Keele University

Synthesis and biological evaluation of polymer-autotaxin inhibitor conjugates for the treatment of ovarian cancer

Natalie Fisher

PhD

July 2016

Keele University

Abstract

Autotaxin is an extracellular phospholipase D that catalyses the hydrolysis of lysophosphatidyl choline (LPC) to bioactive lipid lysophosphatidic acid (LPA). LPA has been implicated in many pathological processes relevant to cancer, including cell migration and invasion, proliferation, and survival. Patients with ovarian cancer often present with an accumulation of ascites fluid in the intraperitoneal cavity which contains LPA at concentrations up to 80 micromolar. Autotaxin is also found at increased levels in the ascites fluid of patients with ovarian cancer and is over-expressed in ovarian cancer tumours that are resistant to chemotherapy. Maintaining a high local concentration of an autotaxin inhibitor within the peritoneal cavity is likely to be important to ensure sufficient and prolonged inhibition of autotaxin. The residence time of small molecular weight drugs in the peritoneal cavity may not be adequate because they are quickly absorbed through the peritoneal capillaries into systemic circulation. Polymers are becoming an increasingly useful tool in the delivery of drugs and have the potential to improve the properties of small molecules, including intraperitoneal residence time. In this thesis, the synthesis of polymer-autotaxin inhibitor conjugates is described, followed by the biological evaluation of the conjugates.

Firstly, the synthesis of a dendrimer-S32826 conjugate and its biological evaluation is reported. S32826 is a LPA analogue with a high potency against autotaxin. This dendrimer-autotaxin inhibitor conjugate was found to inhibit autotaxin activity using two different substrates and two different sources of autotaxin, and to decrease the migration of an ovarian cancer cell line modified to overexpress autotaxin. Furthermore, the conjugate potentiated activation of caspase 3/7 induced by carboplatin. However, conjugation of the drug to the dendrimer significantly reduced its potency.

Subsequently the synthesis of an icodextrin-autotaxin inhibitor conjugate and its biological evaluation was undertaken. Structure-based drug design was used to identify an appropriate locus to cross link icodextrin to an autotaxin inhibitor described by Albers *et al.* with a thiazolidinedione core. The icodextrin-autotaxin inhibitor conjugate was also found to inhibit autotaxin activity using two different substrates and two different sources of autotaxin. Furthermore, the conjugate was found to

reduce migration of an ovarian cell line modified to over express autotaxin. Conjugation to icodextrin led to an increase in solubility and a decrease in permeability compared to the free drug. Finally, the icodextrin-autotaxin inhibitor conjugate was administered to the peritoneal cavity of mice. After 24 hours, 30% of the drug was still detected in the peritoneal cavity. These observations suggest that the drug conjugate may be useful in the treatment of ovarian cancer.

Contents

List of Figures

List of Tables

List of Schemes

List of equations

Acknowledgments

Firstly, I would like to thank my supervisor Dr Alan Richardson for providing unlimited guidance, support and advice throughout this project. And also to my co-supervisor's Dr Michael Edwards, whom has provided excellent support and advice through his expertise in synthetic chemistry and Dr Steve Allin for his input into the design and chemistry of this project and providing me with the opportunity to work at Charnwood Molecular. I would like to thank the MRC for funding this project.

I would like to thank the people at Charnwood Molecular for providing me with an excellent experience whilst on placement. With special thanks to my supervisor Dr Mike Mc Kenzie, and Neilesh, George, Tim and Mel for their patience whilst getting me acquainted with the labs at Charnwood and for their contribution to the chemistry. I am grateful to all those at the animal house for their expertise and assistance with special thanks to Stef, for helping with undertaking the animal studies. I would like to acknowledge Dr Elsegood at Loughborough University for performing the X-ray crystallography. And Dr James Everett for helping with the Caco-2 experiment.

I would like to thank all those in my research group, with a special thanks to Dr Elizabeth Robinson for her support in teaching me cell culture techniques. And to everyone else at the ISTM thank you for your friendship and support over the last four years.

I am eternally grateful to my parents for supporting me through all my choices in life. To my brother Jack and sister Joanne for always being there for me, and my grandparents for their support.

Lastly to James whom has provided me with endless support and encouragement along this journey, not sure I could have done it without you.

Associated publications

Fisher, N.; Hilton-Bolt, T.; Edwards, M. G.; Haxton, K. J.; McKenzie, M.; Allin, S. M.; Richardson, A., Dendrimer Conjugate of 4-(Tetradecanoylamino)benzyl phosphonic Acid (S32826) as an Autotaxin Inhibitor. *ACS Medicinal Chemistry Letters* 2014, *5* (1), 34-39.

Robinson, E.; **Fisher, N**.; Stamelos, V.; Redman, C.; Richardson, A., New strategies for the treatment of ovarian cancer. *Biochemical Society transactions* 2014, *42* (1), 125-9

Abbreviations

ABC	*ATP-binding cassette* transporters
AC	Adenylate cyclase
Akt	Protein Kinase B
AMPK	5' AMP-activated protein kinase
APCI	Atmospheric pressure chemical ionization
ATX	Autotaxin
br	Broad
BSA	Bovine serum albumin
cAMP	Cyclic adenosine monophosphate
CFLIP	FLICE-like inhibitory protein.
CTR1	Copper transporter 1
d	Doublet
DAG	Diacylgylcerol
DMAc	Dimethylacetamide
DMF	Dimethylformamide
DMSO	Dimethylsulfoxide
DNA	Deoxyribonucleic acid
ECM	Extra Cellular Matrix
Edg	Endothelial differentiation gene
EDTA	Ethylenediaminetetraacetic acid
ENPP	Ectonucleotide pyrophosphatase/phosphodiesterase
ENPP-2	Ectonucleotide pyrophosphatase/phosphodiesterase 2
EOC	Epithelial ovarian cancer
EPR	Electron paramagnetic resonance
ES	Electrospray
EtOAc	Ethyl acetate
EtOH	Ethanol
FAF	Fatty acid free
FAK	Focal Adhesion Kinase
G3 PAMAM	3rd Generation polyamidoamine
GAPDH	Glyceraldehyde 3-phosphate dehydrogenase
GEP	Granulin-epithelin precursor
GPCR	G Protein Coupled Receptor
GST	Glutathione S-transferases

HBOC	Hereditary Breast and Ovarian Cancer
HEVs	High endothelial venules
Hex	Hexane
HGSC	High grade serous carcinoma
HMPA	Hexamethylphosphoramide
HNPCC	Hereditary nonpolyposis colorectal cancer
IP_3	inositol trisphosphate
IR	Infra-red
Ki	Inhibitor constant
LC	Liquid Chromatography
LPA	Lysophosphatidic acid
LPA_{1-6}	Lysophosphatidic acid receptors (1-6)
LPAAT	Lysophosphatidic acid acyltransferase-beta
LPAR	Lysophosphatidic acid receptor
LPC	Lysophosphatidylcholine
LPP	Lipid phosphate phosphatases
lysoPLD	Lysophospholipase D
MAG	Monoacylglycerol
MAPK	Mitogen-activated protein kinase
MeOH	Methanol
MMP	Matrix metalloproteinase
mRNA	Messenger RNA
MS	Mass spectrometry
MWCO	Molecular Weight Cut-off
NICE	National Institute for Health and Care Excellence
NMR	Nuclear magnetic resonance
NOE	Nuclear Overhauser Effect
NSAID	Non-steroidal anti-inflammatory drug
NSCLC	Non-small-cell-lung cancer
NUC	Nuclear domain
Papp	Apparent permeability
PARP	Poly ADP ribose polymerase
PC	Phosphatidyl choline
PDE	Phosphodiesterase domain
Pe	Permeability coefficient
PEG	Polyethylene glycol

PEI	Polyethylenimine
PGA	Polyglutamic acid
PI3K	Phosphoinositide 3-Kinase
PKC	Protein Kinase C
PLA1	Phospholipase A1
PLDH	PEGylated Liposomal Doxorubicin Hydrochloride
PPAR	Peroxisome proliferator-activated receptor
PVP	Polyvinylpyrrolidone
q	Quaternary
RGS proteins	Regulator of G protein signalling
RIPA	Radioimmunoprecipitation buffer
Rho	Rho GTPase
ROCK	Rho-associated protein Kinase
rt	Room temperature
s	Singlet
S1P	Sphingosine-1-phosphate
SAR	Structural Activity Relationship
siRNA	Small interfering RNA
SMB1	Somatomedin B-like domain 2
SMB2	Somatomedin B-like domain 1
sPLA2	Secretory Phospholipase A
SRF	Serum response factor
t	Triplet
TBAF	Tetra-*n*-butylammonium fluoride
TEA	Triethylamine
TEER	Trans Epithelial Electrical Resistance
TGA	Thermogravimetric analysis
THF	Tetrahydrofuran
TIPS-Cl	Triisopropylsilyl chloride
TLC	Thin layer chromatography
TMS-I	Trimethylsilyl iodide
TsCl	Tosyl chloride
uPA	Urokinase receptor
UV	Ultraviolet
UV/VIS	Ultraviolet/Visible
VEGF	Vascular endothelial growth factor

Chapter 1

Introduction

1.1 Ovarian cancer

1.1.1 Introduction

Ovarian cancer is the fifth most common cancer in women, with approximately 7,000 women being diagnosed with ovarian cancer in 2011 in the U.K and approximately 4,200 deaths in 2012.[1] Worldwide in 2008 there were approximately 225,000 new cases of ovarian cancer diagnosed, and 140,000 recorded deaths from ovarian cancer.[2] For patients diagnosed between 2008 and 2012 in the U.K survival to five years is 47% with resistance to chemotherapy and reoccurrence of tumour growth a major issue in the long term survival of ovarian cancer patients.[1] Ovarian cancer is a disease produced by the rapid growth and division of one of the three major cell types; germ cells, stromal cells or epithelial cells, with cancer of epithelial origin being the most common.[3] Epithelial ovarian cancer (EOC) has four main histological subtypes, serous (70% of cases), endometrioid (10-15% of cases), clear cell (10% of cases) and mucinous (3% of cases).[4] These subtypes are characterised by their resemblance of differentiated cells found in the fallopian tube (serous), endometrium (endometrioid), endocervix (mucinous) and vagina (clear cell). Serous carcinomas are high grade in 90% of these cases and also account for 70% of deaths from ovarian cancer.[4] Ovarian cancer has few distinctive early symptoms, and is therefore usually diagnosed at an advanced stage of disease with patients presenting with peritoneal metastases. Thus earlier diagnosis would be beneficial and this would be facilitated by an improved understanding of the origin of ovarian cancer.

1.1.1 Origin and histopathology

The epithelial surface of the ovaries was originally identified as the primary origin of ovarian cancer due to the location of the bulk of the tumour and because frequent ovulation has been identified as a major risk factor for ovarian cancer.[3] However, this theory has not been verified and no precancerous lesions have been observed in the ovary.[5] Furthermore, high grade serous carcinomas (HGSC) have the same appearance as fallopian epithelium not ovarian surface epithelium.[5] These observations have led to the suggestion that ovarian cancer may originate from the fallopian tubes.[6] Furthermore,

a link between BRCA1 and BRCA2 mutations and fallopian tube carcinomas led to the analysis of fallopian tubes and ovaries of women with a BRCA1/2 mutation whom had undergone preventative surgery.[7-8] From these studies early serous carcinomas were found in the fallopian tubes.[9-11] Early serous lesions of the fallopian tubes have also been identified in 64-71% of non-hereditary HGSC.[12] Further support for the fallopian tube origin of EOC includes a gene expression analysis which indicated a high degree of similarity between high grade serous ovarian cancer and tubal carcinomas.[13] However, not all HGSC present with tubal carcinomas therefore the origins of EOC require further investigation.[14-17]

Advances in the histology and molecular genetics of ovarian cancer have also changed the idea that ovarian cancer is one disease with many epithelial subtypes and suggest it is several separate diseases.[18] Currently ovarian cancer is classified into two types of tumours.[19] Type I tumours are low grade tumours (well differentiated and slow growing), typically with mutations in BRAF, KRAS and PTEN, including endometrioid, mucinous and clear cell carcinomas. These are slow growing and often resistant to chemotherapy. Type II tumours are high grade tumours (poorly differentiated and fast growing), including serous and endometrioid carcinomas, typically with mutations in p53, BRCA1 and BRCA2.[5] These tumours often grow more rapidly, but are usually sensitive to chemotherapy.

1.1.2 Epidemiology and genetic predisposition

One of the main risk factors associated with ovarian cancer is frequent ovulation,[3] consistent with this observation epidemiological studies have shown a decreased risk of developing ovarian cancer with oral contraceptives, multiple pregnancies and lactation, which reduce ovulation.[20-22] Furthermore, tubal ligation has also been linked with a decrease in ovarian cancer incidences.[23] Fertility treatments have been associated with an increased risk of ovarian cancers; however, more recent studies have disputed this.[24-27] Other risk factors identified include an increase in ovarian cancer incidences in women with endometriosis[28-29] and polycystic ovaries.[30] Further to these biological factors, environmental factors may also increase the risk of developing ovarian cancer.

However, potential risk factors are still disputed such as talcum powder[31] and smoking[32] which were previously linked with an increased risk, have more recently been discounted as a cause for ovarian cancer.[33]

A family history of breast or ovarian cancer is another important risk factor for the development of EOC; 10-15 % of ovarian cancer cases are hereditary in origin.[34] Mutations in the genes *BRCA1* and *BRCA2* are involved in the development of ovarian cancer; this is seen in women with hereditary breast-ovarian cancer syndrome (HBOC).[35] A small number of families present with hereditary ovarian cancer but not breast cancer; this is called site-specific ovarian cancer syndrome.[36] This has been linked to specific mutations in *BRCA1*, and is a unique phenotype of HBOC.[37] *BRCA1* and *BRCA2* are located on chromosome 17q and 13q respectively, and are responsible for the production of DNA repair proteins.[38] These BRCA1/2 DNA repair proteins participate in the homologous recombination pathway. Mutations in BRCA1/2 can cause a loss of function of these proteins, ultimately preventing DNA repair through the faulty homologous recombination pathway leading to an increased risk of ovarian cancer. In most populations these mutations are rare, approximately 1 in 500; however, in some ethnic groups the incidence rate can be as high as 1 in 40.[39] The lifetime risk of developing ovarian cancer in women with a germline *BRCA1* mutation is approximately 40%; a germline *BRCA2* mutation carries a smaller risk of 10-20%.[40] Another hereditary factor linked to ovarian cancer is hereditary non-polyposis colon cancer (HNPCC), which accounts for 1% of all ovarian cancers.[40] HNPCC is also linked with an increased lifetime risk of developing colorectal cancers and endometrial cancers.[41] It originates from inherited mutations in DNA mismatch repair genes.[40-41]

1.1.3 Current treatment

Current treatment generally comprises of cytoreductive surgery in combination with a chemotherapy regime.[14] The course of treatment is dependent on the stage of cancer with which the patient presents. If the patient presents with stage Ia-b and surgical resection is optimal, then no adjuvant systemic chemotherapy is recommended.[42] With high risk (stage Ic) or suboptimal surgical resection it is

recommended that adjuvant chemotherapy is administered.[42] If the patient presents with advanced ovarian cancer (stage II-IV), complete resection of all macroscopic disease is carried out either before or after chemotherapy.[42] First line chemotherapy currently consists of a platinum-based drug, usually carboplatin in USA and European Union due to reduced toxicity compared to cisplatin, in combination with paclitaxel.[43] Platinum based drugs bind to and cause crosslinking of DNA initiating apoptosis. Paclitaxel is part of the taxane class of drugs which act as a mitotic inhibitor by disrupting microtubule function, which is essential to cell division. This combination therapy is effective in approximately 80% of cases; however most patients present with reoccurrence within 3 years of treatment.[42]

Current recommendations on further chemotherapy for ovarian cancer are categorised according to platinum sensitivity.[42] Platinum sensitive or partially platinum sensitive patients, considered to be those who do not relapse within 6 months of initially responding to first line platinum treatment, again receive paclitaxel in combination with carboplatin or cisplatin.[42] For partially platinum sensitive, platinum resistant or platinum refractory advanced ovarian cancer, PEGylated Liposomal Doxorubicin Hydrochloride (PLDH) is considered.[42] Doxorubicin belongs to the class of drugs known as anthracycline these drugs intercalate with DNA, inhibiting DNA synthesis. Doxorubicin is given as a liposomal formulation PLDH, due to increased circulation time and enhanced localisation to the tumour. Furthermore, free doxorubicin accumulates leading to cardiotoxicity and local necrosis, which is reduced in liposomal form. However, liposomal doxorubicin has its own profile of side effects including hand-foot-syndrome.[44] Paclitaxel is recommended for patients who are allergic to platinum based therapy and platinum-resistant patients as a second line option; if the patient is both allergic to platinum and paclitaxel is not deemed appropriate, topotecan may be administered; topotecan is a topoisomerase I inhibitor which works by intercalating DNA bound to topoisomerase I.[42, 45]

1.1.4 New treatments

Olaparib is a poly ADP ribose polymerase (PARP) inhibitor which has recently been approved for the treatment of ovarian cancer.[46] PARP is an enzyme involved in DNA repair. Patients with a *BRCA1/2* mutation are at an increased risk of developing ovarian cancer and are often resistant to conventional chemotherapy.[47] However, their cancers also have an increased reliance on PARP to repair double stranded DNA damage. In the absence of BRCA, repair by homologous recombination is prevented. If PARP is also inhibited, DNA repair depends on the error-prone non-homologous end-joining pathway which leads to further DNA damage. As a result, PARP inhibitors are particularly beneficial for patients with the BRCA1/2 mutation.[48] Several clinical trials have shown therapeutic benefit with the PARP inhibitor Olaparib, for the treatment of ovarian cancer.[49-51] Approval in the European Union and USA has been granted for the treatment of patients with advanced ovarian cancer who have a *BRCA1/2* mutation and have previously received 3 or more lines of treatment.

Bevacizumab, is an anti-VEGF antibody which has shown promise in clinical trials.[52-56] Angiogenesis is an important factor in tumour growth and its inhibition slows tumour progression.[57] Vascular endothelial growth factor (VEGF) is the main target for antiangiogenic treatment.[57] Bevacizumab sequesters VEGF, preventing it from driving angiogenesis and consequently from providing the vascular network necessary for nutrient supply to the tumour. However, NICE have not recommended bevacizumab for treatment of ovarian cancer as they do not believe the benefit justifies the high cost.[58-59]

Although new treatments for ovarian cancer which have been approved are limited, there are many new ovarian cancer treatments currently in development. Often they are targeting specific molecular pathways known to be involved in the pathogenesis of cancer. Some of the more successful treatments include PARP inhibitors, antiangiogenics and PI3/mTOR/Akt pathway inhibitors.

1.1.5 Chemoresistance

Resistance to chemotherapy is a major problem in the treatment of ovarian cancer; it is a key factor in the high mortality rate associated with ovarian cancer. Understanding the mechanisms behind the development of resistance is important in combatting the low survival rate of women with ovarian cancer. So far it has been established that the development of chemoresistance in ovarian cancer is multifactorial and may involve multiple mechanisms.[60]

A mainstay in chemoresistance involve alterations in the drug transport pathways, which can lead to a development of Multiple Drug Resistance. For example, overexpression of ATP-binding cassette (ABC) transporters confers resistance to many chemotherapeutic agents.[61] ABC transporters are responsible for the efflux of endogenous and foreign substances across the cell membrane, when overexpressed this can lead to a reduction in accumulation of chemotherapeutic agents in cancer cells. Copper transporter 1 (CTR1), is the major copper influx transporter protein, it also controls the accumulation of platinum based drugs in tumour cells. Furthermore, CTR1 expression has been correlated with acquired cisplatin resistance in ovarian cancer cells.[62] Alterations in detoxification proteins, such as Glutathione S-Transferase (GST) enzymes and metallothionein, have been shown to confer resistance to chemotherapy. GST's detoxify xenobiotics by catalysing their nucleophilic attack by glutathione preventing interactions with nucleic acids and proteins. GST's have also been shown to detoxify chemotherapeutic drugs such as alkylating agents and platinum-based drugs.[63] Metallothioneins are metal detoxifying proteins, which bind to metal ions to prevent them from interacting inappropriately. The expression and induction of metallothioneins, has been associated with protection against cell damage, apoptosis and oxidative stress.[64]

Alterations in the drug targets themselves is another method of developing resistance, such as changes in β-tubulin, the target of the taxane class of chemotherapeutic agents. β-tubulin is responsible for the production of microtubules which are essential for cell division. Taxanes such as paclitaxel, bind to β-tubulins and inhibit microtubule function preventing cell cycle progression during mitosis. Overexpression of specific β-tubulin iso-types has been suggested as the main

mechanism of the development of resistance to taxanes.[65-66] Another target alteration include that of the topoisomerases. Topoisomerases regulate the under-winding or over-winding of DNA and are the target of many chemotherapeutic agents such as topotecan and doxorubicin, which intercalate the DNA-topoisomerase complex leading to cell death.[66] Mutations in topoisomerase enzymes have been observed causing a reduction in availability of cleavable complexes leading to reduced DNA damage and hence less cell death.[67]

In addition, another mechanism of resistance involves changes in DNA repair mechanisms. Platinum chemotherapeutic agents bind to and cause crosslinking of DNA preventing DNA repair. Therefore, the ability to repair via other mechanisms could confer resistance. A study by Masuda *et al.* found that resistance to cisplatin was related to an increase in the removal of platinum-DNA adducts.[68] Furthermore, Zhen *et al.* reported that acquired cell resistance to cisplatin may be associated with increased gene specific DNA repair efficiency of the interstrand crosslink[69] and Johnson *et al.* found that resistance to cisplatin may be associated with DNA repair and alterations in interstrand crosslink formation.[70] Moreover, alterations in specific genes (oncogenes, tumour suppressor genes, metastasis suppressor genes) appear to be directly associated with the loss of chemosensitivity.[60]

1.1.6 Summary

Although advances in the treatment of ovarian cancer have been made over the past couple of decades due to improvements in cytoreductive surgeries, chemotherapy regimens, such as dose dense chemotherapy, and the use of combinational therapy there are still significant developments required to better treat ovarian cancer, particularly due to resistance to known drugs. More recently morphologic and molecular genetic studies have shown that ovarian cancer is a heterogeneous disease with many distinct subtypes from different origins, therefore ovarian cancer subtypes should be treated on an individual basis. Advances in the understanding of the biology of ovarian cancer has resulted in the development of more targeted therapies, these include PARP inhibitors such as the newly approved olaparib,[46] antiangiogenics and targeting of the PI3/Akt/mTOR network.[43]

1.2 Autotaxin

1.2.1 Introduction

G. Mills *et al.* first discovered that patients with ovarian cancer develop an accumulation of ascites fluid containing factors which support the growth of epithelial cancer cells in the intraperitoneal cavity over two decades ago.[71] Five years later Xu *et al.* discovered that the growth factor lysophosphatidic acid (LPA) is the major ovarian cancer activating agent present in ascites fluid.[72] Levels of LPA in the ascites fluid can reach concentrations up to 80 μM.[73] Since this discovery, LPA has been implicated in a number of mechanisms involved in the pathogenesis and survival of ovarian cancer. However, the development of molecules designed to interfere with this major cancer activating agent are relatively limited. This may largely be due to the complexity of the LPA signalling pathways. More recently the enzymes and receptors involved in the LPA signalling pathway have been defined. One enzyme, autotaxin was discovered by Umezu-Goto *et al.* to produce LPA from lysophosphatidylcholine (LPC).[74] Autotaxin was originally identified as an autocrine motility factor released by human melanoma cells.[75] It was later found to have lysophospholipase D activity and to play a major role in the production of LPA in many biological fluids generated from both normal human cells and cancer cells.[74] It is synthesised as a pre-proenzyme and secreted into the extracellular space.[76]

Lysophosphatidic acid (LPA; mono-acylglycerol-3-phospate) is the simplest glycerophospholipid consisting of a single acyl chain, a glycerol backbone and a phosphate group, (Figure 1.1). There are different molecular species of LPA with varying acyl chain lengths and variants of either saturated, mono- and poly-unsaturated chains. There are also *sn1* or *sn2* regioisomers. The predominant species of LPA is poly-unsaturated 18:2 which accounts for approximately half the amount of LPA present in plasma.[77-78] It plays a vital role as a precursor in phospholipid biosynthesis and also functions as an intercellular lipid mediator inducing many actions including cell proliferation, invasion and migration, inhibition of apoptosis, senescence, angiogenesis and chemoresistance. It acts via specific G protein coupled receptors (GPCRs) on the cell surface to activate a variety of signalling pathways.

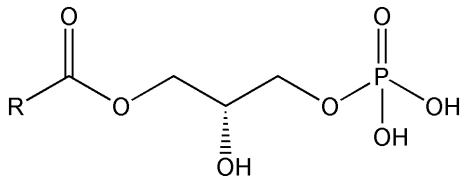

Figure 1.1: Structure of Lysophosphatidic acid.

1.2.2 LPA synthesis

In addition to autotaxin, there are several other enzymatic pathways by which LPA can be produced, (Scheme 1.1). Different species of LPA can be formed via the hydrolysis of phosphatidic acid (PA) by either phospholipase A_1 (PLA_1) or soluble phospholipase A_2 ($sPLA_2$).[77, 79] $sPLA_2$ cleaves the *sn2* positioned fatty acid chain whereas PLA_1 cleaves the fatty acid chain in the *sn1* position. PA itself is produced by hydrolysis of membrane phosphatidylcholine (PC) by phospholipase D (PLD). Another route to LPA formation involves catalysis by ATX/lysophospholipase D (lysoPLD).[74] Autotaxin hydrolyses the choline from lysophosphatidylcholine (LPC) to form LPA. Initially, LPC is formed by hydrolysis of PC by PLA_1 or $sPLA_2$.[77] Due to autotaxins association with cell motility and tumour progression, autotaxin is thought to be the most important catalyst in pathological LPA formation.

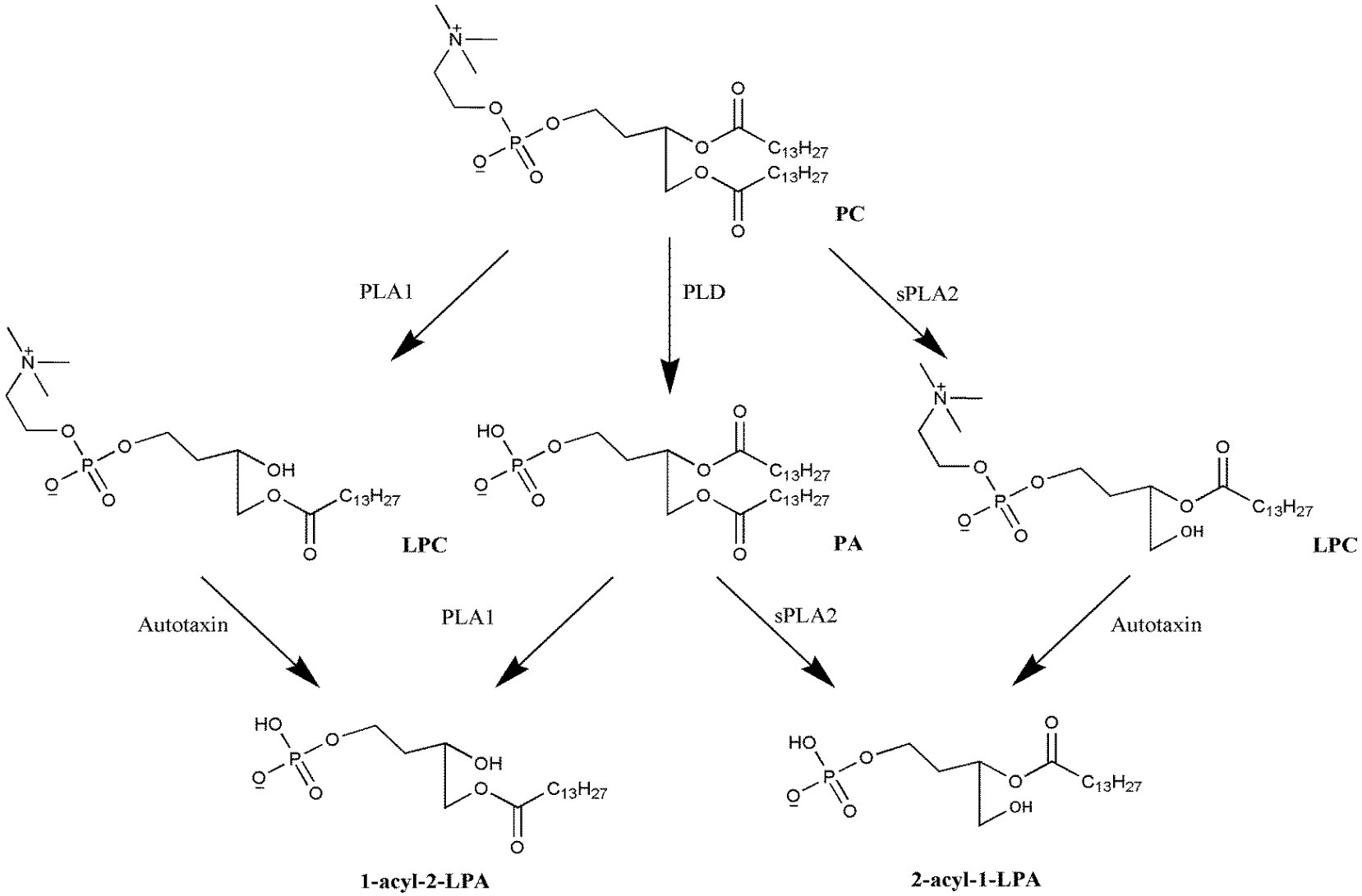

Scheme 1.1: Synthetic scheme of LPA production.

1.2.3 Structure

Autotaxin (ATX) is a 125 kDa glycoprotein extracellular enzyme which is a member of the ecto-nucleotide pyrophosphatase/phosphodiesterase (ENPP) family, encoded by the gene *ENPP-2* on chromosome 8 (Figure 1.2).[75] Transcription of *ENPP2* is regulated by various transcription factors (including Hoxa13, NFAT-1 and v-jun)[80-82] resulting in three different isoforms, ATXα, ATXβ and ATXγ.[75, 83] ATXβ is the most common isoform of autotaxin; it was first identified from tetracarcinoma cells and is the shortest of the isoforms with 863 amino acids.[84] ATXα was first derived from melanoma cells; it is similar to ATXβ but contains an extra 52 residue insertion in the catalytic domain.[85] ATXγ is the least common isoform; it is a brain specific isoform and is similar in structure to ATXβ with an extra 24 residue insertion near the nuclease like domain.[86-88] Determination of the autotaxin crystal structure has only recently been achieved, providing a valuable tool in understanding the binding site of LPA and therefore aiding the development of inhibitors of the enzyme. So far 12 crystal structures have been defined by Nishimasu[89] and Hausmann.[90] Of these PDB entries 3NK(N-R)[89] show autotaxin with LPA bound with varying lengths of acyl chains, PDB entries 3NKM[89] and 2XR9[90] show autotaxin with no inhibitor bound (mouse and rat respectively). PDB entry 2XRG[90] shows autotaxin bound with the known inhibitor HA155 and PDB entries 3WA(V-Y) show autotaxin bound with newly developed inhibitors discovered from a large library of compounds.[91]

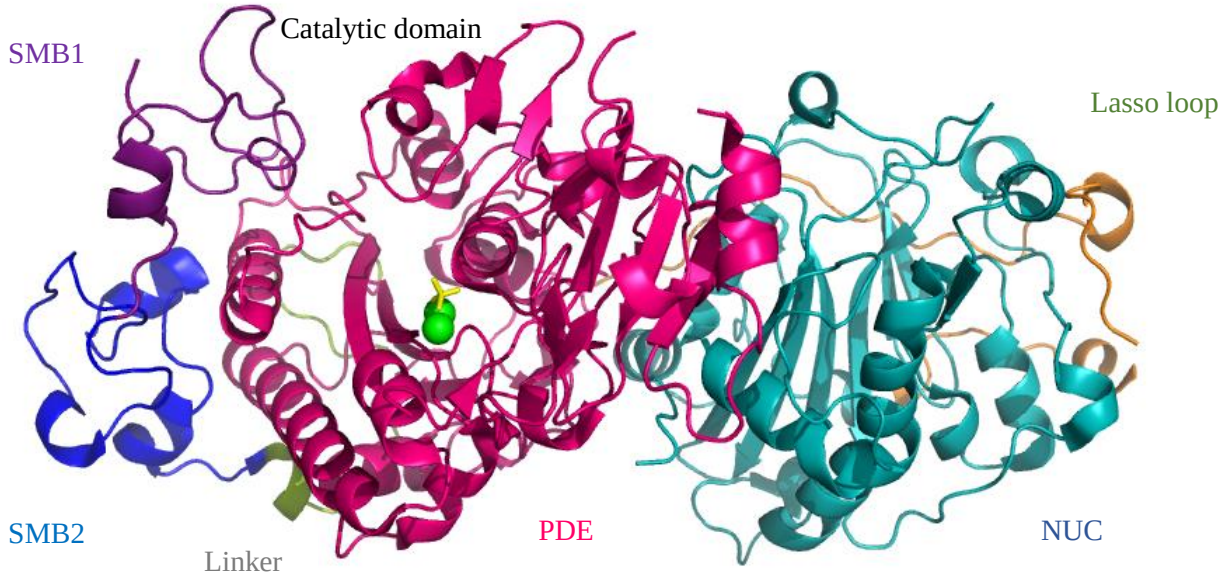

Figure 1.2: Overview of autotaxin structure.

The structure of autotaxin consists of 4 domains; two Somatomedin B like domains (SMB1 & SMB2) at the N-terminus, a central catalytic phosphodiesterase domain (PDE) and a nuclease like domain (NUC) at the C terminus. A linker region (residues 141–160) connects the SMB-like domain 2 with the catalytic domain, and lasso loop region (residues 540–589) connects the catalytic domain with the nuclease-like domain.

The SMB1 (56-96) and SMB2 (96-140) domains are cysteine rich and involved in protein-protein binding. They have also been shown to bind to integrins which are possibly involved in autotaxin's recruitment to the cell surface, bringing it into close proximity with the LPA receptors.[92]

The PDE domain (160-539) is the site of catalysis; it is similar to the catalytic domain of alkaline phosphatases. It consists of a core (161-364, 471-536) and insertion (365-470) subdomain. The core subdomain has an α/β fold and binds to a sulphate and two Zn^{2+} ions.

The NUC domain (590-862) is thought to be catalytically inert. It consists of varied α/β folds and binds a number of ions. It has been suggested that this domain along with the glycan chain is essential for maintaining the structure of the ligand binding site. Computer modelling studies suggest the

existence of an allosteric interaction pathway from the NUC domain to the Thr209 residue in the catalytic domain.[93]

The lasso loop (540–589) wraps around the NUC domain and interacts with the rest of the protein via hydrogen bonds, salt bridges and a disulphide bond. Other features to note include a glycan chain and a cysteine bridge which are assumed to be essential for the interface between the domains, connecting the PDE and NUC domain. It is also thought that a hydrophobic tunnel between the SMB domain and the ligand binding domain may be involved in delivery of LPA to cell surface receptors.[89-90]

1.2.4 Ligand binding site

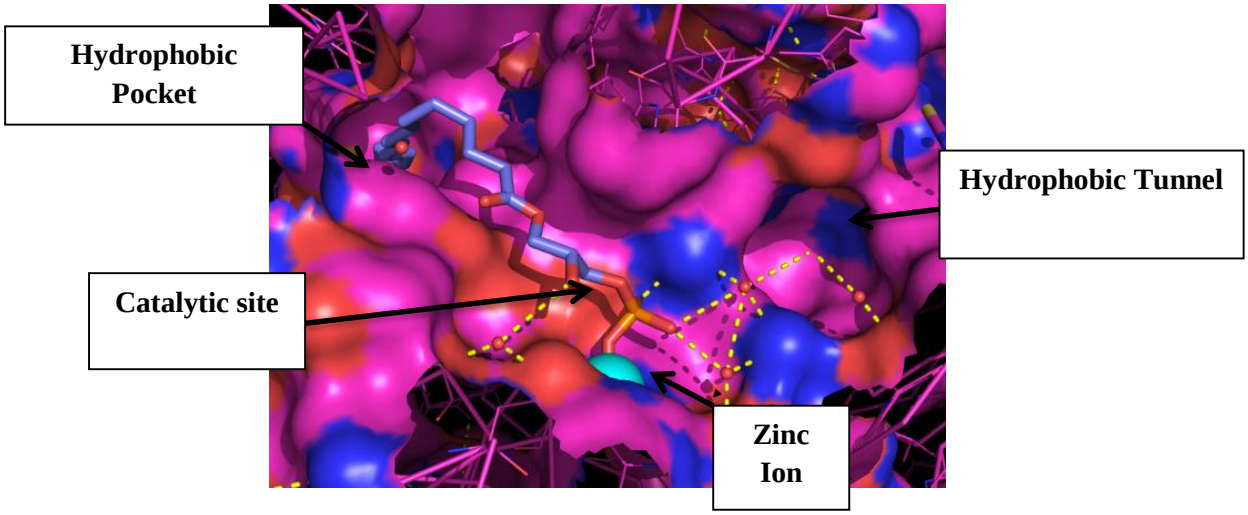

Figure 1.3: Ligand binding site shown with LPA Bound; PDB entry 3NKR.

The main features of the ligand binding site include the two Zn^{2+} ions, and a deep hydrophobic tunnel. One of the zinc ions is coordinated by Asp311, His315 and His474, and the second zinc ion is coordinated by Asp171, Thr209 and His359 residues, leaving one site available on each ion for coordination with another negatively charged molecule, in the ligand free form a sulphate or phosphate is bound here.[89] The Zn^{2+} binding sites are conserved among the ENPP family members and have been shown to be essential for catalytic function as are the highly conserved Asn230 and

Thr209 residues which provide a hydrogen bonding environment for the binding of ligands, (Figure 1.3). [89]

When in complex with LPAs of varying chain lengths the acyl chain, glycerol and phosphate group are all recognised by autotaxin in a similar manner, (Figure 1.4). A slight conformational change occurs on binding to LPA, causing Asp358 which normally forms hydrogen bonds with the OH group of Thr209 to coordinate with one of the $zinc^{2+}$ ions. One oxygen atom of the phosphate coordinates the first $zinc^{2+}$ ion, whilst a second oxygen atom of the phosphate hydrogen bonds to Asn230, and the NH and OH groups of Thr209. The final phosphate oxygen forms a water mediated hydrogen bond with Lys208, Asn230 and Asp473. The glycerol moiety forms van der Waals contacts with Thr209 and Leu243, and its hydroxyl group forms water-mediated hydrogen bonds with Asp311 and Glu308. The acyl chain forms van der Waals contacts with Phe210, Leu213 and Tyr306, and an additional hydrogen bond between the carbonyl group and Tyr306. The lipid tail of the 14:0 LPA, 16:0 LPA and 18:0 LPA sits in a hydrophobic pocket lined by Ile167, Leu216, Ala217, Leu259, Phe273, Trp275 and Met512, the structure is kinked providing specificity for unsaturated substrates. A slight local conformational change occurs in the complexes with Leu216 and Glu308 rotating to accommodate LPA. There was also an observed decrease in electron density with increasing acyl chain length suggesting a decrease in stability.[89-90]

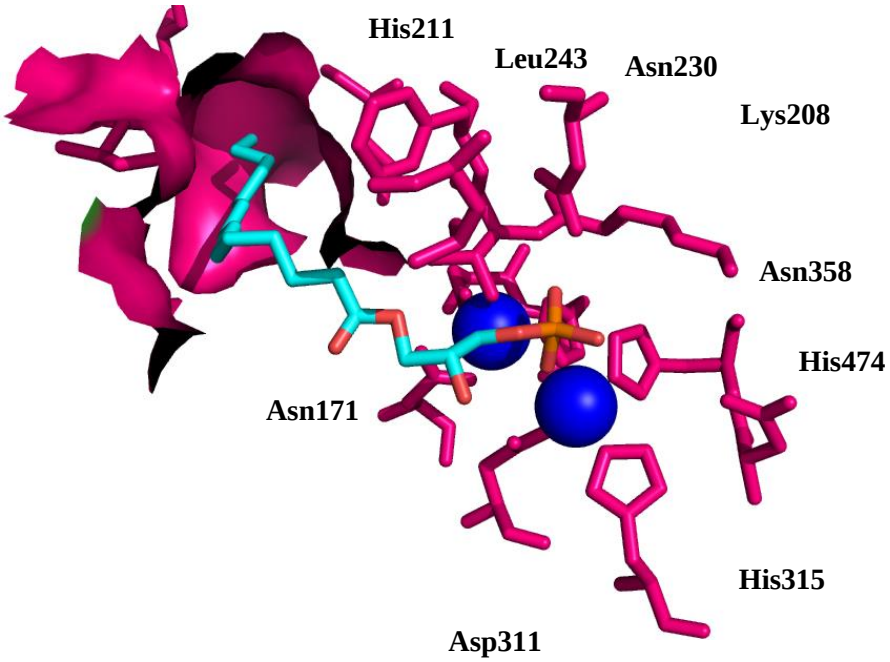

Figure 1.4: Ligand binding site showing residues involve in the binding of LPA; PDB entry 3NKR.

The mechanism of catalysis has not been defined; however, the structural similarity between *X. axonopodis* NPP suggest the mechanism could be similar. The two Zn^{2+} ions, their coordinating residues and the highly conserved Asn230 and Tyr306 of autotaxin were shown to overlap with Asn111 and Tyr205 of *X. axonopodis* NPP, respectively. These observations substantiate that autotaxin hydrolyse LPC through a mechanism similar to that of *X. axonopodis* NPP.[89, 94]

1.2.5 LPA catabolism

There are a number of ways in which LPA can be processed, (Scheme 1.2). Two main pathways are by LPA-acyltransferase (LPAAT) to generate (PA), or dephosphorylation by lipid phosphate phosphohydrolases (LPPs) to mono-acyl glycerol (MAG).[95-98] LPP expression is decreased in ovarian cancer and overexpression has been shown to reduce apoptosis and cell growth in ovarian cancer cells.[95-98] This coupled with increased LPA production by ATX creates “the perfect storm” for cancer cell migration, proliferation and survival.

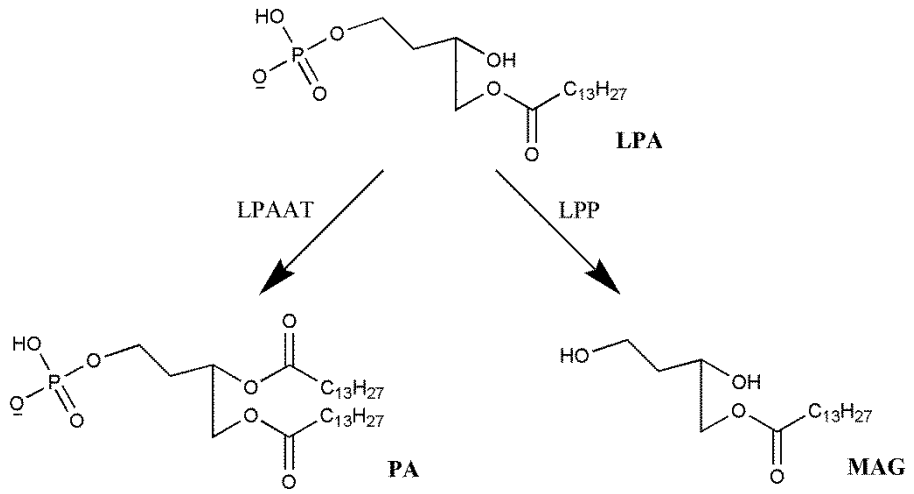

Scheme 1.2: LPA catabolism.

1.2.6 LPA Receptors

The diverse actions of LPA on cells are explained by the existence of at least six GPCRs, LPA_{1-6}, (Figure 1.5) and the different signalling pathways used by each of them.[99] The first LPA receptor was described in 1996 by Chun *et al*., LPA_1 formerly Edg_2 is part of the endothelial differentiation gene (Edg) family.[100] A further two structurally similar LPA receptors LPA_2 and LPA_3[101] (formerly Edg_4 and Edg_7 respectively) were found. These three receptors along with five sphingosine-1-phosphate receptors are the EDG family of receptors. Later Noguchi *et al*. discovered a fourth LPA receptor LPA_4, formerly GPR23/p2y9, which is more closely related to the purinergic receptor family.[103] Two more LPA receptors, structurally similar to LPA_4 were subsequently identified. GPR92/93 and p2y5 now known as LPA_5 [104-105] and LPA_6 [106-108] respectively, along with LPA_4 comprise the non-Edg family of LPA receptors. Other receptors which have been linked to stimulation by LPA include GPR35,[109] GPR87[110] and P2Y10[111]; however more research is needed to fully classify these proteins.[112]

LPA_{1-6} are type 1 rhodopsin-like GPCRs with seven transmembrane domains. LPA receptors couple to one or more heterotrimeric G proteins, namely $G_{12/13}$, G_q, G_i and G_s, resulting in the activation of many signalling pathways leading to many biological responses, (Figure 1.5); and some of which have been implicated in carcinogenesis. Rho and rac are GTPases which are involved in regulating

cell motility in cancer cells.[113] The mitogen-activated protein kinase (MAPK) pathway has been implicated in cancer growth and the Akt pathway in cancer survival. Moreover, downstream events of PLC activation have been shown to promote tumour progression.

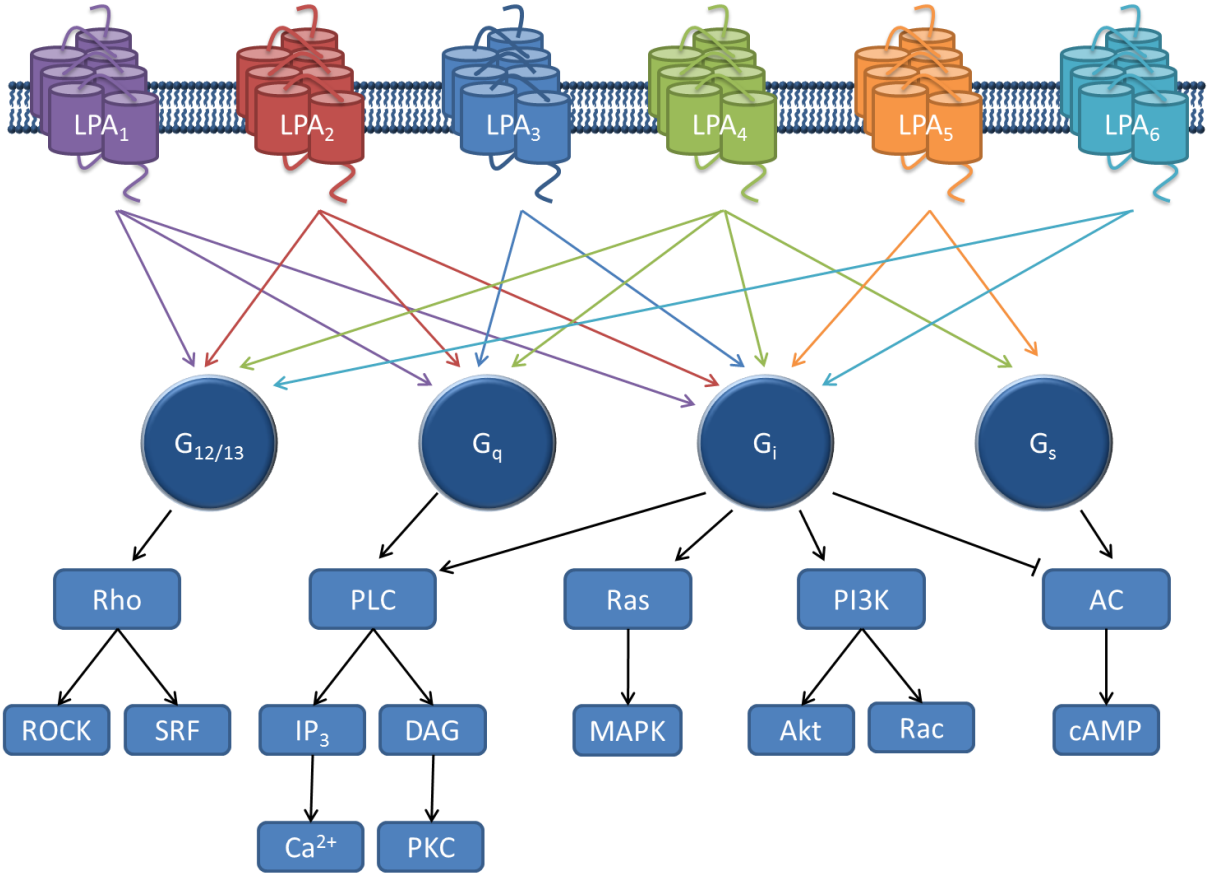

Figure 1.5: LPA receptor signalling cascades.

Expression of LPA receptors has been associated with the pathogenic process of cancer. For example, overexpression of LPA_1 in MDA-MB-231 breast cancer cells promoted skeletal tumour growth in a xenograft model. Also silencing or inhibition of LPA_1 was found to reduce the growth of the tumour and metastasis bone progression.[114] Contradictorily LPA_1 has been found to have a decreased expression in ovarian cancer and when expression was induced it led to an increase in apoptosis independent of LPA.[115] LPA_2 and LPA_3 overexpression has been observed in ovarian cancer,[97,116,117] furthermore, expression was found to correlate with tumour stage.[118]

It has been demonstrated that autotaxin and LPARs can contribute to the initiation and progression of breast cancer.[119] Transgenic mouse models driven by the mouse mammary tumour virus (MMTV) long terminal repeat (LTR) promotor expressing autotaxin (MMTV-ATX) or one of the three main LPA receptors LPA_{1-3} (MMTV-LPA) developed chronic mastitis, hyperplasia, mammary intraepithelial neoplasia and invasive metastatic tumours.[119] A recent study exploring the biological roles of the LPA receptors LPA_{1-3} in the pathogenesis of tumour cells found that LPA_2 and LPA_3 expression lead to an increased activity in cell motility and invasion assays, the activity was further increased by the addition of LPA. Conversely expression of LPA_1 showed decreased intrinsic cell motility and invasion.[120]

In addition to GPCRs LPA activates other receptors such as the peroxisome proliferator-activated receptor, PPARγ, which may also play a role in the carcinogenesis of LPA in ovarian cancer. PPARγ is a transcription factor that drives the expression of genes involved in many biological responses including apoptosis, Zhang *et al.* found that PPARγ is overexpressed in ovarian cancer.[121] Furthermore, Davidson *et al.* observed increased PPARγ expression had a direct correlation with a poor response to chemotherapy and shortened survival.[122] Contradictorily, PPAR agonists inhibit the proliferation of ovarian cancer cells and induce apoptosis.[123] Synergies between PPARγ ligands and platinum based drugs have also been observed.[124] The contradicting evidence for PPARγ contribution to the carcinogenesis of ovarian cancer suggests further clarification of PPARγ's role in cancer is required.

1.3 Physiological and pathophysiological functions

1.3.1 Physiological role of autotaxin

Autotaxin is essential for embryonic development. Transgenic mice lacking autotaxin die as an embryo at embryonic day 9.5.[125-127] Lethality is due to abnormal vascular and neuronal development, indicating autotaxin is vital in the development of vasculature by vasculogenesis and angiogenesis.[125-127] A recent study by Yukiura *et al.* found overexpression of autotaxin in transgenic mice also led to embryonic lethality around embryonic day 9.5 with vascular defects present.[128]

Autotaxin is found in most biological fluids including plasma, serum,[74] urine,[129] synovial fluid,[130-132] peritoneal fluid[73] and cerebrospinal fluid.[133-134] High levels of autotaxin mRNA are found in the ovaries, brain, small intestine and placenta.[84] High levels are also observed in adipose tissue[135] and high endothelial venules (HEVs).[136] HEVs enable lymphocytes to enter lymph nodes. Inactivated autotaxin reduced T-cell homing to the lymph nodes suggesting that autotaxin may regulate lymphocyte migration.[136] Autotaxin may exert other roles not associated with its production of LPA, however most of its biological activity arises from LPA production. Autotaxin is also able to catalyse the production of the sphingolipid, sphingosine-1-phosphate (S1P) which potentially has bioactivity.[137] LPA is present in most biological fluids. There have been many documented effects of LPA in many cell types. The major effects LPA has been associated with include cytoskeletal reorganisation, morphological and physiological cellular changes affecting cellular communication and extracellular matrix interactions.[138] As autotaxin is bioactive and essential to embryonic development there is a possibility that inhibition of autotaxin may produce adverse effects. However, no adverse effects where found from long term inhibition of autotaxin with either siRNA silencing or an autotaxin inhibitor in a mouse model.[139]

1.3.2 Autotaxin and cancer

1.3.2.1 Migration and invasion

Autotaxin and LPA have been well documented in cancer cell migration and invasion. Although autotaxin has not been directly linked to a role in ovarian cancer metastasis and invasiveness, there are many examples of its role in other cancers. First and foremost, autotaxin was initially identified as an autocrine motility factor.[75] Furthermore, expression of $\alpha_6\beta_4$ integrin in advanced breast cancer is associated with a migratory and invasive phenotype, and also led to an increased expression of autotaxin.[81] This overexpression was found to be mediated by the transcription factor NFAT1.[81] Autotaxin has also been directly linked to cell motility and invasive phenotype, knockout of autotaxin leads to inhibition of invasion and motility[140-142] in several cell lines; and over expression of autotaxin has been shown to increase cell invasion[143] and migration.[142-143] The autotaxin/LPA signalling pathway promotes the expression of many pro-migration and invasion factors including the ECM protein osteopontin, an important chemokine involved in the survival, proliferation, migration, invasion and metastasis of gastric cancer cells.[144] Furthermore, autotaxin, through LPA production induces the expression of urokinase plasminogen activator (uPA) and the matrix metalloproteinase MMP3 via activation of the MAPK cascade, which in turn leads to increased invasiveness in human fibrosarcoma HT-1080 cells.[145] Autotaxin activates the small G-proteins cdc42, rac and focal adhesion kinases all of which are key regulators of cell motility.[142, 146-147] Autotaxin has been shown to regulate the formation of invadopodia, cell membrane protrusions involved with invasion, in a LPA dependent manner.[142] Lastly, autotaxin expression by cancer cells also promotes bone metastasis.[148] Thus there is a significant body of evidence linking autotaxin to invasion and migration.

As might be expected from the foregoing discussion LPA has been implicated in these processes. LPA has been extensively studied in a variety of cancer cell migration and invasion models; in ovarian cancer cells an impact of LPA on many pathways has been discovered. LPA induces the activation of the Src family kinase, Fyn, and increases its association within adherens junction protein

p120-catenin, recruiting Fyn to cell-cell junctions, leading to the dispersal of in the ovarian cancer cell line SKOV3.[149]

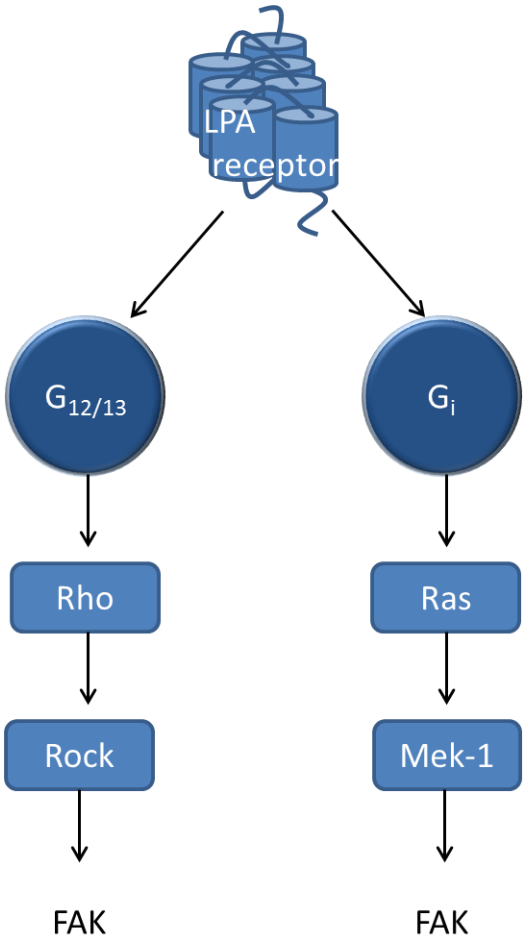

Figure 1.6: Pathways implicated in LPA induced cell migration.

Additionally, LPA activates cytoskeletal reorganisation via the down regulation of RhoA leading to a loss of stress fibres and dissociation of focal adhesion components thereby promoting cell migration.[150] Down regulation of RhoA is dependent on the activation of AMP-activated protein kinase (AMPK).[151] RhoA down regulation has also been shown to be dependent on reorganisation of the cell interface with the ECM by inducing FAK auto-phosphorylation via the $G_{12}/_{13}$–RhoA-ROCK signalling pathway leading to promotion of cell motility.[152-153] Similarly the Gi-Ras-MEK-1 signalling pathway has been shown to mediate LPA-stimulated ovarian cancer cell migration by facilitating focal adhesion kinase (FAK) redistribution to focal contacts, FAK regulates the turnover

of focal contacts therefore contributing to cell migration, (Figure 1.6).[154] Furthermore, induction of the expression of several proteases in ovarian cancer cells by LPA has been observed, including urokinase plasminogen activator (uPA) and the matrix metalloproteinases- MMP1, MMP2, MMP7, and MMP9; which all contribute to the breakdown of ECM facilitating cancer cell invasion.[153, 155-157] LPA also decreases the expression of metalloprotease inhibitors increasing the effect of activation of the MMPs.[158] uPA induction by LPA has been shown to occur in ovarian cancer cells but not in normal epithelial ovarian cells.[159] From the body of evidence discussed in this section, it is clear that the autotaxin-LPA axis is linked to invasion and migration.

1.3.2.2 Inhibition of apoptosis

LPA and autotaxin have been associated with the inhibition of apoptosis via a variety of pathways. LPA induces the translocation of the pro-apoptotic receptor Fas in the extrinsic apoptotic pathway, from the cell surface.[160] Translocation of Fas leads to a reduction in the responsiveness of the cell to apoptotic stimuli. In contrast, LPA also induced the expression of the Fas ligand which induces apoptosis. However, in ovarian cancer this LPA induced Fas Ligand has been implicated in the apoptosis of lymphocytes allowing the cells to avoid immune surveillance.[161-162] Furthermore, LPA increases the expression of the caspase 8 inhibitor CFLIP, preventing caspase 8 activation leading to suppression of the extrinsic apoptotic pathway.[160]

LPA activates the PI-3 kinase/Akt pathway.[160] The PI-3 kinase/Akt pathway is a cell survival pathway, whose activation leads to decreased apoptosis. LPA also promotes the phosphorylation of the pro-apoptotic protein, BAD; unphosphorylated BAD facilitates activation of Bak and Bax to activate the intrinsic apoptotic pathway.[160] Once phosphorylated, BAD can no longer promote activation of Bax and Bak leading to a reduction in apoptosis.[160] LPA also increases the expression of the survival factor, Granulin-epithelin precursor (GEP); which has been shown to be an autocrine growth factor in ovarian cancer.[163] Furthermore, expression of autotaxin has been directly linked to cell survival in fibroblasts with suppression of apoptosis observed in response to serum starvation.[164] The implication of LPA and autotaxin in this wide variety of apoptotic suppressing

pathophysiological pathways together with increased expression of autotaxin and LPA in ovarian cancer provides validation of autotaxin as a target for the treatment of ovarian cancer.

1.3.2.3 Proliferation and senescence

LPA was first described as a growth factor by van Corven *et al.* in 1989, and has since been shown to increase cell growth in several types of cancer.[165-166] In ovarian cancer, LPA stimulated growth via several signalling pathways.[167] Additionally, LPA induces the expression of the growth related oncogene, Groα.[168]

LPA induces the production of the major angiogenic factor VEGF by ovarian cancer cells, and increases the expression of the VEGF receptor in endothelial cells simulating the growth of malignant ovarian tumours.[169-170] It also promotes the expression of pro-angiogenic factor IL-8[171] by ovarian cancer cells signifying that LPA increases the angiogenesis of ovarian cancer cells. Furthermore, VEGF induced expression of autotaxin has been found to increase the effects of LPA.[170]

LPA has also been implicated in the suppression of senescence; LPA has been shown to reduce the amount of the tumour suppressor p53 in A549 lung cancer cells.[172] The effect on LPA was found to be dependent on an increase in proteasome degradation of p53 which leads to a decrease in p53 mediated transcription.[172] It was also found that over expression of the LPA_2 receptor resulted in suppression of the p53-dependent replicative senescence in primary mouse embryo fibroblasts, in a Rho GTPase-dependent manner.[173] It has been suggested that this occurs through the induction of telomerase, allowing indefinite cell proliferation.[174-175]

1.3.2.4 Chemoresistance

LPA and autotaxin have been shown to directly confer resistance to chemotherapy in a number of studies. LPA has been related to the development of resistance to carboplatin in ovarian cancer cells,[176] this has also been observed in colon cancer.[177] Furthermore, expression of autotaxin delayed apoptosis induced by carboplatin in ovarian cancer cells.[178] Apoptosis was also accelerated after inhibition of autotaxin by either siRNA silencing or with a small molecule inhibitor.[178] In addition to

conferring resistance to platinum-based chemotherapy, autotaxin and LPA have been shown to protect breast cancer cells against paclitaxel induced cell death.[179] Paclitaxel disrupts normal spindle function leading to mitotic arrest. LPA was found to restore normal spindle function in breast cancer cells exposed to paclitaxel, leading to the cells escaping mitotic arrest, preventing cell death. This depended on PI3K activation through LPA receptors and involved the displacement of taxol from tublin.[179-180]

Further to autotaxin and LPA, the LPA_2 receptor has been linked to chemoresistance. An increase in irradiation induced apoptosis was observed in LPA_2 null mice.[181-182] The ability of LPA_2 to regulate the pro-apoptotic protein, SIVA1 is one potential way in which LPA is involved with the apoptotic pathway.[183] LPA_2 contains a PDZ domain, which recruit NHERF2 and TRIP6, here they form a complex with SIVA1.[183] SIVA1 is an apoptotic regulatory protein. DNA damage leads to activation of the tumour suppressor p53 which in turn increases the expression of SIVA1, and this contributes to cisplatin induced apoptosis.[184] LPA, through the receptor LPA_2, contributes to the suppression of apoptosis via LPA-induced ubiquitination and turnover of SIVA1, therefore it may be deduced that LPA confers resistance to cisplatin.[185] As SIVA1 inhibits the anti-apoptotic protein Bcl-X_L, part of the Bcl-2 family, which suppresses the activation of Bak/Bax and inhibition of the Bcl-2 family has previously been shown to increase sensitivity to carboplatin.[186-187] This may provide evidence that autotaxin confers resistance to carboplatin via the intrinsic apoptotic pathway.[178]

Further to autotaxin/LPA other proteins associated with LPA Signalling pathway may contribute to chemoresistance, for example, regulator of G protein signalling (RGS) proteins. RGS proteins reduce the signalling of LPA receptors by increasing the GTPase activity of G-proteins that are activated by LPA receptors.[188] The expression of several RGS proteins is decreased in ovarian cell lines which are resistant to cisplatin.[189] When the RGS proteins, RGS10 and RGS17, were knocked down, a reduction in the potency of cytotoxic chemotherapeutic agents was observed. Further to this RGS10 and RGS17 were shown to suppress LPA-induced activation of Akt survival pathways.[189] This suggests a LPA signalling dependent role for RGS proteins in the regulation of chemoresistance in ovarian cancer.

1.3.3 Autotaxin and inflammatory diseases

Further to its role in cancer, the ATX/LPA signalling pathway is implicated in many inflammatory diseases, including cardiovascular diseases,[190] obesity,[191] rheumatoid arthritis,[192] multiple sclerosis,[193] pulmonary fibrosis[194] and chronic hepatitis.[195] Increased autotaxin expression was also observed in the frontal cortex of Alzheimer's like dementia patients.[196]

LPA has been implicated in the progression of rheumatoid arthritis. Genetic ablation of autotaxin resulted in disease attenuation in animal models of rheumatoid arthritis.[192] Autotaxin expression from synovial fibroblasts (SF) induced by TNF, and led to increased LPA which in turn activated SF activation and effector functions in synergy with TNF.[192] Furthermore, inhibition of autotaxin with BrP-LPA reduced arthritis induce by collagen.[197]

In asthmatic patients Broncho alveolar lavage fluid (BALF) increased autotaxin was observed after allergen challenge.[198] This correlated with findings in a murine model, mice which were transgenic for autotaxin expression had a more severe asthmatic phenotype, which was reduced upon addition of an autotaxin inhibitor.[198] Furthermore, LPA concentrations are increased in BALF.[199] Deletion of autotaxin from bronchiolar epithelial cells and macrophages diminishes the severity of bleomycin induced idiopathic pulmonary fibrosis (IPF).[194] Autotaxin inhibition was also able to reduce disease progression in this model.

Additionally, autotaxin's role in obesity and related diseases is currently emerging. White adipose tissue produces autotaxin which produces significant levels of LPA.[191] White adipose tissue with a null autotaxin allele present with reduced plasma autotaxin levels and improvement in glucose tolerance levels.[191] Furthermore, autotaxin expression is increased in the adipose tissue of obese insulin resistant mice and humans.[135] Therefore the role of autotaxin in obesity is unclear and needs further exploration.

Autotaxin in liver disease is a rapidly emerging field. Autotaxin and LPA levels are increased in patients with chronic hepatitis C.[195] Autotaxin and LPA levels were also found to be increased in chronic liver fibrosis model induced by carbon tetrachloride.[200]

The role of autotaxin in cancer and inflammatory diseases suggests inhibitors may be therapeutically useful.

1.4 Autotaxin inhibitors

1.4.1 Introduction

There are three main classes of autotaxin inhibitors; metal chelators, analogues of LPA and small non-lipid molecules. Initially metal chelators where used due to the knowledge that the active site contained two Zn^{2+} ions which are essential to autotaxin's function. The first molecule found to inhibit the activity of autotaxin was L-histidine which was chosen as a potential inhibitor due to its essential role in many metalloenzymatic reactions. L-histidine was found to inhibit autotaxin at millimolar concentrations and also inhibited ovarian cancer and melanoma cell migration.[201] Other metal chelators such as EDTA and phenanthroline have also been shown to inhibit the activity of autotaxin, via the same mechanism of action.[202]

1.4.2 Lipid analogues

Several lipid analogues of LPA have been developed and shown to inhibit autotaxin. Product inhibition of autotaxin by LPA (1-oleoyl) has been observed (IC_{50} = 2.2 μM),[203] this led to the discovery of a large number of biologically active LPA analogues which inhibit autotaxin. These include two fatty acid phosphate analogues of LPA, oleoyl-thiophosphate **1** and tetradecyl-phosphonate **2**, (Figure 1.7).[204] Both **1** and **2** were found to inhibit autotaxin in an LPA-mimicking fashion, the length of the acyl chain of these compounds are consistent in length to the optimal chain length observed in analysis of the crystal structure in complex with LPA of varying acyl-chain lengths.[89] Furthermore, compound **1** was found to be more potent than compound **2** and LPA at inhibiting autotaxin, with micromolar dose-dependent inhibition observed.[204]

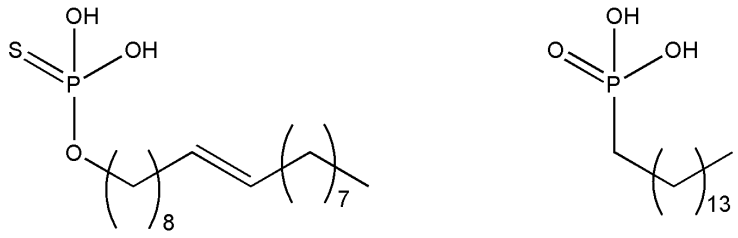

1 **2**

Figure 1.7: Structure of LPA analogues oleoyl-thiophosphate 1 and tetradecyl-phosphonate 2.

Darmstoff **3**, (Figure 1.8), is a naturally occurring molecule of similar structure to LPA, with a dioxolane moiety inserted before the acyl chain. Darmstoff and its analogues were tested for the ability to mimic LPA. They were also tested for inhibition by analysing their ability to agonise/antagonise of a number of LPA receptors were they showed good activity; however when tested for activity against autotaxin they proved to only have mild inhibitory capability.[205]

Cyclic phosphatidic acid (cPA) is another naturally occurring analogue of LPA in which the *sn*-2 hydroxyl group forms a 5-membered ring with the *sn*-3 phosphate. Some cPA's have been shown to have an inhibitory effect on the migration and invasion of cancer cells *in vitro*[206] *and in vivo.*[207] cPA analogues **4-5**, containing the natural 2,3-cyclic phosphate group were poor inhibitors of autotaxin, (Figure 1.8). However, upon stabilisation by replacement of the sn-2 oxygen with an isosteric group, methylene, the compounds showed high inhibition of autotaxin with **6** and **7** (Figure 1.8) achieving IC_{50}s of 140 nM and 370 nM, respectively.[208] Stabilisation at the sn-3 oxygen with a methylene group did not improve the IC_{50}s as significantly with compound **8** and **9** (Figure 1.8) achieving 294 nM and 620 nM potency respectively.[208] Another study investigated the stereoselectivity between the sn-3 *r*- and *s*- stereoisomers and identified no significant difference between the two isomers' inhibition of autotaxin, with binding affinities, K_i's of 0.8 μM and 1.6 μM, respectively.[209] It was also found in this study that the cPA's had a mixed mechanism of inhibition.[209] The effects of chirality of the sn-2 stereoisomers was also separately studied and the stereoisomers showed no significant difference in

inhibition of autotaxin.[210] These studies suggest that the stereoselectivity of cPA's does not influence their activity against autotaxin.

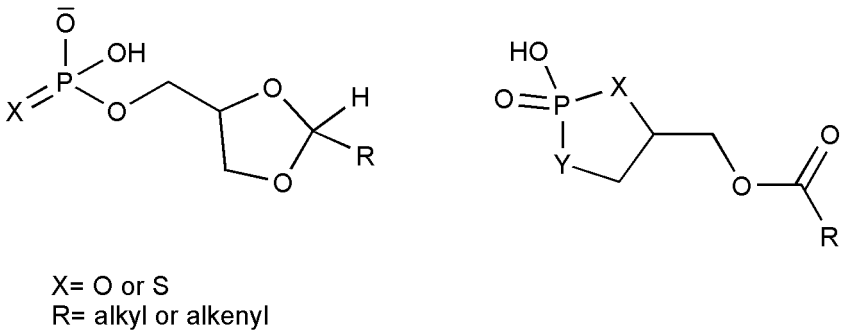

3 **4-9**

Figure 1.8: Darmstoff scaffold and cPA scaffold.

Compound	R	X	Y	IC_{50} (nM)
4	$C_{15}H_{29}$	O	O	-
5	$C_{17}H_{33}$	O	O	-
6	$C_{15}H_{29}$	CH_2	O	140
7	$C_{17}H_{33}$	CH_2	O	370
8	$C_{15}H_{29}$	O	CH_2	294
9	$C_{17}H_{33}$	O	CH_2	620

Table 1.1: Structural variations of cPA tested.

Another set of analogues of LPA that have been investigated are α- and β- substituted phosphonates.[211-213] A study investigating β-keto and β-hydroxyl phosphonates, identified two β-hydroxyl phosphonates **10** and **11**, differing only in their stereochemistry at the β-hydroxy group, (Figure 1.9), as the most potent.[211] The stereochemistry at the α-carbon atom and the 4-methoxy-3,5-dimethyl-pyridyl moiety proved to be important to the activity.[211] Further structural activity relationships (SAR) studies showed that the β-hydroxyl-substituted analogues had a higher potency than α-substituted analogues.[213] Further structural optimisation of the lead compounds did not produce a more potent compound, nevertheless similar potencies were achieved.[213] These tyrosine derived analogues where further analysed by East *et al.* who found that the electron density of the pyridine moiety greatly influenced the potency of these inhibitors, docking modelling found this may

be due to an interaction between the pyridine group and Arg456; therefore it is likely that inhibitors must be electron rich.[214]

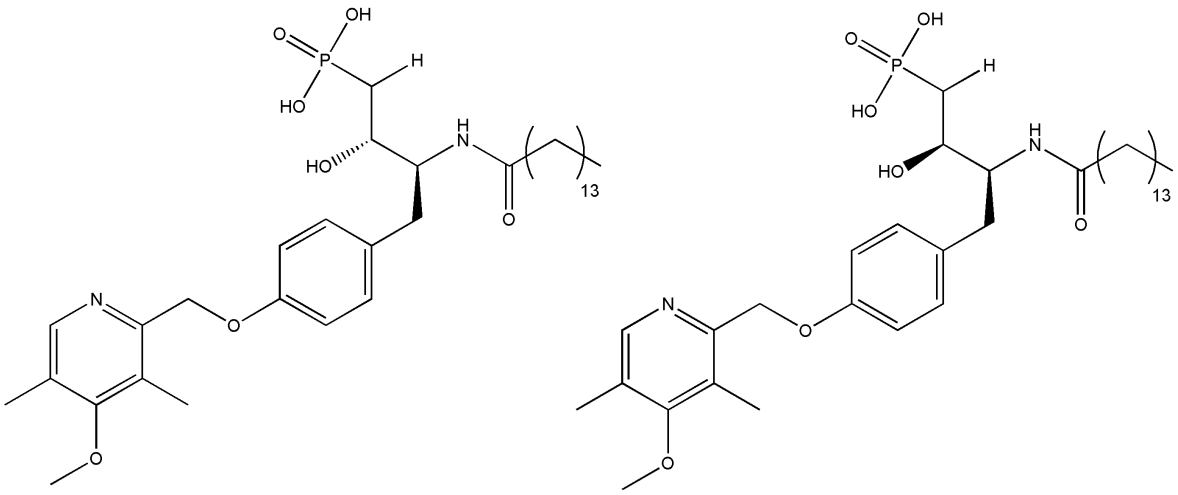

10 **11**

Figure 1.9: Structure of β-hydroxyl phosphonates.

FTY720 (finglimod) **12** (Figure 1.10), an immune-modulator, was recently found to inhibit tumour progression,[215] and, coupled with the structural similarity to LPA, led to the hypothesis that inhibition of autotaxin may be involved in the drug's mechanism of inhibition. The synthesis of FTY720 was established by Kim *et al.* 2006.[216] Phosphorylated FTY720 **13** (Figure 1.10) was observed to inhibit autotaxin by 70% at 1 μM.[217] Further development of SAR based on phosphorylated FTY720 identified FTY720-vinylphosphonate **14**, (Figure 1.10) as effective inhibitors of autotaxin, they also study the effect of the chirality of these compound and found similar inhibition for both (S)-FTY720-vinylphosphonate and (R)-FTY720-vinylphosphonate. However, they differed in mechanism of action with (R)-FTY720-vinylphosphonate inhibiting autotaxin via an uncompetitive mechanism, whereas (S)-FTY720-vinylphosphonate inhibited autotaxin via a competitive mechanism.[218]

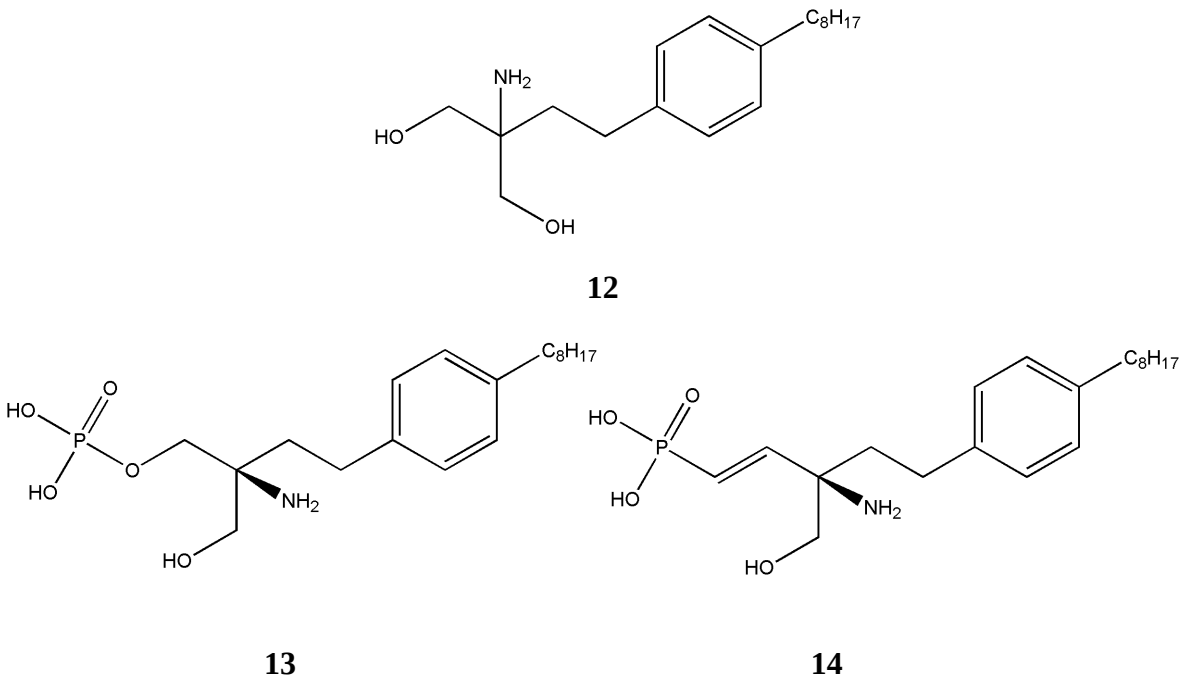

12 **13** **14**

Figure 1.10: Structure of FTY720 and the analogues Phosphorylated-FTY720 and Vinylphosphate-FTY720.

The first described nanomolar inhibitor of autotaxin was S32826, **15** (Figure 1.11) (IC_{50} 9 nM).[83] However, when studied in cellular and *in vivo* models it was found to exhibit little activity and had poor solubility, bioavailability and a lack of stability.[83] Using S32826 as a lead compound several studies have investigated structural variation in order to improve pharmacokinetic properties. Gupte *et al.* developed a library of analogues to try and address the lack of stability of S32826; they suggested this lack of stability may be due to hydrolysis of the amide bond.[219] They identified many compounds with similar activity to S32826, a further two inhibitors, lacking the amide, **16** and **17** (Figure 1.11) were identified as potent inhibitors and maintained stability in *in vivo* models.[219] S32826's poor pharmacokinetics were also addressed by Jiang *et al.* they suggested the poor solubility may be due to the lipophilicity of the compound. And so developed a library of compounds decreasing the lipophilicity, via shortening the lipophilic chain and also substituting at the α position with either a halide or hydroxyl group. This led to the discovery of a new potential inhibitor, an α-hydroxymethylene phosphonate analogue **18** (Figure 1.11) which retained good potency and an increased solubility; they plan to take this compound into clinical studies.[220]

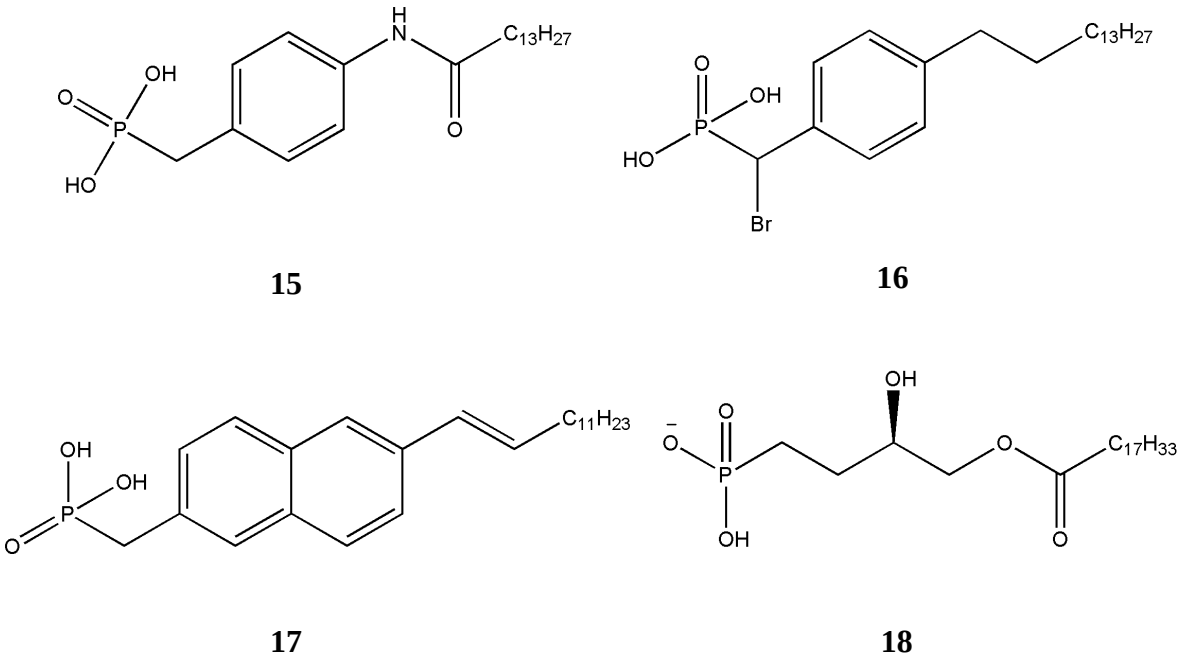

15 **16**

17 **18**

Figure 1.11: Structure of S32826, and analogues based on this scaffold which have achieved nanomolar activity.

Although many of these LPA analogues are potent inhibitors of autotaxin they lack structural diversity and have poor pharmacokinetics. LPA analogues also have the potential to be an agonist or an antagonist of the multiple LPA receptors; this could lead to the development of adverse effects. Thus it may be preferable to develop selective autotaxin inhibitors, although there maybe benefits to simultaneously inhibiting certain LPA receptor subtypes.

1.4.3 Small molecule inhibitors

In order to improve the structural diversity and bioavailability of potential autotaxin inhibitors, Parill *et al.* set out to identify new inhibitor scaffolds utilising virtual throughput screening.[221] Prior to the determination of the autotaxin crystal structure the structure of a bacterial NPP enzyme (which shares a 30% similarity with autotaxin's catalytic domain) was used for the generation of a homology model for use in the structural and computational design of new autotaxin inhibitors. Preliminary docking studies led to the identification of a range of lead compounds based on several structural scaffolds including diphenyl diazerenes, thioureas, isoindoles, and xanthenes, from these a number of bioavailable potent inhibitors of autotaxin were identified. The most effective small molecule

inhibitor developed from this study was H2L 7905958 **19** (IC_{50} 1.6 µM), (Figure 1.12) which has a pipemidic acid core.[222] Studies were carried out in order to improve the potency and further understand the SAR of this compound. Using H2L 7905958 as the lead compound, 70 potential pipemidic analogues where identified via computational screening. 30 of these were chosen to be synthesised for further investigation. Four of these analogues **20-23** (Figure 1.12), were found to have potency similar to H2L 7905958 with the most potent being the R_2 trifluoromethyl- substituted compound, **20** (IC_{50} 900 nM), (Figure 1.12).[222]

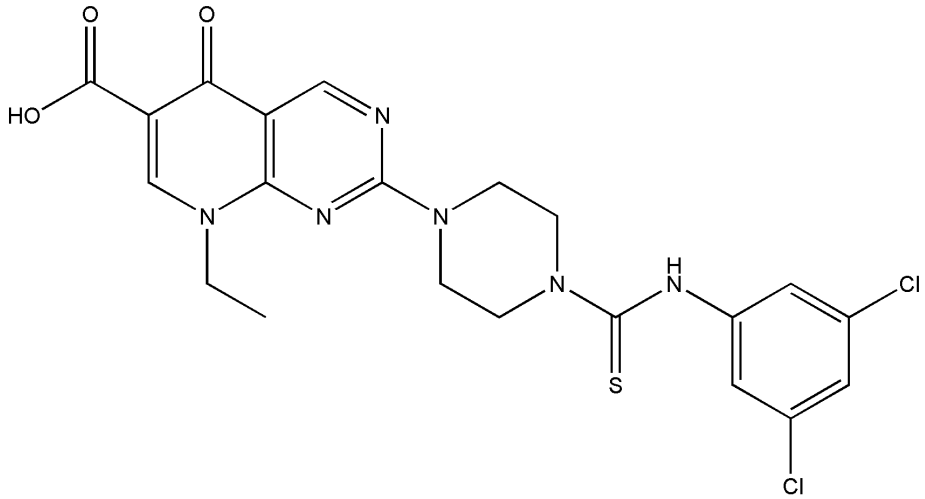

19

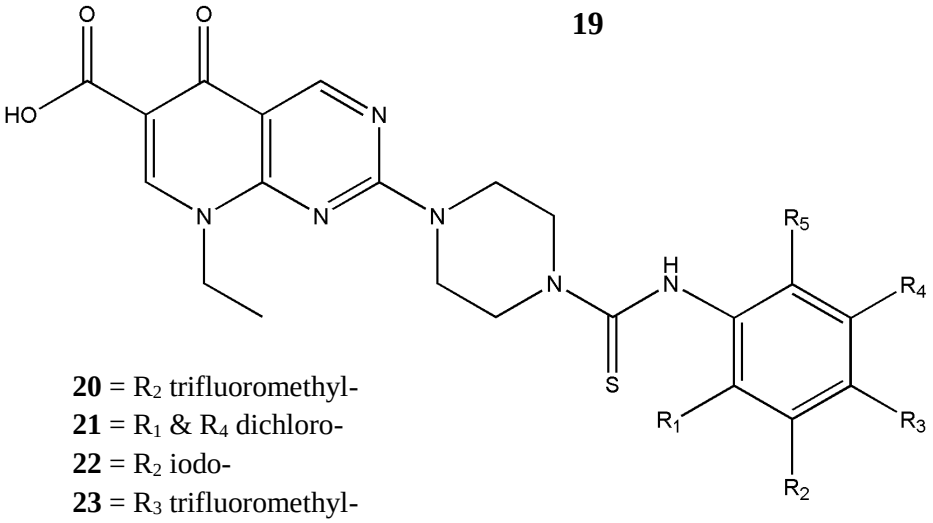

20 = R_2 trifluoromethyl-
21 = R_1 & R_4 dichloro-
22 = R_2 iodo-
23 = R_3 trifluoromethyl-

Figure 1.12: Structure of H2L 7905958 and analogues based on the pipemidic acid core.

Another study by Albers *et al.* discovered a range of thiazolidinediones, through the biochemical screening of a large chemical library.[223] The most potent molecule discovered in the initial screen

was compound **24** (Figure 1.13) which had an IC_{50} of 56 nM. This compound was further optimised but no increased activity from variation of the benzyl and benzylidine groups was observed. However, moving the carboxylic acid group to the *meta*-position led to a 2.5-fold increase in potency. It was hypothesised that the carboxylic acid is involved in strong binding to zinc ions, in order to increase the strength of this interaction the carboxylic acid group was replaced with a boronic acid group, resulting in a 100 fold increase in potency.[223,224] The boronic acid thiazolidinediones are also expected to improve selectivity over hydrolytic enzymes as boronic acids are often present in phosphate ester hydrolysing enzymes. HA130 **25** (Figure 1.13), in which the carboxylic acid was replaced by a boronic acid group and the methoxy- substituent was removed lead to an increase in activity. This compound was found to reduced plasma levels of LPA when tested *in vivo*.[223] So far from all of the SAR and optimisation of thiazolidinediones based inhibitors HA155 **26**, (Figure 1.13) has proven to be the most potent (IC_{50} 6 nM), this compound has also been shown in crystal structure bound with autotaxin.[225] This HA155 autotaxin complex confirmed the theoretical binding mode.[225]

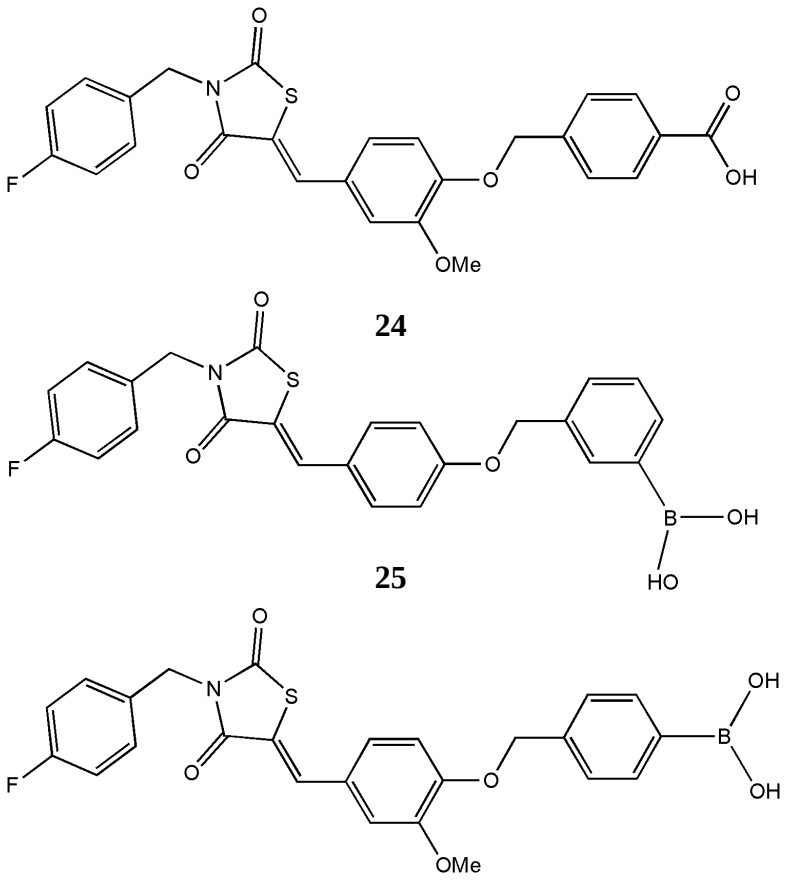

Figure 1.13: Structure of the thiazolidinedione core autotaxin inhibitors.

The recent solution of the crystal structure of autotaxin has also provided a useful tool in the development of autotaxin inhibitors. Kawaguchi *et al.* have taken advantage of this recently describing a set of inhibitors where optimisation was based on the crystal structure of autotaxin. Their most potent inhibitors 3BoA **27** and 4BoA **28** (Figure 1.14), achieved respective IC_{50}s of 13 nM and 22 nM in a TG-mTMP assay. TG-mTMP is a specific autotaxin fluorescence probe developed by the author. 3BoA also exhibited potent activity when studied *in vivo*.[91]

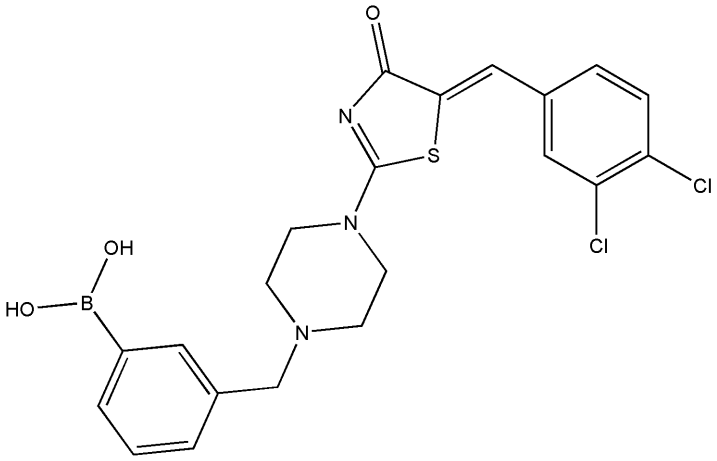

27

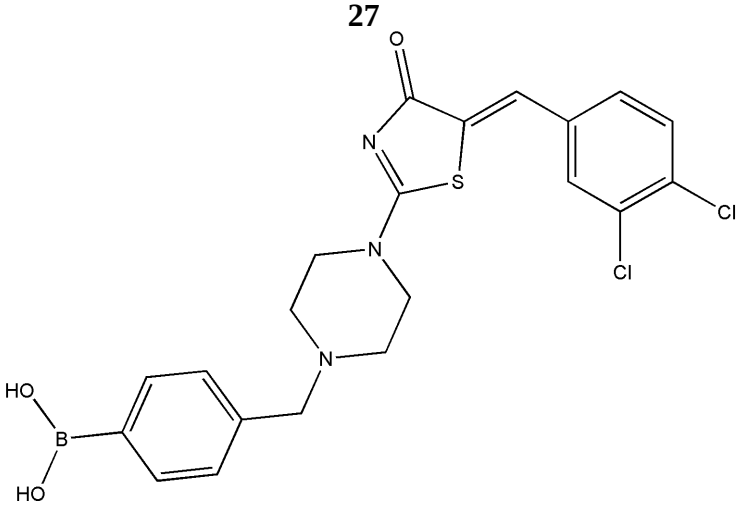

28

Figure 1.14: Structure of 3BoA and 4BoA.

The crystal structure of autotaxin bound with thiazolidinedione **26** shows one of the oxygens of the boronic acid coordinates with the zinc ions in the catalytic domain and the boron forms a covalent bond with the Thr209. Similarly, the boronic acid head group of both 3BoA **27** and 4BoA **28** have been shown to bind to autotaxin in the same manner forming the same contacts.[90-91]

Two of the most recent autotaxin inhibitors described, PF-8380 and ONO-8430506, have shown promise for prolonged inhibition of autotaxin *in vivo*.[226-227]

PF-8380 **29** (Figure 1.15), the most potent inhibitor to date, was based on an autotaxin inhibitor hit identified in the Pfizer compound library and was synthesised in an efficient 3 step process. This compound doesn't contain the carboxylic/boronic acid moiety important in the binding of the

previous set of inhibitors; however, this compound does contain a polar coordinating head group capable of binding to in the catalytic site. PF-8380 exhibited an IC_{50} of 2.8 nM, against isolated autotaxin and 101 nM in whole blood. Furthermore, the ability of this compound to inhibit LPA formation *in vivo* was measured after 4 h; 95% inhibition was observed with a dose of 100 mg/kg. They also demonstrated inhibition of inflammation in a rat tail model.[226]

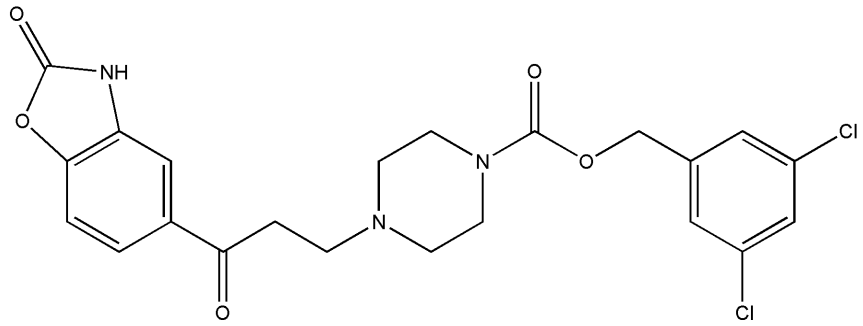

29

Figure 1.15: Structure of PF-8380.

ONO-8430506 is a tetrahydrocarboline derivative, which was identified by *in vitro* screening and subsequent chemical development by ONO pharmaceutical.[227] The structure of ONO-8430506 has not been disclosed. This compound exhibited an IC_{50} of approximately 10 nM against both recombinant autotaxin and plasma. They also investigated the effects of the inhibitor *in vivo* observing complete inhibition of LPA formation for 24 h at a dose of 30mg/kg.[227] Furthermore, ONO-8430506 was found to inhibit autotaxin leading to a delay in breast tumour growth and lung metastasis in mice.[228]

There have been many other autotaxin inhibitors reported, based on a variety of scaffolds. Merck has reported autotaxin inhibitors with nanomolar activity based on benzoxoazolone, benzotriazole and benzopthyridinamine cores.[229-231] Pfizer has developed low nanomolar autotaxin inhibitors with pyridazine and tetrahydropyridopyrimidine scaffolds.[232] Amira Pharmaceuticals have potent autotaxin inhibitors which are indole-thioether carboxylic acid derivatives.[233] And Eli lilly have pyrido-fused pyrimidine and pyrrolo-fused pyrimidine based autotaxin inhibitors.[234] There has also

more recently been bicyclic aryl compounds described as nanomolar autotaxin inhibitors by Biogen.[235]

1.5 Polymer therapeutics

1.5.1 Introduction

Autotaxin inhibitors are small molecule inhibitors which are likely to be rapidly expelled from the peritoneal cavity. Small molecular weight drugs (<20kDa) in the peritoneal cavity are quickly absorbed through the peritoneal capillaries into systemic circulation.[236-237] This leads to frequent or continuous dosing and if drugs are delivered by the intraperitoneal route, this creates problems such as increased risk of infection. In contrast, polymers have a higher molecular size, and are therefore absorbed slowly from the peritoneal cavity mainly via lymphatic drainage. Using polymers as drug carriers would increase the half-life of the drugs in the peritoneal cavity and therefore allow less frequent dosing. Polymers have the potential to increase the half-life of autotaxin inhibitors in the peritoneal cavity.

Polymers have been used in medicine for many years and have a number of biomedical applications. Polymer therapeutics include polymer drugs in which the polymer exhibits bioactivity, polymer-protein conjugates in which a polymer is attached to the protein in order to improve the half-life of the protein, polymeric micelles which encapsulate the drug, and polymer-drug conjugates in which drugs are attached to polymers in order to improve their pharmacokinetics and specificity, (Figure 1.16). Polymer therapeutics differ from conventional drug delivery systems and formulations as they can be chemical tailored to fit specific requirements. This can be through addition of targeting moieties, cleavable linkers or modification of molecular weight.

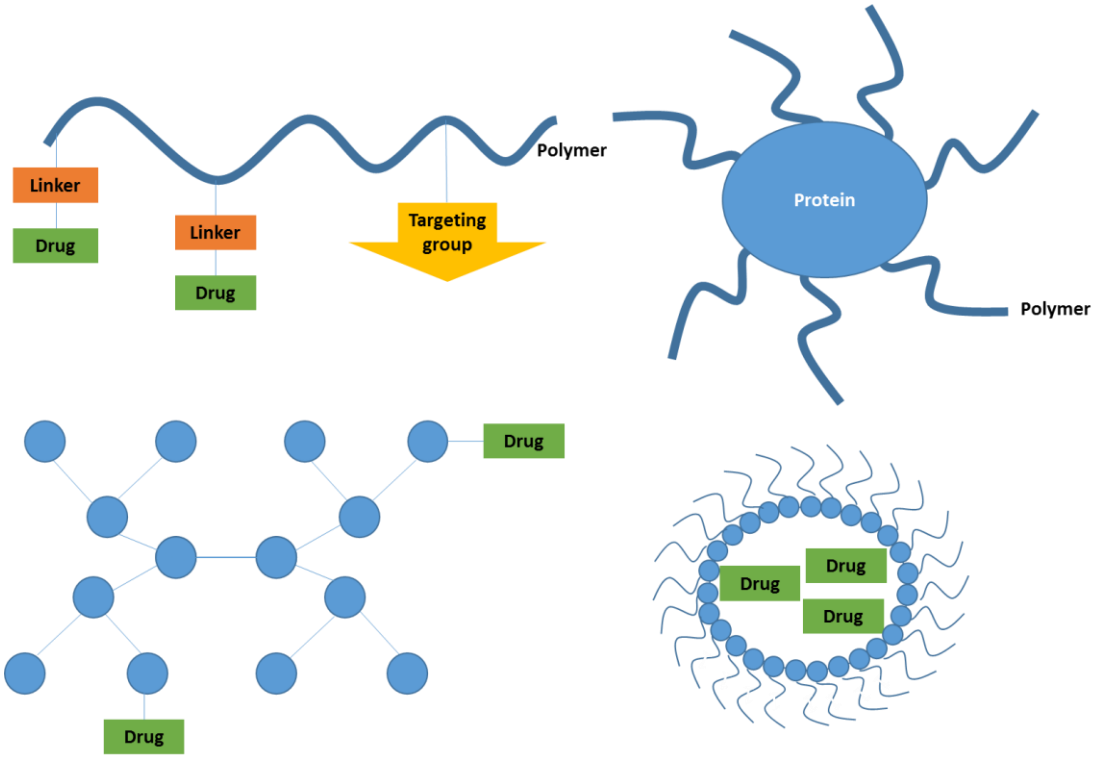

Figure 1.16: Representation of Polymeric therapeutic agents; Polymer-drug conjugate, Polymer-protein conjugate, Dendrimer-drug conjugate and polymeric drug micelle.

There are many different types of polymers which can be chosen to best suit specific requirement of the drug product. The most common polymer currently used is *N-(*2-hydroxypropyl) methacrylamide (HMPA) a synthetic polymer.[238] Other polymers currently used include synthetic polymers (polyethyleneglycol (PEG),[239] poly(vinyl-pyrrolidone) (PVP) and poly(ethylimine) (PEI), or natural polymers (dextrin, dextran and chitosan) or synthetic polymers based on natural products (poly(glutamic acid) (PGA) and poly(malic acid). There are also new classes of polymers being investigated such as dendrimers. Dendrimers are versatile spherical polymers with various functional terminal groups providing a pathway to conjugate potential drugs or targeting molecules furthermore these terminal groups can be modified to control the properties of the dendrimer.[240]

1.5.2 Polymeric anticancer drugs in the clinic

There are many polymeric therapeutics currently in the clinic, the first to be approved was a polymer-protein conjugate in the early 1990's since then, many more polymeric therapies have been

investigated pre-clinically and some have gone on to be approved for clinical use. So far polymer anticancer therapeutics have been beneficial, improving localised bioavailability, increasing solubility, decreasing toxicity and delivering the therapeutic agent to the cancerous tissue. A number of anticancer therapeutics have progressed to routine clinical use (Table 1.2). For instance polymer-protein conjugates have been found to improve the stability of the protein and increase the half-life delivery; such as Pegaspargase (Oncaspar) and Pegfilgrastim (neulasta) and the albumin bound paclitaxel nanoparticle (abraxane) which has been approved for the treatment of breast cancer, more recently this conjugate has been approved for the treatment of non-small cell lung cancer (NSCLC) and pancreatic cancer as a less toxic alternative, to paclitaxel alone.[241] Furthermore, polymeric micelles can also prolong circulation time by encapsulating the drug molecule and preventing its uptake by the macrophage system; Genexol-PM is a polymeric micelle currently used in the clinic. It is a methoxy-PEG-poly (lactide)-paclitaxel micelle used for the treatment of metastatic breast cancer.

Polymer type	**Compound (name)**	**Drug**	**Indication**
Polymer-protein conjugate	SMANCS (Zinostatin, Stimalmer)	neocarzinostatin	Hepatocellular carcinoma (intra-arterial)
	Albumin-paclitaxel (abraxane)	Paclitaxel	Metastatic breast cancer (intravenous), hormone refractory prostate cancer (intravenous)
	PEG-$_{L}$-asparaginase (Oncaspar)	asparaginase	Acute lymphoblastic Leukaemia (intravenous, intramuscular)
	PEG-GCSF (Neulasta)	granulocyte colony-stimulating factor (GCSF)	Prevention of neutropenia (subcutaneous)
Polymeric micelle	Methoxy-peg-poly ($_{D,L}$-lactide)-paclitaxel micelle (Genexol-PM)	Paclitaxel	Metastatic breast cancer (Intravenous)

Table 1.2: Polymeric therapies on the market for the treatment of cancer.

1.5.3 Polymer-drug conjugates

Polymer-drug conjugates are drug molecules chemically conjugated to polymeric molecules. Ringsdorf first suggested the rationale for using pharmacologically active polymeric molecules in the 1970's.[242] Conjugation to a polymer can improve the pharmacokinetic profile of the drug. Polymers increase the half-life of the drug by increased molecular size leading to reduced renal clearing and providing a shielding effect from chemical or enzymatic degradation of the drug. Furthermore, macromolecules such as polymer-drug conjugates can directly target the tumour via the enhanced permeability and retention effect (EPR effect); this occurs due to the increased capillary permeability observed in tumours.[243] A polymer-drug conjugate usually consists of a linker between the drug and the polymer which can be bio-responsive, releasing the drug when at the target site. The polymer needs to be able to carry sufficient drug molecules to be efficacious and potentially also contain a targeting moiety for improved specificity.

Currently, there are a number of polymer-drug conjugates in clinical development (Table 1.3) which are traditional chemotherapeutic agents such as platinum based compounds, paclitaxel, doxorubicin and captothecin conjugated to water soluble polymers in order to improve their pharmacokinetics. The most promising so far appears to be a paclitaxel-polyglutamate conjugate which has reached phase III clinical trials for the treatment of various cancers as single agent or in combination.

Compound (name)	Clinical status	Indication
Polyglumex-paclitaxel (CT-2103, Xyotax)	Phase III	Various cancers; ovarian cancer as single agent or in combination
Polyglutamate-camptothecin (CT-2106)	Phase I/II	Colorectal and ovarian cancers
HPMA copolymer doxorubicin (FCE28068)	Phase II	Various cancers
HPMA copolymer-doxorubicin-galactosamine (FCE28069)	Phase I/II	Hepatocellular carcinoma
HPMA copolymer-paclitaxel (PNU166945)	Phase I	Various cancers
HPMA copolymer-camptothecin (MAG-CPT)	Phase I	Various cancers
HPMA copolymer-carboplatin platinate (AP5280)	Phase I/II	Various cancers
HPMA copolymer-DACH-platinate (AP5346, ProLindac)	Phase II	Ovarian cancers
Dextran-doxorubicin (AD-70, DOX-OXD)	Phase I	Various cancers
Modified dextran camptothecin (DE-310)	Phase I	Various cancers
PEG-camptothecin (Prothecan)	Phase II	Various cancers
PEG-irinitecan (NKTR-102)	Phase II/III	Ovarian, breast and colorectal cancers
Poly(iso-hexyl-cyanoacrylate)-doxorubicin (Transdrug)	Phase I/II	Hepatocellular carcinoma
Polycyclodextrin-camptothecin (IT-101)	Phase I	Metastatic solid tumours

Table 1.3: Polymer-drug conjugates undergoing clinical evaluation for cancer therapeutics.

Polymer-drug conjugates have shown therapeutic benefit in both preclinical and clinical investigations. These benefits include improved pharmacokinetics, such as better distribution and an increased half-life, fewer side effects and enhanced therapeutic efficacy. This is further validated by the polymer based systems which have already made it to the clinic for the treatment of cancer. Polymer-drug conjugates provide a useful platform for the delivery of chemotherapeutic agents.

1.6 Hypothesis

Ovarian cancer is a major disease with only a 40% survival rate; of those who initially respond to chemotherapy the majority relapse with a developed resistance to traditional chemotherapy. The development of resistance is a major downfall for the treatment of ovarian cancer and overcoming this problem is of huge importance for improving the survival of patients with ovarian cancer. Targeting the Autotaxin-LPA signalling pathway is a potential approach in treating drug resistant ovarian cancer because this signalling pathway has been shown to be involved in the pathogenesis of ovarian cancer and also to be instrumental in the development of resistance. There have been many autotaxin inhibitors described to date, however most of these inhibitors have shown poor efficacy *in vivo*, with poor pharmacokinetic profiles. Polymer-drug conjugates have shown therapeutic benefit in both preclinical and clinical investigations. These benefits include improved pharmacokinetics, fewer side effects and enhanced therapeutic efficacy. This is further validated by the polymer based systems which have already made it to the clinic for the treatment of cancer. Delivery of drugs directly to the peritoneal cavity is currently being investigated for the treatment of ovarian cancer, with cisplatin, paclitaxel, carboplatin, and docetaxel suggesting a pharmacokinetic advantage.[244] Because high levels of LPA are found in ascites fluid associated with ovarian cancer and as autotaxin has also been shown to be elevated in ascites fluid, and it is understood to be the main contributor to the production of LPA. Inhibition of autotaxin in the intraperitoneal cavity has the potential to reduce the pathogenic level of LPA present in ascites fluid.

It is proposed that autotaxin inhibitors which are retained in the peritoneal cavity will improve the efficacy of chemotherapy particularly in drug resistant disease.

The overall aim of this thesis was the synthesis and biological evaluation of polymer conjugates of autotaxin inhibitors for use in ovarian cancer treatment with intraperitoneal delivery. Medicinal chemistry and *in vitro* pharmacological studies were employed to achieve the following key objectives:

- Synthesis of polymer-autotaxin inhibitor conjugates; two autotaxin inhibitors were explored: an LPA analogue S32826 coupled to a dendrimer and a small molecule inhibitor with a thiazolidinedione core coupled to icodextrin
- Characterisation of polymer autotaxin inhibitor conjugates; evaluation of the substitution, permeability and solubility of the conjugates and *in vivo* peritoneal retention
- Biological evaluation of polymer autotaxin inhibitor conjugates; the activity of the conjugates against autotaxin in enzymatic activity assays and in cellular assay modelling migration and potentiation of apoptosis

It is hoped that this thesis will benefit the development of new treatments for ovarian cancer.

Chapter 2

Materials and methods

2.1 Synthesis

2.1.1 Materials

Reagents and solvents were obtained from commercial suppliers and were not further purified before use unless stated. G3 PAMAM dendrimer refers to a 3rd generation polyamidoamine (PAMAM) dendrimer (20 wt. % solution methanol) containing 32 surface groups, (Sigma Aldrich, cat no.412422). Icodextrin was obtained as EXTRANEAL™ peritoneal dialysis solution, (7.5% w/v icodextrin in an electrolyte solution, (Baxter)).

2.1.2 General chemistry

Solvents were removed under reduced pressure with a Büchi rotary evaporator. Any remaining solvent was removed under high vacuum. The progress of the reactions was monitored by TLC analysis, using aluminium pre-coated silica gel plates (Merck) visualised by UV irradiation at a wavelength of 254 nm. Flash column chromatography was carried out on silica gel 60 (43-60 mesh); columns were slurry packed in the appropriate solvent/solvent mixture and samples were added as a concentrated solution or pre-absorbed onto silica. Dialysis was carried out using either 8 kDa MWCO (Biodesign) or 20 kDa MWCO (Biotech) dialysis membrane tubing.

2.1.3 Analytical techniques

2.1.3.1 NMR spectroscopy

^{1}H and ^{13}C nuclear magnetic resonance (NMR) were measured on a Bruker DPX300 Fourier transform spectrometer, or a Jeol 400 MHz Fourier transform spectrometer using *d*-DMSO, $CDCl_3$, D_2O or MeOD solvents. Chemical shifts are quoted in ppm downfield from TMS; coupling constants (*J*) are quoted in Hertz (Hz). TMS was defined as 0 in ^{1}H NMR and the residual chloroform triplet as 77.10ppm in ^{13}C NMR. The following abbreviations were used in analysis; broad (br), singlet (s), doublet (d), triplet (t), quartet (q) and multiplet (m).

2.1.3.2 IR spectroscopy

Infra-red (IR) spectra were recorded in their natural state on a Thermo Scientific GladiATR spectrometer and the vibrational frequencies were recorded in cm^{-1}.

2.1.3.3 Mass Spectrometry

Mass Spectra were obtained from the EPSRC National Mass Spectrometry Centre at the University of Wales, Swansea, using electron spray ionisation (ES) or atmospheric pressure chemical ionisation (APCI).

2.1.3.4 Elemental analysis

Elemental analysis was performed by MEDAC Ltd, Chobam. Where appropriate the stoichiometry of coupling was determined by measuring the ratio of elemental phosphorus to the elemental ratio of other elements in the compound.

2.1.3.5 X-ray crystallography

Crystallisation was performed at room temperature in ethyl acetate. Data collection and structural analysis was carried out by Dr. M. Elsegood at the University of Loughborough. See appendix 1 for details of X-ray diffraction data and collection.

2.1.3.6 LC/MS

Liquid chromatography mass spectrometry (LC/MS) was performed whilst at Charnwood Molecular Ltd. LC/MS measurements were performed on an Applied Biosystems API 150EX system, in either acetonitrile or methanol. The purity of all tested compounds as determined by LC/MS analyses was greater than 95%.

2.1.3.7 Thermogravimetric analysis

Thermogravimetric analysis (TGA) was performed using a SDT Q 600 TA instrument, with a constant nitrogen flow of 100 mL/min, heating rate of 20 °C/min, heating was held stable at 100 °C for 10 min to remove any residual solvent. Results were obtained for greater than 10 mg per sample between 20 and 600 °C.

2.1.4 Synthesis of dendrimer-autotaxin inhibitor conjugates

*2.1.4.1 Synthesis of [4-(12-Acetylamino-dodecanoylamino)-benzyl]-phosphonic acid diethyl ester **(34)***

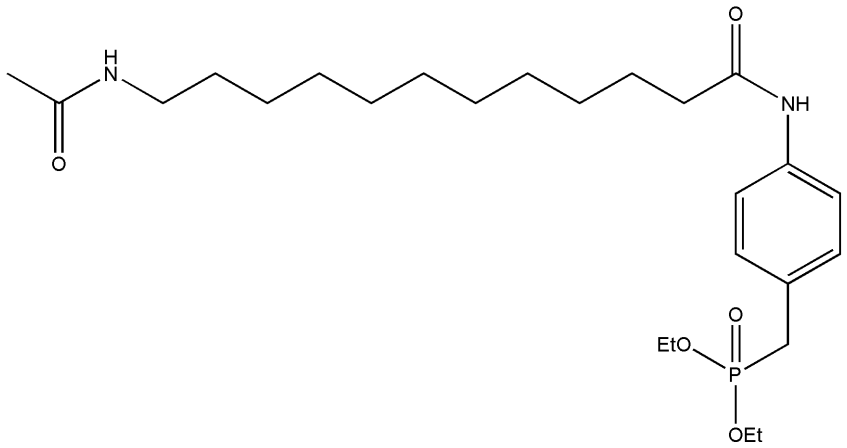

To a solution of [4-(12-Amino-dodecanoylamino)-benzyl]-phosphonic acid diethyl ester (2.00 g, 4.69 mmol, 1.0 equiv.) in pyridine (10 mL) acetic anhydride (0.5 mL, 5.80 mmol, 1.2 equiv.) was added and the reaction mixture was stirred at room temperature for 16 h. The reaction mixture was added to an ice/water mixture (30 mL) and the resultant precipitate was collected *via* filtration to give **[**4-(12-Acetylamino-dodecananoylamino)-benzyl]-phosphonic acid diethyl ester (1.89 g, 4.03 mmol, 85%) as a white crystalline powder.

δ_H (300 MHz *d*-DMSO): 7.99 (s, 1H, NH), 7.49 (d, *J* 6.0, 2H), 7.21 (d, *J* 6.0, 2H), 5.70 (s, 1H, NH), 5.31 (dd, *J* 9.0, 3.0, 2H), 4.04-3.99 (m, 4H), 3.22 (dq, *J* 18.0, 6.0, 4H), 3.14 (s, 1H), 3.08 (s, 1H), 2.36 (t, *J* 6.0, 3H), 2.00 (s, 2H), 1.72 (t, *J* 9.0, 2H) 1.48-1.46 (m, 2H) and 1.28-1.24 (m, 16H).

ν_{max}/cm $^{-1}$ (solid): 3451, 3317, 2982, 2917, 2849, 1671, 1652, 1609, 1542, 1514, 1478, 1411, 1369, 1219.

m/z (ES+) (Found: $[M+H]^+$ 483.2973, $C_{25}H_{44}O_5N_2P_1$ required, 483.2910).

*2.1.4.2 Synthesis of [4-(12-Acetylamino-dodecanoylamino)-benzyl]-phosphonic acid **(35)***

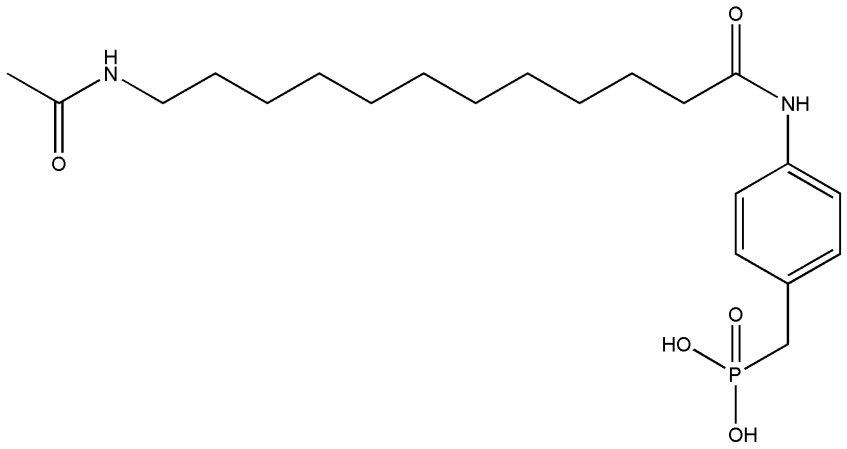

To a solution of [4-(12-Acetylamino-dodecanoylamino)-benzyl]-phosphonic acid diethyl ester (0.700 g, 1.4 mmol, 1.0 equiv.) in anhydrous dichloromethane (10 mL), under N_2, trimethylsilyl iodide (400 µL, 2.8 mmol, 2.0 equiv.) was added *via* syringe. The resulting solution was stirred at room temperature for 8 h, evaporated to dryness and recrystallised from methanol to give [4-(12-Acetylamino-dodecanoylamino)-benzyl]-phosphonic acid (0.581 g, 97%, 1.36 mmol) as a white crystalline powder.

δ_H (300 MHz *d*-DMSO); 9.79 (s, 1H, NH), 7.49 (d, *J* 6.0, 2H), 7.14 (d, *J* 6.0, 2H), 5.31 (dd, *J* 9.0, 3.0, 2H), 4.14 (s, 1H, NH), 3.56 (s, 2H) 3.15 (s, 1H), 3.00 (s, 1H), 2.85 (t, *J* 6.0, 2H), 2.27 (s, 2H), 1.76 (t, *J* 9.0, 2H) and 1.22-1.16 (m, 16H).

ν_{max}/cm^{-1} (solid); 3451, 3302, 2917, 2849, 2160, 1652, 1609, 1541, 1514, 1471, 1412, 1369, 1219.

m/z (ES+) (Found: $[M+H]^+$ 427.2357, $C_{21}H_{36}O_5N_2P_1$ required, 427.2356).

*2.1.4.3 Synthesis of [4-(12-Acryloylamino-dodecanoylamino)-benzyl]-phosphonic acid diethyl ester **(31)***

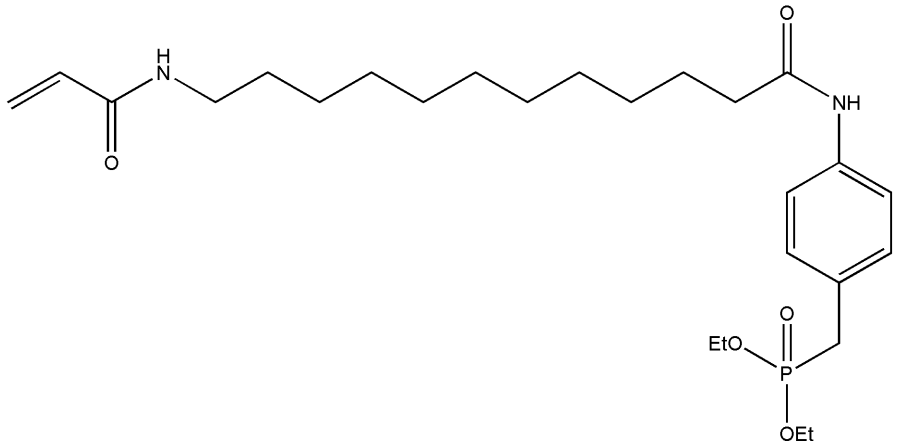

To a solution of [4-(12-amino-dodecanoylamino)-benzyl]-phosphonic acid diethyl ester (1.50 g, 3.40 mmol, 1.0 equiv.) and triethylamine (0.9 mL, 6.80 mmol, 2.0 equiv.) in anhydrous dichloromethane (25 mL) cooled to −20 °C, a solution of acryloyl chloride (0.340 g, 3.75 mmol, 1.1 equiv.) in anhydrous dichloromethane (15 mL) was added dropwise. The reaction mixture was warmed to 0 °C and stirred for a further 4 h under N_2. The reaction mixture was then washed with saturated aqueous $NaHCO_3$ (3x 30 mL), water (3x 50 mL) and saturated brine (3x 30 mL), dried ($MgSO_4$) and evaporated. The resultant product was stirred in ethyl acetate: petrol (3:7) for 16 h and collected *via* filtration to give [4-(12-acryloylamino-dodecanoylamino)-benzyl]-phosphonic acid diethyl ester (0.715 g, 1.44 mmol, 43%) as a white crystalline powder.

δ_H (300 MHz *d*-DMSO): 8.31 (s, 1H, NH), 7.42 (d, *J* 6.0, 2H), 7.12 (d, *J* 6.0, 2H), 6.23 (m, 1H), 6.08 (m, 1H), 5.98 (br. s, 1H, NH), 5.53 (dd, *J* 9.0, 3, 2H), 3.99-3.88 (m, 4H), 3.23 (q, *J* 18.0, 6.0, 2H), 3.07 (s, 1H), 3.00 (s, 1H), 2.29 (t, *J* 6.0, 3H), 1.63 (t, *J* 9.0, 2H) 1.46-1.42 (m, 2H) and 1.20-1.16 (m, 16H).

ν_{max}/cm $^{-1}$ (solid): 3293, 2985, 2918, 2850, 1674, 1656, 1627, 1601, 1538, 1470, 1456, 1330, 1305, 1239.

m/z (ES+) (Found: $[M+H]^+$, 495.2978, $C_{26}H_{44}O_5N_2P_1$ required, 495.2982).

*2.1.4.4 Synthesis of [4-(12-Acryloylamino-dodecanoylamino)-benzyl]-phosphonic acid diethyl ester dendrimer conjugate **(32)***

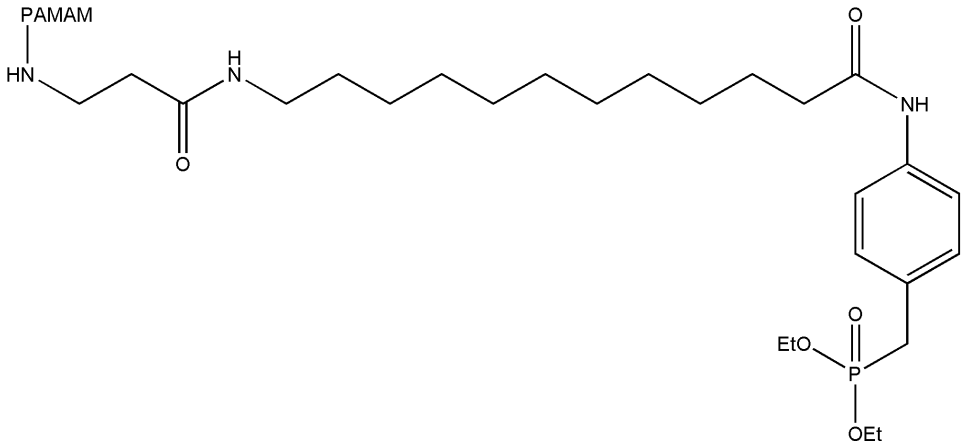

A solution of G3 PAMAM dendrimer (0.250 g, 7.24×10^{-3} mmol, 1.0 equiv.) and [4-(12-Acryloylamino-dodecanoylamino)-benzyl] phosphonic acid diethyl ester (0.458 g, 0.92 mmol, 128 equiv.) in ethanol (10 mL) was heated with stirring at 100 °C for 48 h in an ACE™ pressure tube. The solution was then transferred to dialysis tubing (MWCO 8 kDa (Biodesign)) and dialyzed in methanol (500 mL), being changed 3 times per day for 3 days. The methanol was then evaporated to yield [4-(12-Acryloylamino-dodecanoylamino)-benzyl]-phosphonic acid diethyl ester dendrimer conjugate (0.200 g, 0.009 mmol, 30% based on complete substitution) as a yellow solid.

ν_{max}/cm^{-1} (solid): 3385, 2970, 1621, 1541, 1448, 1361, 1303, 1239.

2.1.4.5 Synthesis of conjugate 1 ***(33)***

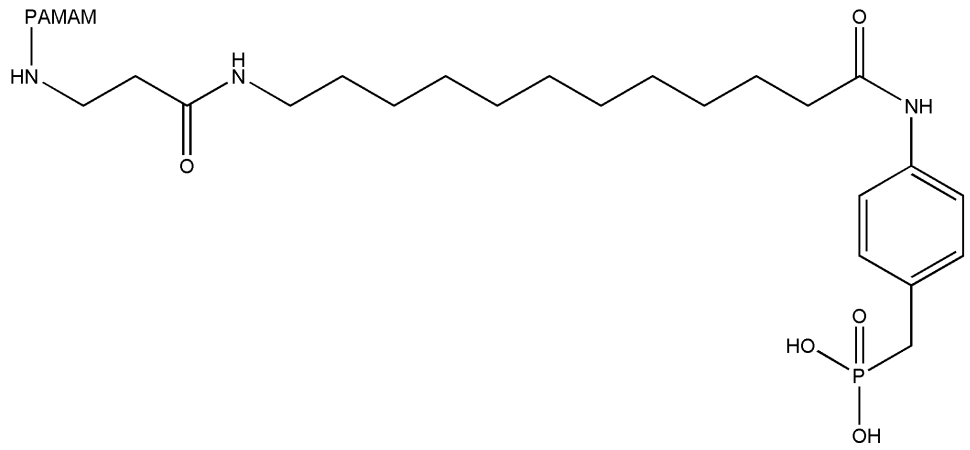

To a solution of [4-(12-Acryloylamino-dodecanoylamino)-benzyl]-phosphonic acid diethyl ester dendrimer conjugate (0.200 g, approx. 0.009 mmol, 1.0 equiv.) in anhydrous dichloromethane (5 mL), under N_2, trimethylsilyl iodide (0.28 mL, 2.00 mmol, 222 equiv.) was added *via* syringe. The resulting solution was stirred at room temperature for 8 h. The reaction mixture was then directly transferred into dialysis tubing (MWCO 8 kDa (Biodesign)) and dialyzed in methanol (500 mL), being changed 3 times per day for 3 days. The methanol was then evaporated to give conjugate 1 (0.016 g, 7.73×10^{-4} mmol, 9% based on complete substitution) as an orange oil.

ν_{max}/cm^{-1} (solid): 3242, 2952, 2927, 2860, 1709, 1671, 1585, 1508, 1438, 1414, 1388, 1341, 1276.

Elemental analysis: $C_{718}H_{1310}N_{154}O_{148}P_{16}$: Theory; C 58.13%, H 8.90%, N 14.54%, P 3.34%; Found; C 45.65%, H 6.14%, N 8.45%, P 3.38%.

^{1}H NMR analysis is shown in section 3.3.3.

2.1.5 Synthesis of icodextrin-autotaxin inhibitor conjugates

*2.1.5.1 Synthesis of 3-(4-Fluorobenzyl)-thiazolane-2,4-dione **(38)***

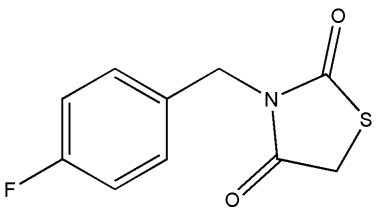

A solution of thiazolidine-2,4-dione (2.94 g, 25 mmol, 1.5 equiv.) in anhydrous DMF (50 mL), under N_2, was cooled to 0 °C. Sodium hydride (60% dispersed in oil, 0.92 g, 23 mmol, 1.35 equiv.) and a solution of 4-fluorobenzyl chloride (2.1 mL, 17 mmol) in anhydrous DMF (10 mL) were added. The reaction mixture was allowed to warm to room temperature over 4 h. The mixture was transferred into an ice/water mixture (100 mL) and hexane (50 mL) was added. The mixture was allowed to crystallise overnight at 4 °C, and collected *via* filtration to yield 3-(4-Fluoro-benzyl)-thiazolane-2,4-dione (4.2 g, 19 mmol, 75%) as white crystalline needles.

δ_H (300 MHz $CDCl_3$): 7.35 (m, 2H) 6.91 (m 2H), 4.65 (s, 2H), 3.87 (s, 2H).

δ_C (75 MHz $CDCl_3$); 171.7, 171.2, 162.6 (d, $^1J_{CF}$ 247.5), 131.7 (d, $^2J_{CF}$ 8.3), 130.9 (d, $^3J_{CF}$ 3.3), 115.7 (d, $^4J_{CF}$ 21.4)5, 44.6, 33.8.

ν_{max}/cm $^{-1}$ (solid): 1719, 1677 (C=O), 1589, 1520, 1447, 1385, 1342.

m/z (APCI) (Found: $[M+H]^+$, 226.0333. $C_{10}H_9O_2N_1F_1S_1$ required, 226.0333).

^{1}H NMR and IR data agrees with that published in the literature.[224]

*2.1.5.2 Synthesis of 4-(4-Formyl-2-methoxy-phenoxymethyl)-benzoic acid **(41)***

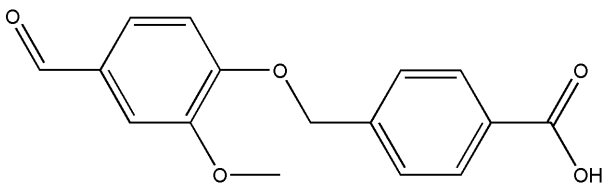

Vanillin (0.70 g, 4.60 mmol, 1.05 equiv.) and potassium hydroxide (0.32 g, 5.70 mmol, 1.3 equiv.) were suspended in anhydrous DMSO (10 mL). Methyl 4-(bromomethyl)-benzoate (1.00 g, 4.37 mmol 1.0 equiv.) was added and the mixture was stirred at room temperature for 30 min. Water (50 mL) was added and the solution was heated to 115 °C for 2 h. 1 M NaOH (10 mL) was added and the solution was refluxed for approximately 4 h until the solution became clear. The reaction mixture was diluted with water (100 mL) and acidified with 1 M HCl to pH 2. The product was collected *via* filtration to give 4-(4-Formyl-2-methoxy-phenoxymethyl)-benzoic acid (1.21 g, 4.20 mmol, 71%) as a yellow crystalline powder.

δ_H (300 MHz d-DMSO): 13.03 (bs, 1H, OH), 9.84 (s, 1H), 7.99 (d, *J* 8.3, 2H), 7.58 (d, *J* 8.3, 2H), 7.54 (dd, *J* 8.3, 1.9, 1H), 7.43 (d, *J* 1.8, 1H), 7.26 (d, *J* 8.3, 1H), 5.31 (s, 2H), 3.85 (s, 3H).

δ_C (75 MHz d-DMSO); 191.4, 167.0, 152.8, 149.3, 141.3, 140.2, 130.3, 129.9, 129.5, 128.6, 127.6, 125.8, 112.6, 109.7, 69.3, 55.6.

ν_{max}/cm $^{-1}$ (solid): 3726, 2988, 2529, 1989, 1716 (C=O), 1674 (C=O), 1583, 1504, 1278, 1257.

m/z (ES-) (Found: $[M-H]^-$, 285.0762. $C_{16}H_{13}O_5$ required, 285.0768).

^{1}H NMR and IR data agrees with that published in the literature.[224]

*2.1.5.3 Synthesis of 4-{4-[3-(4-Fluoro-benzyl)-2,4-dioxo-thiazolidin-5-ylidenemethyl]-2-methoxy-phenoxymethyl}-benzoic acid **(24)***

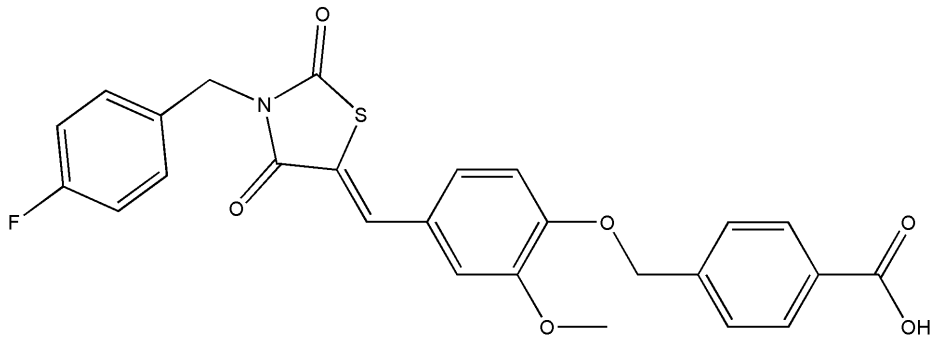

3-(4-Fluoro-benzyl)-thiazolane-2,4-dione (0.51 g, 2.25 mmol, 1.1 equiv.) was dissolved in ethanol (10 mL). Piperidine (0.014 mL, 2.07 mmol, 1.0 equiv.) and 4-(4-formyl-2-methoxy-phenoxymethyl) benzoic acid (0.70 g, 2.25 mmol, 1.1 equiv.) was added and the solution was heated at reflux for 24 h. The mixture was cooled to room temperature and the resulting precipitate was collected *via* filtration to yield 4-{4-[3-(4-fluoro-benzyl)-2,4-dioxo-thiazolidin-5-ylidenemethyl]-2-methoxy-phenoxymethyl}-benzoic acid (1.03 g, 2.08 mmol, 93%) as yellow crystalline powder.

δ_H (300 MHz $CDCl_3$): 13.03 (bs, 1H, OH), 9.84 (s, 1H), 7.99 (d, *J* 9.0, 2H), 7.57 (d, *J* 6.0, 2H), 7.53-7.23 (m, 7H), 5.31 (s, 2H), 4.82 (s, 2H), 3.85 (s, 3H).

δ_C (75 MHz $CDCl_3$); 167.8, 166.7, 166.2, 162.6 (d, $^1J_{CF}$ 247), 150.0, 149.8, 141.4, 134.2, 131.1 (d, $^4J_{CF}$ 3.3), 130.9 (d, $^3J_{CF}$ 8.2), 130.0, 129.9, 126.8, 126.7, 124.4, 118.9, 115.6 (d, $^2J_{CF}$ 21.5), 113.6, 112.9, 76.6, 70.2, 56.0, 44.5.

ν_{max}/cm^{-1} (solid): 3734, 2988, 2880, 2826, 2519, 2190, 2155, 1541 (C=O), 1448, 1404, 1279, 1250.

m/z (ES-): (Found: $[M-H]^-$, 492.0924, $C_{26}H_{19}O_6N_1F_1S_1$ required, 492.0923).

^{1}H NMR and IR data agrees with that published in the literature.[224]

*2.1.5.4 Synthesis of 3-Acetoxy-4-hydroxybenzaldehyde **(44)***

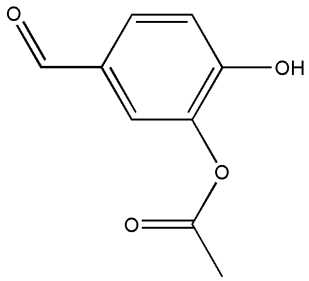

3,4-Dihydroxybenzaldehyde (0.300 g, 2.20 mmol, 1.0 equiv.), was suspended in THF (3 mL) and cooled to 0 °C. 2 M NaOH (3 mL, 5.40 mmol, 2.5 equiv.) was added dropwise followed by dropwise addition of acetic anhydride (0.25 mL, 2.64 mmol, 1.2 equiv.). The solution was stirred at 0 °C for 20 min. The solution was diluted with ethyl acetate (5 mL) and then acidified with concentrated HCl (0.25 mL) and pH 2.5 phosphate buffer (2 mL). THF was removed *via* evaporation, followed by filtration through a celite pad and washed with ethyl acetate. The combined organic layers were dried ($MgSO_4$) and ethyl acetate was evaporated. The resulting yellow oil was purified by column chromatography (dichloromethane/methanol, gradient 1-10% methanol). The product 3-Acetoxy-4-hydroxybenzaldehyde (0.247 g, 1.30 mmol, 62%) was collected as a colourless oil with approximately 20% 4-acetoxy-3-hydroxy-benzaldehyde impurity.

δ_H (300 MHz $CDCl_3$): 9.77 (s, 1H), 7.61-7.58 (m, 2H), 7.20 (s, 1H), 6.74 (bs, 1H, OH), 3.68 (s, 3H).

δ_C (75 MHz $CDCl_3$): 191.5, 169.1, 153.1, 138.7, 129.7, 124.0, 123.3, 117.7, 21.0.

No further analysis was performed.

*2.1.5.5 Synthesis of Methyl-4-(4-formyl-2-hydroxy-phenoxymethyl)-benzoate **(45)***

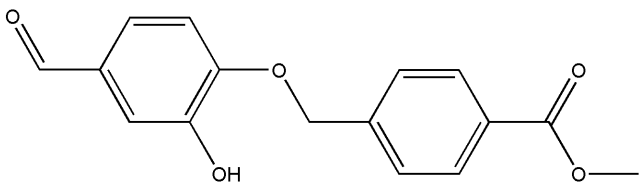

3,4-Dihydroxybenzaldehyde (0.15 g, 1.1 mmol, 1.0 equiv.) was dissolved in DMF (5 mL), sodium bicarbonate (0.13 g, 1.5 mmol, 1.5 equiv.), methyl-4-(bromomethyl)-benzoate (0.456 g, 2.00 mmol, 2.0 equiv.) and sodium iodide (0.044 g, 0.30 mmol, 0.3 equiv.) was added. The reaction mixture was heated at 40 °C for 24 h. the reaction was quenched with 10 % aqueous HCl (10 mL) and extracted with ethyl acetate (3 x 10 mL), washed with brine (3 x 10 mL), dried ($MgSO_4$) and the solvent was evaporated to yield the crude product as a brown oil. The resulting product was purified by column chromatography (ethyl acetate/hexane (1:4)). The product methyl-4-(4-formyl-2-hydroxy-phenoxymethyl)-benzoate (0.22 g, 0.76 mmol, 70%) was collected as a colourless solid with slight impurities.

δ_H (300 MHz *d*-DMSO): 9.77 (s, 1H), 8.01-7.98 (m, 2H), 7.64-7.61 (m, 2H), 7.47 (d, *J* 7.5, 1H), 7.23 (s, 1H), 6.92 (d, *J* 7.5, 1H), 5.41 (s, 2H), 4.58 (br s, 1H), 3.83 (s, 3H).

δ_C (75 MHz *d*-DMSO): 191.1, 166.2, 152.1, 152.0, 148.3, 147.3, 145.8, 129.3, 129.0, 128.8, 126.3, 124.5, 115.5, 114.2, 62.3, 52.0.

ν_{max}/cm^{-1} (solid): 3672, 2988, 1713 (C=O), 1672 (C=O), 1583, 1428, 1406, 1394, 1310, 1276.

m/z: 284.8

The crystal structure was also determined for this compound, see section 4.2.2.3.

*2.1.5.6 Synthesis of Methyl 4-{4-[3-(4-fluoro-benzyl)-2,4-dioxo-thiazolidin-5-ylidenemethyl]-2-hydroxy-phenoxymethyl}-benzoate **(46)***

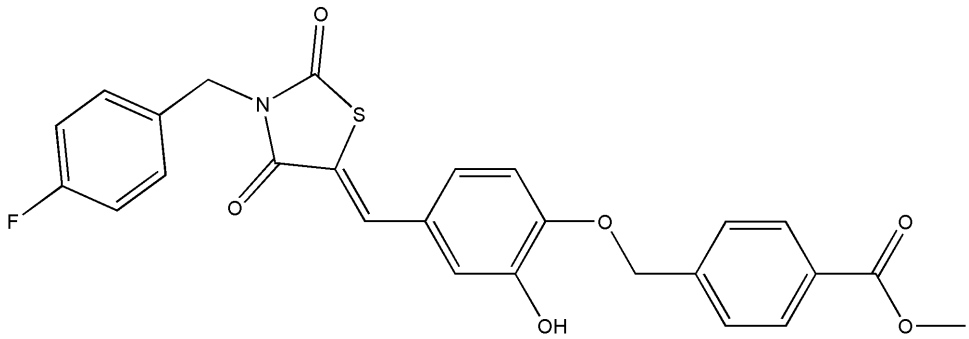

3-(4-Fluoro-benzyl)-thiazolane-2,4-dione (0.390 g, 0.176 mmol 1.0 equiv.) was dissolved in ethanol (10 mL). Piperidine (0.017 mL, 0.176 mmol 1.0 equiv.) and methyl-4-(4-Formyl-2-hydroxy-phenoxymethyl)-benzoate (0.504 g, 0.176 mmol 1.0 equiv.) was added and the reaction mixture was heated at reflux for 24 h. The mixture was cooled to room temperature resulting in precipitation. The precipitate was collected *via* filtration to yield methyl-4-{4-[3-(4-fluoro-benzyl)-2,4-dioxo-thiazolidin-5-ylidenemethyl]-2-hydroxy-phenoxymethyl}-benzoate (0.594 g, 0.12 mmol, 69%) as yellow crystalline powder.

δ_H (300 MHz *d*-DMSO): 7.99 (d, *J* 9.0, 2H), 7.80 (s, 1H), 7.63 (d, *J* 9.0, 2H), 7.35 (dd, *J* 9.0 2H), 7.20 (d, *J* 9.0, 2H), 7.15-7.06 (m, 3H), 5.29 (s, 2H), 4.80 (s, 2H), 3.85 (s, 3H).

ν_{max}/cm $^{-1}$ (solid): 3627, 2988, 1712 (C=O), 1672 (C=O), 1583, 1504, 1428, 1406, 1394.

m/z (ES+) (Found: $[M + NH_4]^+$ 511.1330, $C_{26}H_{24}O_6N_2F_1S_1$ required, 511.1334).

*2.1.5.7 Synthesis of 4-(4-Formyl-2-hydroxy-phenoxymethyl)-benzoic acid **(47)***

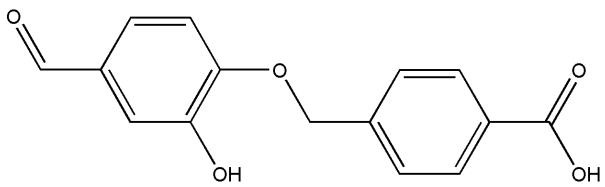

Methyl-4-(4-formyl-2-hydroxyl-phenoxymethyl) benzoate (0.100 g, 0.34 mmol) was dissolved in DMSO (1 mL). Water (5 mL) was added and the reaction was heated to 70 °C for 2 h. 1 M NaOH (1 mL) was added and reaction was heated at 70 °C until the solution became clear. The reaction mixture was diluted with water (20 mL) and acidified to pH 2 with 1 M HCl, resulting in precipitation. The resulting precipitate was collected *via* filtration to yield 4-(4-Formyl-2-hydroxy-phenoxymethyl)-benzoic acid (0.092 g, 0.33 mmol, 98%) as a pale yellow crystalline powder.

δ_H (300 MHz, *d*-DMSO): 9.79 (s, 1H), 8.00 (m, 2H), 7.62 (m, 2H), 7.39 (dd, *J* 9.0, 3, 1H), 7.33 (d, *J* 3.0, 1H), 7.20 (d, *J* 9.0, 1H), 5.34 (2H, s).

δ_C (75 MHz, *d*-DMSO): 196.2, 166.9, 157.4, 155.6, 148.7, 147.2, 145.8, 131.5, 129.8, 129.7, 129.4, 119.6, 117.5, 76.2.

ν_{max}/cm $^{-1}$ (solid): 3726, 3705, 2988, 2529, 1674 (C=O), 1583 (C=O), 1406.

m/z: 270.8.

*2.1.5.8 Synthesis of 4-{4-[3-(4-Fluoro-benzyl)-2,4-dioxo-thiazolidin-5-ylidenemethyl]-2-hydroxy-phenoxymethyl}-benzoic acid **(42)***

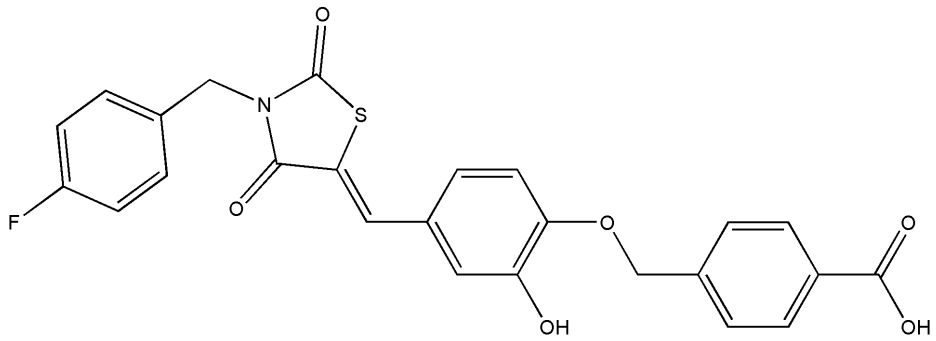

3-(4-Fluorobenzyl)-1,3-thiazolane-2,4-dione (4.00 g, 17.70 mmol, 1.0 equiv.) was dissolved in ethanol (100 mL). Piperidine (1.72 mL, 17.70 mmol 1.0 equiv.) and 4-(4-formyl-2-hydroxy-phenoxymethyl)-benzoic acid (4.80 g, 17.7 mmol 1.0 equiv.) was added and the reaction mixture was heated at reflux for 24 h. The mixture was cooled to room temperature and acidified to pH 2 with 1 M HCl resulting in precipitation of the product. The precipitate was collected *via* filtration to yield 4-{4-[3-(4-fluoro-benzyl)-2,4-dioxo-thiazolidin-5-ylidenemethyl]-2-hydroxy-phenoxymethyl}-benzoic acid (6.78 g, 14.16 mmol, 80%) as a yellow crystalline powder.

δ_H (400 MHz *d*-DMSO); 7.87 (d, *J* 9.0, 2H), 7.75 (s, 1H), 7.47 (d, *J* 9.0, 2H), 7.29-7.24 (m, 2H), 7.12-7.06 (m, 5H), 5.19 (s, 2H), 4.75 (s, 2H).

δ_C (75 MHz *d*-DMSO); 167.2, 165.7, 162.4 (d, $^1J_{CF}$ 278.0), 149.1, 147.4, 145.2, 141.8, 133.9, 131.9 (d $^4J_{CF}$ 3.3), 130.0 (d, $^3J_{CF}$ 8.2),129.5, 127.5, 126.0, 117.8, 115.5 (d, $^2J_{CF}$ 21.4), 114.9, 114.1, 69.2, 56.7.

m/z: 477.6.

*2.1.5.9 Synthesis of tosylated icodextrin **(49)***

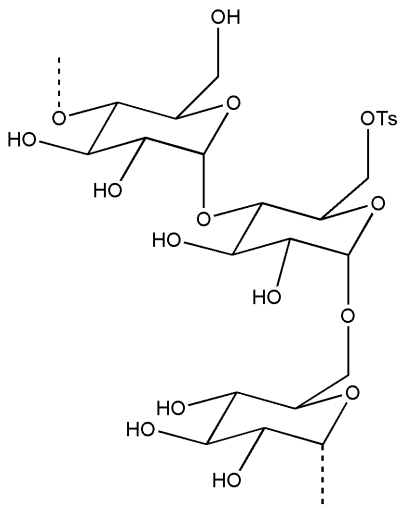

Extraneal™ (30 mL) was transferred to dialysis tubing (MWCO 8 kDa (Biodesign)) and dialysed in water (1 L), being changed 3 times per day for 3 days. The dialysate was then added to an excess of acetone (100 mL) and stirred overnight. The resulting precipitate was collected *via* vacuum filtration, washed (acetone) and desiccated for 16 h over potassium pentoxide. Icodextrin (1.5 g) was added to anhydrous DMAc (30 mL) and was heated to 160 °C for 3 h. LiCl (anhydrous, 1.5 g, 30 mmol) was added and the mixture was heated at 100 °C for 16 h. the reaction was cooled to 50 °C and tosyl chloride (7.8 g, 40 mmol) was added and the reaction was heated for 8 h. The solution was then cooled to room temperature and transferred to dialysis tubing (MWCO 8 kDa (Biodesign)) and dialyzed in water (1 L), being changed 3 times per day for 3 days to yield tosylated icodextrin (1.15 g, 77%) as a colourless crystalline solid.

δ_H (300 MHz *d*-DMSO); 7.47 (d, *J* 6.0, 2H), 7.12 (d, *J* 9.0, 2H), 5.14 (br. s, 1H, anomeric proton), 2.29 (s, 3H). Other peaks were too broad to be characterized, see NMR spectrum in section 4.2.3.2.

ν_{max}/cm^{-1} (solid): 3325, 1646, 1361, 1151.

Elemental analysis: Found: C 38.79%, H 6.21%, S 2.23%. Theoretical: C 46.70%, H 5.43%, S 9.59%.

*2.1.5.10 Synthesis of Methyl-4-{4-[3-(4-fluoro-benzyl)-2,4-dioxo-thiazolidin-5-ylidenemethyl]-2-hydroxy-phenoxymethyl-} benzoate icodextrin conjugate **(50)***

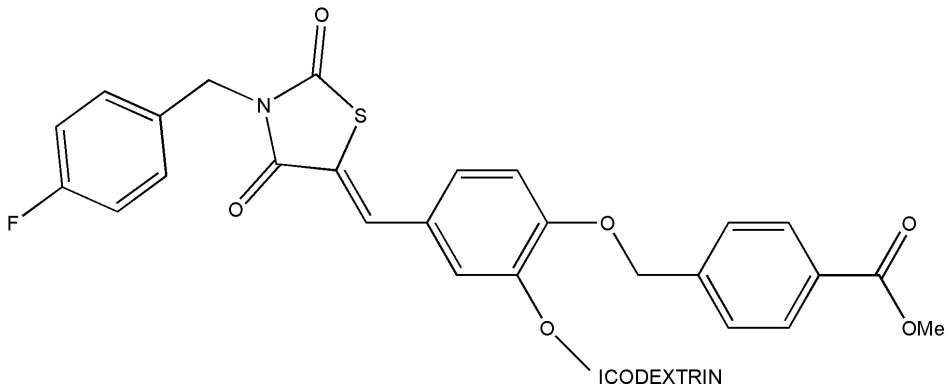

To a solution of tosylated icodextrin (0.050 g) and methyl-4-{4-[3-(4-fluoro-benzyl)-2,4-dioxo-thiazolidin-5-ylidenemethyl]-2-hydroxy-phenoxymethyl-} benzoate (0.250 g, 0.717 mmol) in anhydrous DMSO (10 mL), triethylamine (0.5 mL, 3.70 mmol) was added and the solution was heated to 100 °C for 20 h. The solution was cooled to room temperature and transferred to dialysis tubing (MWCO 8 kDa (Biodesign)) and dialysed against methanol (1 L), being changed 3 times per day for 3 days to yield thiazolidine-2,4-dione ester conjugate (0.145 g, 48% mass recovered) as an orange oily solid.

See section 4.2.4 for characterisation.

*2.1.5.11 Synthesis of Triisopropylsilyl-4-{4-[3-(4-fluoro-benzyl)-2,4-dioxo-thiazolidin-5-ylidenemethyl]-2-hydroxy-phenoxymethyl}-benzoate **(52)***

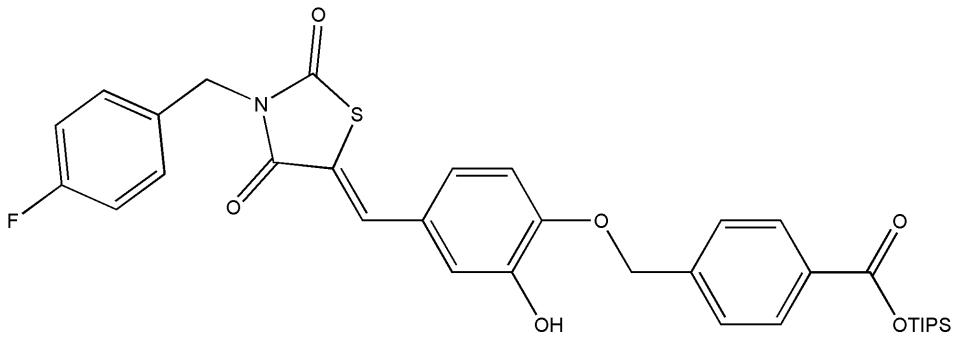

To a cooled solution of 4-{4-[3-(4-fluoro-benzyl)-2,4-dioxo-thiazolidin-5-ylidenemethyl]-2-hydroxy-phenoxymethyl-}-benzoic acid (0.100 g, 0.20 mmol, 1.0 equiv.) in anhydrous DMF (10 mL), under N_2, sodium hydride (0.005 g, 0.20 mmol, 1.0 equiv.) was added. The reaction was stirred and allowed to warm to room temperature over 1 h. Triisopropylsilyl chloride (0.043 g, 0.02 mL, 0.22 mmol, 1.1 equiv.) was added and the reaction was stirred at room temperature for 4 h. The solution was poured into ice/water mixture and the product was extracted with ethyl acetate (3 x 20 mL), washed with brine (3 x 20 mL) and dried ($MgSO_4$). The solvent was evaporated to yield triisopropylsilyl-4-{4-[3-(4-fluoro-benzyl)-2,4-dioxo-thiazolidin-5-ylidenemethyl]-2-hydroxy-phenoxymethyl}-benzoate (0.046 g, 0.07 mmol, 49%) as a yellow crystalline powder.

δ_H (400 MHz $CDCl_3$): 8.00 (d, *J* 7.4, 2H), 7.69 (s, 1H), 7.40-7.38 (m, 4H), 7.01 (s, 1H), 6.95-6.81 (m, 4H), 5.84 (s, 1H), 5.15 (s, 2H), 4.75 (s, 2H), 1.35 (m, 3H), 1.04 (m, 18H).

δ_C (75 MHz $CDCl_3$): 173.6, 164.1, 151.9, 148.7, 147.3, 146.2, 135.9, 134.1, 130.7, 130.0, 127.4, 116.1, 115.5, 112.2, 107.8, 98.4, 87.4, 70.5, 59.1, 46.5, 44.4, 43.0, 32.7, 28.3, 26.8, 23.2, 17.9, 12.0.

m/z: 635.0.

2.1.5.12 Synthesis of Triisopropylsilyl-4-{4-[3-(4-fluoro-benzyl)-2,4-dioxo-thiazolidin-5-ylidenemethyl]-2-hydroxy-phenoxymethyl}-benzoate icodextrin conjugate

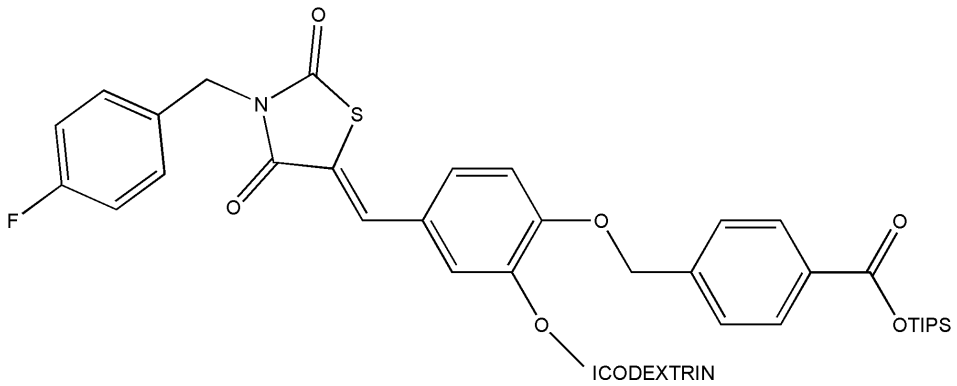

Triisopropylsilyl-4-{4-[3-(4-fluoro-benzyl)-2,4-dioxo-thiazolidin-5-ylidenemethyl]-2-hydroxy-phenoxymethyl}-benzoate (0.050 g, 0.078 mmol), was stirred in anhydrous DMSO (10 mL). Triethylamine (0.5 mL, 3.70 mmol) and tosylated icodextrin (0.010 g, >8 kDa), were added and the solution was heated at 100 °C for 16 h. The solution was cooled to room temperature and transferred to dialysis tubing (MWCO 8 kDa (Biodesign)) and dialyzed against methanol (1 L), being changed 3 times per day for 3 days to yield triisopropylsilyl-4-{4-[3-(4-fluoro-benzyl)-2,4-dioxo-thiazolidin-5-ylidenemethyl]-2-hydroxy-phenoxymethyl}-benzoate icodextrin conjugate (0.020 g, 33% mass recovered) as an orange oily solid.

Used directly in next step.

2.1.5.13 Synthesis of conjugate 2

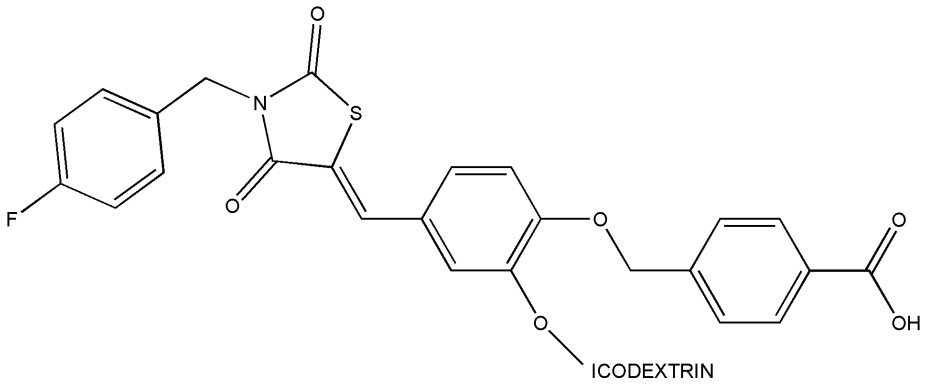

To a solution of triisopropylsilyl-4-{4-[3-(4-fluoro-benzyl)-2,4-dioxo-thiazolidin-5-ylidenemethyl]-2-hydroxy-phenoxymethyl}-benzoate icodextrin conjugate (0.020 g) in methanol (10 mL) tetra-n-butyl ammonium fluoride (0.050 g, 0.19 mmol) was added and the solution was stirred at room temperature for 3 h. The solution was transferred to dialysis tubing (MWCO 8 kDa (Biodesign)) and dialyzed against methanol (1 L), being changed 3 times per day for 3 days to yield conjugate 2 (0.018 g, 22% mass recovered) as a brown oil.

ν_{max}/cm^{-1} (solid): 3325, 2922, 2853, 1700 (C=O), 1673, 1601, 1551, 1456, 1434.

See section 4.2.7 for characterisation.

*2.1.5.14 Synthesis of 2-(2-Bromo-ethoxy)-ethanol **(54)***

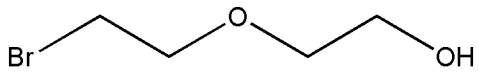

To a solution of ethylene glycol (1.79 mL, 18.85 mmol, 1.0 equiv.) in MeCN (30 mL), carbon tetrabromide (6.88 g, 20.74 mmol, 1.1 equiv.) and triphenylphosphine (4.90 g, 18.85 mmol, 1.0 equiv.) were added sequentially and the mixture was stirred at room temperature for 16 h. 1 M NaOH (25 mL) was added and the solvent was removed *via* evaporation. The aqueous residue was extracted with ethyl acetate (3 x 30 mL), washed with brine (2 x 30 mL), dried ($MgSO_4$), and concentrated *via* rotary evaporation, to yield the crude product (6.9 g). The crude residue was purified by column chromatography (hexane/ethyl acetate (1:3)) to yield 2-(2-Bromo-ethoxy)-ethanol (1.57 g, 9.3 mmol, 49%) as a yellow oil.

δ_H (300 MHz *d*-DMSO); 3.60 (m, 4H), 3.40 (m, 4H), 2.41 (s, OH).

No further analysis was performed.

^{1}H NMR data agrees with that published in the literature.[245]

2.1.5.15 Synthesis of Methyl-4-{4-[3-(4-fluoro-benzyl)-2,4-dioxo-thiazolidin-5-ylidenemethyl]-2-[2-(2-hydroxy-ethoxy)-ethoxy]-phenoxymethyl}-benzoate ***(55)***

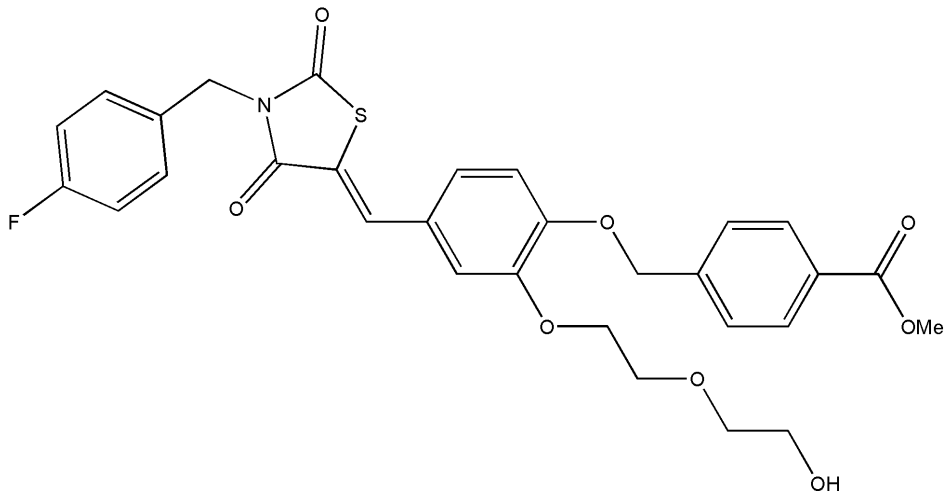

To a solution of methyl-4-{4-[3-(4-fluoro-benzyl)-2,4-dioxo-thiazolidin-5-ylidenemethyl]-2-hydroxy-phenoxymethyl}-benzoate (0.465 g, 0.94 mmol 1.0 equiv.) in MeCN (5 mL), potassium hydroxide (0.112 g, 1.86 mmol, 2.0 equiv.) was added and the reaction mixture was heated at 60 °C for 2 h. Potassium iodide (0.155 g, 0.94 mmol, 1.0 equiv.) and 2-(2-bromo-ethoxy)-ethanol (0.315 g, 1.86 mmol, 2.0 equiv.) was added and the reaction mixture was stirred for 16 h. The mixture was diluted with water, extracted with ethyl acetate (3 x 20 mL), washed with brine (3x 20 mL) dried ($MgSO_4$) and concentrated *via* evaporation to yield the crude product. The crude product was purified *via* column chromatography (petroleum ether/ethyl acetate gradient 40-100% ethyl acetate) to yield methyl-4-{4-[3-(4-fluoro-benzyl)-2,4-dioxo-thiazolidin-5-ylidenemethyl]-2-[2-(2-hydroxy-ethoxy)-ethoxy]-phenoxymethy}-benzoate (0.366 g, 0.64 mmol, 68%) as a yellow crystalline powder.

δ_H (400 MHz *d*-DMSO); 7.98 (d, *J* 8.0, 2H), 7.75 (s, 1H), 7.45 (d, *J* 7.0, 2H), 7.19 (dd, *J* 8.0, 3.0, 2H), 6.99-6.96 (m, 2H), 6.94 (d, *J* 7.0, 1H), 5.17 (s, 2H), 4.75 (s, 2H), 4.28 (d, *J* 6.0, 1H), 4.16 (d, *J* 6, 2H), 3.85-3.83 (m, 5H), 3.73-3.55 (m, 6H).

m/z: 580.7.

2.1.5.16 Synthesis of Methyl 4-{4-formyl-2-[2-(2-hydroxy-ethoxy)-ethoxy]-phenoxymethyl}-benzoate

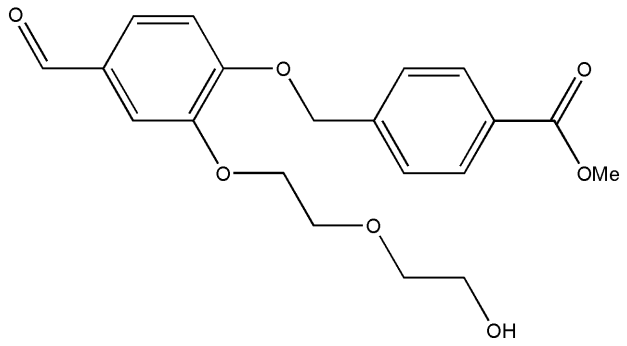

Methyl-4-{4-[3-(4-fluorobenzyl)-2,4-dioxo-thiazolidine-5-ylidenemethyl]-2-hydroxy-phenoxymethyl}-benzoate (0.310 g, 0.627 mmol, 1.0 equiv.) was stirred in DMF (5 mL). Potassium carbonate (0.173 g, 1.25 mmol, 2.0 equiv.), potassium iodide (0.110 g, 0.627 mmol, 1.0 equiv.) and 2-(2-chloro-ethoxy)-ethanol (0.2 mL, 1.88 mmol, 2.9 equiv.) was added and the reaction was heated to 70 °C for 18 h. The next day the solution was diluted with water (50 mL) and extracted with ethyl acetate (3 x 20 mL), washed with water (3 x 20 mL) and brine (3 x 20 mL). The solvent was removed by evaporation to yield the crude product. The crude product was purified *via* column chromatography (hexane/ethyl acetate (1:3)) to yield methyl-4-{4-formyl-2-[2-(2-hydroxy-ethoxy)-ethoxy]-phenoxymethyl}-benzoate (0.239 g, 0.41 mmol, 58%) as a pale yellow crystalline powder.

δ_H (400 MHz $CDCl_3$): 9.82 (s, 1H), 8.04 (d, *J* 7.0, 2H), 7.51-7.48 (m, 3H), 7.40 (d, *J* 7.0, 1H), 6.96 (d, *J* 7.0, 1H), 5.27 (s, 2H), 4.25 (d, *J* 7.0, 2H), 3.94-3.90 (m, 5H), 3.69-3.65 (m, 4H).

δc (75 MHz, *d*-DMSO): 201.0, 188.1, 184.9, 151.2, 144.7, 134.7, 134.0, 127.3, 118.9, 118.0, 102.9, 96.7, 96.0, 79.2, 72.5, 60.7, 60.2, 44.8.

m/z: 375.0.

*2.1.5.17 Synthesis of 4-(4-Formyl-2-[2-(2-hydroxy-ethoxy)-ethoxy]-phenoxymethyl}-benzoic acid (**57**)*

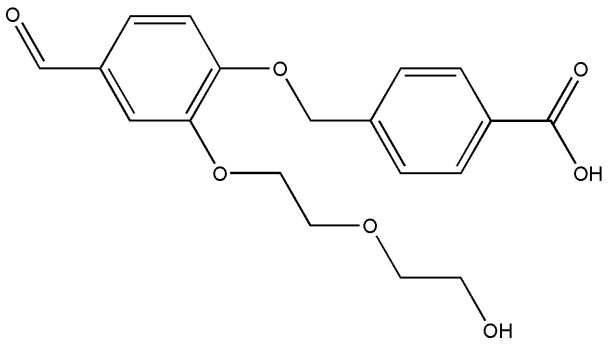

Methyl-4-(4-formyl-2-[2-(2-hydroxy-ethoxy)-ethoxy]-phenoxymethyl}-benzoate (0.100 g, 0.34 mmol) was dissolved in DMSO (1 mL), water (5 mL) was added and the reaction was heated to 70 °C for 2 h. 1 M NaOH (1 mL) was added and reaction was heated at 70 °C until the solution became clear. The reaction mixture was diluted with water (10 mL) and acidified to pH 2 with 1 M HCl, the resulting precipitate was collected *via* filtration to yield 4-(4-formyl-2-[2-(2-hydroxy-ethoxy)-ethoxy]-phenoxymethyl}-benzoic acid (0.092 g, 0.33 mmol, 98%) as a pale yellow crystalline powder.

δ_H (300 MHz $CDCl_3$): 9.83 (s, 1H), 7.98 (d, J 9.0, 2H), 7.60, (d, *J* 9.0, 2H), 7.51 (dd *J* 9.0, 3, 1H), 7.46-7.45 (m, 1H), 7.22 (d, *J* 9.0, 1H), 5.34 (s, 2H), 4.40 (br s, 1H, OH), 4.20 (m, 2H), 3.85 (m, 2H), 3.80 (m, 4H), 3.41 (br s, 1H OH).

δ_C (75 MHz, CDCl3): 200.1, 167.1, 159.7, 155.1, 135.5, 131.5, 130.6, 129.9, 127.2, 123.9, 115.6, 115.3, 103.1, 72.5, 68.7, 66.9, 61.2, 60.2.

m/z: 358.9

*2.1.5.18 Synthesis of 4-{4-[3-(4-Fluoro-benzyl)-2,4-dioxo-thiazolidin-5-ylidenemethyl]-2-[2-(2-hydroxy-ethoxy)-ethoxy]-phenoxymethyl}-benzoic acid **(58)***

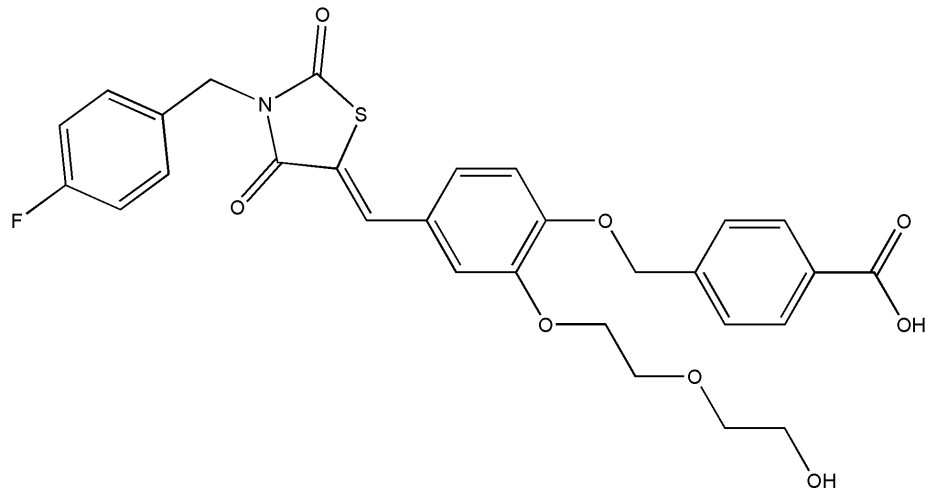

3-(4-Fluorobenzyl)-1,3-thiazolane-2,4-dione (0.51 g, 2.25 mmol, 1.0 equiv.) was dissolved in ethanol (10 mL). Piperidine (0.014 mL, 2.25 mmol, 1.0 equiv.) and 4-[(4-formyl-2-methoxyphenoxy)methyl] benzoic acid (0.70 g, 2.24 mmol, 1.0 equiv.) was added and the solution was heated at reflux for 24 h. The mixture was cooled to room temperature and the resulting precipitate was collected *via* filtration to yield 4-[(4-{[3-(4-fluorobenzyl)-2,4-dioxo-1,3-thiazolan-5-yliden]-methyl-2-methoxyphenoxy)methyl] benzoic acid (1.03 g, 2.08 mmol, 93%) as a yellow crystalline powder.

δ_H (400 MHz d-DMSO); 7.98 (d, *J* 8.3, 2H), 7.75 (s, 1H), 7.45 (d, *J* 7.0, 2H), 7.19 (dd, *J* 8.3, 3.0, 2H), 6.99-6.96 (m, 3H), 6.94 (d, *J* 7.0, 1H), 5.17 (s, 2H), 4.75 (s, 2H), 4.70 (s, 1H, OH), 4.28 (d, *J* 6.0, 1H), 4.16 (d, *J* 6.0, 2H), 3.93-3.90 (m, 2H), 3.73-3.55 (m, 6H), 3.44 (br. s, 1H, OH).

m/z: 565.8.

2.1.5.19 Synthesis of Triisopropyl-4-{4-[3-(4-fluoro-benzyl)-2,4-dioxo-thiazolidin-5-ylidenemethyl]-2-[2-(2-hydroxy-ethoxy)-ethoxy]-phenoxymethyl}-benzoate ***(59)***

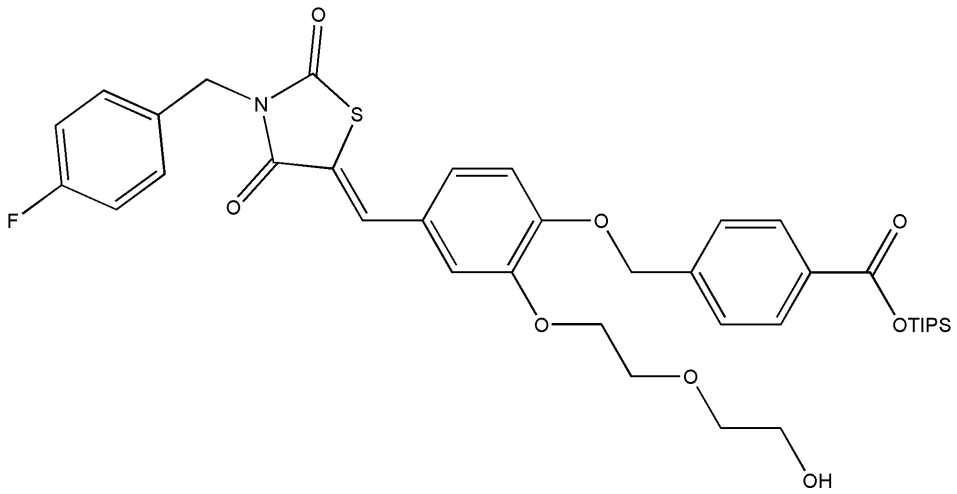

4-{4-[3-(4-Fluoro-benzyl)-2,4-dioxo-thiazolidin-5-ylidenemethyl]-2-[2-(2-hydroxy-ethoxy)-ethoxy]-phenoxymethyl}-benzoic acid (6.00 g, 10.5 mmol, 1.0 equiv.) and triisopropylsilyl chloride (3.4 mL, 15 mmol, 1.42 equiv.) were stirred in anhydrous THF (200 mL). Triethylamine (1.6 mL, 11.55 mmol, 1.1 equiv.) was added and the reaction mixture was stirred for 15 min at room temperature. The resulting mixture was diluted with diethyl ether (200 mL) and the solvent was removed by rotary evaporation to yield the crude product 9.00 g as an oily yellow solid. The crude material was purified by column chromatography (hexane/ethyl acetate (1:1)) to yield triisopropyl-4-{4-[3-(4-fluoro-benzyl)-2,4-dioxo-thiazolidin-5-ylidenemethyl]-2-[2-(2-hydroxy-ethoxy)-ethoxy]-phenoxymethyl}-benzoate (5.78 g, 8.00 mmol, 76%) as a bright yellow crystalline powder.

δ_H (400 MHz $CDCl_3$): 8.06-8.04 (m, 2H), 7.78 (s, 1H), 7.49 (d, *J* 8.3, 2H), 7.39-7.35 (m, 2H), 7.00-6.96 (m, 4H), 6.92-6.90 (m, 1H), 5.23 (s, 2H), 4.82 (s, 2H), 4.21-4.18 (m, 2H), 3.93-3.90 (m, 2H), 3.68-3.65 (m, 4H), 1.40 (q, *J* 7.2, 3 H), 1.12 (d, *J* 7.6, 18H).

δ_C (75 MHz $CDCl_3$): 174.2, 167.8, 166.5, 155.1, 151.8, 149.0, 141.3, 134.0, 130.6, 126.8, 125.1, 120.9, 115.8, 115.5, 112.2, 105.0, 102.8, 88.9, 82.1, 76.5, 69.4, 63.0, 61.8, 58.3, 44.5, 39.8, 39.0, 20.5, 17.9, 12.0.

m/z: 724.7.

2.1.5.20 Synthesis of Triisopropyl-4-{4-[3-(4-fluoro-benzyl)-2,4-dioxo-thiazolidin-5-ylidenemethyl]-2-[2-(2-hydroxy-ethoxy)-ethoxy]-phenoxymethyl}-benzoate icodextrin conjugate

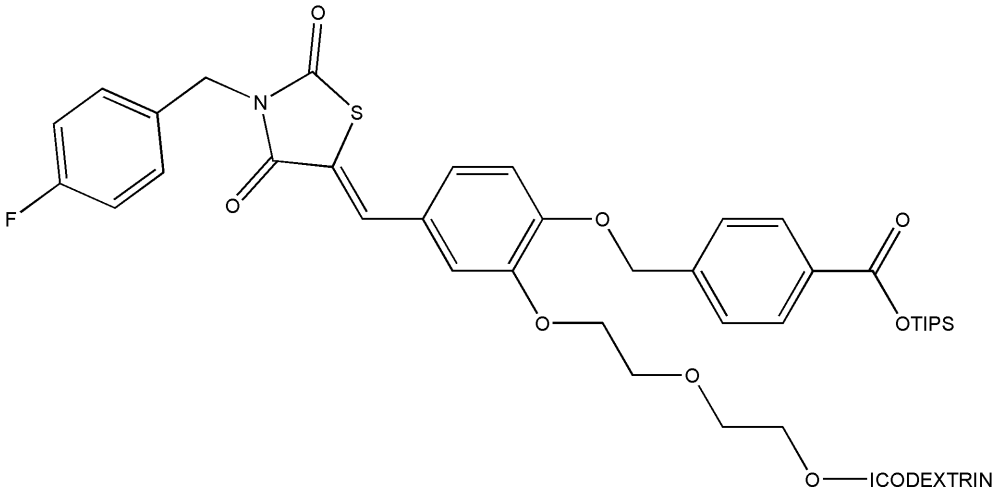

Tosylated icodextrin was dialysed against water (1 L) using a 20 kDa MWCO (biotech) dialysis membrane, being changed 3 times a day for 3 days, 4-{4-[3-(4-fluoro-benzyl)-2,4-dioxo-thiazolidin-5-ylidenemethyl]-2-hydroxy-phenoxymethyl-triisopropylsilyl-benzoate (0.05 g, 0.057 mmol), was stirred in DMSO (10 mL). Triethylamine (0.5 mL, 3.7 mmol) and tosylated icodextrin (0.01 g, 20 kDa MWCO) was added and the solution was heated at 100 °C for 16 h. The solution was then cooled to room temperature and transferred to dialysis tubing (MWCO 8 kDa (Biodesign)) and dialysed in methanol (1 L), being changed 3 times per day for 3 days to yield triisopropyl-4-{4-[3-(4-fluoro-benzyl)-2,4-dioxo-thiazolidin-5-ylidenemethyl]-2-[2-(2-hydroxy-ethoxy)-ethoxy]-phenoxymethyl}-benzoate icodextrin conjugate (0.018 g, 30% mass recovered) as a brown oil.

Used directly in next step.

2.1.5.21 Synthesis of conjugate 3

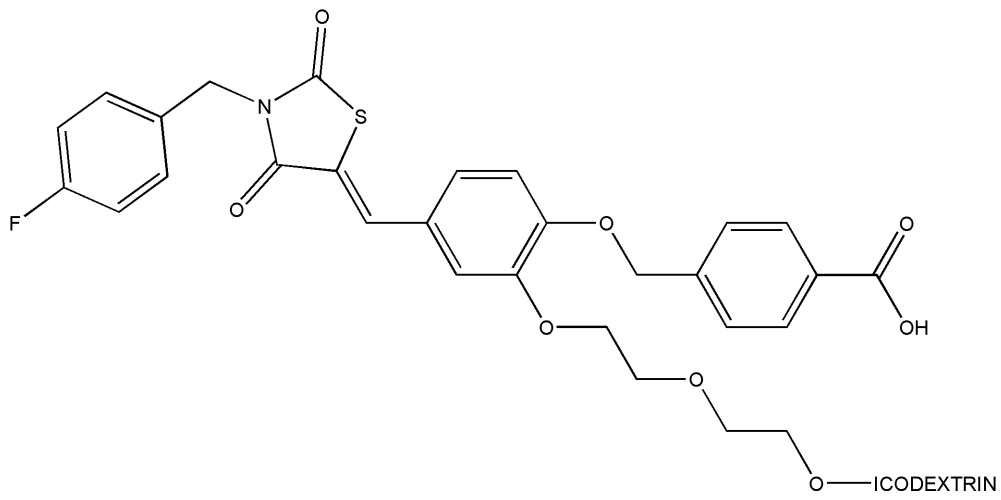

To a solution of triisopropyl-4-{4-[3-(4-fluoro-benzyl)-2,4-dioxo-thiazolidin-5-ylidenemethyl]-2-[2-(2-hydroxy-ethoxy)-ethoxy]-phenoxymethyl}-benzoate icodextrin conjugate (0.02 g) in methanol (10 mL), tetra-n-butyl ammonium fluoride (0.05 g, 0.19 mmol) was added and the solution was stirred at room temperature for 3 h. The solution was transferred to dialysis tubing (MWCO 20 kDa (Biotech)) and dialyzed against methanol (1 L), being changed 3 times per day for 3 days to yield 4-{4-[3-(4-fluoro-benzyl)-2,4-dioxo-thiazolidin-5-ylidenemethyl]-2-[2-(2-hydroxy-ethoxy)-ethoxy]-phenoxymethyl}-benzoic acid icodextrin conjugate (0.018 g, 30%, mass recovered) as a colourless oil.

ν_{max}/cm^{-1} (solid): 3320, 2922, 2872, 1700, 1673, 1550.

2.1.5.22 *Synthesis of Methyl-4-(4-[3-(fluoro-benzyl)-2,4-dioxo-thiazolidin-5ylidenemethyl]-2-{2-[2-(toluene-4-sulfonyloxy)-ethoxy]-ethoxy}-phenoxymethyl)-benzoate* ***(60)***

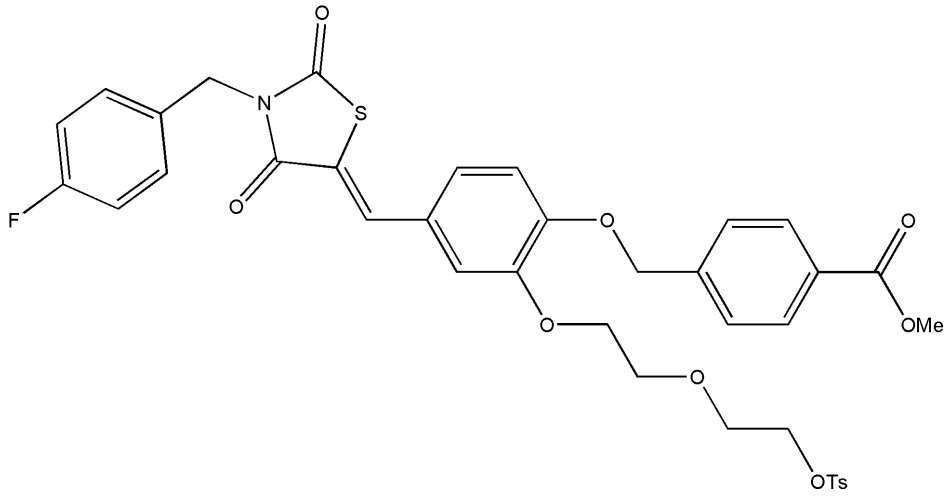

Methyl-4-{4-[3-(4-fluoro-benzyl)-2,4-dioxo-thiazolidin-5-ylidenemethyl]-2-[2-(2-hydroxy-ethoxy)-ethoxy]-phenoxymethyl}-benzoate (0.200 g, 0.343 mmol, 1.0 equiv.) was stirred in dichloromethane (5 mL) in a reaction vial. Triethylamine (0.095 mL, 0.686 mmol, 2.0 equiv.) and tosyl chloride (0.065 g, 0.343 mmol, 2.0 equiv.) were added and the reaction was stirred at room temperature and monitored *via* LC/MS; for 20 h. The reaction mixture was washed with water (3 x 2 mL), followed by drying ($NaSO_4$), the solvent was removed *via* evaporation to yield methyl-4-(4-[3-(fluoro-benzyl)-2,4-dioxo-thiazolidin-5ylidenemethyl]-2-{2-[2-(toluene-4-sulfonyloxy)-ethoxy]-ethoxy}-phenoxymethyl)-benzoate (0.145 g, 57%, 0.197 mmol) as a yellow oil.

δ_H (400 MHz $CDCl_3$): 7.97 (d, *J* 8.3, 2H), 7.75 (s, 1H), 7.73-7.69 (m, 2H), 7.42 (d, *J* 7.0, 2H), 7.35 (m, 2H), 7.19 (dd, *J* 8.0, 3.0, 2H), 6.94-6.86 (m, 5H), 5.22 (s, 2H), 4.77 (s, 2H), 4.25 (d, *J* 6.0, 1H), 4.06 -4.03 (m, 4H), 3.85-3.82 (m, 3H), 3.75-3.71 (m, 2H), 3.69-3.65 (m, 2H).

2.1.5.23 Synthesis of Triisopropylsilyl-4-(4-[3-(fluoro-benzyl)-2,4-dioxo-thiazolidin-5-ylidenemethyl]-2-{2-[2-(toluene-4-sulfonyloxy)-ethoxy]-ethoxy}-phenoxymethyl)-benzoate ***(61)***

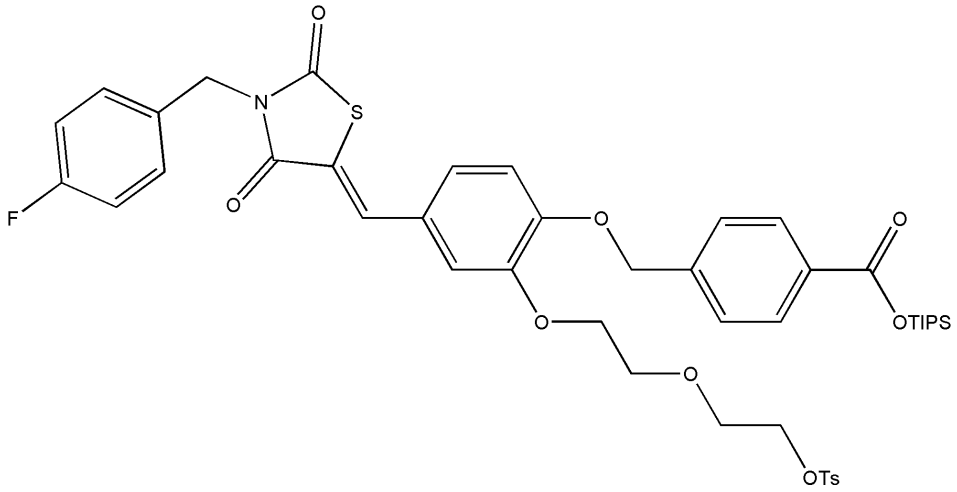

Triisopropyl-4-{4-[3-(4-fluoro-benzyl)-2,4-dioxo-thiazolidin-5-ylidenemethyl]-2-[2-(2-hydroxy-ethoxy)-ethoxy]-phenoxymethyl}-benzoate (2.02 g, 2.75 mmol, 1.0 equiv.), was stirred in dichloromethane (40 mL). Tosyl chloride (0.58 g, 3.00 mmol, 1.1 equiv.) and triethylamine (0.383 mL, 2.75 mmol, 1.0 equiv.) were added and the reaction mixture was stirred at room temperature for 20 h. The crude product was collected *via* evaporation of the solvent and the residue was purified by column chromatography (ethyl acetate/hexane (1:1) with 1% triethylamine). Triisopropylsilyl-4-(4-[3-(fluoro-benzyl)-2,4-dioxo-thiazolidin-5ylidenemethyl]-2-{2-[2-(toluene-4-sulfonyloxy)-ethoxy]-ethoxy}-phenoxymethyl)-benzoate (1.20 g, 1.4 mmol, 50%) was collected as a waxy yellow solid.

δ_H (400 MHz $CDCl_3$): 8.03 (d, *J* 8, 2H), 7.77 (s, 1H), 7.74 (d, *J* 8.0, 2H), 7.45 (d, *J* 8.0, 2H), 7.40-7.37 (m, 2H), 7.25 (d, *J* 8.0, 2H), 7.02-6.96 (m, 4H), 6.90 (d, *J* 8.0, 1H), 5.21 (s, 2H), 4.83 (s, 2H), 4.14-4.06 (m, 4H), 3.82 (t, *J* 6.0, 2H), 3.76-3.73 (m, 2H), 2.36 (s, 3H), 1.39 (q, *J* 6.0, 3H), 1.11 (d, *J* 8.0, 18H).

δ_C (100 MHz $CDCl_3$): 167.8, 166.2, 165.9, 162.8 (d $^1J_{CF}$ 250), 150.8, 149.3, 146.8, 144.8, 141.6, 134.0, 133.2,131.4, 131.2, 131.2, 131.0, 130.9, 130.6, 130.3, 129.8, 128.0, 127.1, 126.9, 126.9, 125.2,

119.2, 115.7 (d, $^{2}J_{CF}$ 21.5), 115.7, 114.6, 77.4, 70.5, 69.9, 69.2, 69.2, 69.2, 44.6, 21.9, 21.6, 17.9, 12.2.

m/z: 879.7.

2.1.5.24 Synthesis of 4-(4-[3-(4-Fluoro-benzyl)-2,4-dioxo-thiazolidin-5-ylidenemethyl]-2-{2-[2-(3,4,5-tris-benzyloxy-6-methoxy-tetrahydro-pyran-2-ylmethoxy)-ethoxy]-ethoxy}-phenoxymethyl)-benzoic acid ***(62)***

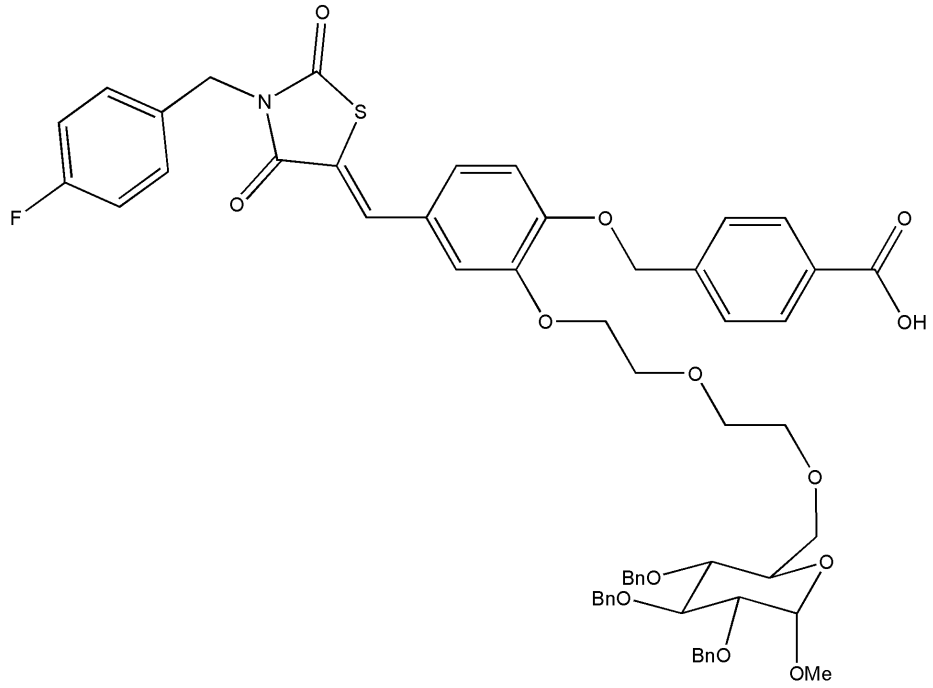

Methyl-2,3,4-tri-o-benzyl-α-D-glucopyranoside (0.100 g, 0.22 mmol, 1.1 equiv.) was stirred in anhydrous DMF (5 mL) and cooled to 0 °C. Sodium hydride (0.040 g, 0.22 mmol, 1.1 equiv.) was added and the reaction mixture was allowed to warm to room temperature. After 2 h triisopropylsilyl-4-(4-[3-(fluoro-benzyl)-2,4-dioxo-thiazolidin-5-ylidenemethyl]-2-{2-[2-(toluene-4-sulfonyloxy)-ethoxy]-ethoxy}-phenoxymethyl)-benzoate (0.19 g, 0.215 mmol, 1.0 equiv.) was added and the reaction mixture was stirred for 6 h. The reaction was quenched with NH_4Cl (sat.) (0.5 mL) and the solvent was removed *via* evaporation to yield a brown oil. The crude product was dissolved in dichloromethane (5 mL), washed with $NaHCO_3$ (3x 5 mL), brine (3x 5 mL), the organic layer was collected and the solvent was removed *via* rotary evaporation. The crude product was purified by column chromatography (methanol/dichloromethane (1:20)). 4-(4-[3-(4-Fluoro-benzyl)-2,4-dioxo-thiazolidin-5-ylidenemethyl]-2-{2-[2-(3,4,5-tris-benzyloxy-6-methoxy-tetrahydro-pyran-2-ylmethoxy)-ethoxy]-ethoxy}-phenoxymethyl)-benzoic acid (0.100 g, 0.09 mmol, 46%) was collected as a colourless oil.

δ_H (400 MHz $CDCl_3$): 9.24 (s, 1H), 8.06 (d, *J* 8.3, 2H), 7.96 (s, 1H), 7.48 (d, *J* 8.3, 2H),7.32-7.18 (m, 18H), 6.82 (d, *J* 8.3, 1H), 6.75 (d, *J* 8.3, 1H), 5.23 (s, 2H), 4.91 (d, 1H), 4.78 (d, 1H), 4.75-4.72 (m, 2H), 4.61-4.45 (m, 6H), 4.40 (d, *J* 6.0, 1H), 4.29 (d, *J* 6.0, 1H), 3.97-3.94 (m, 1H), 3.88-3.83 (m, 1H), 3.49-3.47 (m, 3H), 3.31 (s, 3H), 2.86-2.83 (m, 3H).

δ_C (100 MHz $CDCl_3$): 167.1, 150.5, 148.4, 146.3, 142.7, 138.7, 138.2, 138.0, 130.6, 128.6, 128.5, 128.4, 128.2, 128.2, 128.1, 128.0, 128.0, 127.8, 127.7, 127.0, 122.1, 117.3, 113.2, 98.1, 82.2, 80.2, 78.0, 77.4, 76.8, 76.0, 75.2, 73.5, 70.3, 70.2, 70.4, 69.2, 68.9, 65.9, 64.5, 55.3, 53.5, 36.4, 29.8, 15.3.

A mass spectrum was not obtained for this compound as it did not ionise.

2.1.5.25 Synthesis of conjugate 4

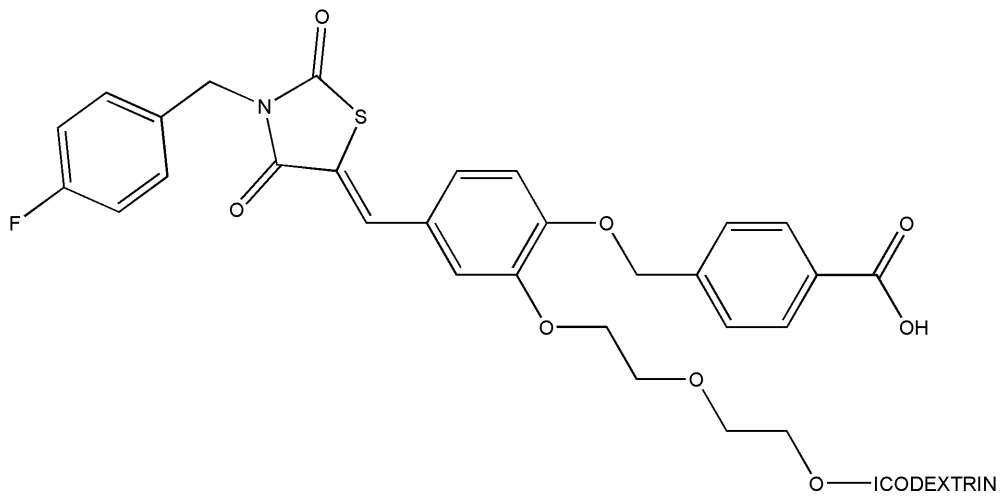

Icodextrin (0.325 g, approx. 0.016 mmol) was suspended in DMAc (10 mL) and heated to 100 °C with stirring until dissolved. The solution was then cooled to room temperature and sodium hydride (0.036 g, 0.89 mmol) was added and stirred under N_2 for 2 h. Triisopropylsilyl-4-(4-[3-(fluoro-benzyl)-2,4-dioxo-thiazolidin-5-ylidenemethyl]-2-{2-[2-(toluene-4-sulfonyloxy)-ethoxy]-ethoxy}-phenoxymethyl)-benzoate (0.784 g, 0.89 mmol) was dissolved in DMAc (1 mL) and added to the reaction mixture dropwise. The reaction was monitored by TLC (hexane/ethyl acetate (4:2)) and stirred at room temperature for 20 h. The reaction mixture was transferred into a dialysis membrane and dialysed against methanol (1 L) being changed 3 times per day for 3 days to yield conjugate 4 (0. 504 g, 42%).

See section 4.2.7 for characterisation.

2.1.5.26 Synthesis of conjugate 5

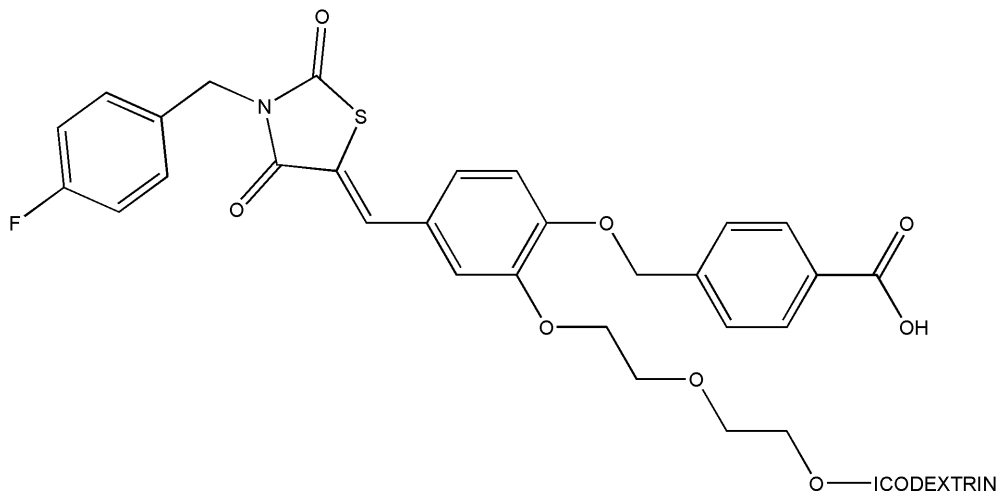

Icodextrin (0.25 g, approx. 0.016 mmol) was suspended in DMAc (5 mL) and heated to 100 °C with stirring until dissolved. The solution was then cooled to room temperature and sodium hydride (0.040 g, 1 mmol) was added and stirred under N_2 for 2 h. Triisopropylsilyl-4-(4-[3-(fluoro-benzyl)-2,4-dioxo-thiazolidin-5-ylidenemethyl]-2-{2-[2-(toluene-4-sulfonyloxy)-ethoxy]-ethoxy}-phenoxymethyl)-benzoate (0.220 g, 0.25 mmol) was dissolved in DMAc (1 mL) and added to the reaction mixture dropwise. The reaction was monitored by TLC (hexane/ethyl acetate (4:2)) and was stirred at room temp for 4 h. the reaction mixture was transferred into a dialysis membrane and dialysed against methanol (1 L) being changed 3 times per day for 3 days to yield conjugate 4 (0. 407 g, 56%).

ν_{max}/cm^{-1} (solid): 3362, 2361, 2342, 1557, 1155.

See section 4.2.7 for characterisation.

2.1.5.27 Synthesis conjugate 6

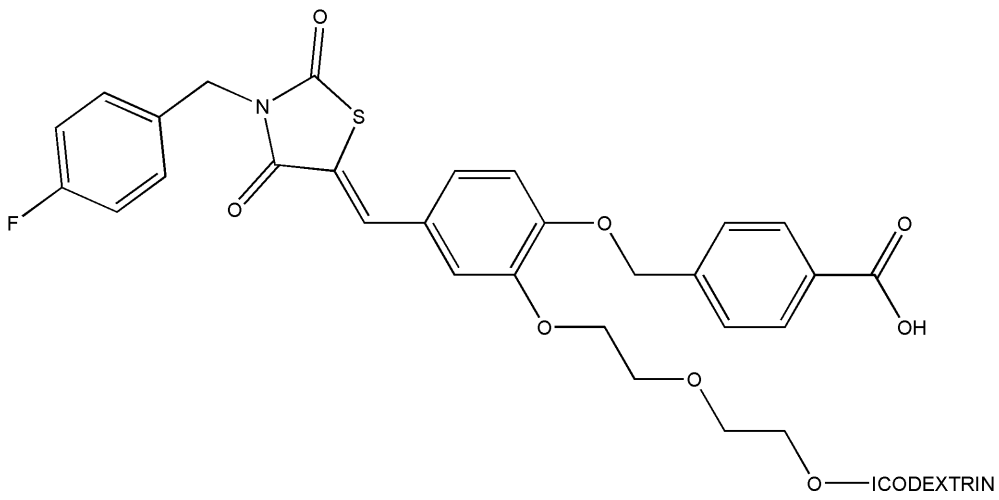

Icodextrin (0.25 g, approx. 0.016 mmol) was suspended in DMAc (5 mL) and heated to 100 °C with stirring until dissolved. The solution was then cooled to room temperature and sodium hydride (0.040 g, 1.00 mmol) was added and stirred under N_2 for 4 h. Triisopropylsilyl-4-(4-[3-(fluoro-benzyl)-2,4-dioxo-thiazolidin-5-ylidenemethyl]-2-{2-[2-(toluene-4-sulfonyloxy)-ethoxy]-ethoxy}-phenoxymethyl)-benzoate (0.449 g, 0.57 mmol) was dissolved in DMAc (1 mL) and added to the reaction mixture dropwise. The reaction was monitored by TLC (hexane/ethyl acetate (4:2)) and stirred at room temperature for 4 h. The reaction mixture was transferred into a dialysis membrane and dialysed against methanol (1 L) being changed 3 times per day for 3 days to yield conjugate 6 (0. 401 g, 43%).

ν_{max}/cm^{-1} (solid): 3362, 1507, 1146, 2361, 2342, 1078, 1019.

The ^1H NMR spectrum is shown in section 4.2.6.3.

2.1.6 Degree of substitution

The degree of substitution of icodextrin-drug conjugates was determined by measuring the inherent fluorescence of the inhibitor molecule, (λ_{Ex} = 360 nm, λ_{Em} = 440 nm) using a Synergy 2 microplate reader (BioTek instruments, Inc.). A calibration curve for fluorescence against concentration was generated by dissolving a known concentration of the molecule in DMSO and creating a dilution series with PBS (pH 7.4). Fluorescence was then measured for the test compound and compared to the standard curve and the inhibitor. The amount of inhibitor present could then be determined as a mol/w or w/w ratio.

2.2 Biological evaluation

2.2.1 Cell lines and culture

3E3 and 3V5 cell lines were obtained from CRUK, Clare Hall, South Mimms. 3E3 ovarian cancer cells have previously been engineered from Ovcar-3 cells to express autotaxin[178] whereas 3V5 cells were transfected with the empty vector. 3E3 and 3V5 cells were maintained in either RPMI growth medium (RPMI 1640, Lonza) supplemented with 10% fetal bovine serum (FBS, Lonza), Penicillin/Streptomycin (50 µg/mL, Lonza) and glutamine (2 mM, Lonza). Caco2 cells were obtained from Sigma Aldrich and maintained in Eagle's Minimum Essential medium (EMEM, Lonza) supplemented with 10% fetal bovine serum (FBS, Lonza), Penicillin/Streptomycin (50 U/mL, Lonza) and glutamine (2 mM, Lonza), HEPES (1% v/v, Lonza), MEM non-essential amino acid solution (1% v/v, Sigma). Cells were grown at 37 °C in 5% CO_2 in a NAPCO heater jacket incubator (Precision Scientific).

2.2.2 Cell passage and counting

To passage cells, the growth medium was removed and cells were washed with phosphate buffered saline (PBS, 2 mL, Lonza). To detach the cells, trypsin (1 mL, Lonza) was added and the cells were incubated at 37 °C for up to 10 min until cells were detached. The trypsin was quenched with appropriate growth medium (1 mL) and the cells were transferred into a sterile 15 mL tube (Sarstedt). The cells were centrifuged (150 g, 3 min, room temperature, Thermo Scientific Heraeus Megafuge 8), the supernatant was aspirated and the cell pellet re-suspended in the appropriate growth medium before adding to a new flask containing fresh medium (sterile T25 or T75 cell culture flask, Sarstedt). When the cells were prepared for an experiment the re-suspended cells were counted using a Neubauer haemocytometer (Reichert Brightline), and the appropriate amount of cells were seeded into cell culture plates (96-well, 6-well, Sarstedt).

2.2.3 Cell freezing and recovery

Cells of a low passage number, 50% confluent in a T75 cell culture flask were detached from the plastic with trypsin (2 mL) and the trypsin was quenched with growth medium (2 mL). The cells were collected by centrifugation (150 g, 3 min, room temperature), the supernatant was aspirated and the cells re-suspended in 1 mL freezing medium (growth medium supplemented with FBS (10%) and DMSO (8%, (Sigma Aldrich)). Re-suspended cells were then dispensed into cryovials (0.2 mL, Triple Red) and stored in liquid nitrogen after an initial 24 h at -80 °C in an ultralow freezer (Nuaire).

For cell recovery from liquid nitrogen storage, cells were quickly thawed in a water bath (37 °C, Grant instruments), suspended in growth medium (5 mL), collected by centrifugation (150 g, 3 min, room temperature), the medium was aspirated and the cells were suspended in growth media (1 mL) before adding to a T25 cell culture flask containing growth medium (7 mL). The cells were then maintained as described in section 2.2.2.

2.2.4 Cell proliferation assay

Cells were prepared as described in section 2.2.2. 5,000 cells were seeded per well in 80 µL growth medium in a 96-well plate and incubated for 24 h. The growth medium was removed and the cells were washed with PBS (100 µL). Serum free growth medium containing the desired drug treatment (final volume 100 µL) was then added to the cells which were incubated for 16-72 h. The relative cell number was determined by sulforhodamine B (SRB, Sigma Aldrich) assay. The growth medium was removed from the cells and 100 µL trichloroacetic acid (10%, TCA, Sigma Aldrich) and the cells were incubated on ice for 30 min. The TCA was removed and the plate washed 3 times by immersion in water and dried at room temperature. Once dry, SRB (0.4% in 1% acetic acid, Sigma Aldrich) was added to stain the cells (30 min, room temperature). Excess SRB was removed by washing with acetic acid ((1%) 3 x 100 µL) and the plate was dried at room temperature. The bound stain was solubilized (100 µL, 10 mM Tris (pH 10, Sigma Aldrich)) and absorbance was measured using a Synergy 2 microplate reader (BioTek instruments, Inc.) (λ = 570 nm).

2.2.5 Protein extraction and quantification

Cells were lysed in (100 µl per 10 cm^2) radio-immunoprecipitation buffer (RIPA) containing Hepes (20 mM, CalbioChem), sodium chloride (150 mM, Sigma-Aldrich), ethylene-diamino-tetraacetic acid (2 mM EDTA, Sigma Aldrich), sodium deoxycholate (0.5%, Sigma Aldrich), NP40 (1%, Sigma Aldrich), Leupeptin (120 µM, Sigma Aldrich), Pepstatin (10 µM, Sigma Aldrich) and phenylmethanesulfonyl fluoride (PMSF, 1 mM, Sigma Aldrich). The cell lysate was cleared by centrifugation (2500 g, 4 ℃, 10 min) and the supernatant was transferred into new microcentrifuge tubes and stored at -80°C.

Protein concentration was determined using a Bicinchonic acid (BCA) assay. Bovine serum albumin (BSA, Sigma Aldrich) solution was prepared containing 0.1, 0.25, 0.5, 0.75, 1.0, 1.5 and 2.0 mg/mL BSA to create a standard curve for the assay. BCA reagent was prepared by adding 1:50 copper (II) sulphate solution (Sigma Aldrich) to Bicinchonic acid solution (Sigma Aldrich). The samples or standards (10 µL of sample appropriately diluted with RIPA buffer or BSA standards (10 µL)) were treated with 100 µL of the BCA reagent. After incubation (37°C, 30 min), absorbance was measured using a Synergy 2 multimode microplate reader (BioTek instruments, Inc.) (λ=570 nm). The protein concentration of the lysate was calculated from a calibration curve constructed using the protein standard by linear regression.

2.2.6 Western blotting

The cell lysates were prepared as described above and diluted 1:4 with NuSep sample buffer ((Invitrogen), containing 5% v/v 2-mercaptoethanol, (Sigma Aldrich)) and mixed. The samples were denatured by heating (15 min, 70 °C) and collected by brief centrifugation (10,000 g, 30 secs, room temperature). The appropriate volume of sample (10 µg protein) was loaded on a 4-20% Tris-Glycine gel (NuSep) and run in an electrophoresis module (XCell SureLock Mini Cell, Invitrogen), at 75 V for 1 h 15 min in hepes running buffer (100 mM hepes, 100 mM Tris and 1% sodium dodecyl sulphate (SDS, Sigma Aldrich), a PageRuler protein Ladder (Thermo Scientific) was loaded onto each gel to estimate protein size. Protein was then transferred to polyvinylidene difluoride (PVDF) membranes

(GE healthcare Life Sciences) at 25 V for 2 h in NuSep transfer buffer (25 mM Tris HCl (pH 7.5, Sigma Aldrich), 200 mM glycine (Sigma Aldrich), 0.075% SDS and 10% methanol (Sigma Aldrich)). The membrane was blocked using Tris-buffered saline with Tween (TBST, (50 mM Tris HCl, 150 mM NaCl and 1% Tween) containing 5% w/v low-fat dry milk powder) for 1 h at room temperature with shaking (Stuart Scientific Platform Shaker STR6). The blocking solution was removed and the primary antibody, diluted to the appropriate concentration in TBST containing 5% w/v low-fat dry milk powder (see Table 2.1), was added and incubated for 16 h at 5 °C with shaking. The membrane was washed (TBST, 3x 5 min) and the secondary antibody, diluted to the appropriate concentration in TBST containing 5% w/v low-fat dry milk powder (see Table 2.1), was then added and the membrane was incubated for 1 h at room temperature with shaking. The membrane was washed (TBST 5x 5 min) and then incubated with the chemiluminescent substrate (uptilight HS HRP, Uptima) and visualised using FluorChem M imager (Protein Simple).

Antibody	**Dilution factor**	**Source**
GAPDH	1:5000	Millipore
Anti-mouse	1:2000	Cell Signaling Technology
Anti-rabbit	1:2000	Cell Signaling Technology
Autotaxin	1:500	Santa Cruz Biotechnology

Table 2.1: Antibodies used for protein immunodection.

2.2.7 Purification of autotaxin

In order to efficiently test compounds for activity against autotaxin, a suitable assay was required. The cell line 3E3 has previously been derived from OVCAR-3 to ectopically express autotaxin.[178] And this was used as one source of autotaxin. The cell line 3V5 which had been transfected with the empty vector was used as a control.

Purification of autotaxin from 3E3 cell supernatant was achieved with Concanavalin A (Con A) affinity chromatography. Con A is a protein which specifically binds to carbohydrate molecules, allowing the separation of glycoproteins. Autotaxin is a glycoprotein and so is retained by the Con A on the column. Autotaxin can be eluted with α-methylmannoside which has a high affinity for Con A.

To purify autotaxin, 3E3 cells were seeded in a T75 flask and when 50% confluent the medium was replaced with serum free medium (10 mL) and incubated overnight. The next day the supernatant was collected and cleared by centrifugation (2600 g, 4 °C, 15 min). The supernatant was loaded onto a HiTrap Con A sepharose column (GE healthcare) and recirculated for 1 h at 4 °C. 20 mL Tris buffered saline (TBS; 20 mM Tris, 0.5 M NaCl, pH 7.4) was passed through the column and autotaxin was eluted with 2 mL α-methylmannoside (0.5 M, (Sigma Aldrich)) in TBS at 4 °C for 24 h. The next day, a 2 mL fraction was collected, and dialysed against TBS (1 L) with a dialysis membrane (MWCO 8 KDa, Biodesign) at 4 °C. The retentate was then used directly as the source of autotaxin for the bis-*p*NPP assay.

2.2.8 Bis-*p*NPP Assay

In order to quantify autotaxin activity the previously described bis-*p*NPP assay was employed.[203] Bis-*para*-nitrophenylphosphate (bis-*p*NPP) also contains a phosphodiester moiety and so can be considered an analogue of the autotaxin substrate LPC. Autotaxin hydrolyses bis-*p*NPP to form the chromophore *p*-nitrophenol, whose concentration is then measured by absorbance (λ = 405 nm), (Figure 2.1).

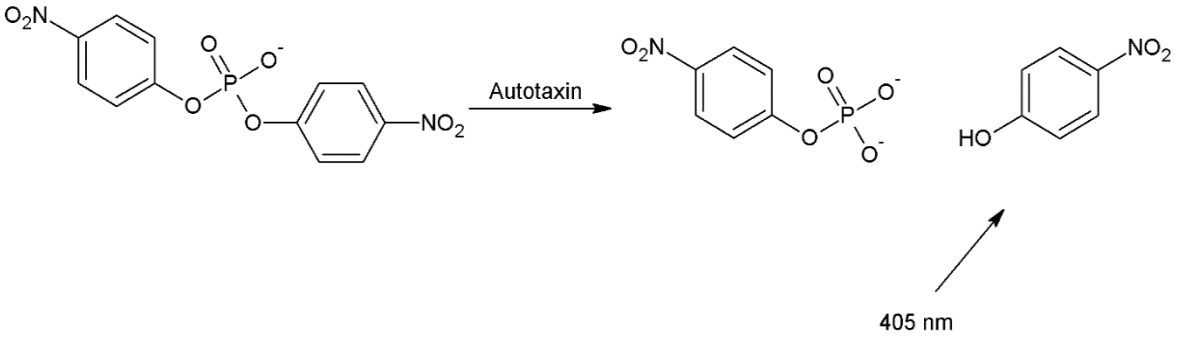

Figure 2.1: Bis-*p*NPP assay reaction; Autotaxin hydrolyses bis-*p*NPP to the chromophore *p*-nitrophenol.

In a 96-well plate, 20 µL 5X reaction buffer (250 mM Tris HCl, 25 mM KCl, 5 mM $CaCl_2$, 5 mM $MgCl_2.6H_2O$, NaCl 700 mM, pH 7.8), 10 µL bis-*p*NPP (1 mM prepared in *d*H_2O), and 20 µL of the test compound were added to each well, followed by the addition of recombinant autotaxin (50 µL per well), purified as described in section 2.2.7. After incubation (37°C, 4 h) absorbance was measured using a Synergy 2 multimode microplate reader (BioTek instruments, Inc.) (λ = 405 nm). Data was analysed using GraphPad Prism software (GraphPad Software, Inc.). Non-linear regression was used to fit a 4 parameter (Hill equation) sigmoidal dose-response curve to determine the IC_{50}.

2.2.9 FS-3 assay

Inhibition of autotaxin activity was also evaluated using a commercially available assay to measure the hydrolysis of FS-3, a fluorescence-quenched analogue of LPC (Echelon Biosciences, Inc. Salt Lake City, UT), (Figure 2.2).[246]

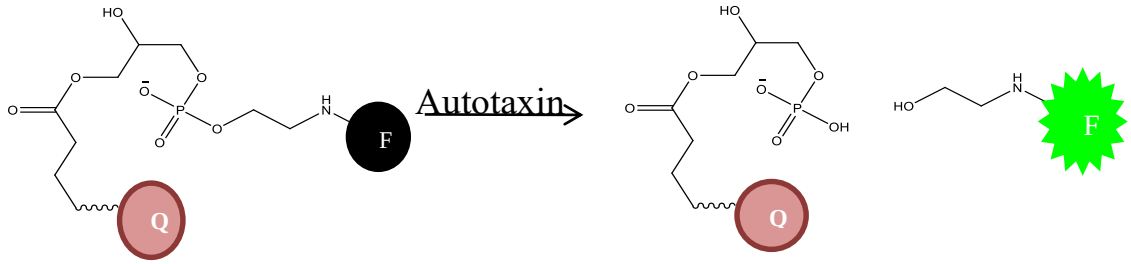

Figure 2.2: FS-3 assay reaction; Autotaxin hydrolyses FS-3 which releases the fluorescent molecule to be measured.

Reaction buffer containing autotaxin (80 µL per well, made as specified in the autotaxin inhibition kit protocol) and sample compounds (10 µL per well) appropriately diluted, were mixed in a white 96 well plate using a rocker for 1 min and then pre-incubated for 10 min at 37 °C. Subsequently, FS-3 substrate ((10 µL per well), 10 µM stock solution in dH$_2$O) was added and mixed for 3 minutes on a rocker. The final concentration of autotaxin and FS-3 substrate per well was 2 nM and 1 µM, respectively. The Synergy 2 multimode microplate reader (BioTek instruments, Inc.) was used to maintain the samples (λ_{Ex} = 485 nm, λ_{Em} = 528 nm) at 37 °C and fluorescence was measured every two minutes for 30 min. The rate of hydrolysis was determined using linear regression for the data from the period over which the fluorescence increased linearly with time. The reaction rates for each sample were analysed using GraphPad Prism software. Non-linear regression was used to fit a 4 parameter (Hill equation) sigmoidal dose-response to determine the IC_{50}. A control using BrP-LPA standards was performed with each screen. A secondary screen was performed to ensure the inhibitor activity identified in the initial screen was not due to interference with the fluorescence of hydrolysed FS-3. In the second screen the fluorescence of fluorescein was measured in the presence of the compounds. Fluorescein buffer ((90 µL per well) made as specified in autotaxin inhibition kit protocol) and either dH$_2$O, BrP-LPA or sample compound (10 µL per well) were added per well and the plate was incubated at 37°C for 10 mins. Fluorescence was then measured (λ_{Ex} = 485 nm, λ_{Em} = 528 nm). The data was then averaged and the background fluorescence was subtracted. The percentage inhibition of fluorescein fluorescence was calculated using the following equation:

$$Percent\ inhibition\ Sample = \left[1 - \left(\left(\frac{(C1 + C2)}{2}\right) - \left(\frac{(A1 + A2)}{2}\right)\right) / \left(\left(\frac{(B1 + B2)}{2}\right) - \left(\frac{(A1 + A2)}{2}\right)\right)\right] * 100$$

Equation 2.1: Percentage sample inhibition; Where A represents the background fluorescence in the absence of inhibitor and fluorescein, B represents fluorescence in the absence of the inhibitor and C represents fluorescent in the presence of the inhibitor; "1" and "2" represent duplicate readings.

2.2.10 Wound healing assay

Cells were plated at a density of 200,000 cells/mL in 6-well plates using growth medium. When the cells had reached confluence the medium was removed and a P200 plastic pipette tip was drawn across the centre of the plate to produce a clean wound area. The wells were washed gently twice with PBS to remove any debris and remaining FBS. The medium was then replaced with serum free medium supplemented with lysophosphatidyl choline (0.5 μM), and the compound to be tested. DMSO was added to each well as necessary to normalise the DMSO concentration to 0.5%. The cells were viewed and photographed by phase contrast microscopy immediately after wounding. After incubation at 37 °C for 16 h the cells were stained and fixed with methylene blue (200 μL, 30 min, room temperature, (Sigma Aldrich); 0.5% w/v in 50% H_2O, 50% EtOH) and photographed by phase contrast microscopy. The wound closure was measured using imageJ software. A calibration image was used to determine distance (μm). The area of a section of the wound pre- and post-migration was then measured and the percentage wound closure was calculated as;

$$Percentage\ wound\ closure = \left(\frac{(a_b - a_a)}{a_b}\right) * 100$$

Equation 2.2: Calculation of percentage wound closure; Where a_b represents the area of the wound immediately after wounding and a_a represents the area of the wound after migration.

2.2.11 Caspase 3/7 activity assay

3E3 and 3V5 cells were plated at a density of 5,000 cells per well in a 96-well plate in 80 μL of growth medium and incubated for 24 h. The medium was removed and the cells were washed with PBS. 100 μL of serum free medium supplemented with LPC (0.5 μM, Sigma Aldrich) and the indicated combinations of carboplatin (300 μM), and compound to be tested were then added and the cells were incubated for 18 h. The cells were centrifuged (1000 g, 2 min), the supernatant was removed and 30 μL PBS and 30 μL of Caspase-Glo 3/7 reagent (Promega) were added and cells were incubated for 30 minutes at room temperature in the dark. Luminescence was then measured using

Synergy 2 multimode microplate reader. To normalise for cell number, identical samples were prepared in parallel and stained with SRB as described in section 2.2.4.[247]

2.2.12 Parallel Artificial Membrane Permeation Assay (PAMPA)

MultiScreen Filter Plates (Millipore) were used for PAMPA. Test compounds were dissolved in DMSO and diluted with PBS (pH 7.4) to a final 2% DMSO concentration. Propranolol (highly permeable) and furosemide (poorly permeable) were used as a controls for permeability alongside each assay; solutions of these (100 µM) were made in PBS (containing 2% DMSO). The limit of quantification (LOQ) by UV/Vis spectroscopy and fluorescence spectroscopy of each compound was determined before each experiment. A 2-fold serial dilution for each compound in PBS (2% DSMO) starting at 100 µM was performed and the absorption or fluorescence measured and a peak maximum was plotted for each compound against concentration. The LOQ was defined as the concentration of compound whose absorbance/emission background + 5 S.D. A 1% solution (w/v) of Lecithin (Sigma Aldrich) in dodecane (Sigma Aldrich) was prepared and sonicated for 30 mins until complete dissolution. 5 µL per well of the lecithin mixture was pipetted onto each well of the donor plate (MAIPN4510, Millipore), directly followed by the addition of 150 µL of the test compound solution. The donor plate top compartment was then placed in the PTFE acceptor plate (MSSACCEPTOR, Millipore), each well of the acceptor plate contained 300 µL of PBS (2% DMSO). The plates were incubated in a moist environment, to avoid evaporation, at room temperature for 48 h. After incubation, UV/Vis absorption from 250 nm to 500 nm or the fluorescence emission (λ_{Ex} = 485 nm, λ_{Em} = 528 nm), was measured using 100 µL per well of the donor solution and 100 µL per well of the acceptor solution. Compound solutions were also made up at the theoretical equilibrium concentration and the fluorescence emission or UV/Vis absorption was measured sing 100 µL per compound. The analysis was performed in triplicate. The following equation was used to calculate Log Pe.

$$Log\ Pe = Log\left\{C \cdot \ln\left(1 - \frac{[Drug]_{acceptor}}{[Drug]_{equilibrium}}\right)\right\}$$

$$where\ C = (V_D \cdot \frac{V_A}{(V_D + V_A)Area} \cdot time)$$

Equation 2.3: Calculation of Log Pe; Where V_D is the volume of the donor solution in cm^3 and V_A is the volume of the acceptor solution in cm^3. Area is the Surface area of the membrane in cm^2 and time is the length of incubation in seconds.

2.2.13 Caco-2 permeability

Caco-2 cells were maintained as described in section 2.2.2. 100,000 cell/cm^2 were plated in transwells (surface area 0.33 cm^2, 0.4 µm pore size, Greiner Bio-One) which were placed in 24-well plates containing 500 µL medium per well and cultures for 28 days changing the medium every three days. On the day of the experiment the Trans Epithelial Electrical Resistance (TEER) was measured using a Millicell® ERS-2 Voltohmmeter (MerkMilipore) a TEER value threshold of 200 Ω.cm^2 was used to confirm an intact monolayer. Medium was changed to serum free medium in both the apical and basolateral side. After 3 h, the medium was removed, the cells were washed twice with Hank's Balance Salt Solution (HBSS, Lonza). 500 µL of HBSS was placed in the basolateral side and 500 µL of HBSS containing the test compound was added to the apical side. 200 µL was immediately removed from the apical side for a T0 reading. The cells were incubated for 2 h at 37 °C, after which the supernatant was collected from both the apical and basolateral side. The fluorescence ($\lambda_{Ex.}$ = 360 nm, $\lambda_{Em.}$ = 440 nm) of 100 µL of each sample was measured using a Synergy 2 multimode microplate reader. The concentration of the compounds was calculated from a standard curve of fluorescence and the permeability was calculated according to the following equation:

$$P_{app} = \left(\frac{D_Q}{D_t}\right).SA.[drug]$$

Equation 2.4: Calculation of P_{app}; Where D_Q is the molar concentration Dt is the time in seconds, SA is the surface area of the membrane in cm^2.

2.2.14 Solubility

2.2.14.1 Kinetic solubility

The compound was diluted in Tris HCl buffer from a 1 mM stock in DMSO. The solution was shaken on a rocker for 2 h to dissolve followed by centrifugation at 10, 000 g for 20 min. The absorbance was measure using a NanoDrop 2000 spectrophotometer (ThermoScientific). The analysis was performed in duplicate. The concentration of the sample was calculated from a standard absorbance curve of the test compound in Tris buffer containing DMSO, utilising the beer-lambert law.

$$A = \varepsilon cl$$

Equation 2.5: Beer-Lambert law.

2.2.14.2 Thermodynamic solubility

The miniaturised shake flask method was used to measure the thermodynamic solubility of the compounds. An excess of the compound to be tested was placed into a 1.5 mL microcentrifuge tube and to this 200 µL of PBS was added. Compounds were shaken for 24 h at room temperature in order to achieve equilibrium. After equilibration, the tubes were centrifuged at 10000 g for 20 min. The fluorescence, ($\lambda_{Ex.}$ = 360 nm, $\lambda_{Em.}$ = 440 nm) of 100 µL of the supernatant was measured using a Synergy 2 multimode microplate reader. The concentration of the solution was determined according to a calibration curve of test compound. The calibration curve was generated by linear regression analysis of the fluorescence of the reference samples. The analysis was performed in triplicate.

Chapter 3

Synthesis and biological evaluation of a dendrimer-autotaxin inhibitor conjugate

3.1 Introduction

As previously discussed, autotaxin is the main enzyme which catalyses the production of LPA, and consequently stimulates cell migration, proliferation and survival in many cancer types including ovarian cancer. There are currently many autotaxin inhibitors in development due to autotaxin's emerging role in the pathogenesis of cancer and other diseases. Some of the first autotaxin inhibitors were analogues of LPA, based on observed product inhibition.[203] Analogues of LPA which function as competitive autotaxin inhibitors are lipophilic due to the extended alkyl chain and therefore have poor bioavailability and poor solubility; they may also be susceptible to degradation by endogenous hydrolytic pathways. One of the most potent LPA analogues described to date is S32826, **15,** as shown in Figure 3.1.[83] This compound exhibited nanomolar inhibition of autotaxin *in vitro* and reduced the amount of LPA present in plasma and ascites *ex vivo*.[83] However, when tested *in vivo* no inhibition of LPA production in plasma was observed a few minutes after administration.[83] This may be due to the poor pharmacokinetic profile associated with LPA analogues.

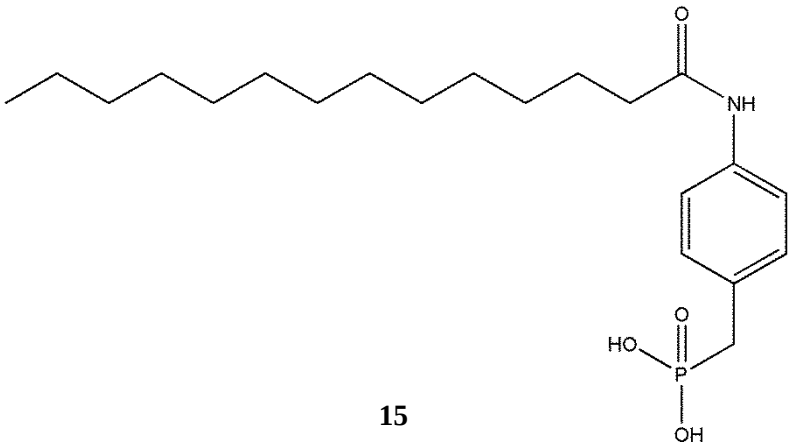

15

Figure 3.1: Structure of S32826.

Dendrimers are highly branched macromolecules of low poly-dispersity with a multifunctional central core molecule, and branches of various lengths, as shown in Figure 3.2.[240, 248] In general dendrimers are spherical with small molecular size but high molecular weights. The multiple surface groups of dendrimers offer the opportunity to covalently attach multiple drug molecules per dendrimer.[249-250] The larger hydrodynamic volume of polymers has the potential to increase the half-

life of a drug molecule in plasma and ascites, increasing the probability of tumour accumulation.[251-252] A larger hydrodynamic volume leads to reduced renal clearing and can also provide a shielding effect from chemical or enzymatic degradation of the drug. Macromolecules such as dendrimers can directly target the tumour via the EPR effect; this occurs due to the increased capillary permeability observed in tumours.[243] Furthermore, the multiple surface groups of dendrimers also allow the possibility of attaching targeting agents such as folic acid which has a high affinity for the folate receptor that is overexpressed in many epithelial cancers including ovarian cancer.[253] The conjugation of drug molecules to dendrimers can also increase their metabolic stability.[240, 254] An example of improved pharmacokinetics due to conjugation to a dendrimer is a PAMAM-cisplatin conjugate. Cisplatin is poorly soluble in aqueous solution and associated with significant toxicity. Upon conjugation, increased solubility and a decrease in systemic toxicity was observed.[255]

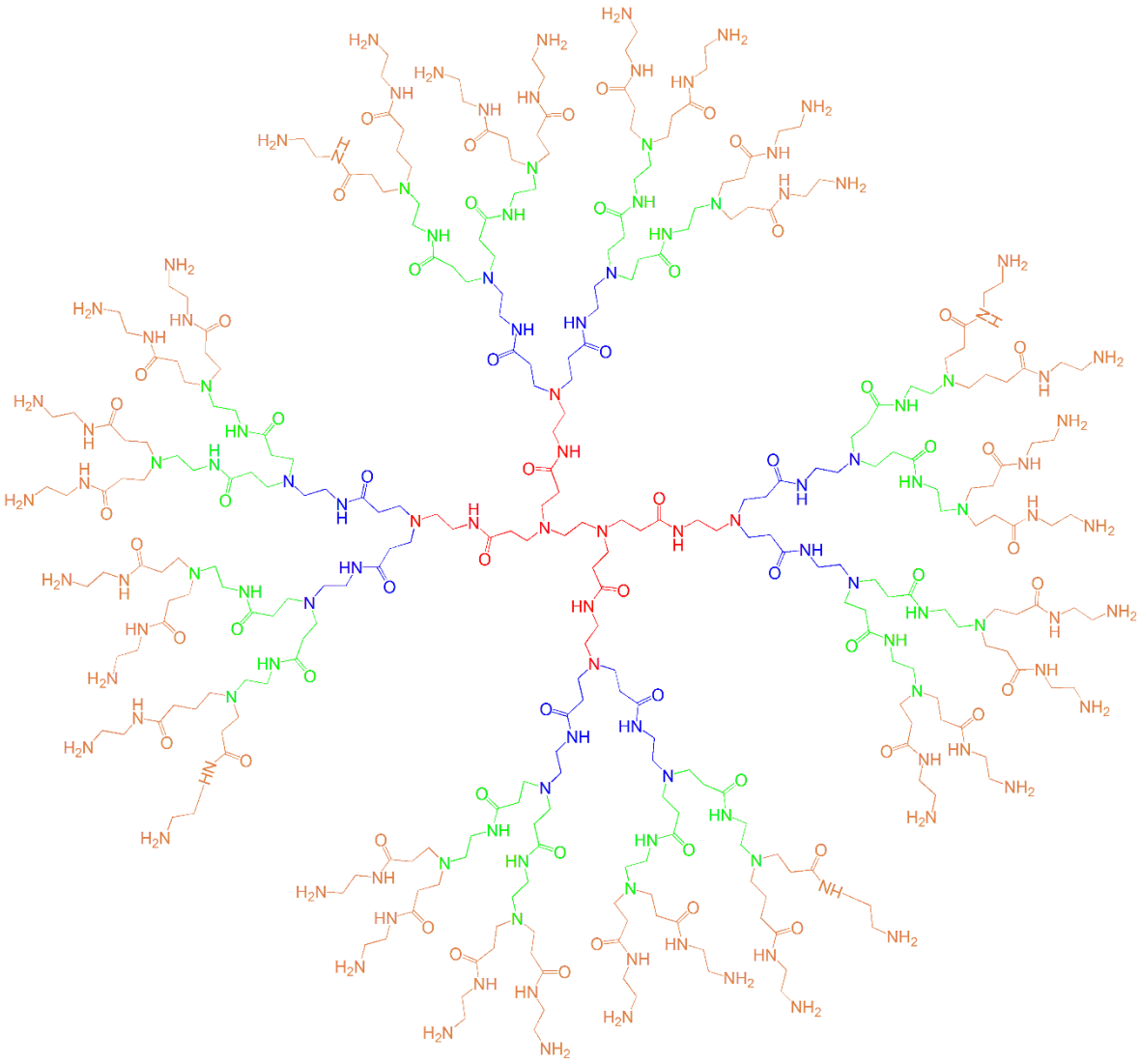

Figure 3.2: Structure of G3 PAMAM dendrimer. The Core is shown in red and successive generations are shown in blue, green and orange, respectively.

Attaching the lipophilic autotaxin inhibitor S32826 **15** to a G3 PAMAM dendrimer has the potential to prolong the retention of the inhibitor in circulation and in the peritoneal cavity. When designing the dendrimer-S32826 conjugate the crystal structure of autotaxin had not yet been determined. It was theorised that the alkyl chain of LPC would be buried in the plasma membrane and therefore be free from the enzyme. It was also hypothesised that the alkyl chain of S32826 would behave similarly to the alkyl chain of LPC leaving the alkyl chain free from the active site and so a suitable place to attach to the dendrimer.

In this chapter the conjugation of S32826 to a dendrimer was evaluated. However, this necessitated confirmation that conjugation of the autotaxin inhibitor to a dendrimer would not impair its ability

to inhibit autotaxin. Firstly, the synthesis of a novel drug conjugate of the potent autotaxin inhibitor, S32826 with a 3rd generation (G3) PAMAM dendrimer is described. Then the conjugate's ability to inhibit autotaxin *in vitro*, was assessed using two autotaxin inhibitor assays. Two assays were used to confirm the conjugate retained biological activity. The role of autotaxin and LPA in cell migration is well documented, with inhibition of autotaxin previously shown to decrease migration. The conjugate was assessed for activity in an ovarian cancer cell migration model. Due to autotaxin previously being shown to delay apoptosis induced by carboplatin;[178] the conjugate's ability to potentiate apoptosis in a cytotoxicity assay in combination with carboplatin was investigated.

3.2 Materials and methods

3.2.1 Solubility

Solubility was measured as described in section 2.2.14.1 and adapted as follows. A solution of conjugate 1 in DMSO (1 mM) was diluted in Tris HCl buffer increasing the concentration of the conjugate until the conjugate began to precipitate. The saturated solution was shaken on a rocker for 2 h to equilibrate followed by centrifugation at 10000 g for 20 min. Absorbance (λ 277) of the solution was measured. The concentration of the solution was determined using a standard curve of absorbance.

3.2.2 FS-3 assay

Compounds were tested for autotaxin inhibition using the FS-3 assay as described in section 2.2.11 and adapted as follows. Conjugate 1 (10 μM) was prepared as a stock solution in DMSO, and the G3 PAMAM dendrimer (1 mM) in Tris HCl buffer. A range of concentrations were prepared with a 3-fold serial dilution in Tris buffer. 80 μL reaction buffer, containing autotaxin, and 10 μL of standard, compound or vehicle were pre-incubated for 10 min at 37 °C. 10 μL FS-3 substrate was added and fluorescence was measured at 37 °C every two minutes for 30 min.

3.2.3 Bis-pNPP Assay

Compounds were further tested for their ability to inhibit autotaxin in the bis-*p*NPP assay as described in section 2.2.10 and adapted as follows. S32826 (1 mM), S32826-acetamide (10 μM) and conjugate 1 (10 μM) were prepared as a stock solution in DMSO, and the G3 PAMAM dendrimer (1 mM) in Tris HCl buffer. S32826-acetamide, conjugate 1 and G3 PAMAM dendrimer were diluted 2-fold in Tris HCl buffer to yield a range of concentrations. 5X Bis-*p*NPP assay reaction buffer 20 μL, 10 μL bis-*p*NPP (1 mM) and 20 μL of compound dilution or solvent was added to each well, followed by the addition of 50 μL autotaxin solution. Absorbance was measured after 4 h incubation.

3.2.4 Wound healing assay

The ability of the compound to inhibit migration was tested in the wound healing assay as described in section 2.2.12 and adapted as follows. Serum free growth medium was supplemented with LPC (0.5 μM), DMSO (normalised to 0.5%) and either no inhibitor, S32826 (30 nM) or conjugate 1 (1.3 μM or 2.6 μM) and 1 mL of the medium mixture was added per well. The percentage wound closure was measured after 16 h.

3.2.5 Caspase 3/7 activity assay

The ability of the compounds to potentiate apoptosis induced by carboplatin was tested using the Caspase 3/7 assay as described in section 2.2.13 and adapted as follows. The cells were incubated with serum free medium supplemented with LPC (0.5 μM) and the indicated combinations of carboplatin (300 μM), S32826 (300 nM) or Conjugate 1 (10 μM) for 18 h. After 30 min incubation with the Caspase-Glo 3/7 reagent, the fluorescence was measured.

3.3 Results

3.3.1 Synthesis of Conjugate 1

To couple S32826 to the PAMAM dendrimer, a reactive moiety was required. The commercially available [4-(12-amino-dodecanoylamino) benzyl] phosphonic acid diethyl ester **30** was converted to the intermediate acrylamide phosphonate **31** via a nucleophilic addition-elimination with acryloyl chloride. This reaction was performed at 0 °C with triethylamine in dichloromethane to yield the desired intermediate **31** (43%), as shown in Scheme 3.1.

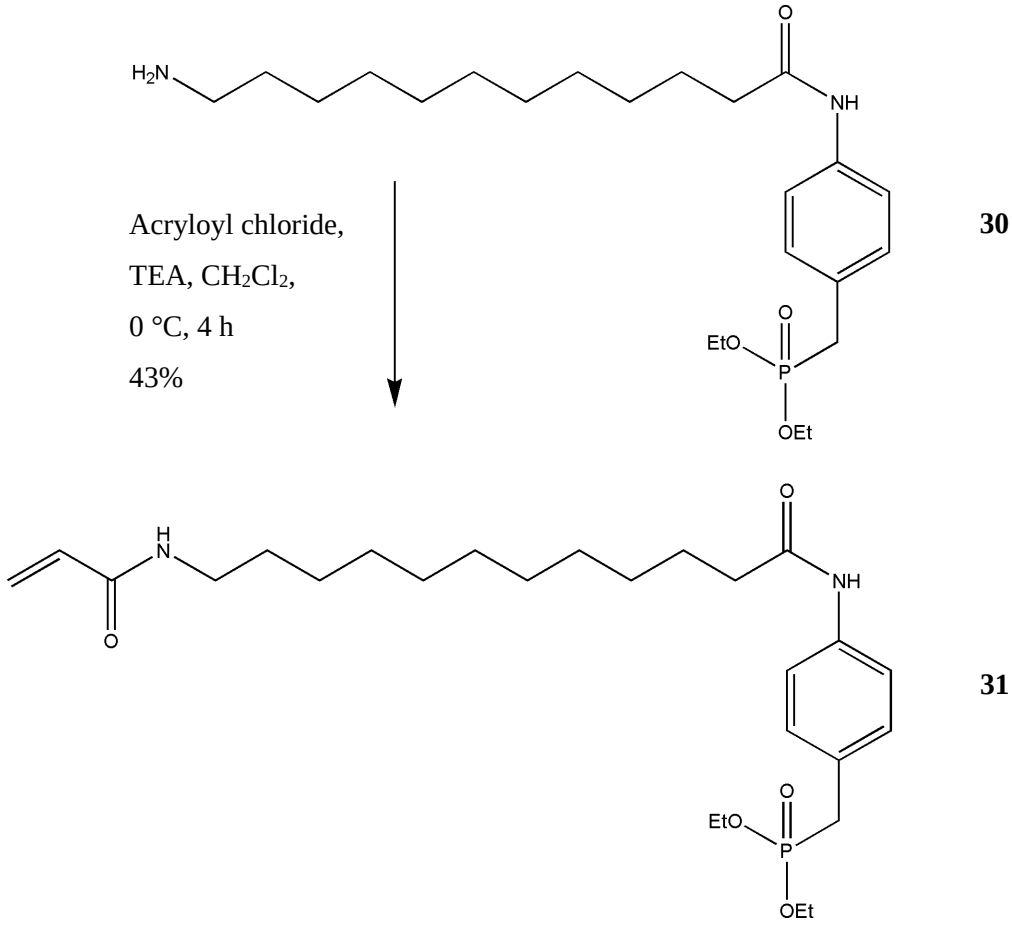

Scheme 3.1: Synthesis of S32826-acrylamide.

Intermediate **31** was then conjugated to the G3 PAMAM dendrimer through a conjugate addition reaction. The intermediate (128 equiv.) and G3 PAMAM dendrimer were dissolved in ethanol and heated to 100°C in a sealed reaction tube for 48 h. The reaction mixture was then dialysed in methanol

to remove any unreacted acrylamide, yielding the desired dendrimer S32826-ester conjugate **32** (30%) based on the dendrimer used, as shown in Scheme 3.2.

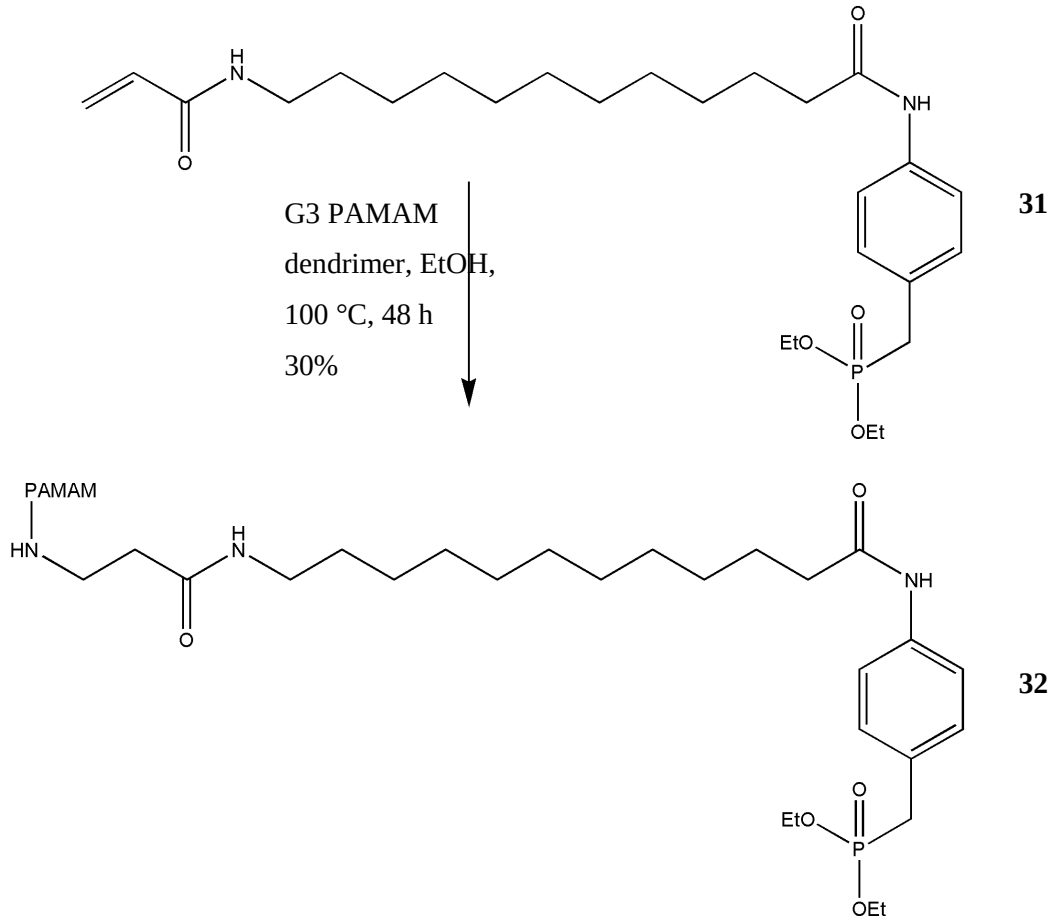

Scheme 3.2: Conjugation to the dendrimer.

Removal of the ethyl protecting groups to reveal the phosphonic acid necessary for binding to the zinc ions in the catalytic site of autotaxin was achieved by treating compound **31** with an excess of trimethylsilyl iodide in methanol to yield the final dendrimer-autotaxin inhibitor conjugate, conjugate 1 (9%), as shown in Scheme 3.3.

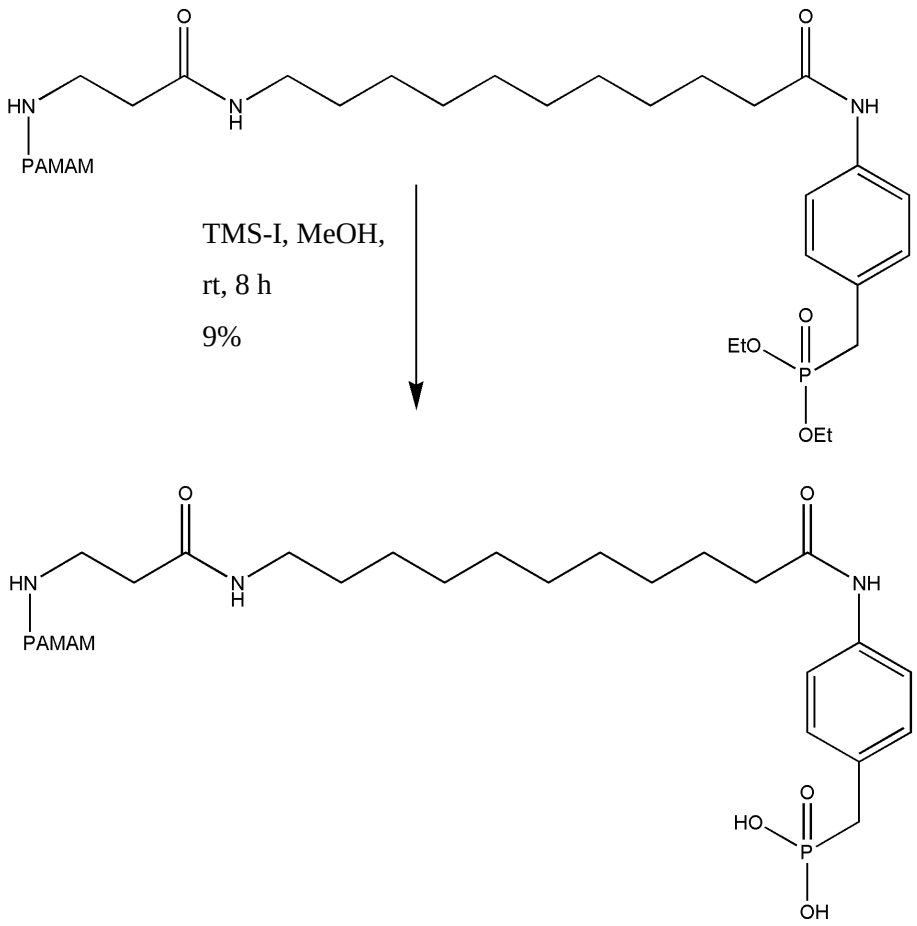

Scheme 3.3: Phosphonate deprotection of the conjugate.

The mechanism for cleavage of phosphonate esters with TMS-I proceeds via a two-step reaction the lone pair of the phosphoryl oxygen attacks the partially positive silicon of TMS-I, the displaced halide ion then attacks one of the alkoxy groups of the phosphonate forming the trimethylsilyl phosphonate, the process is then repeated with the other alkoxy group. This is followed by hydrolysis of the bis(trimethylsilyl)-phosphonate to form the desired phosphonic acid, as shown in Scheme 3.4.

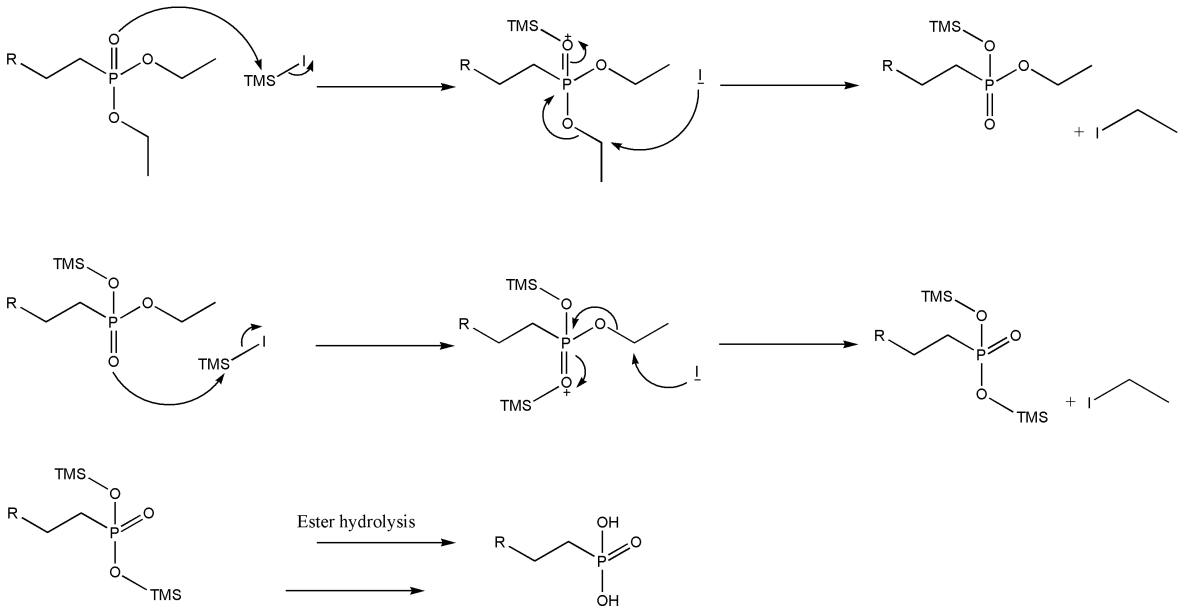

Scheme 3.4: Mechanism of hydrolysis of dialkylphosphonate with trimethylsilyl iodide.

3.3.2 Derivatisation of the terminal amine of S32826

A further analogue of S32826 was prepared in which the terminal amine was converted to an acetamide moiety. This compound mimics the inhibitor coupled to the amine (in particular, lacking the positive charge that the free amine would endow) but lacks the steric bulk of the dendrimer. It provides a useful control to help understand the effect of modifying the inhibitor on the inhibitor's activity. The terminal amine of [4-(12-amino-dodecanoylamino) benzyl] phosphonic acid diethyl ester **30** was converted to the amide with acetic anhydride, in pyridine to yield the acrylamide phosphonic diethyl ester **34** (85%), The resulting acetamide **34** was deprotected as before utilising TMS-I to yield the acetamide phosphonic acid **35** (97%), as shown in Scheme 3.5.

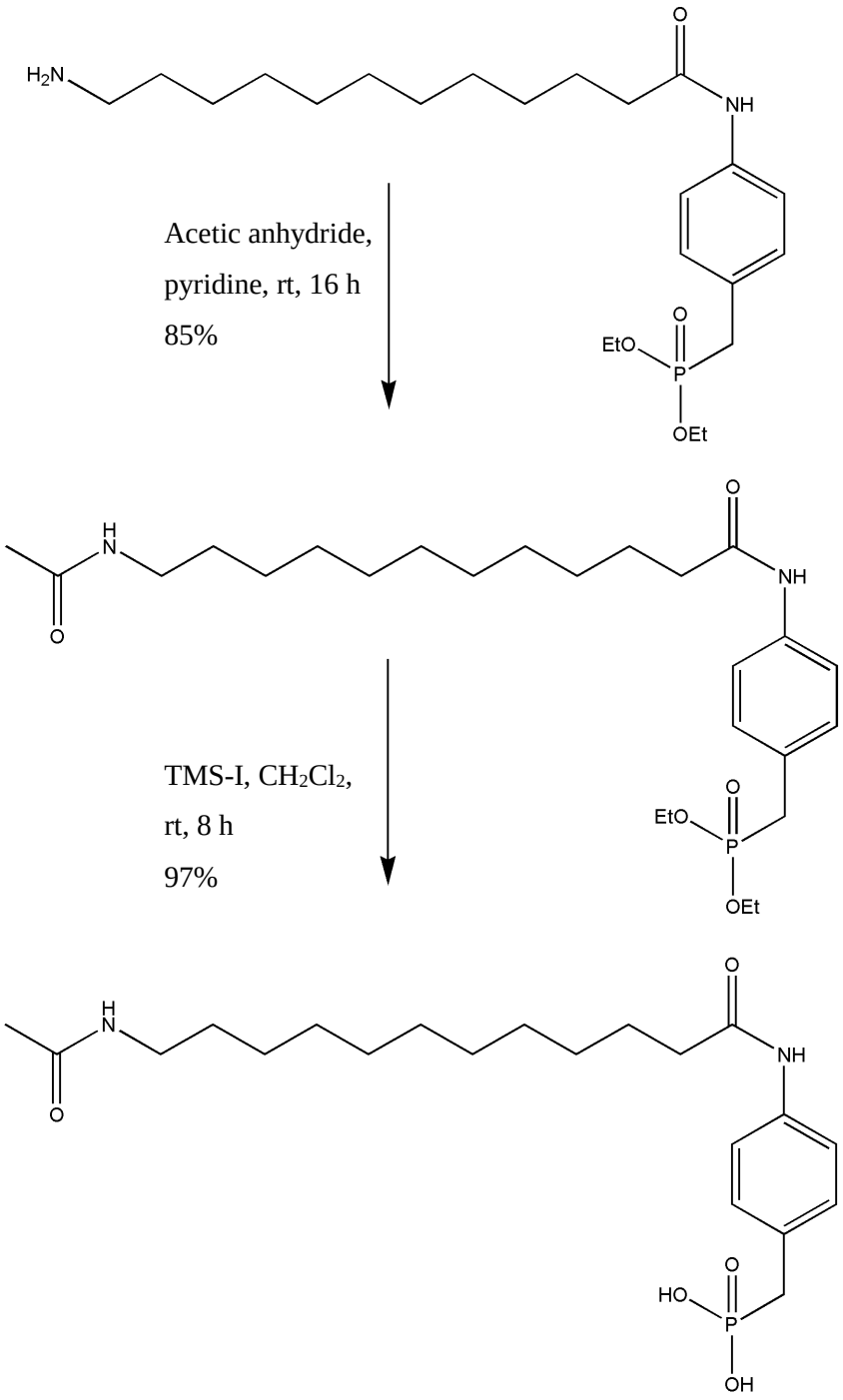

Scheme 3.5: Synthesis of S32826-acetamide.

3.3.3 Structural analysis of Conjugate 1

The structure of conjugate 1 was supported by ^{1}H NMR, IR spectroscopy and elemental analysis. The ^{1}H NMR spectrum showed evidence that conjugation has occurred

by presence of the aromatic peaks at 7.00-7.600 ppm, as shown in Figure 3.3.

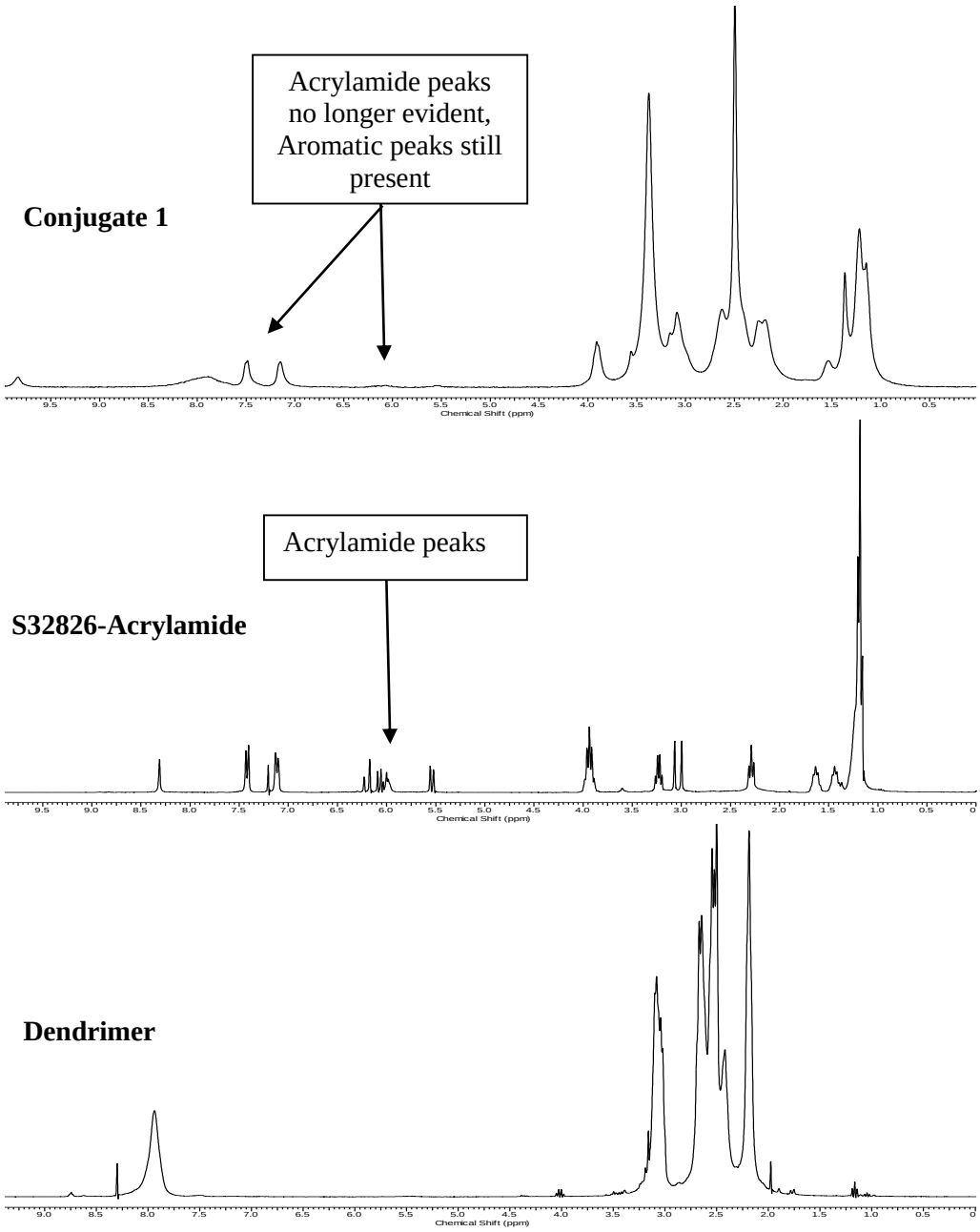

Figure 3.3: ^{1}H NMR spectrum for conjugate 1.Comparison of the ^{1}H NMR spectrum for acrylamide intermediate, G3 PAMAM dendrimer and conjugate 1.

The structure of conjugate 1 was further confirmed by IR analysis. Analysis shows the presence of a peak at 1709 cm^{-1} which may correspond to the amide formed when conjugated, not present in either the S32826-acrylamide or the G3 PAMAM dendrimer, as shown in Figure 3.4.

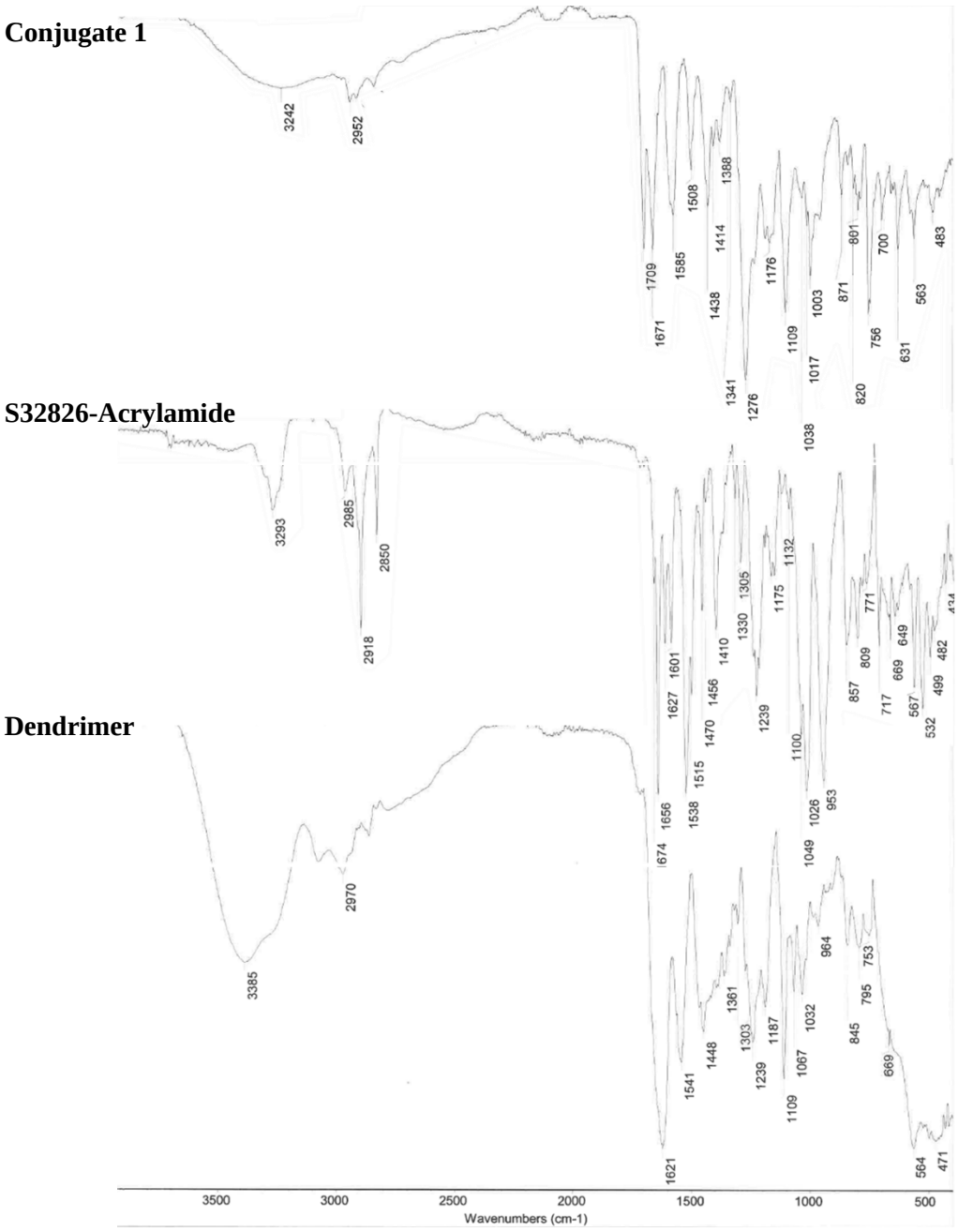

Figure 3.4: IR spectra of conjugate 1; Dendrimer (Bottom), S32826-acrylamide (Middle), Conjugate 1 (Top).

3.3.4 Determination of degree of substitution

The success of coupling the inhibitor to the G3 PAMAM dendrimer was established by measuring the elemental ratio of the phosphorus (only present in the inhibitor molecule) compared to nitrogen in conjugate 1. The elemental analysis suggested essentially complete coupling to the 32 terminal amines in the G3 PAMAM dendrimer, with a ratio of Phosphorus to Nitrogen of ~0.38 which

corresponds favourably to the theoretical ratio for maximum conjugation, 0.43. The elemental ratio of the phosphorous was also compared to carbon and hydrogen. The ratio of phosphorus to carbon and hydrogen also gave similar ratios to that expected of maximum conjugation, as shown in Table 3.1.

	Percentage (%)		**Ratio compared to P**	
Element	**Theoretical**	**Found**	**Theoretical**	**Found**
C	56.92	45.65	0.0834	0.0740
H	8.47	6.14	0.207	0.550
N	12.68	8.45	0.380	0.400
O	17.11	-	-	-
P	4.82	3.38	-	-

Table 3.1: Elemental analysis of conjugate 1; Comparison to theoretical fully substituted G3 PAMAM dendrimer of the elemental analysis results of conjugate 1.

3.3.5 Solubility

The kinetic solubility of conjugate 1 was measured. Solubility was determined by measuring absorbance of a 2mg/mL solution of conjugate 1 in Tris HCl buffer. The concentration was calculated using a standard curve of absorbance versus concentration. The concentration of conjugate 1 in solution was found to be 91 µM.

3.3.6 Inhibition of autotaxin activity

The ability of conjugate 1 to inhibit autotaxin was evaluated in two autotaxin enzyme assays measuring hydrolysis of either FS-3 [246] or bis-*p*NPP [203] substrates.

3.3.6.1 FS-3 assay

Conjugate 1 demonstrated only a moderate decrease in apparent potency after coupling to the dendrimer with an IC_{50} of 160 nM (Figure 3.5), compared to the literature value for the free

compound, S32826 with an IC_{50} of 9 nM.[220] The unconjugated dendrimer had no measureable effect in this assay. A secondary screen was also undertaken to ensure the compounds did not interfere with the fluorescence of the FS-3 substrate. None of the compounds tested interfered with substrate fluorescence.

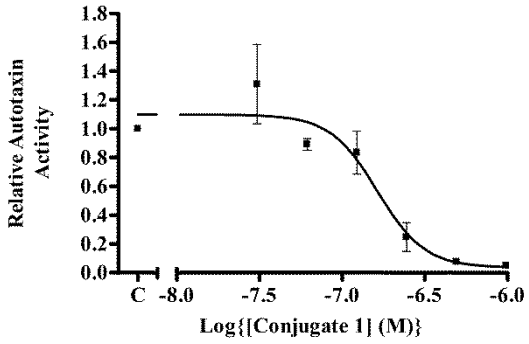

Figure 3.5: Inhibition of autotaxin enzymatic activity by conjugate 1, tested in FS-3 assay; The results are expressed as a fraction (mean ±S.D. n=2) of the activity measured in the absence of the inhibitor. IC_{50} values were calculated as means of IC_{50}s from separate experiments.

3.3.6.2 Bis-pNPP assay

The supernatant from 3E3 cells was used as a source of autotaxin for this assay. To confirm the level of expression of autotaxin the supernatant was analysed in the FS-3 autotaxin inhibitor assay for activity and by western blotting as described in sections 2.2.9 and 2.2.6, respectively. The 3E3 cell supernatant showed sufficient activity in the FS-3 assay and the western blot indicated the presence of autotaxin, (Figure 3.6).

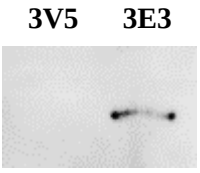

Figure 3.6: 3E3 western blot for autotaxin presence. Conjugate 1 was tested for activity using bis-*p*NPP as the substrate. Autotaxin was purified from 3E3 cells as described in section 2.2.7. A comparable potency was measured using this substrate. Conjugate 1 exhibited an IC_{50} of 1.7 μM,

whereas S32826 had an IC_{50} of 30 nM, (Figure 3.7). The unconjugated dendrimer had no measurable effect on autotaxin activity in this assay.

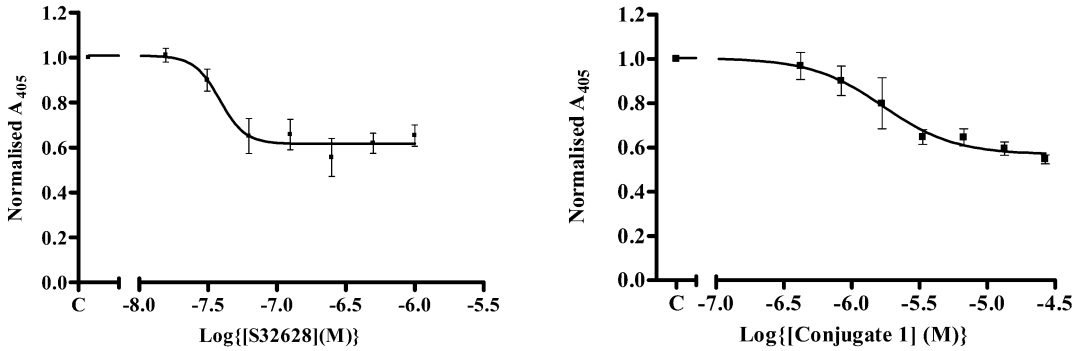

Figure 3.7: Inhibition of autotaxin activity by conjugate 1 and S32826, tested in bis-*p*NPP assay; The results are expressed as a fraction (mean ±S.D. n=3) of the activity measured in the absence of the inhibitor. IC_{50} values were calculated as means of IC_{50}s from separate experiments.

Furthermore, derivatisation of S32826 terminal amine group to an acetamide had no significant effect on autotaxin inhibition, with the compound demonstrating an IC_{50} of 50 nM using bis-*p*NPP as the substrate, (Figure 3.8).

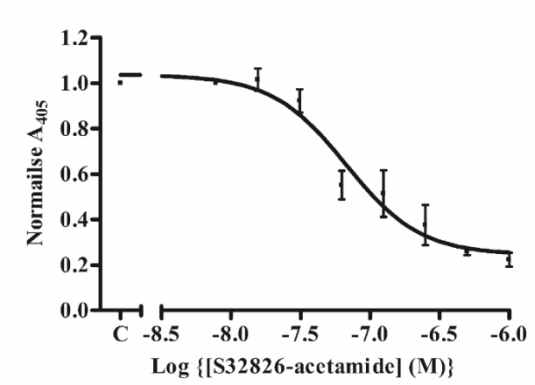

Figure 3.8: Inhibition of autotaxin activity by S32826-acetamide, tested in bis-*p*NPP assay; The results are expressed as a fraction (mean ±S.D. n=2) of the activity measured in the absence of the inhibitor. IC_{50} values were calculated as means of IC_{50}s from separate experiments.

3.3.7 Inhibition of migration

LPA and autotaxin have been shown to regulate cell migration in many cancer cell types including ovarian carcinomas.[141, 256-257] To ensure conjugate 1 retained the ability to inhibit autotaxin in a biological assay, the effect of conjugate 1 on wound healing was evaluated using 3E3 ovarian cancer

cells. 3E3 cells, derived from Ovcar-3 cells and previously engineered to over express autotaxin,[178] were grown to a confluent monolayer. Once an even monolayer had formed a wound was inflicted and the migration of the cells was measured as percentage wound closure, in serum free medium, supplemented with LPC (0.5 μM), containing the autotaxin inhibitor S32826 (30 nM) or conjugate 1 (0.65 μM or 1.3 μM). Both autotaxin inhibitors reduced would closure almost two-fold compared to the wound closure measured with cells exposed to vehicle alone, as shown in Figure 3.9. The dendrimer alone was also tested in the wound healing experiment at a concentration comparable to conjugate 1 and was found to have no measurable effect on wound closure.

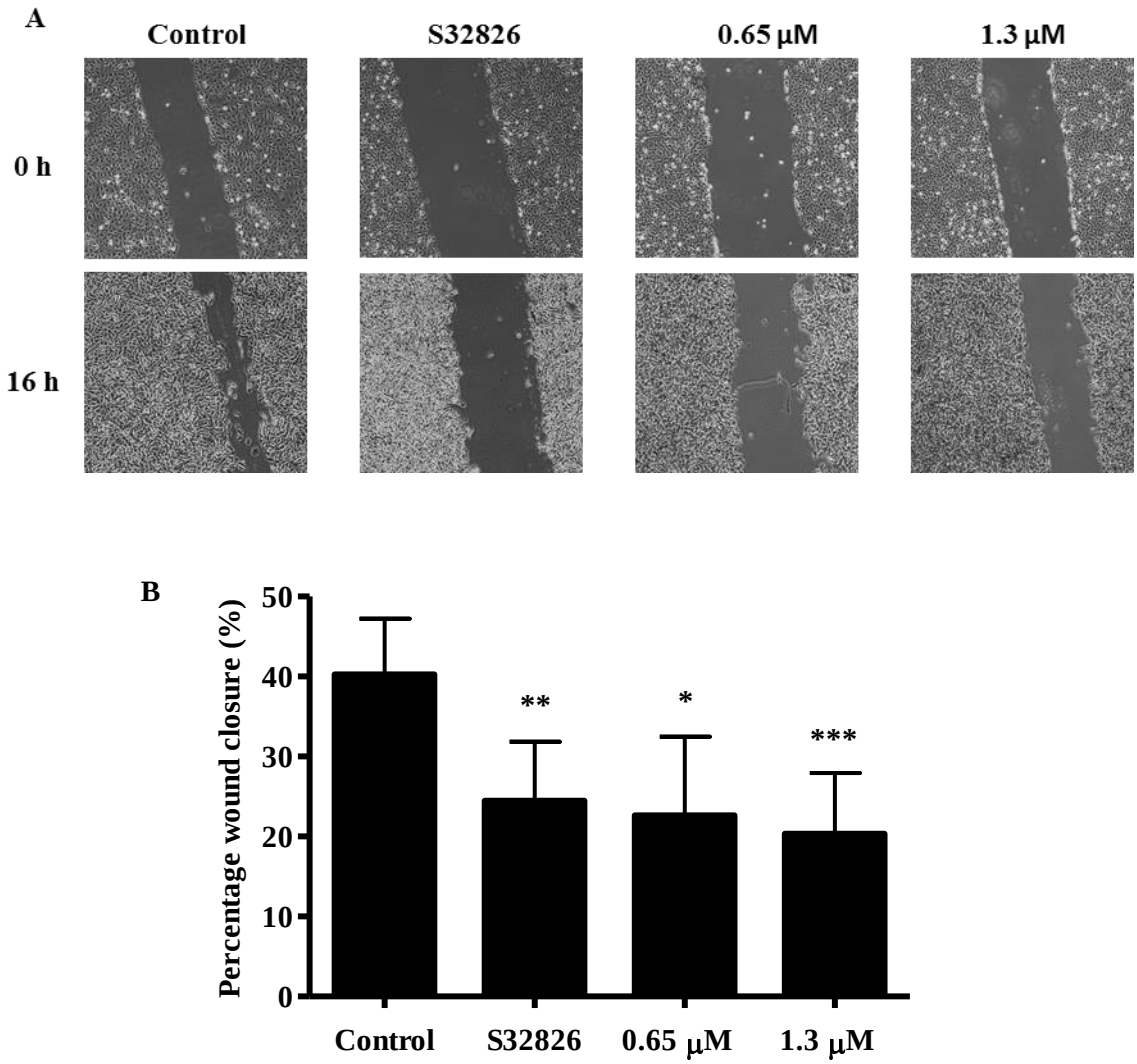

Figure 3.9: Effect of autotaxin inhibition with conjugate 1 on wound closure, in 3E3 cells. A. Inhibition of autotaxin with S32826 and conjugate 1. 3E3 cells were grown to confluence, a wound was created and serum free media containing 30 nM S32826, 0.65 µM conjugate 1 or 1.3 µM conjugate 1 was added and wound closure was measured after 16 h. B. The percentage wound closure was measured, wound closure = ((pre-migration area – post-migration area)/pre-migration area) *100. (Bars show mean +S.D., n=3–5, S32826 n=5, 0.65 µM n=3, 1.3 µM n=5). Control cells were treated with vehicle (0.5% DMSO). * $P < 0.05$, ** $P < 0.01$, *** $P < 0.001$ vs. control (paired t-test comparing treatment to corresponding control within experiment).

The effect of the inhibitors on the migration of 3V5 cells, which were transfected with the empty vector, and do not over express autotaxin was measured concurrently, as shown in Figure 3.10. Both the free inhibitor and the inhibitor bound to the G3 PAMAM dendrimer had no measurable effect on the percentage wound closure.

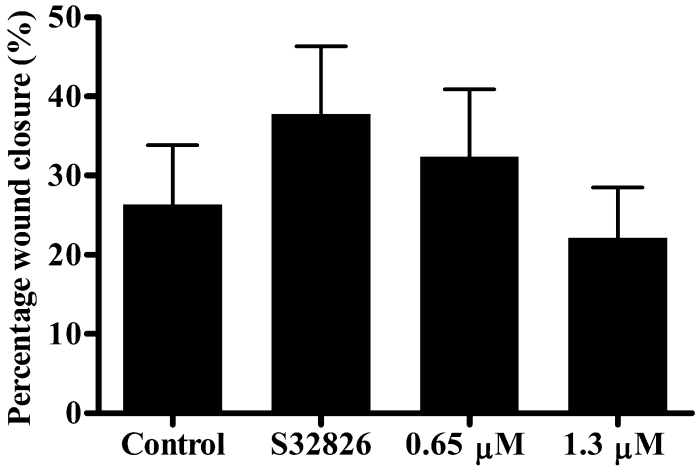

Figure 3.10: Effect of autotaxin inhibition with conjugate 1 on wound closure, in 3V5 cells. Inhibition of autotaxin with S32826 and conjugate 1. 3V5 cells were grown to confluence, a wound was created and serum free media containing 30 nM S32826, 0.65 μM conjugate 1 or 1.3 μM conjugate 1 was added and wound closure was measured after 16 h. B. The percentage wound closure was measured, wound closure = ((pre-migration area – post-migration area)/pre-migration area) *100. (Bars show mean +S.D., n=3). Control cells were treated with vehicle (0.5% DMSO).

3.3.8 Potentiation of apoptosis induced by carboplatin

Previous work has shown that expression of autotaxin delays apoptosis induced by carboplatin, while apoptosis was accelerated after inhibition of autotaxin by either siRNA or with a small molecule inhibitor.[178] To investigate the ability of conjugate 1 to potentiate apoptosis induced by carboplatin, caspase 3/7 activity was measured in 3E3 and 3V5 cells. The cells were treated with either carboplatin (300 μM), in the presence or absence of LPC (0.5 μM), and either vehicle, S32826 (300 nM) or conjugate 1 (10 μM). After 18 h, cell death was assessed by measuring caspase 3/7 activity.

Carboplatin increases caspase 3/7 activity in 3E3 cells, and this could be substantially repressed by the addition of the substrate of autotaxin, LPC. However, the inclusion of the autotaxin inhibitors, S32826 or conjugate 1 prevented the suppression of caspase activity induced by LPC, as shown in Figure 3.11. On otherwise untreated cells, the autotaxin inhibitors had no measurable effect on caspase activity.

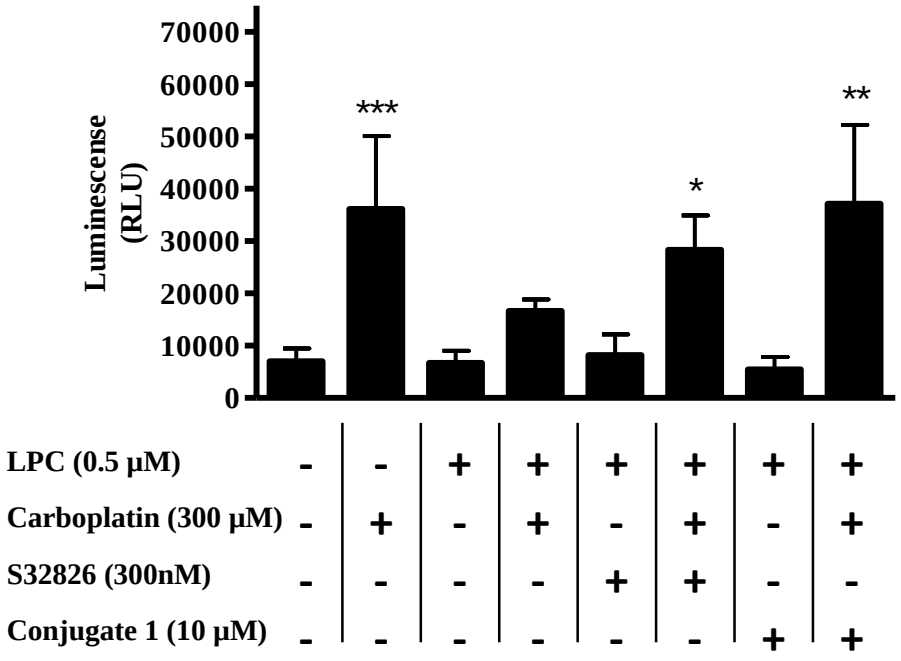

Figure 3.11: Caspase 3/7 activity measured in the presence of carboplatin and conjugate 1 in 3E3 cells. Ovarian cancer cells (3E3) engineered to overexpress autotaxin were treated and caspase 3/7 activity was measured following incubation with 10 μM conjugate 1, 300 nM S32826 with or without 300 μM carboplatin for 18 h. Caspase 3/7 activity was normalised for cell death (SRB assay). (Bars show mean + S.D., n = 3–5). * $P < 0.05$, ** $P < 0.01$, *** $P < 0.001$ vs. LPC + carboplatin only (one-way anova, post-hoc Tukey test).

In contrast, in 3V5 cells, which were transfected with the empty vector and which do not ectopically expressed autotaxin, addition of LPC was unable to supress the increase in caspase activity induced by carboplatin, as shown in Figure 3.12. Addition of the autotaxin inhibitors S32826 or conjugate 1 with carboplatin did not significantly alter the caspase 3/7 activity from that measured in the presence of carboplatin alone. The effect of the G3 PAMAM dendrimer on caspase activity in the presence of carboplatin was also measured, no significant difference between the carboplatin treated and the carboplatin with G3 PAMAM dendrimer was observed.

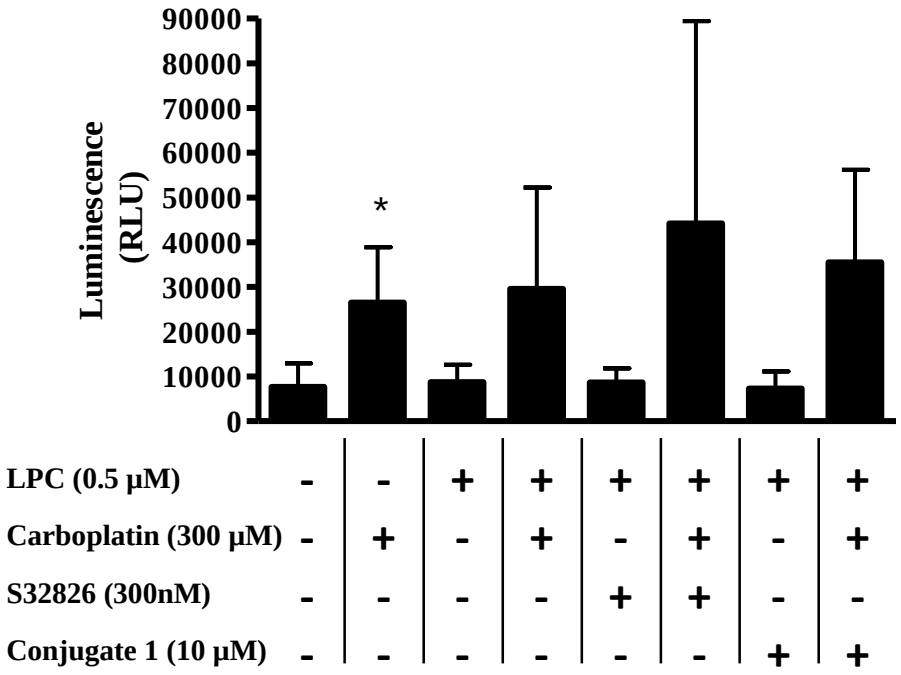

Figure 3.12: Caspase 3/7 activity measured in the presence of carboplatin and conjugate 1 in 3V5 cells ; Ovarian cancer cells (3V5) transferred with the vector were treated and caspase 3/7 activity was measured following incubation with 10 µM conjugate 1, 300 nM S32826 with or without 300 µM carboplatin for 18 h. Caspase 3/7 activity was normalised for cell death (SRB assay). (Bars show mean + S.D., n = 3–5). * $P < 0.05$, ** $P < 0.01$, *** $P < 0.001$ vs. LPC + carboplatin only (one-way anova, post-hoc Tukey test).

3.4 Discussion

Inhibition of autotaxin has the potential to decrease the survival, migration and proliferation of cancerous cells. Attaching an autotaxin inhibitor to a dendrimer has the potential to improve the pharmaceutical properties of the inhibitor and also increase the retention of the inhibitor in the intraperitoneal cavity. In the work described in this chapter the autotaxin inhibitor S32826 has been attached to a dendrimer and the effect of this conjugation on the biological activity of the inhibitor has been investigated.

The LPA analogue S32826 was chosen as unlike many other autotaxin inhibitors, S32826 has been described as having a low potency for LPA receptors.[83] Due to the similarity of structure of LPA analogues they have the potential to be an agonist or antagonist of the multiple LPA receptors, alongside their potent inhibition of autotaxin. The effects of LPA analogues on LPA receptors is not well established and therefore it was considered appropriate to use a drug which inhibits autotaxin without agonistic/antagonistic effects on LPA inhibitors. This was considered particularly important because the LPA receptors LPA2 and LPA3 have been shown to promote ovarian cancer tumorigenesis.[97, 118, 258] In contrast, LPA1 expression is decreased in ovarian cancer cells and it has been shown to promote apoptosis.[115] Thus, the agonist/antagonist profile of autotaxin inhibitors at LPA receptors may influence their clinical efficacy. S32826 has no affinity for the LPA1 receptor up to concentrations of 10 μM.[83] This study also showed S32826 had no affinity for a panel of other receptors.

Initial work had attempted to derivatise the G3 PAMAM dendrimer using ester groups as electrophiles. The aim was to react the ester groups with the terminal amine of the inhibitor to provide an amide linkage with the dendrimer, followed by deprotection of the phosphonate esters to give the desired phosphonic acid terminus, which is known to be important in binding to autotaxin.

Although initial attempts to functionalise the G3 PAMAM dendrimer in this way were unsuccessful, this was easily resolved by switching to a conjugate addition reaction to provide an amide linkage. Conjugate 1 was synthesised in an effective three step process involving acyl derivatisation of the

drug molecule to form the acrylamide, conjugate addition to the terminal amines of G3 PAMAM dendrimer and finally phosphonate ester deprotection.

The structure of conjugate 1 was confirmed through standard ^{1}H NMR and IR studies, and the degree of substitution was determined via elemental analysis. Elemental analysis suggested almost complete coupling of the inhibitor to each of the 32 terminal amines of the G3 PAMAM dendrimer was achieved. Although complete substitution was achieved it is unlikely that each inhibitor molecule can bind to autotaxin simultaneously due to steric constraints. While the primary objective of this study was to determine if conjugating autotaxin to a dendrimer would impair its activity, and several lines of evidence have shown retention of activity, different degrees of substitution could be investigated in the future to establish the effect this has on the potency of autotaxin inhibition and the physicochemical properties expressed by conjugate 1. Gas Phase chromatography (GPC) could be used to determine the polydispersity onto the dendrimer.

Conjugate 1 was initially evaluated for biological activity, by assessing its ability to inhibit autotaxin obtained from two different sources (commercial kit or purified from 3E3 cells) and measured using two different substrates. Conjugate 1 showed an approximate 10-60-fold reduction in potency compared to unconjugated S32826. This suggests that conjugation to the dendrimer has notably impaired the inhibitor's ability to bind to autotaxin, however conjugate 1 has retained some pharmacological activity. This reduction in activity may be due to the way in which the inhibitor binds to the ligand binding site of autotaxin. When this conjugate was designed the crystal structure of autotaxin had not been determined. In 2011 the crystal structure of LPA bound to autotaxin was elucidated and this showed the lipophilic chain of LPA sitting within a hydrophobic pocket.[89-90] As the dendrimer is attached to the end of the lipophilic chain of the drug molecule; this chain is unlikely to be able to sit in this pocket anymore, forcing an alternative binding conformation which might explain the observed reduction in potency.

Consistent with this interpretation, the S32826 analogue in which the terminal amine was converted to an acetamide retained potency comparable to the parent compound. Thus derivatisation of the inhibitor at the terminal end did not have a significant effect on the pharmacological activity of S32826 per se, rather the steric bulk of the dendrimer is likely to have prevented the drug molecule

binding with high affinity to the enzyme. It is possible that this prevents the alkyl group entering the hydrophobic pocket, causing a substantial reduction in the binding interactions that drive high affinity binding of S32826.

The Autotaxin/LPA pathway is known to regulate cell migration, in many cancer cell types, including ovarian cancer. Inhibition of autotaxin has been shown to reduce cancer cell migration. A monolayer wound healing experiment was used to confirm S32826 inhibits migration in ovarian cancer cells overexpressing autotaxin. The same assay was used to confirm conjugate 1 retained its biological activity, conjugate 1, at a concentration relative to potency, explain inhibited wound healing in this assay.

Autotaxin is over-expressed in tumours that are relatively resistant to chemotherapy[259] and autotaxin can contribute to resistance to carboplatin.[178] Thus, autotaxin inhibitors may be useful in the treatment of ovarian cancer as agents to overcome the resistance to chemotherapy. LPA has previously been shown to inhibit cell death induced by cisplatin in ovarian cancer cells.[176] Furthermore autotaxin inhibited apoptosis induced by paclitaxel in breast cancer and melanoma cells.[179] Previous work in cells engineered to over-express autotaxin, has shown that inhibition of autotaxin with the inhibitor ccPA 16:1 potentiates cell death induced by carboplatin.[178] Based on this previous work, the ability of conjugate 1 to potentiate apoptosis induced by carboplatin was evaluated by measuring caspase 3/7 activity. LPC was shown to protect cells from carboplatin induced caspase 3/7 activity in 3E3 cells, engineered to overexpress autotaxin, whereas no protective effect was observed in 3V5 cells which were transfected with the empty vector. Addition of the LPC provides autotaxin with the substrate to synthesise LPA which in turn promotes cell survival, as the cells transfected with the vector do not express autotaxin this protection is not observed. The addition of the free inhibitor S32826 or conjugate 1 was able to supress the decreased activation of caspase 3/7, producing caspase activity similar to that induced by carboplatin in the absence of LPC. The free inhibitor did not induce caspase 3/7 activity on its own. Lack of protection in 3V5 cells gives confidence the conjugate is biologically active through inhibition of autotaxin.

The primary aim of attaching an autotaxin inhibitor to a polymer, such as a dendrimer, was to increase the retention of the drug molecule in the intraperitoneal cavity. Providing continual and prolonged

inhibition of autotaxin may reduce the production of LPA and potentially prevent metastasis and reduce chemoresistance. However, although dendrimers were initially thought to be a good choice for this purpose due to their large hydrodynamic volume; there is evidence that dendrimers are rapidly cleared from the intraperitoneal cavity. Intraperitoneal injection of ^{125}I-labelled PAMAM dendrimers were found to be rapidly expelled from the intraperitoneal cavity.[248] A similar study investigating the bio-distribution of ^{125}I-labelled biotinylated-PAMAM dendrimers after intravenously administration and obtained similar results[260] with most of the dendrimers accumulating in the kidneys after 4 h. Furthermore, attaching the drug to a dendrimer resulted in reduced potency. This led to different drugs and different polymers being investigated. The elucidation of the crystal structure of autotaxin bound to LPA and also to a small molecule inhibitor allowed the design of more structured polymer-autotaxin inhibitor conjugates as described in the following chapters.

3.5 Conclusion

The results from this study suggest that in principle autotaxin inhibitors may be conjugated to dendrimers and retain their pharmacologic activity. While dendrimers are rapidly cleared from the intraperitoneal cavity, limiting their use for prolonging intraperitoneal retention of autotaxin inhibitors, they may still be of use for improving the physicochemical properties of the highly lipophilic class of autotaxin inhibitors based on LPA. Attaching the autotaxin inhibitor S32826 to a dendrimer has the potential to improve the pharmacokinetic profile, reducing the rapid clearance observed when tested with *in vivo* models.[83] Although the focus of the studies described here are to evaluate autotaxin inhibitors for the treatment of ovarian cancer, autotaxin inhibitors have potential in other cancers and other diseases. A dendrimer-autotaxin inhibitor may be therapeutically beneficial for retaining autotaxin in other cavities such as joints, autotaxin expression has been shown to be increased in rheumatoid arthritis. It would be useful to evaluate this conjugate in a rheumatoid arthritis model. It will also be useful to evaluate this approach using other autotaxin inhibitors and to further explore the effect attaching to dendrimers may have on reducing autotaxin inhibitor clearance from circulation.

Chapter 4

Synthesis of an icodextrin-autotaxin inhibitor conjugate

4.1 Introduction

As discussed in chapter 1, there are many potent autotaxin inhibitors currently in development. Albers *et al*. discovered a series of inhibitors based on a thiazolidinedione core, this series produced several inhibitors with nanomolar potency.[224] Additionally, Hausmann *et al.* determined the crystal structure of autotaxin in complex with one of the series a boronic acid inhibitor, HA155, as shown in Figure 4.1.[90]

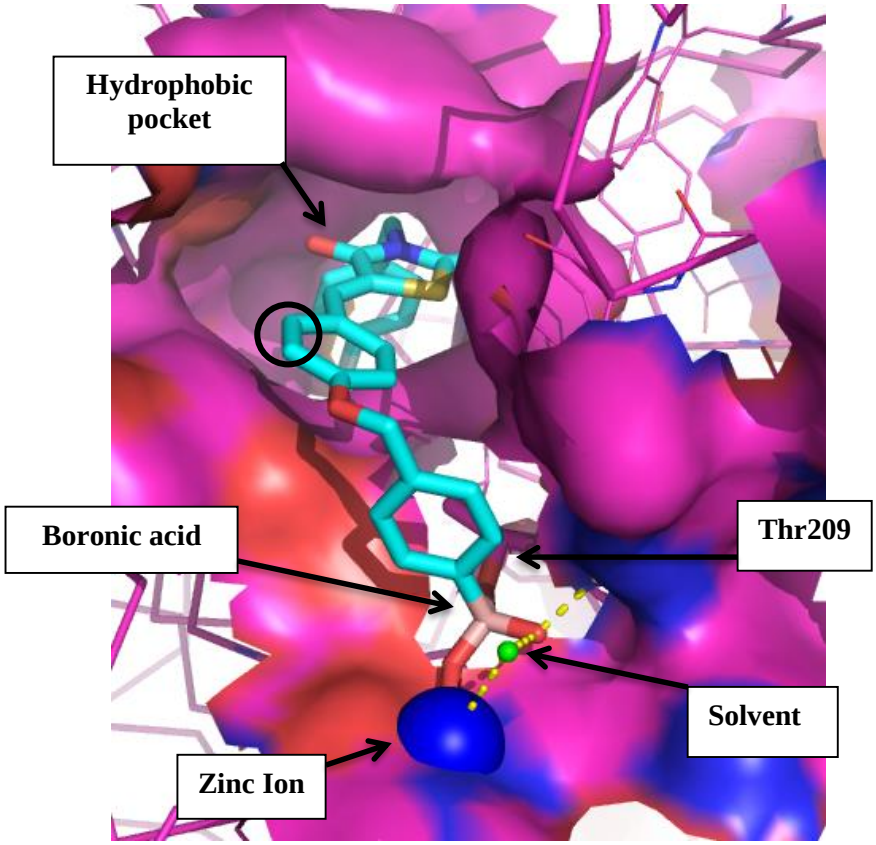

Figure 4.1: Ligand binding site with HA155 bound, PDB entry 2XRG.

The availability of the crystal structure of this compound in complex with autotaxin enables structure based design of polymer inhibitor conjugates based on this scaffold. Comparing the crystal structure of autotaxin in complex with LPA obtained by Nishimasu *et al.* it can be deduced that the inhibitor shares the same binding pocket as LPA.[89] The inhibitor binds to autotaxin in the catalytic domain, and the boron atom forms a reversible covalent bond with Thr209 and one of the two boron hydroxyl

groups is stabilised by the two zinc ions.[90] The four membered hydrophobic ring system forms a network of van der Waal interactions and the 4-fluorobenzyl moiety binds with the hydrophobic pocket which is also the site of binding of the acyl chain of LPA.[90] The thiazolidine-2,4-dione and its conjugated ring lie between the hydrophobic pocket and catalytic site, similar to the glycerol moiety of LPA,[90] as shown in Figure 4.1, circled in black.

The design of a conjugate was based upon a comparison of the structure of compound **24** and the crystal structure of the similar boronic acid. Compound **24** was the first potent autotaxin inhibitor discovered in this thiazolidine-2,4-dione series and had an IC_{50} of 56 nM in the Bis-*p*NPP assay, (Figure 4.2).[224] This compound was chosen for attachment to a polymer due to the potential of the methoxy group to serve as a point of conjugation. Analysis of the conformation of the similar boronic acid inhibitor in complex with autotaxin suggests this methoxy group sits in an accessible position.

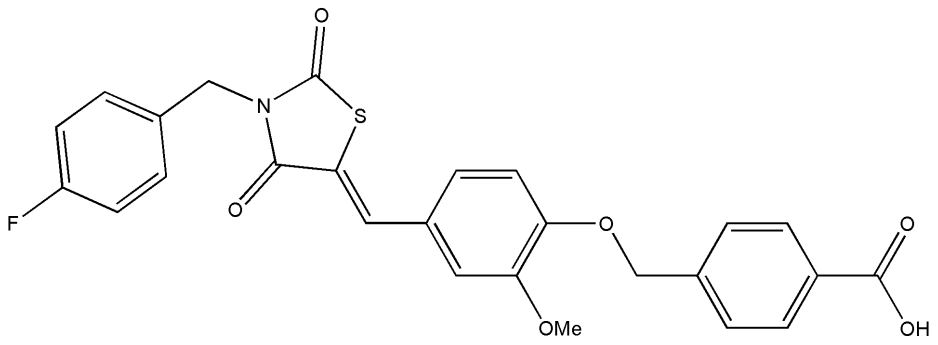

24

Figure 4.2: Structure of 2,4-thiazolidinedione autotaxin inhibitor.

As dendrimers are rapidly cleared from the intraperitoneal cavity, a polymer was required possessing features which would enable long-term retention. Icodextrin, is the main constituent of Extraneal™, a peritoneal dialysis solution, already established for clinical use. Icodextrin is a water soluble glucose polymer derived from maltodextrin with α 1-4 glyosidic bonds and approximately 10% α 1-6 glyosidic bonds. It has a weigh average molecular weight between 13 and 19 kDa. The retention

of icodextrin in the intraperitoneal cavity has been studied, with approximately sixty per cent remaining in the intraperitoneal cavity after 12 hours.[261]

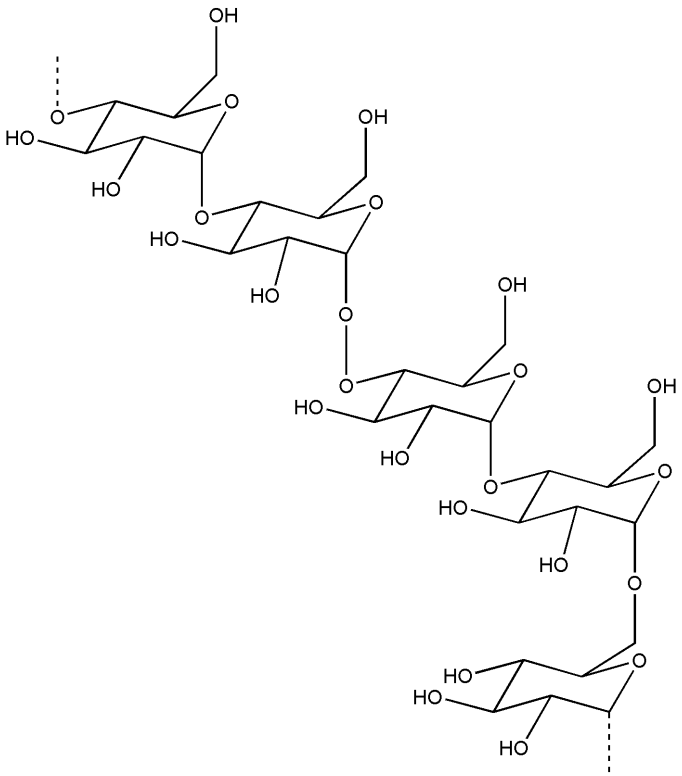

Figure 4.3: Structure of icodextrin.

This chapter will discuss the synthetic approach for both the autotaxin inhibitor and the conjugation of the inhibitor to icodextrin. This will be followed by structural analysis of the conjugates.

4.2 Results

4.2.1 Synthesis of thiazolidine-2,4-dione autotaxin inhibitor

Initially, synthesis of the autotaxin inhibitor **24** was employed as a starting point to develop a novel compound which could be conjugated to Icodextrin. This was achieved utilising the previously described synthetic method used by Albers and co-workers, as shown in Scheme 4.1.[224]

Firstly, intermediate **38** was prepared by *N*-benzylating thiazolidine-2,4-dione **36** with 4-fluorobenzyl chloride **37**, following deprotonation with sodium hydride, in anhydrous DMF, (75%).

The second intermediate **41** was prepared by *O*-benzylating vanillin **39** with methyl-4-(bromomethyl)-benzoate **40** in the presence of potassium hydroxide. The ester functionality in this compound was then hydrolysed *in situ* with sodium hydroxide to give the benzoic acid **41**, (71%).

Finally, both intermediates, thiazolane-2,4-dione **38** and aldehyde **41**, were combined via a Knoevenagel condensation mediated by piperidine in ethanol to yield the previously described autotaxin inhibitor **24**, (93%). The identity of the product was secured from the ^{1}H-NMR with the characteristic alkene singlet of the newly formed double bond at 4.82 ppm.

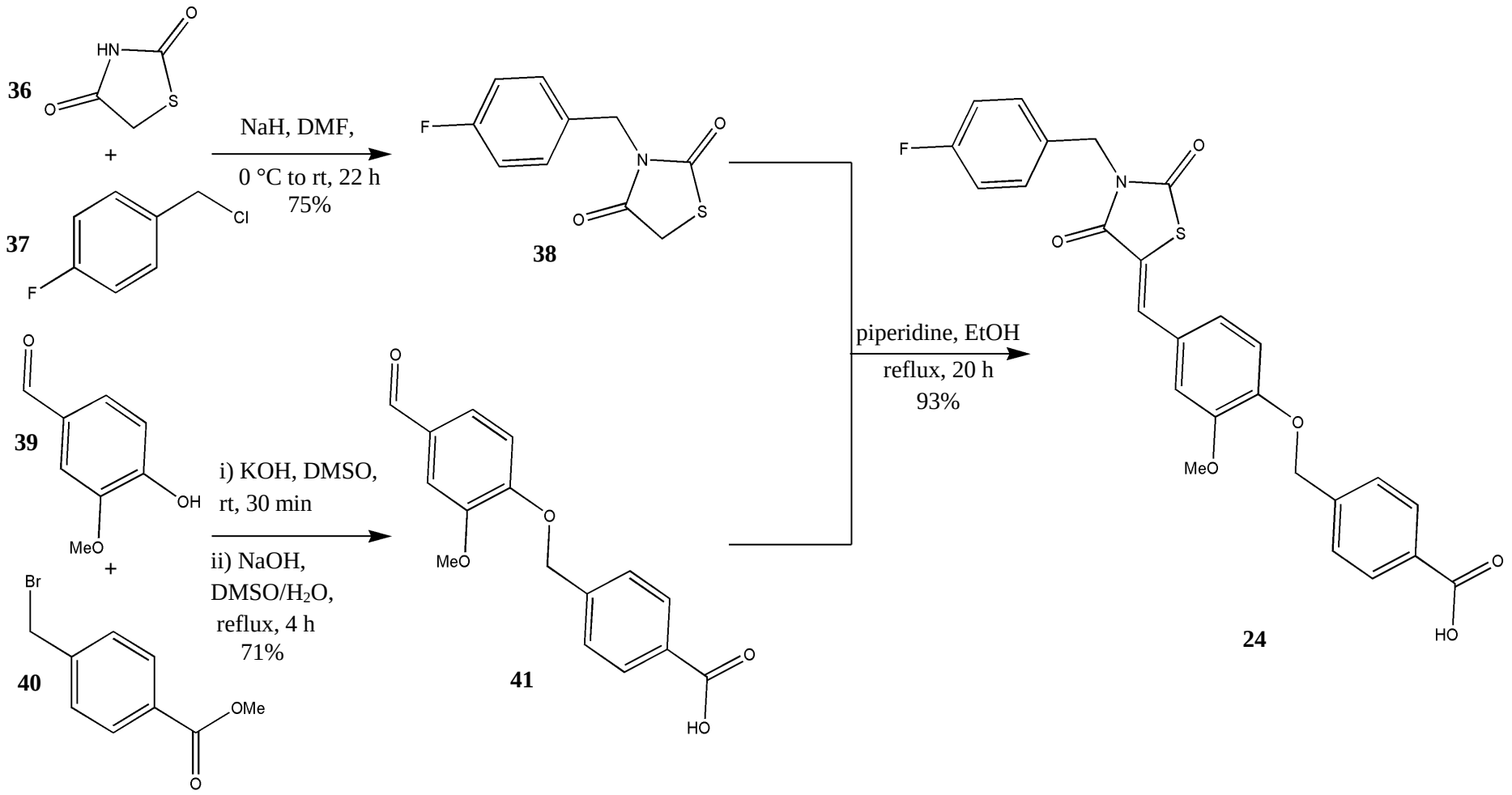

Scheme 4.1: Synthesis of thiazolidine-2,4-dione autotaxin inhibitor.

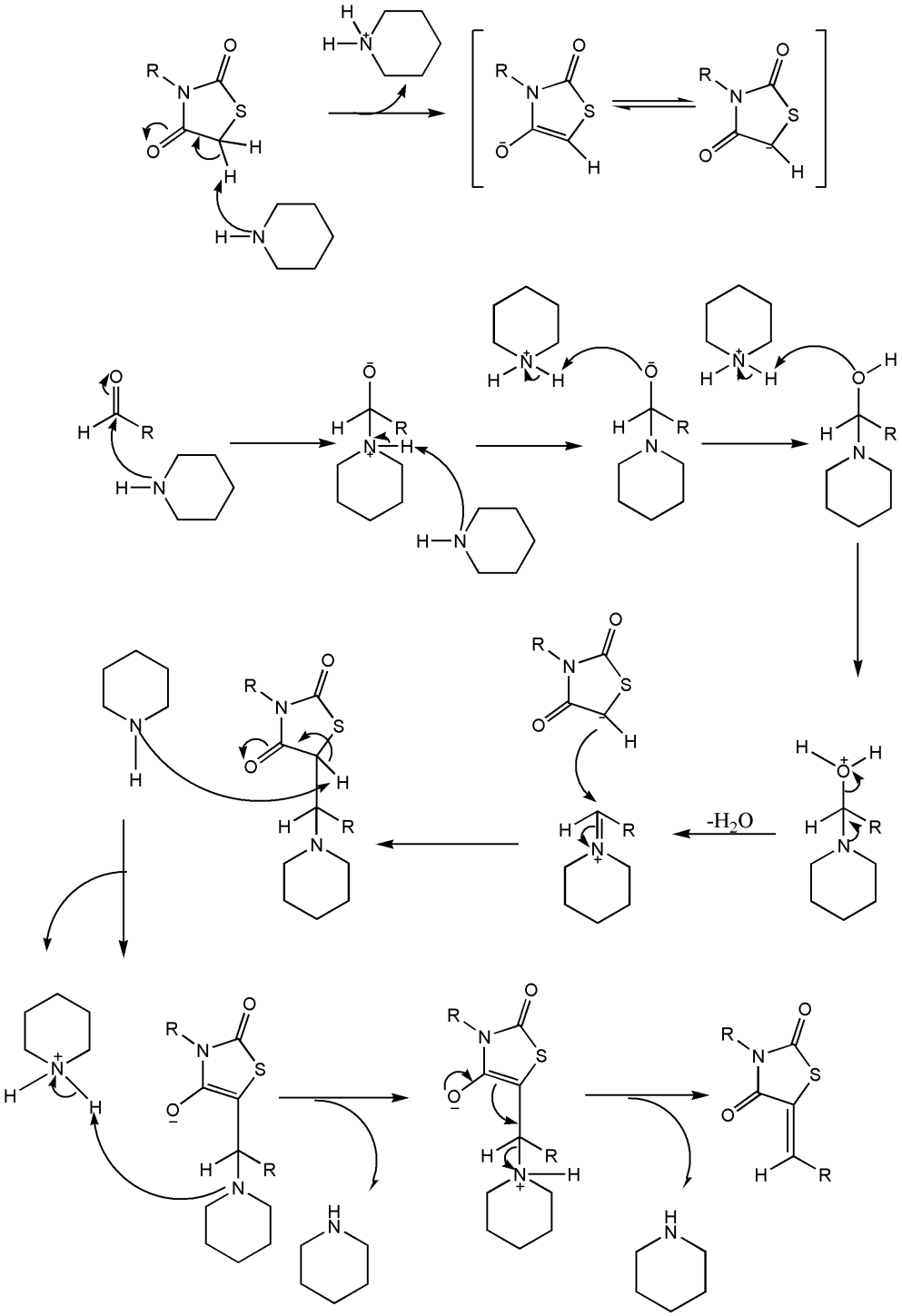

Scheme 4.2: Mechanism of Knoevenagel condensation.

The Knoevenagel condensation begins by deprotonation of the activated methylene by piperidine to give a resonance stabilised enolate. Piperidine also reacts with the aldehyde to form an iminium ion intermediate, which is then attacked by the enolate. The intermediate compound formed is then

deprotonated by piperidine to give another enolate while the amine of the intermediate is protonated. A rearrangement releases the piperidine to yield the final olefin product, as shown in Scheme 4.2.

4.2.2 Exposing the hydroxyl group

4.2.2.1 Demethylation of the aryl methyl ether

Demethylation of the aryl methyl ether of compound **24** to expose the phenolic hydroxyl group was required to create a reactive moiety for future attachment to icodextrin. Demethylation was initially attempted using the Lewis acid boron tribromide at room temperature; as described by McOmie *et al*.[262]

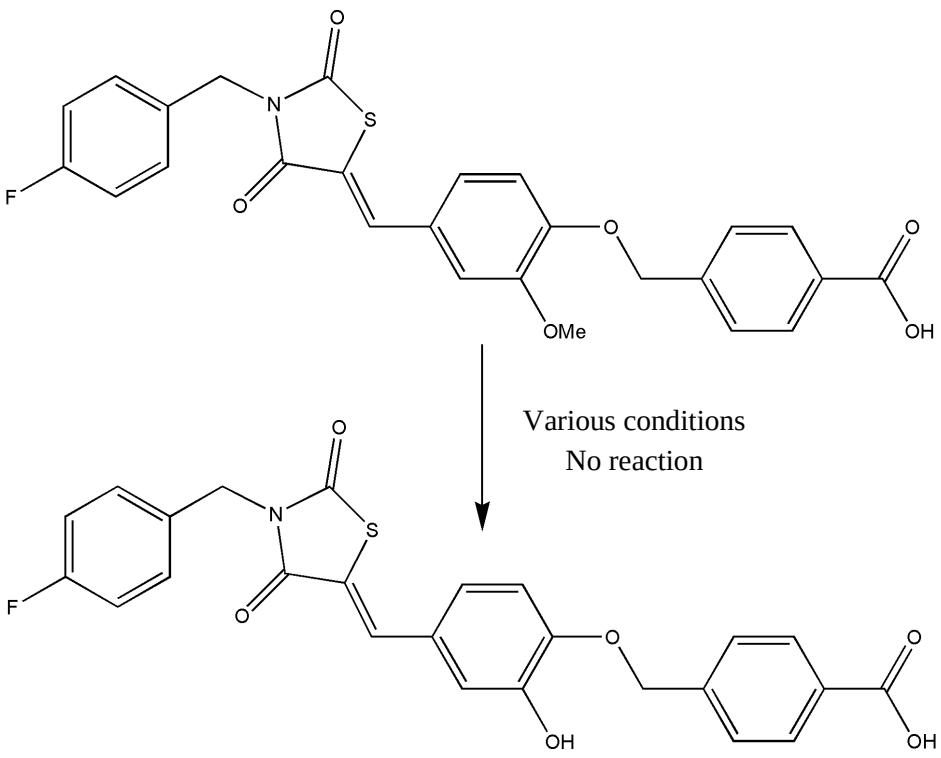

Scheme 4.3: Attempted demethylation of thiazolidine-2,4-dione.

This reaction failed under a variety of conditions, resulting in either the removal of both the methyl and benzyl ether groups or recovery of the starting material. Cerium trichloride and TMS-iodide,

both milder Lewis acids, were also attempted. However, both were unsuccessful resulting in recovery of the starting material. Conditions attempted are shown in Table 4.1.

Reducing agent	Equivalents	Time (h)	Temperature (°C)	Outcome
BBr_3	2	2	0	No reaction
BBr_3	2	16	0	No reaction
BBr_3	2	4	23	No reaction
BBr_3	10	16	23	Demethylation and debenzylation
BBr_3	10	2	23	Demethylation and debenzylation
BBr_3	5	16	23	No reaction
$CeCl_3$	1.5	16	reflux	No Reaction
TMS-I	10	8	reflux	No reaction

Table 4.1: Conditions attempted for demethylation of the phenolic methyl ether.

4.2.2.2 Acetylation of 3,4-dihydroxy-benzaldehyde

Selective acetylation of the 3-hydroxyl group of 3,4-dihydroxy-benzaldehyde **43** was attempted to create a more labile protecting group. Synthesis was achieved with acetic anhydride in the presence of sodium hydroxide and subsequent acidification with hydrochloric acid and phosphate buffer, to yield compound **44** in an impure state in approximately 62%, as shown in Scheme 4.4.

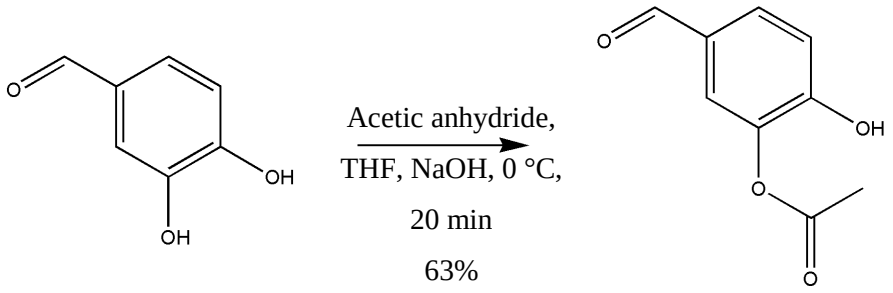

43 **44**

Scheme 4.4: Acetylation of 3,4-dihydroxy-benzaldehyde.

TLC and ^{1}H NMR analysis showed by-products 3,4-diacetoxy-benzaldehyde and 4-acetoxy-3-hydroxy-benzaldehyde were present. These by-products were separated from the desired 3-monosubstituted isomer **44** via column chromatography. ^{1}H NMR analysis showed the 4-monosubstituted product was still present in a ratio of approximately 1:6, indicating that further purification would be required. No further action was taken with this route.

4.2.2.3 Selective benzylation of 3,4-dihydroxy-benzaldehyde

A method by Plourde *et al.* for the selective benzylation of the 4-hydroxyl position of 3,4-dihydroxy-benzaldehyde was investigated.[263] This method utilising the mild base sodium bicarbonate (1.5 equiv.) resulted in the 4-mono-substituted benzaldehyde **45**, with small 3-mono-subsituted and di-substituted impurities. Impurities were removed via column chromatography and recrystallization to yield compound **45**, (70%), as shown in Scheme 4.5.

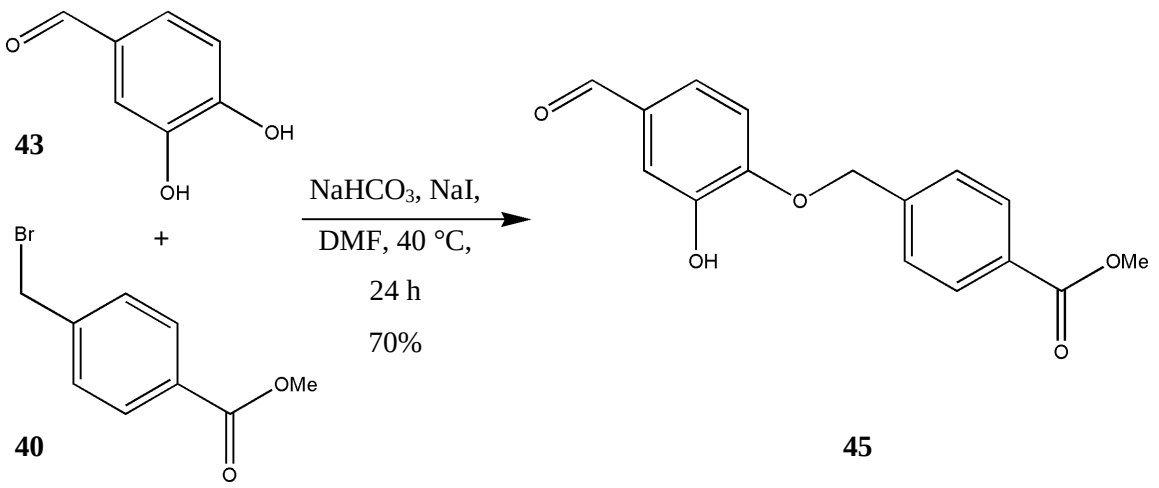

Scheme 4.5: Selective benzylation of 3,4-dihyroxy-benzaldehyde.

Since sodium bicarbonate is not basic enough to deprotonate the phenol the mechanism for this reaction could either progress through S_N2 followed by deprotonation or deprotonation followed by S_N2.

The regiochemistry was confirmed by Nuclear Overhauser Effect (nOe) NMR analysis and X-ray crystallography. nOe NMR analysis showed a correlation between the 5-position hydrogen of the aromatic ring and the CH_2 of the ether linkage, which would not be present if the 3-hydroxyl group had been benzylated. Single crystal X-ray diffraction confirmed the structure as shown in Figure 4.4.

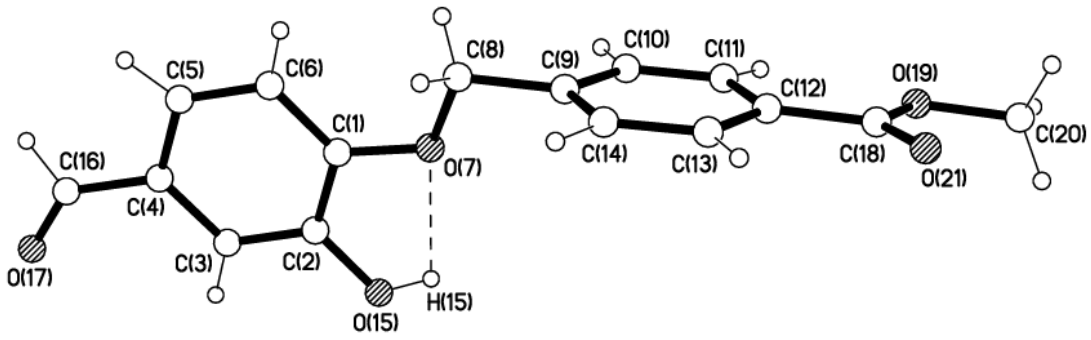

Figure 4.4: Crystal structure of compound **45**.

4.2.2.4 Synthesis of thiazolidine-2,4-dione with exposed hydroxyl group

Aldehyde **45,** which possessed the desired hydroxyl functional group, then underwent piperidine mediated Knoevenagel condensation, as described in section 4.2.1, with thiazolidine-2,4-dione **38**, to yield the desired compound **46**, (69%), as shown in Scheme 4.6.

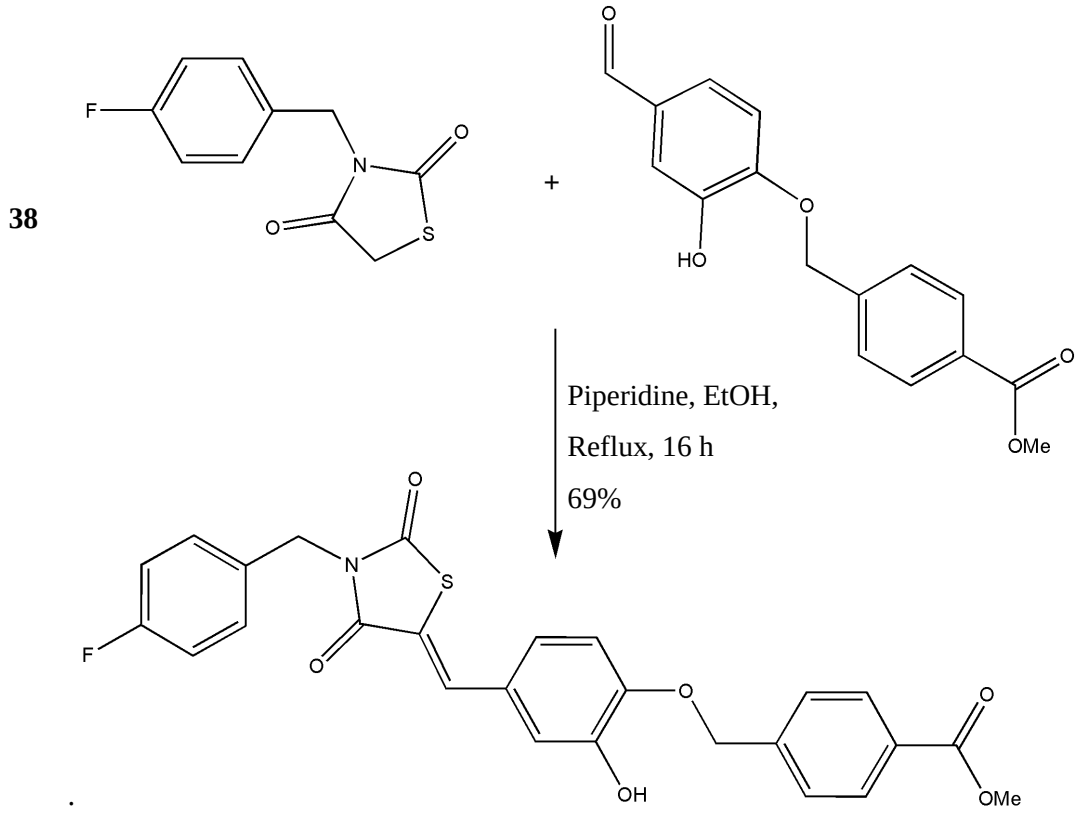

Scheme 4.6: Synthesis of thiazolidine-2,4-dione with free hydroxyl group.

The methyl ester was not converted to the carboxylic acid. The methyl ester would act as a protecting group to prevent any unwanted reactions during future conjugation to icodextrin.

4.2.2.5 Synthesis of thiazolidine-2,4-dione carboxylic acid

The carboxylic acid **42** was also synthesised to investigate the effect of changing the methoxy functional group to a hydroxyl group on the biological activity of the compound. To obtain the

carboxylic acid, benzaldehyde **45** underwent saponification with NaOH and heating to yield intermediate, **47** (98%), as shown in Scheme 4.7.

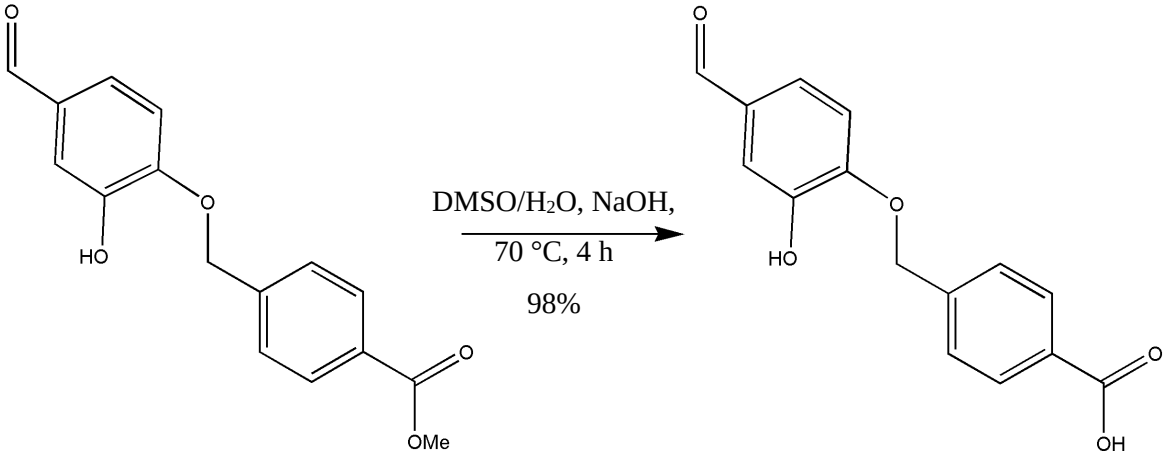

45 **47**

Scheme 4.7: Saponification of benzaldehyde benzoate.

Compound **47**, was condensed with thiazolidine-2,4-dione **38** as described in section 4.2.1 to yield the desire compound **42**, (80%), as shown in Figure 4.5.

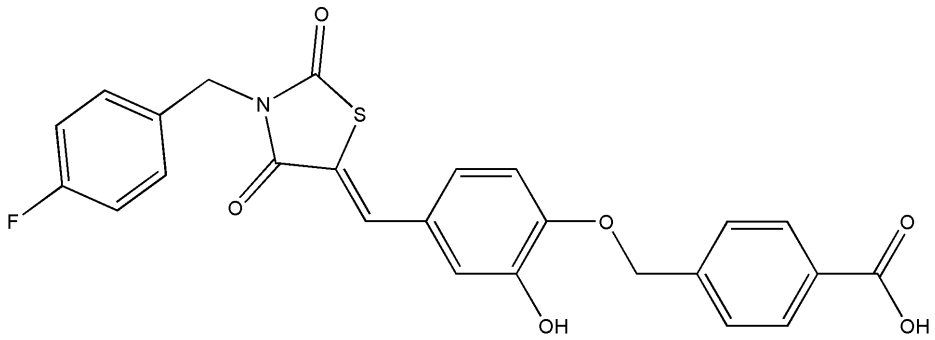

42

Figure 4.5: Structure of thiazolidine-2,4-dione inhibitor with free hydroxyl group.

4.2.3 Activation of icodextrin

Icodextrin was tosylated to provide a suitable leaving group for conjugation to the inhibitor molecule. It was assumed that the sterically most accessible C6-position hydroxyl group would be tosylated selectively given the precedent for D-glucose.[264]

4.2.3.1 Dissolution of icodextrin

Icodextrin is insoluble in most organic solvents. After much experimentation and a screen of potential solvents, icodextrin was solubilised based upon a method utilised by Liu *et al*. to solubilise cellulose.[265] Icodextrin was suspended in a DMAc-LiCl co-solvent system and heated to 160 °C for 8 h until completely dissolved. LiCl is used to disrupt the strong hydrogen bonding formed within icodextrin due to the formation of hydrogen bonds between the hydroxyl groups of icodextrin and chloride ions. Once in solution cooling to room temperature was possible without precipitation of icodextrin.

4.2.3.2 Tosylation of icodextrin

Tosylation was performed in DMAc-LiCl with 5 w/w equivalents of tosyl chloride in the presence of pyridine. The reaction was heated for 16 h, cooled and dialysed against deionised water to yield icodextrin-tosylate **49**, (50% mass recovery), as shown in Scheme 4.8.

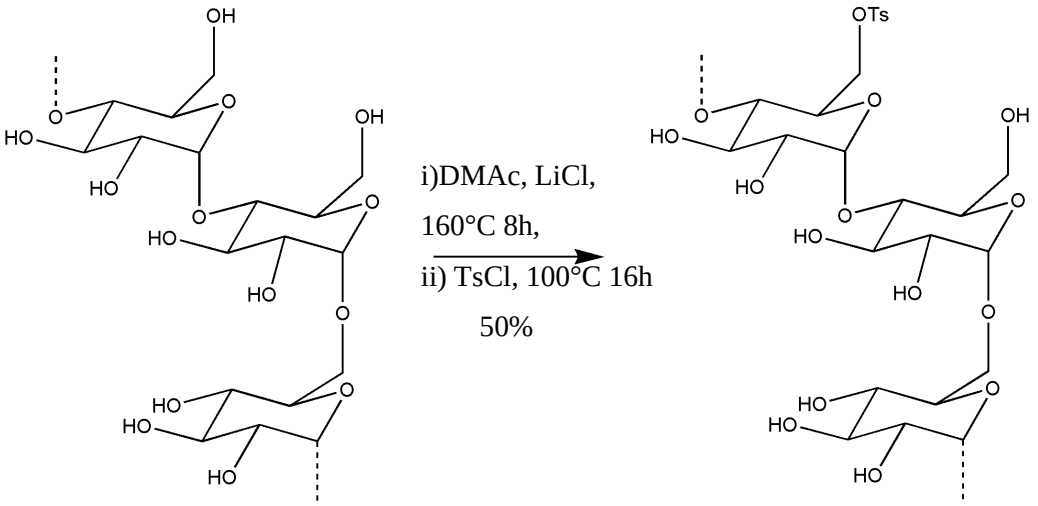

48 **49**

Scheme 4.8: Synthetic route to icodextrin tosylate.

Tosylation of icodextrin was determined via ^{1}H NMR and IR analysis. ^{1}H NMR analysis showed the presence of two aromatic peaks at 7.47 ppm and 7.12 ppm, most likely corresponding to the AA′BB′ aromatic ring protons of the tosyl group. The degree of tosylation can be approximated from the ratio of the signal from the aromatic tosyl peaks which each correspond to two hydrogens and the anomeric hydrogen of icodextrin, as shown in Figure 4.6. This suggests a ratio of 1 in 9 icodextrin monomers have been tosylated. The NMR spectrum peaks of the tosylated icodextrin are much broader than that of the icodextrin alone, this may be due to a higher water content possible cause by more water getting trapped due to sterical conformation changes.

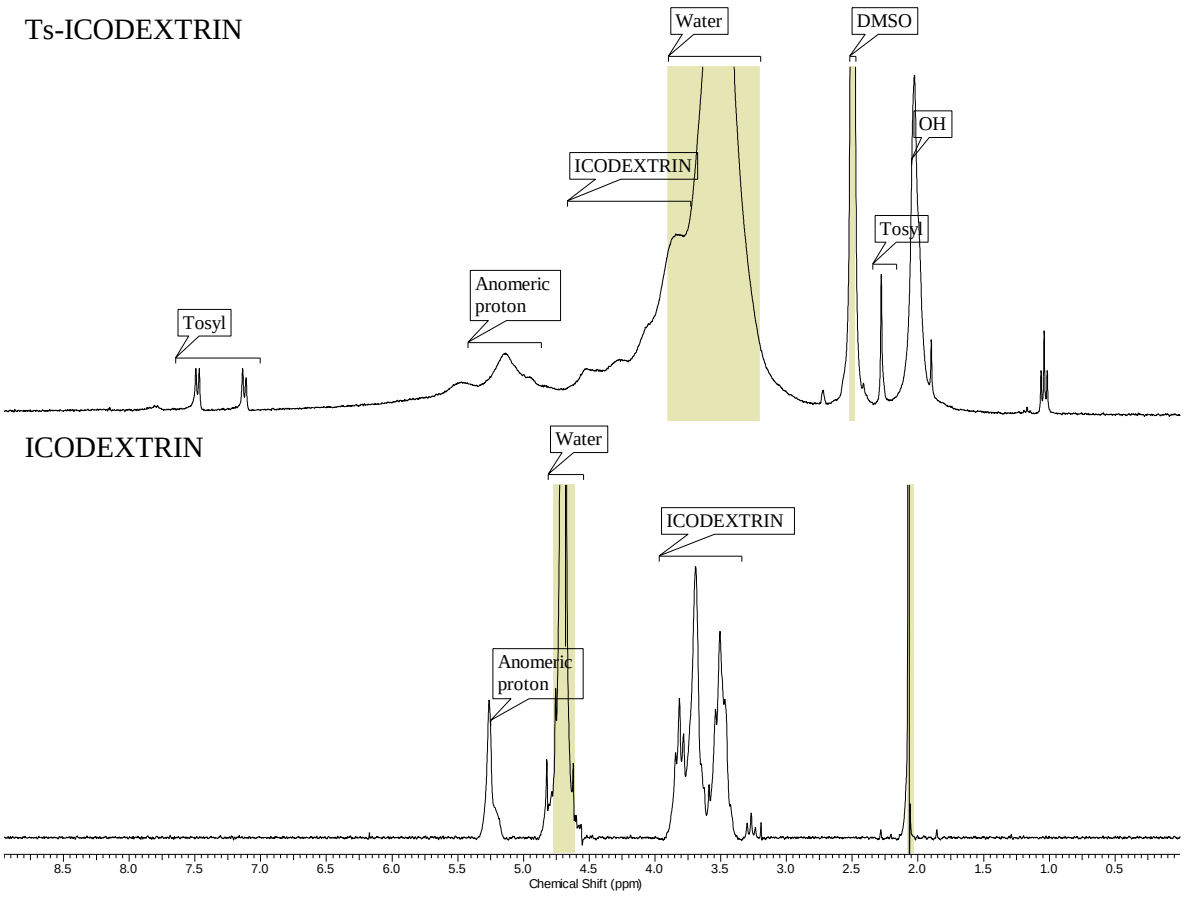

Figure 4.6: ^{1}H NMR of icodextrin tosylate.

4.2.4 Synthesis of conjugate 2

Conjugation of the inhibitor to icodextrin was achieved via ether formation between icodextrin-tosylate and the inhibitor (5 mass equiv.) in DMSO in the presence of pyridine, heated for 24 h. The cooled reaction mixture was then dialysed against deionised water, yielding compound **50** (22% mass recovery), as shown in Scheme 4.9.

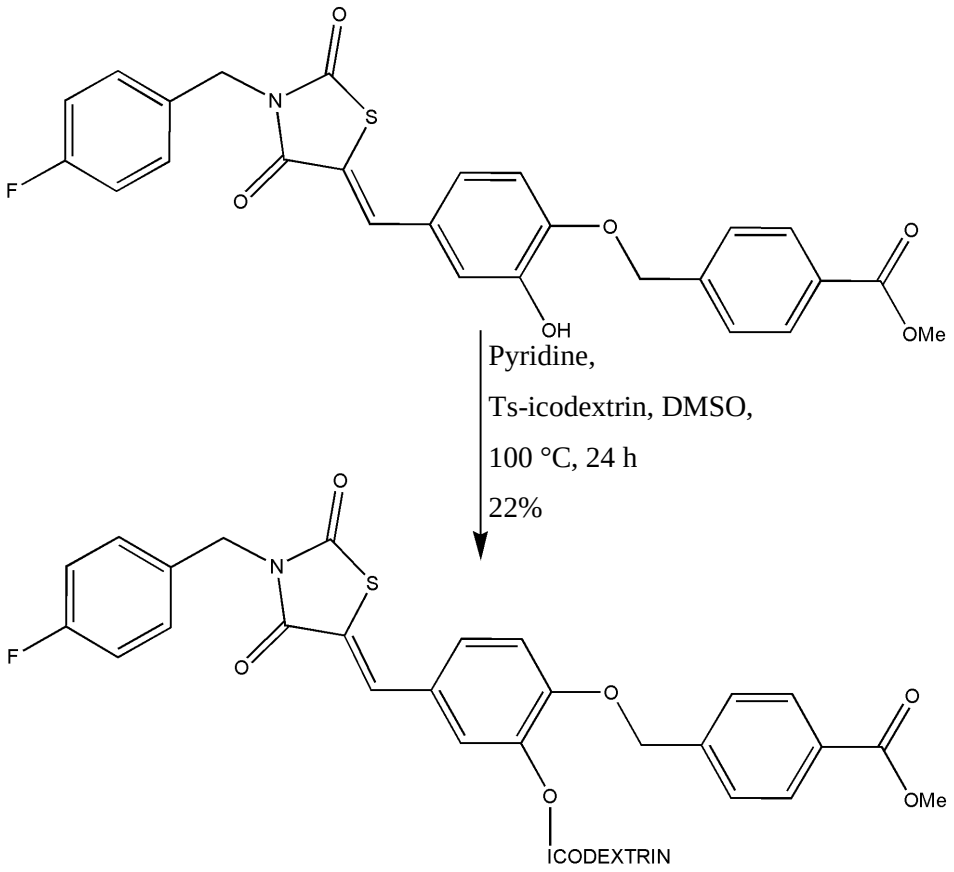

46

50

Scheme 4.9: Synthetic route for conjugation to icodextrin.

The conversion of the ester of compound **50** to expose the essential carboxylic acid of the inhibitor was attempted via saponification. However, these conditions appeared too harsh for the compound possibly due to degradation as evident by NMR analysis, as shown in Scheme 4.10.

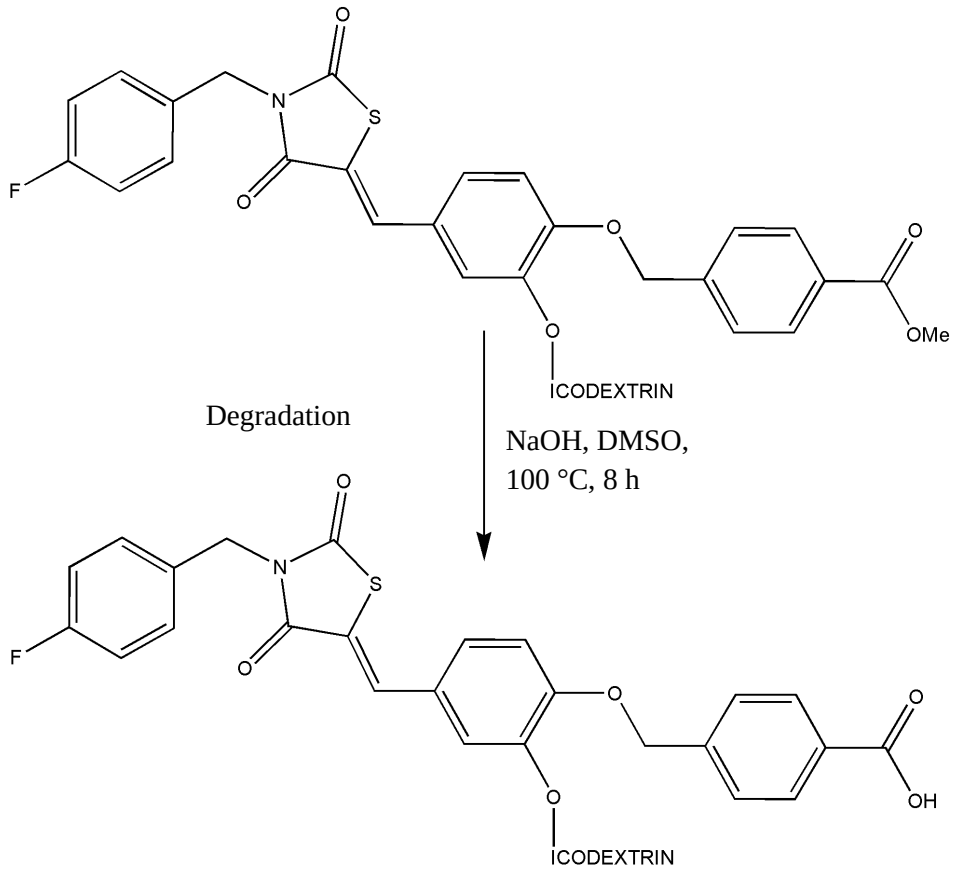

50

51

Scheme 4.10: Attempted deprotection of compound **50**.

4.2.4.1 Silyl protection of carboxylic acid

The carboxylic acid protecting group was replaced with a silyl group. Silyl protecting groups can be selectively removed using fluoride ions. The carboxylic acid was protected with a triisopropylsilyl group because this is sufficiently stable to the mildly basic conditions used in the other synthetic steps. Protection was achieved with triisopropylsilyl chloride in anhydrous DMF in the presence of sodium hydride, to yield compound **52** (72%)**,** as shown in Scheme 4.11.

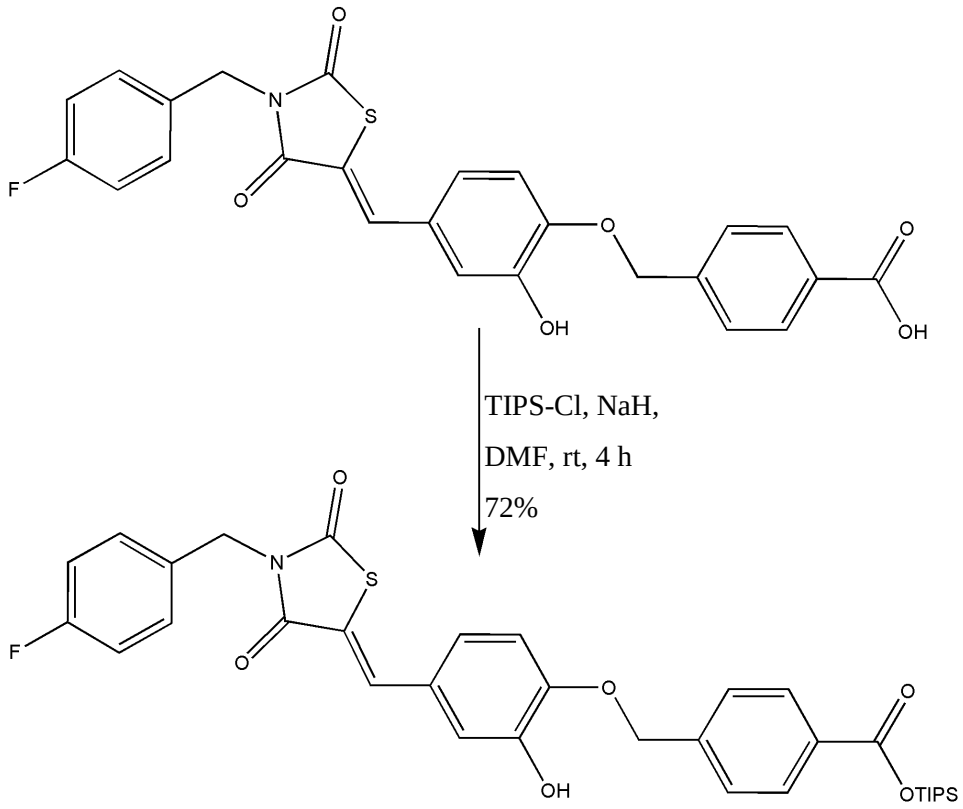

Scheme 4.11: Silyl protection of carboxylic acid.

4.2.4.2 Conjugation to icodextrin

The newly protected inhibitor **52** was conjugated to tosylated icodextrin according to the method described in section 4.2.4. The conjugate was then treated with tetrabutylammonium fluoride (TBAF) in methanol to expose the essential carboxylic acid, yielding conjugate 2, (22% mass recovery) as shown in Scheme 4.12.

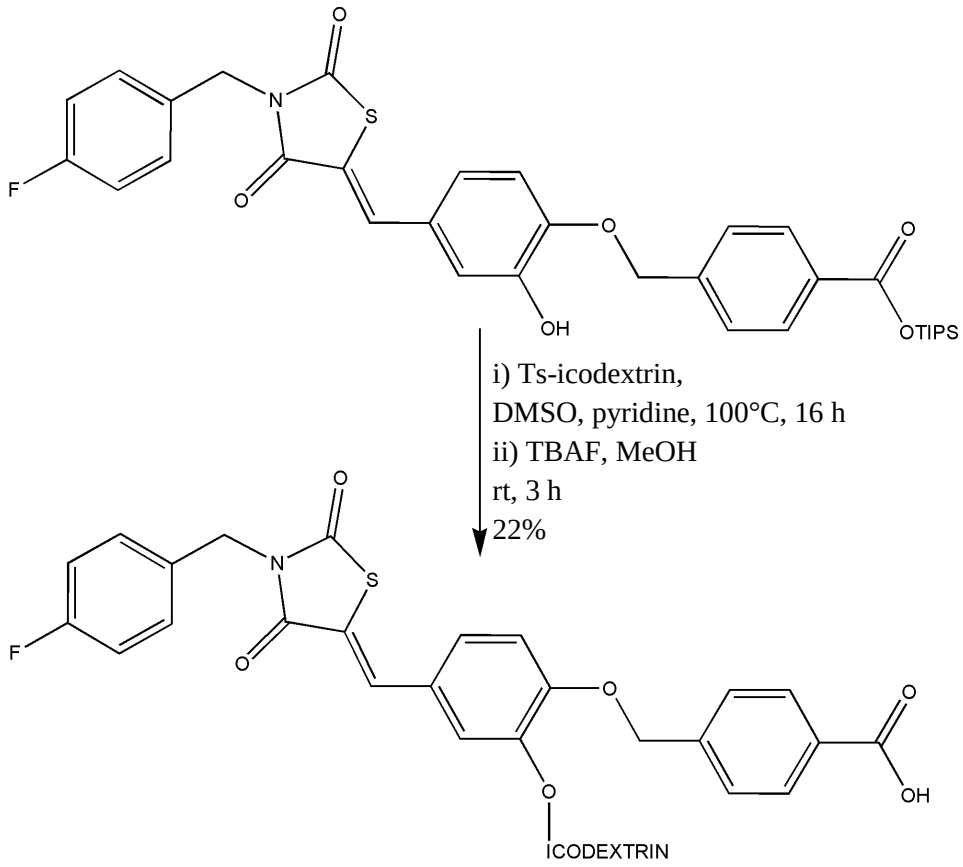

52

Conjugate 2

Scheme 4.12: Synthesis of Conjugate 2.

This compound had a molecular weight greater than 8 kDa, as per the MWCO of dialysis membrane. In order to improve retention time in the intraperitoneal cavity a larger molecular weight was desired. The synthesis was attempted again using icodextrin which had been dialysed using a membrane with a molecular mass cut off of 20 kDa.

4.2.5 Synthesis of conjugate 3

Synthesis of the conjugate with icodextrin with a larger molecular mass was required. The synthesis of Conjugate 3 was initially attempted according to the previously employed method, described in section 4.2.4., using tosylated icodextrin >20 kDa. However, no conjugation was observed, resulting in recovery of icodextrin. This was postulated to be due to steric interactions, possibly caused by secondary interactions with the longer icodextrin; which make the alkylation reaction which couples

the drug to the icodextrin more difficult; the yield for the first attempt of this reaction was already low.

4.2.5.1 Addition of a linker moiety

A linker moiety was added to the inhibitor molecule to increase the distance between the two molecules. A diethylene glycol linker was chosen due to its stability and to retain the oxidation level of the functionality and method of attachment from the initial synthesis. The diethylene glycol linker was added by Williamson synthesis.[245]

Firstly, diethylene glycol was converted to 2-(2-bromo-ethoxy)-ethanol via the Appel reaction with triphenylphosphine and carbon tetrabromide, to yield compound **54**, (49%), as shown in Scheme 4.13.

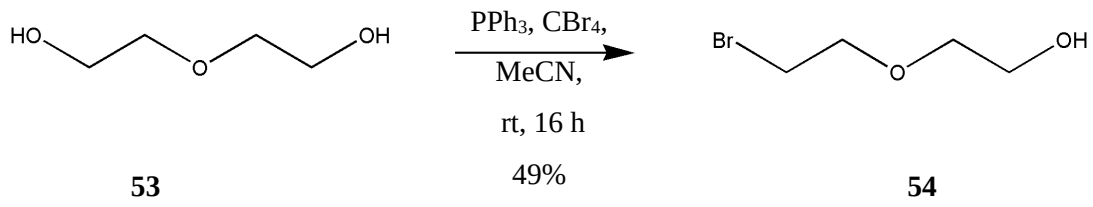

53 **54**

Scheme 4.13: Synthesis of 2-(2-bromoethoxy)-ethanol.

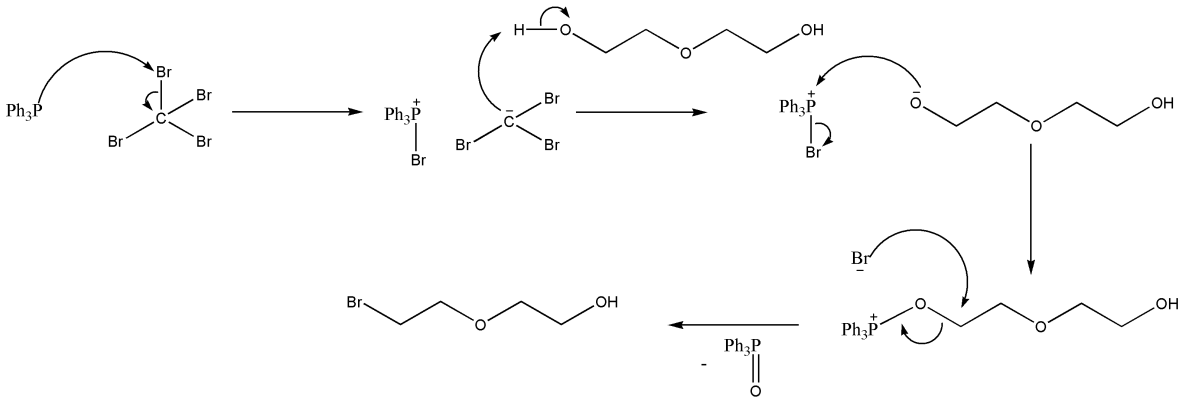

Scheme 4.14: Mechanism of Appel reaction.

Compound **46** was alkylated with 2-(2-bromoethoxy)-ethanol in the presence of potassium hydroxide. Potassium iodide was added to further activate the alkyl bromide with an *in situ* Finkelstein reaction, substituting the bromide for the more reactive iodide group. This yielded compound **55**, (68%), as shown in Scheme 4.15.

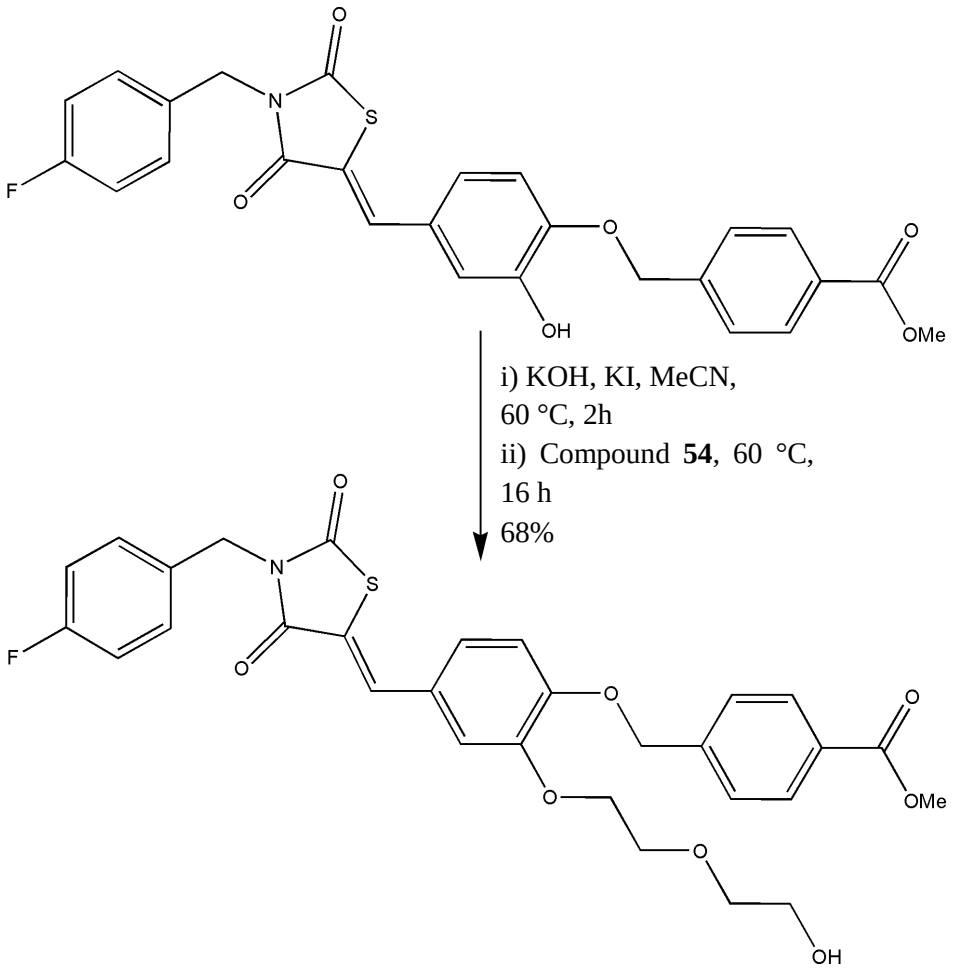

Scheme 4.15: Alkylation of thiazolidine-2,4-dione methyl ester.

The alkylation of compound **52** with 2-(2-bromo-ethoxy)-ethanol, was attempted according to the previously employed method and variations of the conditions as shown in Table 4.2.

Base	Equivalents	Solvent	Time (h)	Temperature (°C)	Outcome
KOH	1.1	MeCN	2	21 to 70	Removal of TIPS
Na_2CO_3	1.1	DMF	4	21 to 70	Removal of TIPS
K_2CO_3	1.1	MeCN	4	21 to 70	TIPS removal and undesired alkylation
Na_2CO_3	1.1	MeCN	20	21 to 70	No change
NaH	1.1	DMF	4	0 to 21	Removal of TIPS

Table 4.2: Conditions for alkylation.

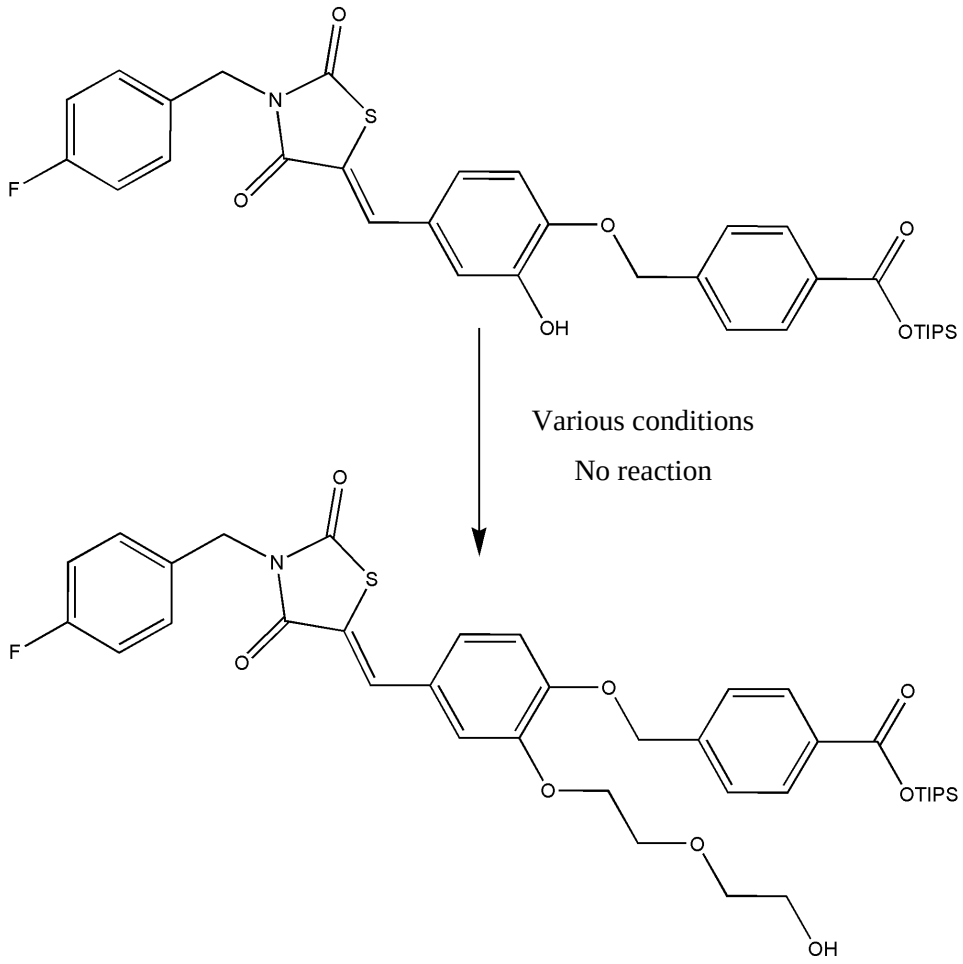

Scheme 4.16: Attempted alkylation of thiazolidine-2,4-dione TIPS ester.

The synthesis of the inhibitor molecule with linker, compound **56** was changed to incorporate the linker at an earlier stage. At this point commercially available 2-(2-chloroethoxy)-ethanol was substituted for the 2-(2-bromoethoxy)-ethanol reducing the amount of required synthetic steps. Alkylation of compound **45** was achieved with 2-(2-chloroethoxy)-ethanol in anhydrous DMF in the presence of potassium carbonate. Again potassium iodide was added for *in situ* Finkelstein reaction.

This was followed by saponification with sodium hydroxide, to yield compound **57**, (91%), as shown in Scheme 4.17.

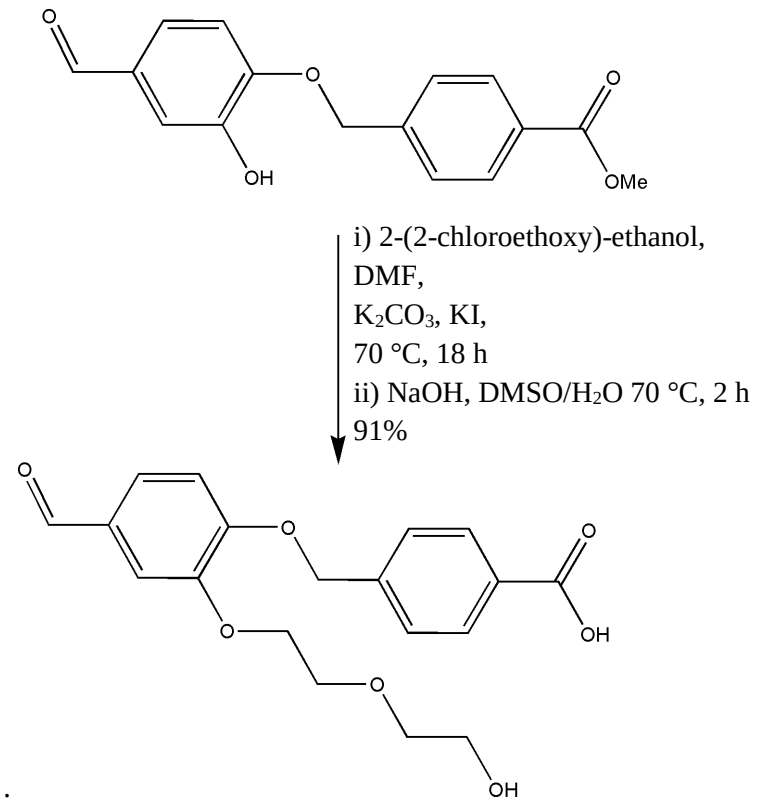

Scheme 4.17: Alkylation of benzaldehyde.

Compound **57** underwent Knoevenagel condensation with compound **41** according to the standard method described in section 4.2.1., yielding the desired compound **60**, (54%), as shown in Scheme 4.18.

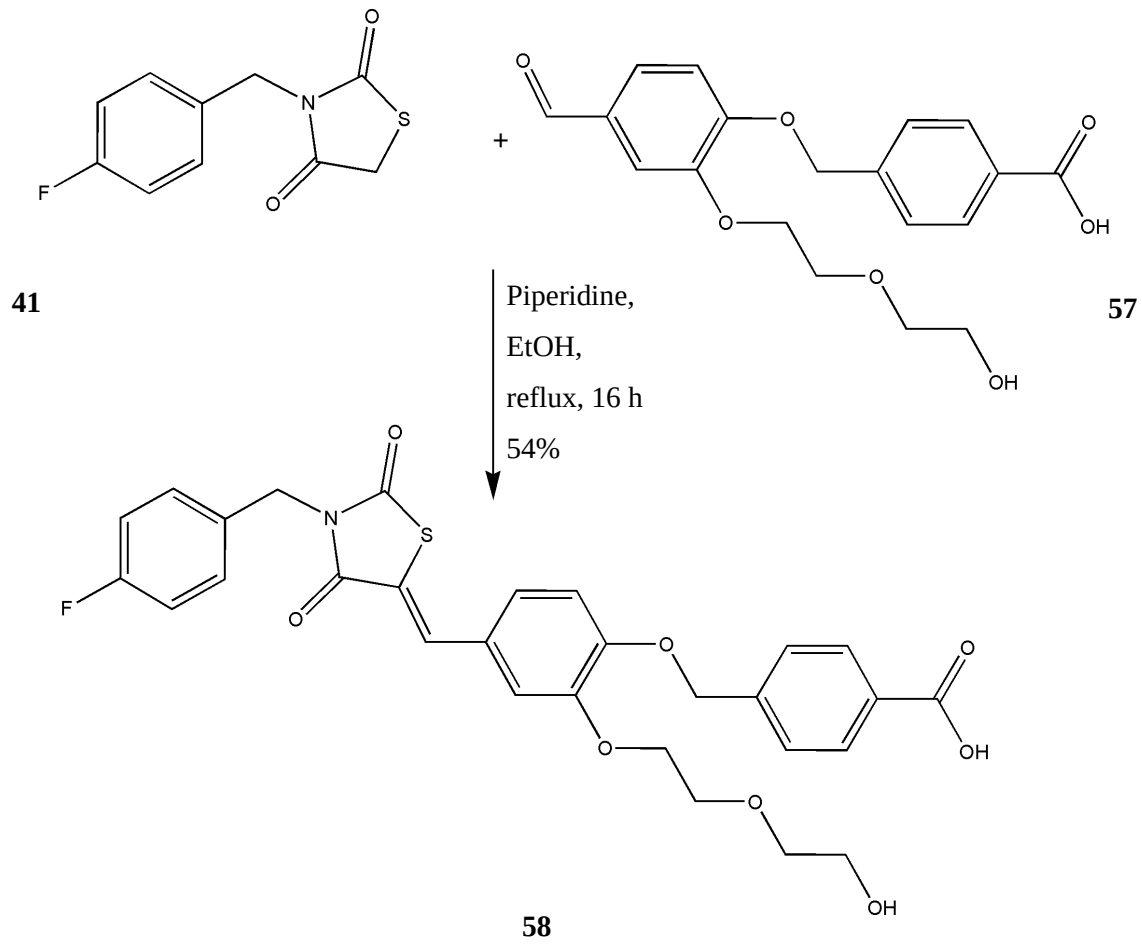

Scheme 4.18: Synthesis of thiazolidine-2,4-dione with linker.

The carboxylic acid of compound **58** was then protected using triisopropylsilyl chloride according to a method described by Smith *et al*. for selective ester formation.[266] The selectivity of this reaction is based on the pKa, although triethylamine is a weak based it is able to deprotonate the acid and therefore make the acid more reactive than the primary alcohol. This was achieved in anhydrous tetrahydrofuran in the presence of triethylamine to yield compound **59**, (76%), as shown in.

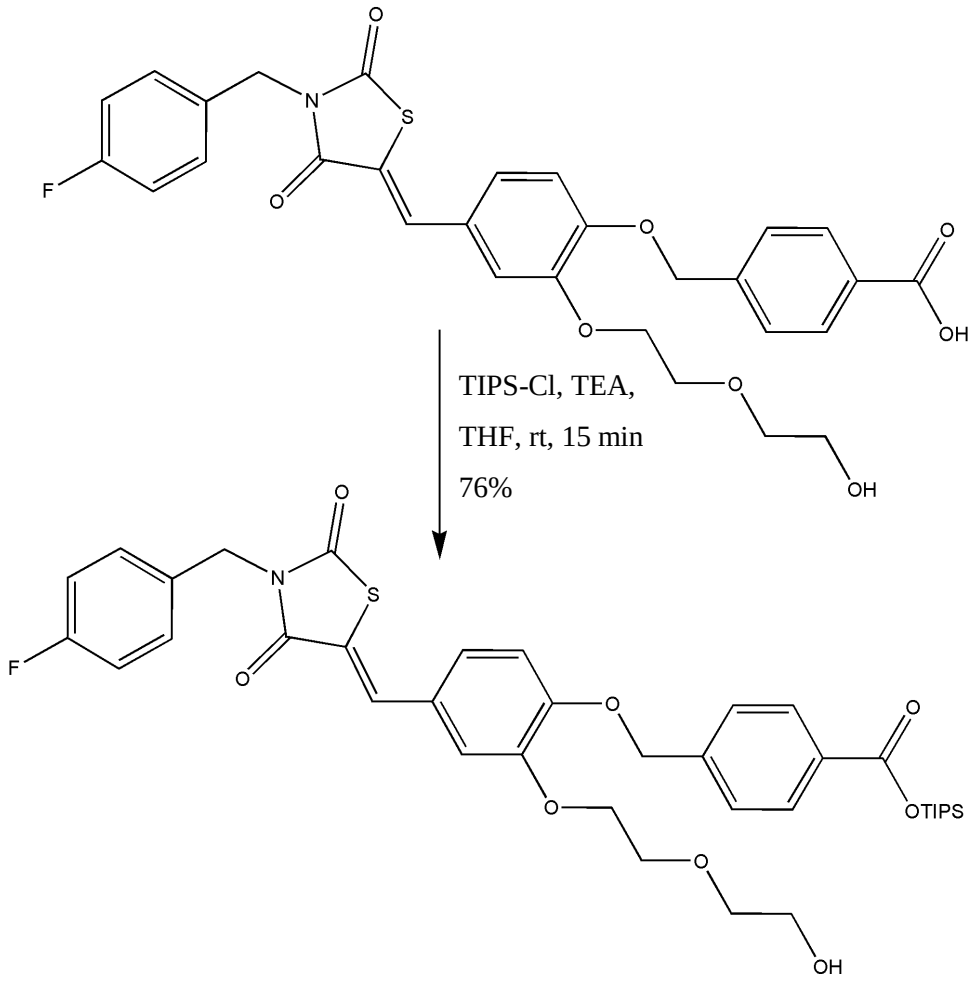

58

59

Scheme 4.19: Silyl protection of thiazolidine-2,4-dione with linker.

4.2.5.2 Conjugation to icodextrin

Compound **59** was conjugated to 20 kDa icodextrin as previously described in section 4.2.4.2. resulting in desired Conjugate 3, (30% mass recovered), as shown in Scheme 4.20.

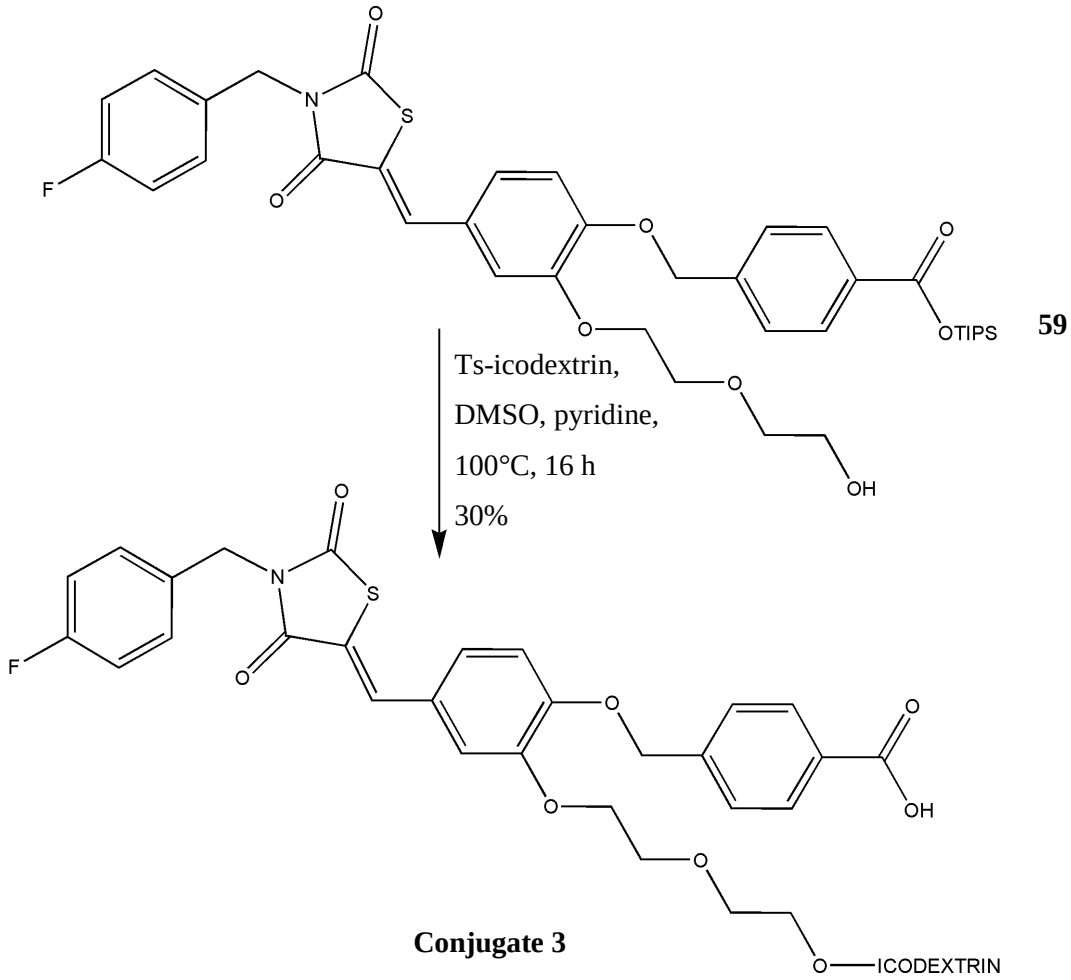

Scheme 4.20: Synthesis of conjugate 3.

4.2.6 Alternative route to conjugation

Tosyl groups have the potential to act as alkylating agents *in vivo*, therefore the synthetic route was altered to guarantee no tosyl groups were present in the final conjugate. This was achieved by reversing the reactivity, tosylating the inhibitor-linker molecule.

4.2.6.1 Tosylation of the inhibitor

Tosylation of compound **55** was investigated as a model reaction. This was achieved with tosyl chloride in dichloromethane with 1 equivalent of triethylamine. The product was purified by column chromatography to yield compound **60**, (57%).

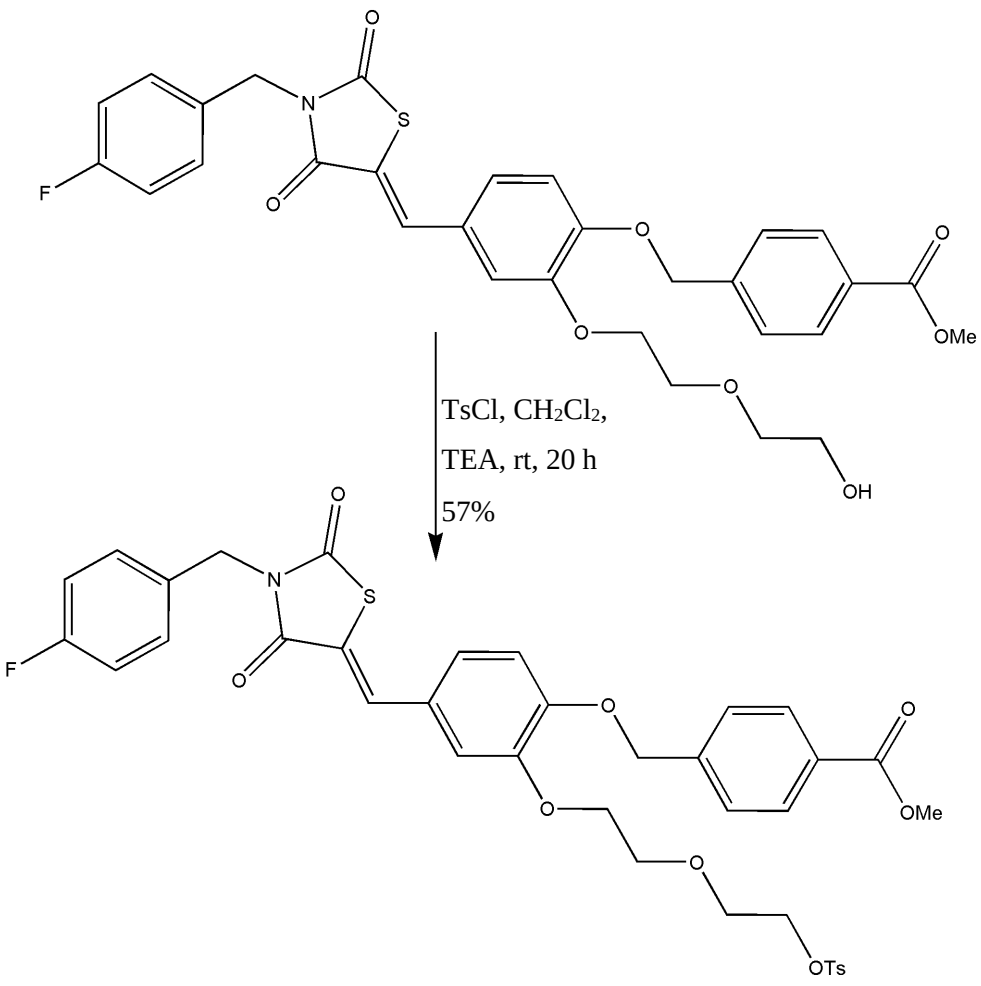

55

60

Scheme 4.21: Synthesis of tosylated thiazolidine-2,4-dione methyl ester.

Tosylation of compound **59**, was achieved according to the previously described method yielding compound **61**, (50%), as shown in Scheme 4.22.

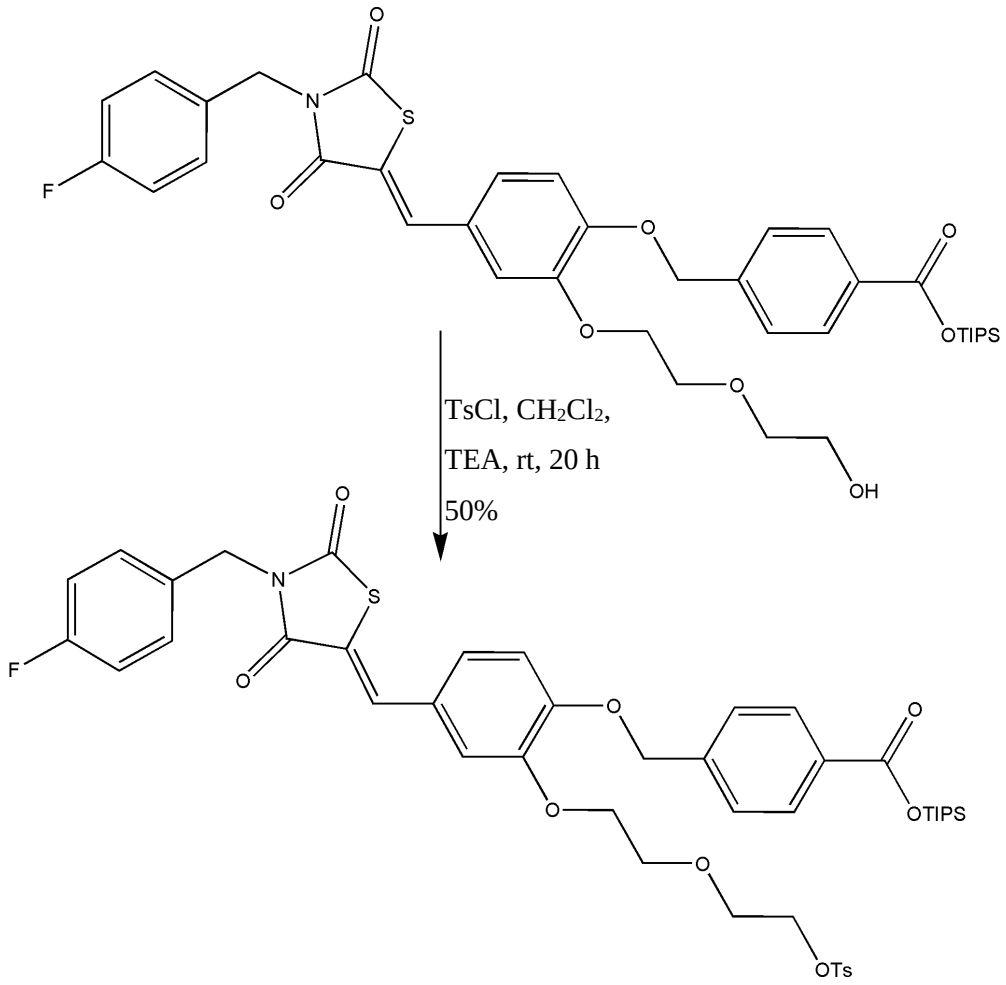

59

61

Scheme 4.22: Tosylation of thiazolidine-2,4-dione TIPS ester linker.

4.2.6.2 Gluco model study

A model study using the commercially available 2-methyl-3,4,5-pyranoside was performed to enable better structural analysis. The pyranoside was solubilised in anhydrous dimethyl-acetamide (DMAc) and sodium hydride was applied to deprotonate. The tosylate was added and the reaction was monitored by LC/MS. The resulting product was purified via column chromatography, to yield the desired compound **62**, (46%), as shown in Scheme 4.23.

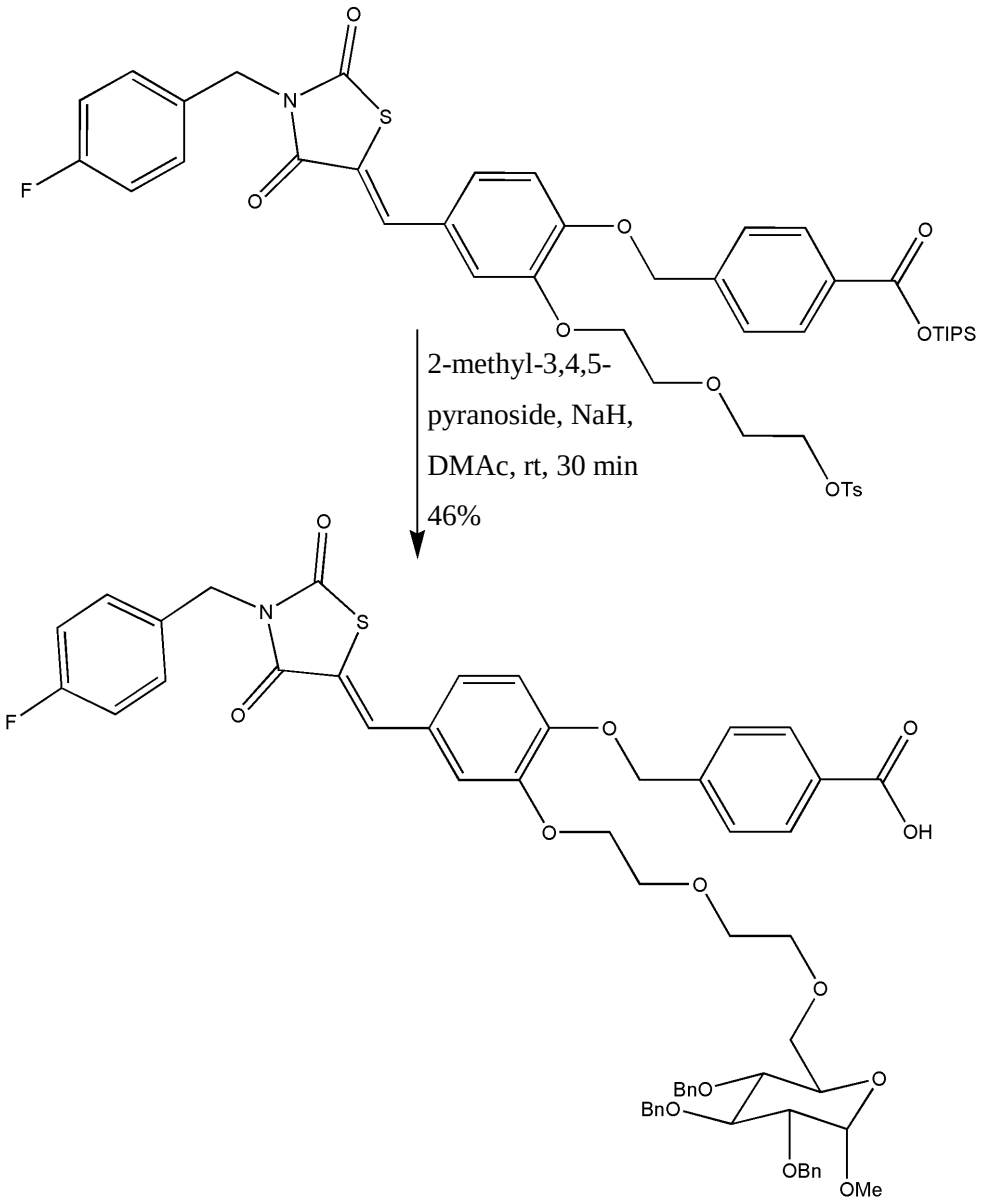

Scheme 4.23: Synthesis of model conjugate.

The structure of the conjugate was determined via NMR studies. ^{1}H NMR and ^{13}C NMR suggest that the coupling was complete, with the presence of all expected protons. It was also apparent that the triisopropylsilyl ester had been cleaved either during conjugation or work-up. Mass spectrometry was also performed however the compound had low ionisation and therefore could not be detected.

4.2.6.3 Synthesis of conjugates 4, 5 and 6

This approach was then attempted with icodextrin. Icodextrin was solubilised as described in section 4.2.3.1. Sodium hydride was used to deprotonate icodextrin, followed by addition of tosylate **61**. The reaction was stirred at room temperature and followed by TLC, to yield conjugates 4, 5 and 6.

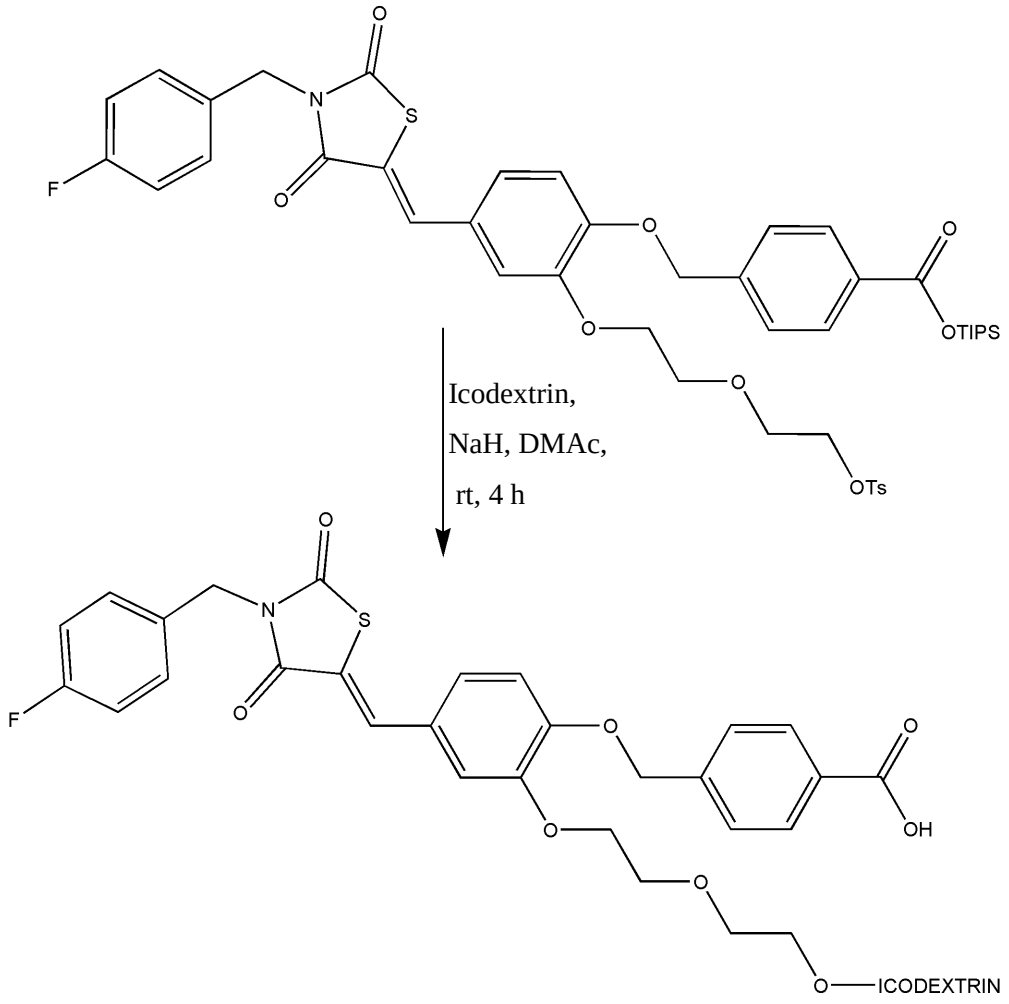

63

Conjugate 4, 5 and 6

Scheme 4.24: Synthetic strategy for conjugation to icodextrin.

A series of compounds were synthesised using different amounts of tosylate as shown in Table 4.3.

Conjugate	Equivalents	Yield (g)	Yield (%)
4	50	0.504	42
5	30	0.407	56
6	10	0.401	43

Table 4.3: Different equivalents of inhibitor molecule added.

4.2.7 Structural analysis

The structure of the conjugates was analysed via ^{1}H and ^{13}C NMR studies, IR spectroscopy and TGA analysis. Conjugate 4 was insoluble in several different solvents and therefore further characterisation was not possible.

^{1}H NMR analysis shows the presence of proton peaks representative of the inhibitor molecule, for example those in the aromatic region and the characteristic peaks of icodextrin, as shown in Figure 4.7.

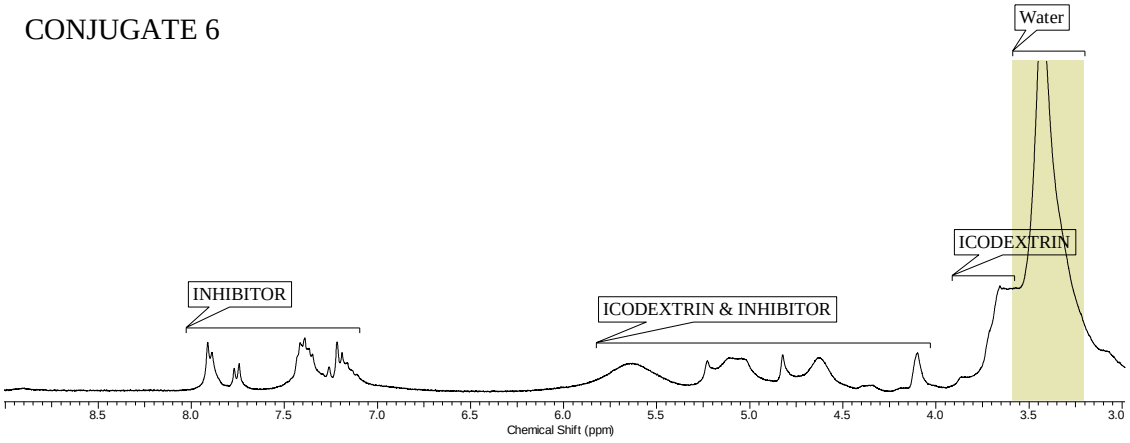

Figure 4.7: Representative ^{1}H NMR analysis of conjugate; Spectra of conjugate 6 shown.

The IR spectra of the conjugates when compared to icodextrin alone show peaks at 2852 and 1704 cm^{-1} which most likely correspond to the carboxylic acid of the inhibitor and a peak at 3386 cm^{-1} corresponding to the icodextrin OH peaks, as shown in Figure 4.8.

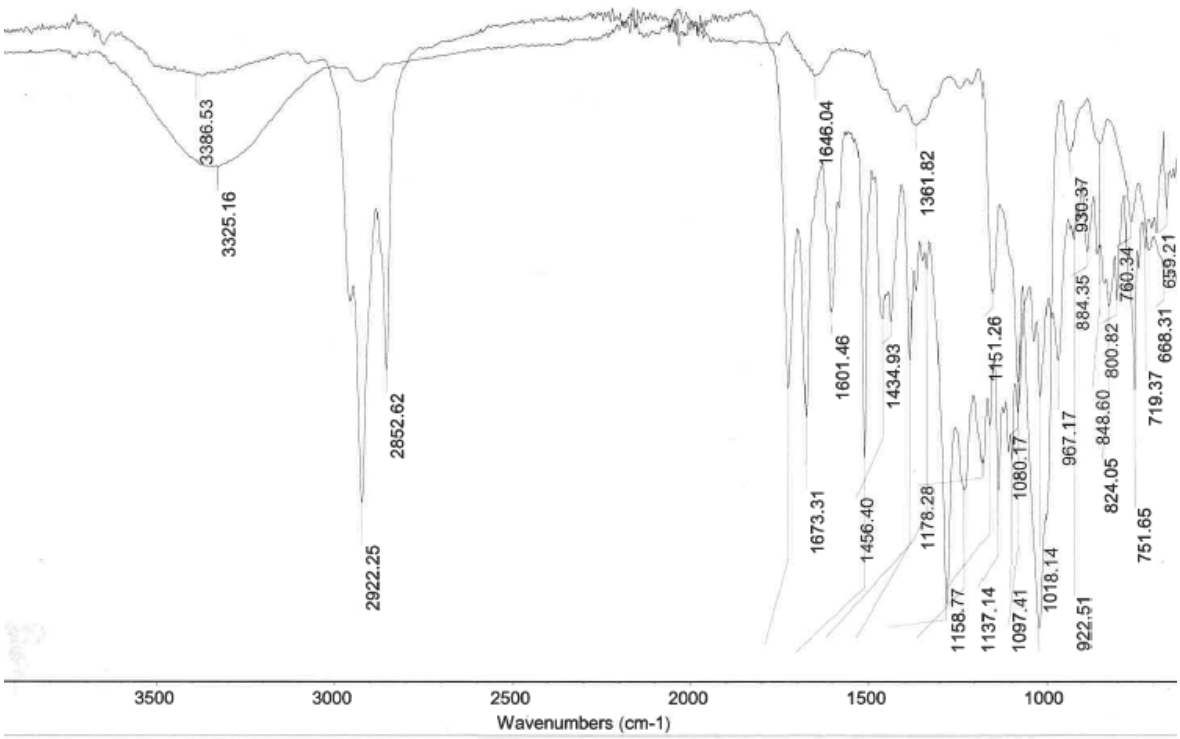

Figure 4.8: Representative IR spectrum; Icodextrin and conjugate 6.

TGA analysis was also performed. This showed conjugation to the inhibitor created a different profile to that of the inhibitor and the icodextrin, as shown in Figure 4.9. Weight loss below 100 °C was due to water evaporation, the weight loss above 100 °C is the thermal decomposition of the compound. Both icodextrin and the inhibitor have a single weight loss peak around 310 °C. Whereas the conjugate shows an earlier and more gradual decomposition starting at approximately 230 °C. The shallower decomposition pattern of the conjugate may be due to moisture escaping upon melting.

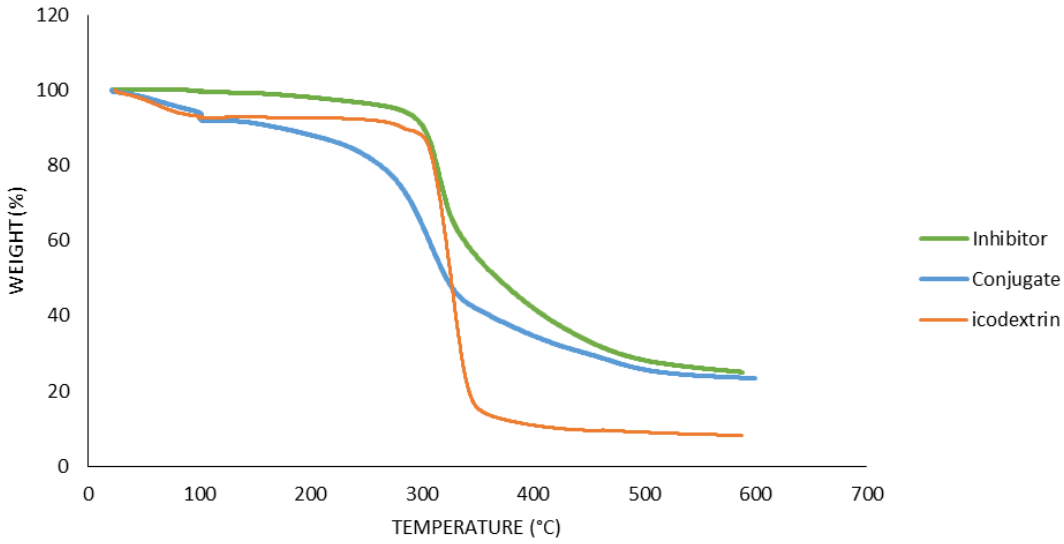

Figure 4.9: TGA analysis of conjugate 6.

The inhibitor inherent fluorescence was utilised to establish the degree of substitution of the conjugate. The fluorescence of a known amount of conjugate was measured and the fluorescence was compared to a standard curve of inhibitor fluorescence to calculate how much inhibitor was present. The amount of inhibitor molecule found to be present in the conjugates is shown in Table 4.4.

Conjugate	Inhibitor (μM)	Inhibitor/icodextrin (mmol/g)	Inhibitor/icodextrin (g/g)	Substitution (%)
2	43	0.0043	0.00212	0.07
3	15	0.0026	0.00129	0.04
5	95	0.095	0.0468	1.46
6	109	0.184	0.091	2.90

Table 4.4: Degree of substitution of conjugates 5 and 6; (Results shown are a mean of n=2).

4.3 Discussion

The initial strategy was to synthesise the lead compound and then expose the required hydroxyl group, utilising a mild base such as boron tribromide. However, selective removal of the aryl methyl ether was unsuccessful with the benzylic group also being cleaved. It was therefore attempted to substitute the methyl for a more selective leaving group. Derivitisation of this functional group with an acetyl group was attempted, however the selectivity for the 3-position was relatively low resulting in a mixture of compounds. Concurrently a method for selective substitution of the 4-hydroxyl group of 3,4-dihydroxy-benzaldehyde was investigated. This method proved successful with the mono-4-hydroxyl group being benzylated. The structure of this compound was confirmed by NMR studies and X-ray crystallography. This compound was condensed with the thiazolidinedione as previously described to yield the desired inhibitor with a functional group in the correct position to attach to icodextrin. The carboxylic acid moiety was left as an ester in order to act as a protecting group during conjugation to icodextrin.

Icodextrin was purchased as Extraneal™ peritoneal dialysis solution. This was an aqueous solution containing electrolytes and small organic molecules which required removal. This was achieved via dialysis against water. Icodextrin as a solid was then isolated utilising its poor solubility in organic solvents or were possible via freeze-drying to remove the water present. Solubilisation of icodextrin in an organic solvent was achieved utilising a DMAc/LiCl co-solvent system. The mechanism of dissolution is via disruption of hydrogen bonds between the OH of the polymer and chloride ions.[267] In order to conjugate to the inhibitor molecule icodextrin a good leaving group was required. This was achieved via the addition of a tosyl group, substitution at the C-6 OH was anticipated due to the increased reactivity of this primary position.

The next step was to conjugate the inhibitor molecule with the icodextrin tosylate. This was achieved under mild basic conditions with heat. The conjugation was determined via NMR analysis. However, after this, upon attempting to remove the methyl protecting group to expose the carboxylic acid which

is essential for autotaxin inhibition, the stronger basic conditions required for this saponification appeared too harsh, as evident by NMR analysis. Possible reason for this are interactions with the allyl group present in the drug molecule. Saponification of the drug molecule not conjugate to icodextrin also proved unsuccessful. It was therefore decided that a more liable protecting group was required for the carboxylic acid. A silyl group was chosen due to the selective cleavage of silyl groups using fluoride ions. Conjugation and subsequent deprotection utilising fluoride ions proved successful generating the desired thiazolidine-2,4-dione autotaxin inhibitor icodextrin conjugate.

As one of the primary aims of the conjugation to icodextrin is to increase the retention time of the autotaxin inhibitor in the intraperitoneal cavity; a larger icodextrin was desired in order to increase retention due to a larger hydrostatic volume. However, the previously employed synthetic route was unsuccessful. It was hypothesised this may be due to an increase in steric hindrance created by the larger chain of icodextrin present. Inclusion of a PEG linker was explored to act as a spacer between the icodextrin and the inhibitor molecule. This linker was chosen due to its stability and the retention of the terminal functional group to attach to icodextrin. This required a new synthetic route to the inhibitor molecule with linker attached which was successfully achieved in an eight step convergent synthetic route. Silyl esters were found to be very liable to cleavage and therefore chemistry was performed before the addition of this protecting group. In the future it may be beneficial to explore different carboxylic acid protecting groups. The new inhibitor molecule was conjugated to the larger icodextrin successfully and the degree of substitution was determined using the intrinsic fluorescence of the inhibitor molecule.

Tosyl groups have the potential to act as alkylating agents *in vivo*. To guarantee no tosyl groups were present after conjugation the reactivity was reversed, tosylating the inhibitor molecule. The potentially hazardous tosyl groups would therefore be removed during the dialysis step. This required synthesis of the inhibitor tosylate. This was achieved via selective tosylation of the terminal hydroxyl group of the inhibitor molecule. The inhibitor tosylate was then conjugated to icodextrin which had been deprotonated with sodium hydride. This was performed with multiple equivalents of the

inhibitor tosylate to further explore the effect the degree of substitution had on the physicochemical properties of the conjugate. Again the degree of substitution of these conjugates was determined via measurement of fluorescence.

4.4 Conclusion

A synthetic procedure to yield an icodextrin conjugate has been described. This synthetic route has the potential to be exploited for conjugation of many molecules to icodextrin. The conjugates described in this chapter will be investigated further for their biological activity.

Chapter 5

Biological evaluation of icodextrin autotaxin inhibitor conjugates

5.1 Introduction

The autotaxin/LPA pathway has been shown to promote migration and resistance to chemotherapy in ovarian cancer. Inhibition of this pathway has the potential to reduce these effects. In ovarian cancer LPA is present in ascites in concentrations up to 80 μM.[73] Autotaxin has also been shown to be elevated in the ascites of ovarian cancer patients. It is thought this contributes to chemoresistance and metastasis often associated with late stage ovarian cancer. Inhibition of autotaxin has been shown to increase the sensitivity of ovarian cancer cells to carboplatin[178] and breast cancer cells to paclitaxel.[179]

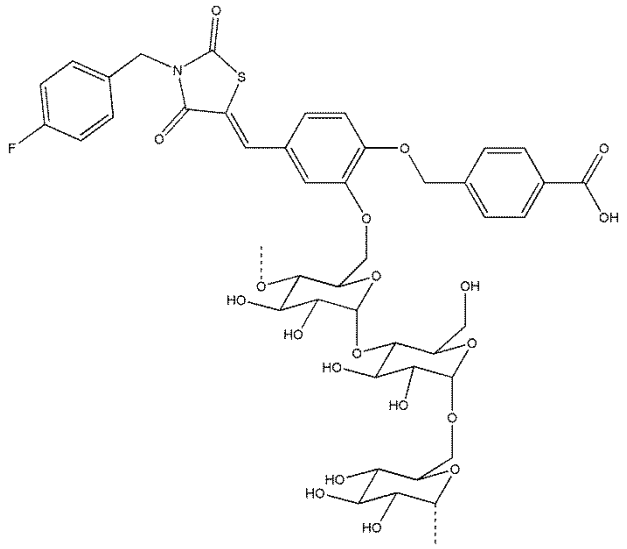

Figure 5.1: Structure of Icodextrin-autotaxin inhibitor, conjugate 2.

Reducing these high levels of LPA present in ascites has the potential to prolong the time until relapse after chemotherapy and reduce drug resistance. Autotaxin inhibitors are small molecules which are likely rapidly cleared from the peritoneal cavity. Attaching autotaxin inhibitors to polymers has the potential increase the half-life of the inhibitor in the peritoneal cavity. Icodextrin is a polymer which is already established in the clinic for peritoneal dialysis. The intraperitoneal pharmacokinetics of icodextrin have been defined and icodextrin is eliminated from the peritoneal cavity slowly ($t_{½}$ > 12

hr).[261] Higher molecular weight icodextrin fractions are anticipated to be eliminated even more slowly. Icodextrin is therefore an ideal candidate for conjugation with autotaxin inhibitors.

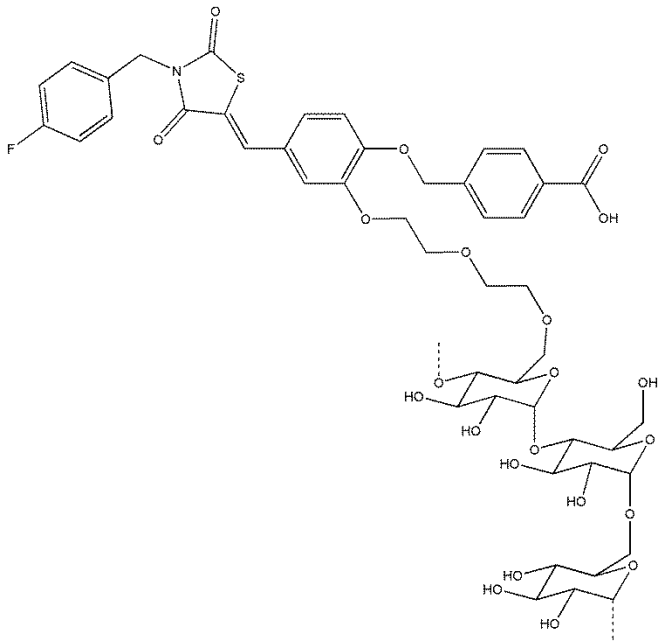

Figure 5.2: Structure of Icodextrin-autotaxin inhibitor conjugates 3-6.

Chapter 4 discussed the synthesis of icodextrin-autotaxin inhibitor conjugates, (Figure 5.2). This chapter will focus on the biological evaluation of these described conjugates. The conjugates were tested for *in vitro* activity employing the methods described in chapter 3. Firstly, the ability of these conjugates to inhibit recombinant autotaxin was evaluated using autotaxin from two sources. The effect on the autotaxin inhibitors' biological activity was assessed with a wound healing assay. The solubility and permeability of the conjugates was also characterised, this was achieved using the miniaturized shake flask method and a PAMPA assay for transport across an artificial bilayer, and a Caco-2 cell permeability assay. Preliminary studies were also carried out for *in vivo* compatibility and determination of the pharmacokinetic profile, achieved in a murine model.

5.2 Methods

5.2.1 Solubility

The solubility was measured as described in section 2.2.14.2 using the miniaturized shake flask method and adapted as follows. An excess of the test compound was suspended in 200 µL PBS (pH 7.4) and shaken for 24 h at room temperature, followed by centrifugation. Fluorescence of the supernatant was measured and the concentration of the solution was determined according to a standard curve.

5.2.2 FS-3 assay

Compounds were tested for autotaxin inhibition using the FS-3 assay as described in section 2.2.9 and adapted as follows. The free inhibitor (1 mM), conjugate 3 (6 mg/mL), conjugate 5 (10 mg/mL) and conjugate 6 (10 mg/mL) were prepared as a stock solution in DMSO, icodextrin (10 mg/mL) in water. The compounds were diluted 2-fold in PBS (pH 7.4). 80 µL of reaction buffer containing autotaxin and 10 µL of standard, compound dilution or solvent were pre-incubated for 10 min at 37 °C. 10 µL of FS-3 substrate were added and the rate of FS-3 hydrolysis was measured at 37 °C every two minutes for 30 min.

5.2.3 Bis-*p*NPP Assay

Compounds were also tested for their ability to inhibit autotaxin in the bis-*p*NPP assay as described in section 2.2.8 and adapted as follows. The free inhibitor (1 mM), conjugate 3 (6 mg/mL), conjugate 5 (10 mg/mL) and conjugate 6 (10 mg/mL) were prepared as a stock solution in DMSO and icodextrin (10 mg/mL) in water. Compounds were diluted 2-fold in PBS (pH 7.4). 20 µL of 5X reaction buffer, 10 µL bis-*p*NPP (1 mM) and 20 µL of compound dilution or solvent was added to each well, followed by the addition of 50 µL autotaxin solution. Absorbance was measured after 4 h incubation.

5.2.4 PAMPA

Permeability across an artificial bilayer was tested as described in section 2.2.12 and adapted as follows. The free inhibitor (1 mM), conjugate 3 (6 mg/mL), conjugate 5 (10 mg/mL) and conjugate 6 (10 mg/mL) were prepared as a stock solution in DMSO, icodextrin (10 mg/mL) in water and diluted with PBS (pH 7.4) to a final 2% DMSO. Membranes were wet with dodecane containing PC (5 mg/mL) 5 µL per well. Immediately after wetting 150 µL of either furosemide (10 µM), propranolol (10 µM), free inhibitor (10 µM), conjugate 2, (100 µg/mL), conjugate 3 (100 µg/mL), conjugate 5 (100 µg/mL) and conjugate 6 (100 µg/mL) was added to the appropriate donor well, and the donor compartment was placed in the acceptor plate, each acceptor well containing 300 µL of PBS (2% DMSO). The plates were incubated in a moist environment at room temperature for 48 h. The amount of compound present in the donor and acceptor compartments was measured by UV/VIS or fluorescence spectroscopy.

5.2.5 Caco-2 permeability assay

Permeability was further assessed in a cell based permeability assay as described in section 2.2.13 and adapted as follows. After incubation with serum free medium for 3 h, two HBSS washes were performed. 500 µL of HBSS was placed in the basolateral side and 500 µL of HBSS containing either paracetamol (10µg/mL), the free inhibitor (10 µg/mL) or conjugate 6 (100 µg/mL) was added to the apical side. 200 µL was immediately removed from the apical side for a T0 reading. The cells were incubated for 2 h, after which the supernatant was collected from both the apical and basolateral side. The concentration of the compounds was calculated from a standard curve of fluorescence.

5.2.6 Wound healing assay

The ability of the compound to inhibit migration was tested in the wound healing assay as described in section 2.2.10 and adapted as follows. Serum free growth medium was supplemented with LPC (0.5 µM), DMSO (normalised to 0.4%) and either no inhibitor, icodextrin (50 µg/mL), the free

inhibitor (500 nM), conjugate 3 (50 µg/mL), or conjugate 6 (50 µg/mL), 1 mL was added per well. The percentage wound closure was measured after 16 h.

5.2.7 *In vivo* experiments

Animal experiments were performed under the guidelines of UK Home office regulations under the Animals (Scientific Procedures) Act 1986 and UKCCR guidelines for animal experimentation and were approved by the animal welfare commission of Keele University. Female NCR Nu/Nu mice between 5 and 7 weeks were used and allowed to acclimatise for 1 week after arrival.

5.2.7.1 Sterilisation of compound NF440

Before use, the compound was sterilised by suspending a known amount in 70% ethanol followed by freeze-drying (Edwards Modulyo), for 4 h to remove all traces of solvent. The compound was then dissolved in sterile PBS and diluted to concentrations of 0.22 mg/mL, 0.1 mg/mL and 0.03 mg/mL.

5.2.7.2 In vivo toxicity study

Mice were weighed and received intraperitoneal injection of 0.4 mL of either 0.03 mg/mL, 0.1 mg/mL or 0.22 mg/mL NF440 in sterile PBS using a 26G syringe in the lower left quadrant. The mice where monitored over 24 h for adverse effects. After 24 h the mice were weighed and euthanized by cervical dislocation. Ventral skin was removed and 0.5 mL sterile PBS was added to the peritoneal cavity, the wash was collected after gentle massage with the blunt end of forceps. An autopsy was then performed to check for signs of toxicity or adverse effects.

5.2.7.3 In vivo peritoneal retention

Mice were injected with 0.4 mL of 0.22 mg/mL NF440 into the peritoneum with a 26G syringe in the lower left quadrant. 3 mice per time point were euthanized by cervical dislocation at 1 min, 30 min, 60 min, 3 h, 6 h and 24 h after injection. 0.4 mL PBS was used as a control for background

fluorescence (see below) and mice in this group were euthanized after 1 min by cervical dislocation. Ventral skin was removed and 0.5 mL sterile PBS was added to the peritoneal cavity, the wash was collected after gentle massage with the blunt end of forceps. The washes were immediately centrifuged (5, 000 g 10 min) and the supernatant was transferred to a new microcentrifuge tube. The volume collected was measured and the fluorescence, ($\lambda_{Ex.}$ = 360 nm, $\lambda_{Em.}$ = 440 nm) of 100 µL of each wash was measured using a Synergy 2 multimode microplate reader. The amount of compound present was calculated from the standard curve to determine drug concentration and from the sample volume. The data was analysed using GraphPad software to fit an exponential decay to calculate the half-life. The drug recovery by peritoneal lavage was estimated by comparison of the mass of drug inject to the mass recovered 1 minute after injection.

5.3 Results

5.3.1 Inhibition of autotaxin

The ability of the conjugates to inhibit autotaxin was measured in two autotaxin inhibition assays, using two sources of autotaxin and two substrates, FS-3 and bis-*p*NPP.

5.3.1.1 FS-3 assay

The ability of the conjugates to inhibit autotaxin was tested using FS-3 as the substrate. The conjugates demonstrated IC_{50} values ranging from 0.85 µg/mL to 6.7 µg/mL. The IC_{50} of the conjugates are between 2 and 20 fold higher than that of the free inhibitor when expressed in terms of the concentration of pharmacophore attached to the polymer, with IC_{50}s of 76-640 nM compared to 35 nM of the free inhibitor, (Figure 5.3 and Table 1.1). The reduction in potency was more pronounced in the conjugates with the higher amounts of pharmacophore attached. The unconjugated icodextrin had no measureable effect in this assay. A secondary screen was also performed to ensure the compounds did not interfere with the fluorescence of the assay substrate, FS-3. None of the compounds tested in this assay interfered with fluorescence.

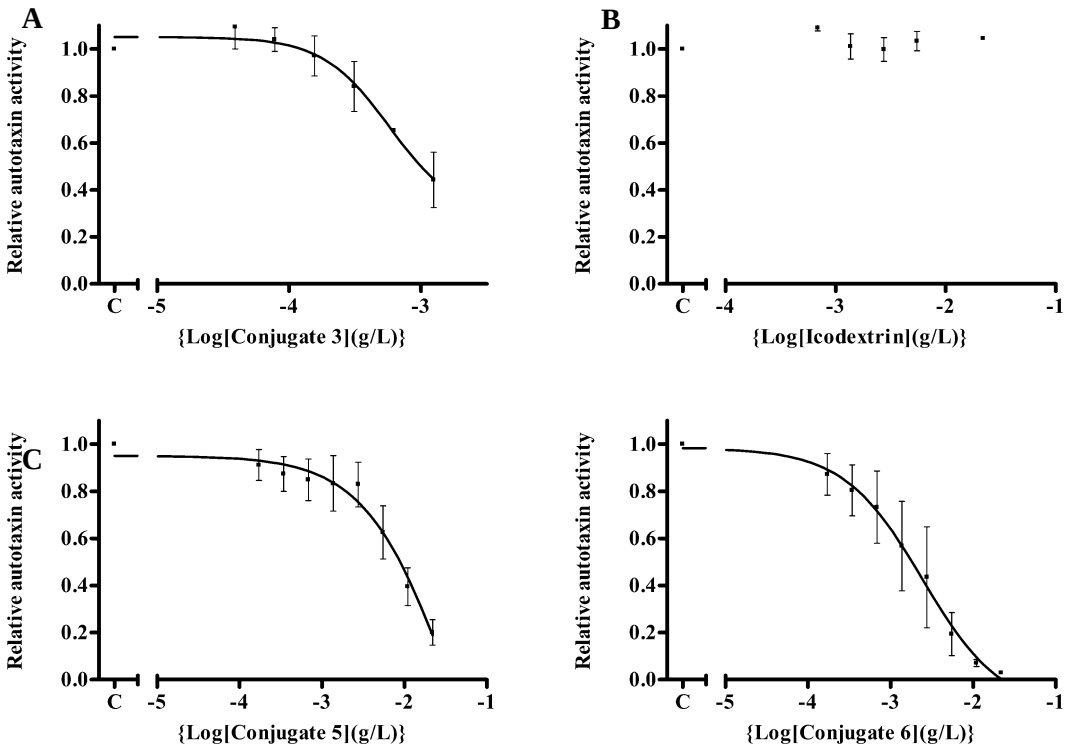

Figure 5.3: Inhibition of autotaxin enzymatic activity by conjugates, 3, 5 and 6, tested in FS-3 assay; A. inhibition with conjugate 3; B. with icodextrin; C. inhibition with conjugate 5; D. inhibition with conjugate 6. The results are expressed as a fraction (mean ±S.D. n=2) of the activity measured in the absence of the inhibitor.

Compound	**IC_{50} [pharmacophore] (nM)**	**IC_{50} [conjugate] (µg/mL)**
Free inhibitor	35	-
Conjugate 3	76	1.3, 0.87
Conjugate 5	189, 125	6.4, 7.3
Conjugate 6	699, 611	1.0, 0.68

Table 5.1: Inhibition of autotaxin enzymatic activity by the free inhibitor, conjugates 3, 5 and 6, tested FS-3 assay; IC_{50}s are shown as either the concentration of conjugate (µg/mL) or the concentration of pharmacophore present in the conjugate (nM). (IC_{50} values of the conjugates are given as µg/mL because the MW of icodextrin is varied about 20 kDa). Both the mean average and standard deviation were calculated using IC_{50} values from repeat experiments.

5.3.1.2 Bis-pNPP assay

The ability of compounds to inhibit autotaxin was also investigated using bis-*p*NPP as the substrate. Autotaxin was purified from 3E3 cells as described in section 2.2.7. The conjugates had a comparable IC_{50} to that obtained in the FS-3 assay, with IC_{50}s ranging from 90 nM to 640 nM, (Figure 5.4). This was similarly comparable to the amount of pharmacophore present. Maximal inhibition varied with conjugate 2 and 3 unable to completely inhibit autotaxin, this may be due to lower solubility of these conjugates. As these compounds have different maximal inhibitions comparing IC_{50} values is limited. Unconjugated icodextrin (100 µg/mL) had no measureable effect in this assay. The results are summarised in Table 5.2.

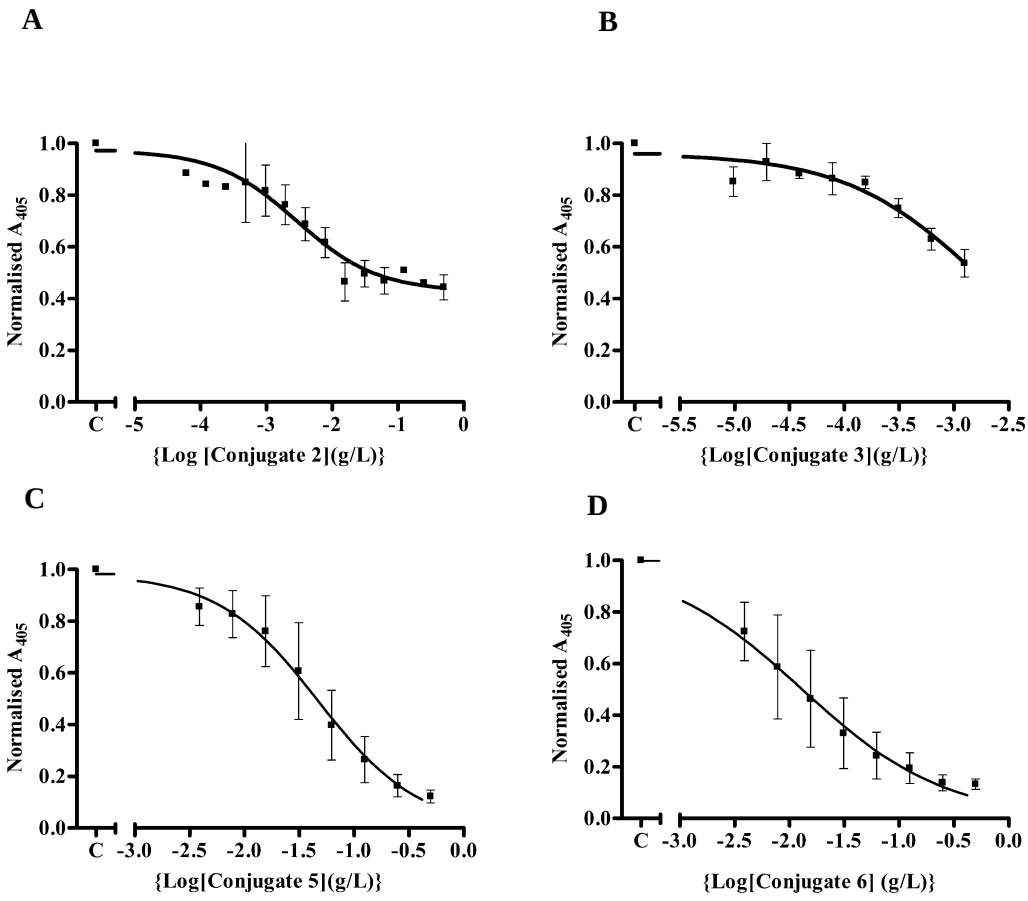

Figure 5.4: Inhibition of autotaxin enzymatic activity by conjugates 2, 3, 5 and 6, tested in bis-*p*NPP assay; A. inhibition with conjugate 2; B. inhibition with conjugate 3; C. inhibition with conjugate 5; D. inhibition with conjugate 6. The results are expressed as a fraction (mean ±S.D. n = 2-3) of the activity measured in the absence of the inhibitor.

Compound	**IC_{50} [pharmacophore] (nM)**	**IC_{50} [conjugate] (µg/mL)**
Free inhibitor	56	-
Conjugate 2	120	2.9 ± 2.2
Conjugate 3	99 ± 45	2.2 ± 1.9
Conjugate 5	495 ± 448	6.2 ± 6.7
Conjugate 6	392 ± 527	2.1 ± 2.9

Table 5.2: Inhibition of autotaxin enzymatic activity by the free inhibitor conjugates 2, 3, 5 and 6, tested in Bis-*p*NPP assay; IC_{50}s are shown as either the concentration of conjugate (µg/mL) or as a relative concentration to the amount of pharmacophore present in the conjugate (nM). (Results are expressed as mean ± S.D. n=3). Both the mean average and standard deviation were calculated using IC_{50} values from repeat experiments.

5.3.2 Solubility

The aqueous solubility of the compounds in PBS (pH 7.4) was tested using a miniaturised shake flask method. Conjugation to icodextrin increased the solubility of the pharmacophore compared to the free inhibitor, compound **24**. (Table 1.3) The solubility of the conjugate 6 is less than conjugate 5, probably reflecting the higher density of pharmacophore attached to icodextrin in conjugate 6.

Compound	**Solubility (g/L)**	**Degree of substitution Inhibitor/icodextrin (g/g)**
Free inhibitor	0.08 ± 0.015	-
Conjugate 5	1.52 ± 0.263	0.0468
Conjugate 6	0.22 ± 0.015	0.091

Table 5.3: Solubility of conjugates; measured using a miniaturised shake flask method. (Results are expressed as mean ± S.D. n=3).

5.3.3 Permeability

The autotaxin inhibitor was attached to icodextrin in order to increase retention of the inhibitor in the intraperitoneal cavity. The effect of conjugation on the permeability of the compound was tested in two assays, across an artificial bilayer and across an epithelial cell layer.

5.3.3.1 PAMPA

The ability of icodextrin to decrease the permeability of the pharmacophore across an artificial bilayer was measured using PAMPA assay. Furosemide and propranolol were used as a control for low and high permeability, respectively. These compounds showed the anticipated differences in permeability. The free inhibitor was moderately permeable across the membrane, but all the icodextrin conjugates showed substantially less permeability than the free inhibitor and were in some cases less permeable than furosemide, Figure 5.5.

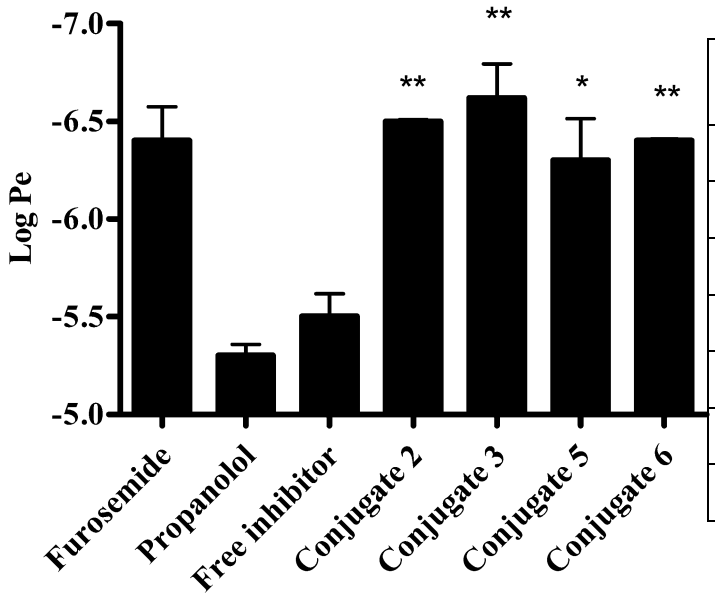

Compound	Permeability (Log Pe)
Furosemide	-6.4 ± 0.3
Propranolol	-5.3 ± 0.1
Free inhibitor	-5.5 ± 0.2
Conjugate 2	-6.5 ± 0.01
Conjugate 3	-6.9 ± 0.3
Conjugate 4	-6.3 ± 0.3
Conjugate 5	-6.4 ± 0.01

Figure 5.5: Permeability of conjugates measured in PAMPA assay; Permeability of the free inhibitor and conjugates 2, 3, 5 and 6, Furosemide and Propranolol are shown as a control for low and high permeable drugs respectively. Furosemide (100 µM), Propranolol (100 µM), Free inhibitor (100 µM), Conjugate 2 (100 µg/mL), Conjugate 3 (100 µg/mL), Conjugate 5 (100 µg/mL) or Conjugate 6 (100 µg/mL) were applied to the artificial bilayer. After 48 h Log Pe was calculated. (Bars show mean +S.D., n=2–3). Control cells were treated with vehicle (0.4% DMSO). * $P < 0.05$, ** $P < 0.01$, *** $P < 0.001$, vs. control (paired t-test).

To further confirm a decrease in permeability when conjugated to icodextrin conjugate 6 was tested in a Caco-2 cell permeability assay. The effect of the conjugate on the trans epithelial electrical resistance (TEER) of Caco-2 cells was measured over 2 h, this determined the compound had no effect on the cell monolayer. The permeability of the conjugate was approximately 9 fold less than the free inhibitor, as shown in Table 5.4.

Compound	Permeability (P_{app} x 10^{-6})
Paracetamol	38
Free inhibitor	65.6
Conjugate 6	7.4

Table 5.4: Permeability of the free inhibitor and conjugate 6 measured in Caco-2 assay; Paracetamol was used as a control. Paracetamol (10 µg/mL) or Conjugate 6 (100 µg/mL) were applied to the artificial bilayer. (Results are expressed as mean ± S.D. n=3).

5.3.4 Inhibition of migration

LPA and autotaxin have been shown to regulate cell migration. To confirm the biological activity of the conjugates their effect on wound healing was evaluated using 3E3 ovarian cancer cells; these cells were previously engineered to overexpress autotaxin.[178] The cells transfected with the vector, 3V5, were used as a control. Once an even monolayer had formed a wound was inflicted and the migration of the cells was measured. The free autotaxin inhibitor reduced wound closure by approximately 50% compared to the wound closure measured with cells exposed to vehicle alone. The conjugates at a comparable concentration in terms of the amount of pharmacophores present, were also able to reduce wound closure by approximately 50%, (Figure 5.6).

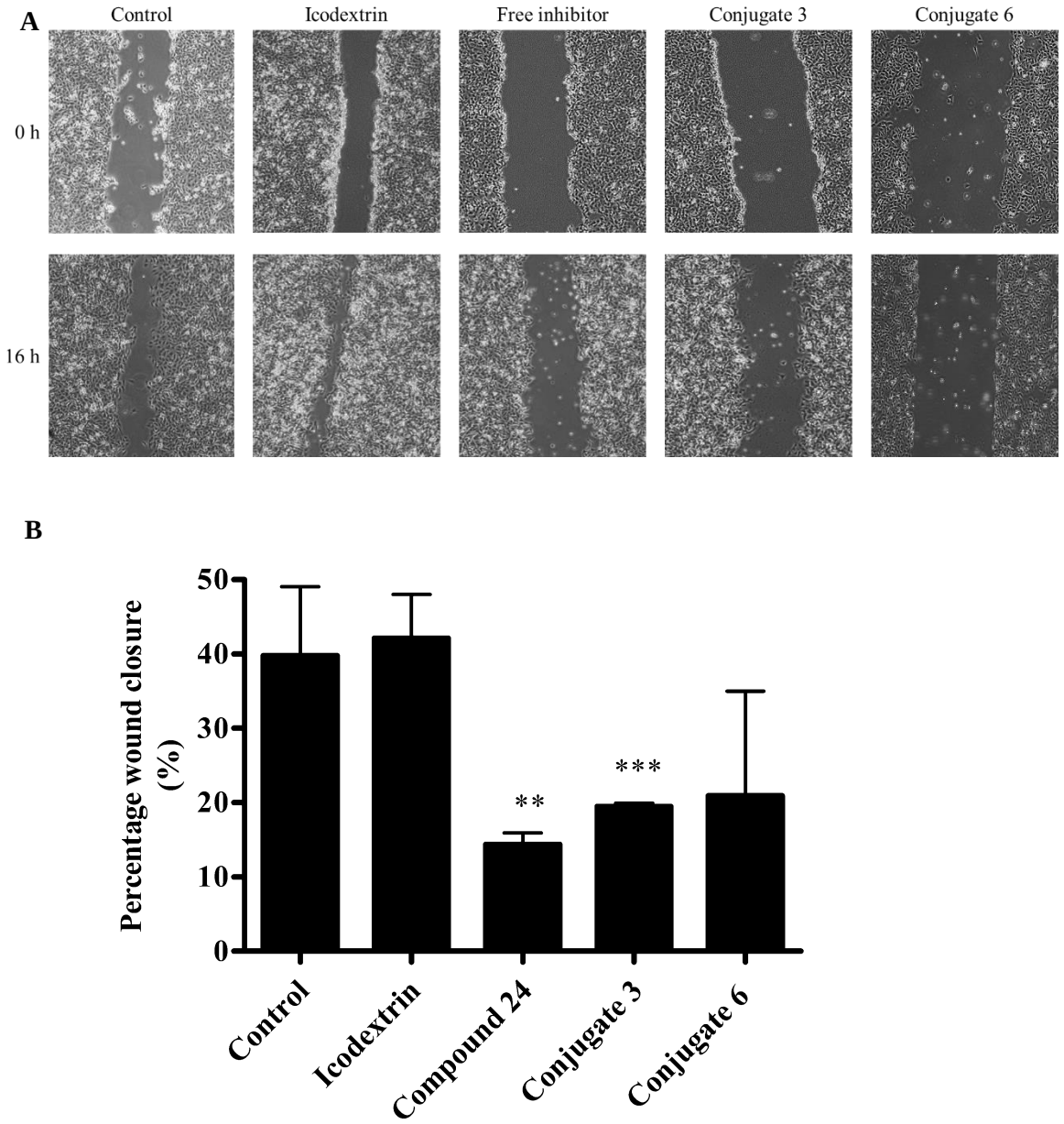

Figure 5.6: Effect of autotaxin inhibition with the free inhibitor, conjugates, 3 and 6 on wound closure; A. Inhibition of autotaxin with the free inhibitor and conjugate. 3E3 cells were grown to confluence, a wound was created and serum free media containing the free inhibitor (100 nM), conjugate 3 (5 µg/mL), or conjugate 6 (10 µg/mL) was added and wound closure was measured after 16 h. B. The percentage wound closure was measured, wound closure = ((pre-migration area – post-migration area)/pre-migration area) *100. (Bars show mean +S.D., n=2–5, compound 24 n=5, conjugate 3 n=3, conjugate 6 n=2). Control cells were treated with vehicle (0.4% DMSO). * $P < 0.05$, ** $P < 0.01$, *** $P < 0.001$, vs. control (paired t-test, compared to corresponding control).

Icodextrin alone was also tested in the wound healing experiment at a concentration comparable to that of conjugate used, this was found to have no significant effect on wound closure, (Figure 5.7). The effect of the inhibitors on the migration of 3V5 cells, which were transfected with the empty vector, and do not over express autotaxin was measured concurrently. Both the free autotaxin inhibitor and conjugates had no significant effect on the percentage wound closure.

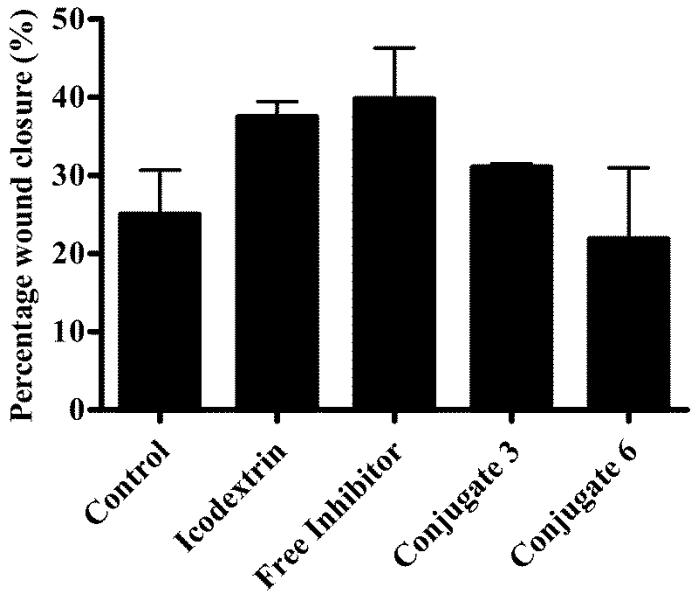

Figure 5.7: Effect of autotaxin inhibition with the free inhibitor, conjugates, 3, and 6 on wound closure in 3V5 cells, transfected with the vector; 3V5 cells were grown to confluence, a wound was created and serum free media containing the free inhibitor (100 nM), conjugate 3 (5 µg/mL), or conjugate 6 (10 µg/mL) was added and wound closure was measured after 16 h. The percentage wound closure was measured, wound closure = ((pre-migration area – post-migration area)/pre-migration area) *100. (Bars show mean +S.D., n=2–5, compound 24 n=5, conjugate 3 n=3, conjugate 6 n=2). Control cells were treated with vehicle (0.4% DMSO).

5.3.5 *In vivo* pharmacokinetics

5.3.5.1 Toxicity

Before initiating *in vivo* experiments to assess the pharmacokinetics of the conjugates, the effect of intraperitoneal administration of the conjugate was evaluated for acute overt toxicity and to establish a safe dose for subsequent experiments. Conjugate 6 was formulated in sterile PBS at concentrations

of 0.03 mg/mL, 0.1 mg/mL and 0.22 mg/mL. nu/nu mice at 6-7 weeks were injected with 400 µL of the formulation into the peritoneal cavity. Mice were monitored for adverse effects for 24 h but no overt toxicity was seen. Furthermore, there was no significant difference in the weight of the mice before administration and after 24 h. After sacrificing the mice, autopsies did not reveal any gross pathological effects.

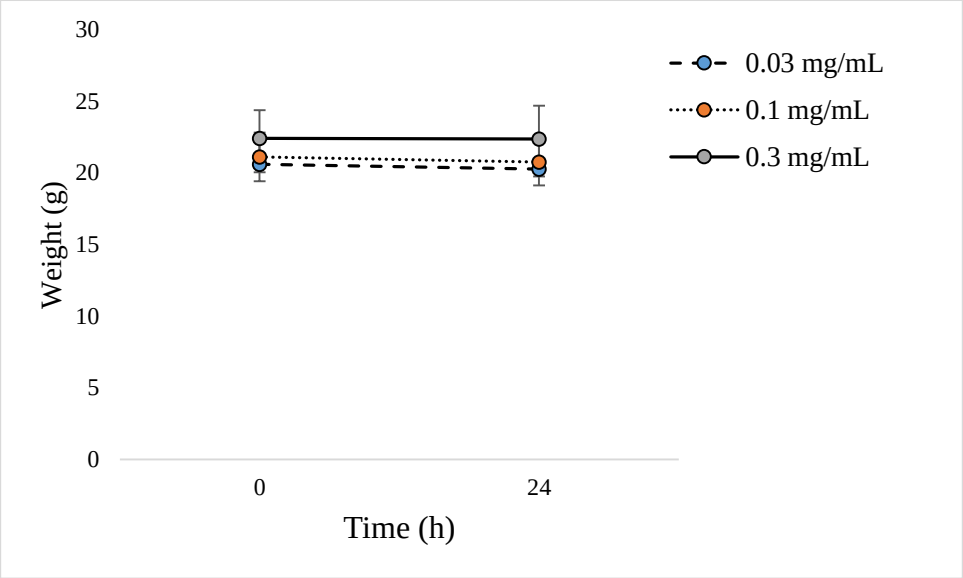

Figure 5.8: Weight difference in mice treated with conjugate 6 at varying concentrations over 24 h (Results are express as a mean ± S.D. of n=2).

5.3.5.2 Peritoneal retention

To assess whether intraperitoneal administration of the conjugates could allow prolonged inhibition of autotaxin, the retention of conjugate 6 in the intraperitoneal cavity of nu/nu mice was evaluated over 24 h. 0.4 mL of conjugate 6 (0.22 mg/mL) was administered i.p. and mice were sacrificed 1 min, 30 min, 60 min, 3 h, 6 h, and 24 h after administration. The peritoneal cavity was washed and the amount of conjugate present in the wash was measured. The half-life of the conjugate in the peritoneal cavity was found to be 0.59 h, as shown in Figure 5.9. Notably, however, 30% of the drug remained after 24 hours, compared to the amount recovered after 1 min. These data suggest that drug

elimination does not follow monophasic kinetics although insufficient data points were obtained to conduct a robust analysis.

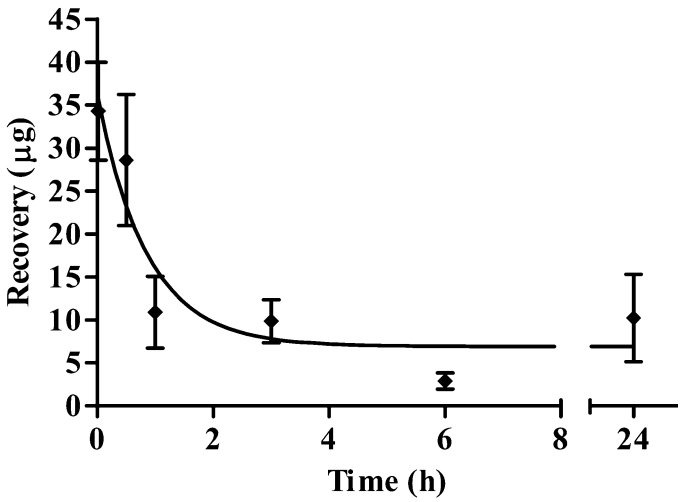

Figure 5.9: Conjugate 6 peritoneal retention; Conjugate 6 recovered from intraperitoneal washes versus time in the peritoneal cavity is plotted. (Results are express as a mean ± S.D. of n=3).

The percentage recovery from the peritoneal cavity was calculated. The intercept of a linear regression of natural log of retention plotted against time was used to estimate the amount of drug present at time zero (from the y intercept). This value did not differ substantially from the mass of drug measured in the peritoneal cavity immediately after drug administration. The estimated amount present from linear regression analysis suggests that approximately 40% of the conjugate was recovered from the peritoneal cavity at time 0h.

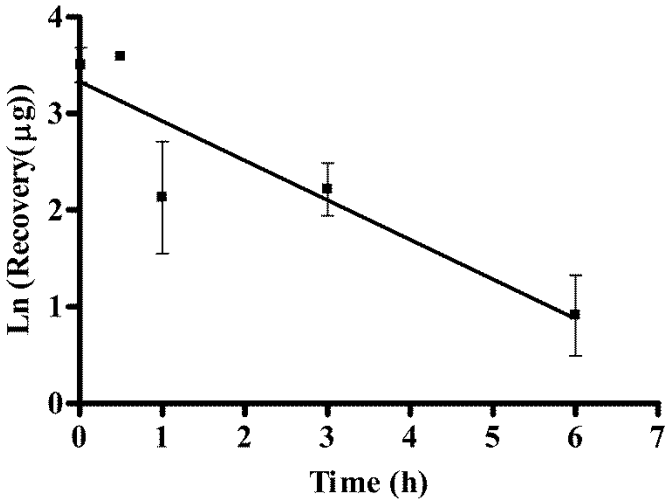

Figure 5.10: Linear regression to calculate recovery from intraperitoneal cavity; Ln(recovery(µg)) against time. (Results are express as a mean ± S.D. of n=3).

5.4 Discussion

Autotaxin catalyses the production of LPA which is present at high concentrations in the peritoneal cavity of ovarian cancer patients. Inhibition of autotaxin has the potential to decrease the survival, migration and proliferation of cancerous cells. Maintaining a high local drug concentration within the peritoneal cavity is important to provide sufficient prolonged inhibition of autotaxin.

The major processes for eliminating drugs from the peritoneal cavity are either via the blood and lymphatic system or diffusion across the peritoneal membrane.[236, 268] The peritoneal membrane is thin and highly permeable to molecules with molecular weights of less than 20 kDa. Transfer into the blood vessels is limited by transfer across the capillary membrane and blood flow. The lymphatic system absorbs compounds with a molecular weight greater than 500 Da. Therefore, the residence time of small molecular weight drugs in the peritoneal cavity may not be adequate because they are quickly absorbed through the peritoneal capillaries into the systemic circulation, or they are lost by diffusion across the peritoneum. Attaching an autotaxin inhibitor to icodextrin has the potential to increase the retention of the inhibitor in the intraperitoneal cavity, by preventing diffusion of the compounds across the peritoneal membrane. In the previous chapter the synthesis of an icodextrin-autotaxin inhibitor conjugate was described. The work described in this chapter explores the effect conjugation has on the pharmacokinetics and the biological activity of the inhibitor.

The autotaxin inhibitor chosen to attach to icodextrin was a potent inhibitor with a thiazolidinedione core previously described by Albers *et al*.[224] This compound had a terminal carboxylic acid but, a relative of this inhibitor, a boronic acid based inhibitor, has been shown to reduce plasma LPA levels *in vivo*. Although this reduction was short lived it shows promise as a candidate to target autotaxin.[223]

The conjugates were initially investigated for retained activity by assessing their ability to inhibit autotaxin obtained from two different sources (commercial kit or purified from 3E3 cells) and measured using two different substrates. The conjugate retained activity in both assays giving confidence the drug is active. The degree of substitution appeared to have an effect on the ability of the conjugate to inhibit autotaxin. Having more inhibitor conjugated led to a decrease in potency

when expressed in terms of the pharmacophore present. This may be due to steric hindrance caused by having too much drug attached to icodextrin, preventing more autotaxin from binding and therefore some of the drug becomes redundant.

Conjugation to icodextrin increased the aqueous solubility of the inhibitor. However, similar to the observed reduction in potency with increased substitution, the aqueous solubility decreased as the amount of inhibitor attached was increased. This is not surprising considering that the pharmacophore is significantly more hydrophobic than icodextrin. It may be appropriate to optimise the substitution ratio to optimize the solubility/potency profile, in order to maximize the therapeutic benefit of the drug.

The Autotaxin/LPA pathway is known to regulate cell migration, in many cancer cell types, including ovarian cancer.[141, 256-257] Inhibition of autotaxin has been shown to reduce cancer cell migration. A monolayer wound healing experiment was used to confirm the free drug inhibits migration in ovarian cancer cells overexpressing autotaxin. The same assay was used to confirm the conjugates retained biological activity. Neither the free inhibitor nor the conjugate reduced migration in 3V5 cells, which were transfected with the vector and do not overexpress autotaxin. This suggests that the compounds are inhibiting migration by reducing the activity of autotaxin rather than as a result of activity at some other target. The activity of this conjugate as an inhibitor of migration suggests that the conjugate could be used to inhibit metastasis.

Once the conjugates had demonstrated retained pharmacological activity, conjugate 6 was taken forward for *in vivo* pharmacokinetic analysis. Initially the toxicity of the conjugates was investigated to establish a safe dosage. The conjugate was found to have no evident adverse effects on the health of the mice. It is not surprising that the conjugate showed no toxicity because icodextrin is already established clinically and the drug is quickly metabolised. The pharmacophore itself has previously been reported to undergo rapid metabolism. This may be advantageous because once the drug becomes systemically available, its rapid metabolism is likely to reduce the chance of toxicity. It is possible, however, that the drug metabolites could be toxic. Thus, the studies here were only

preliminary tolerability tests to allow further *in vivo* testing and formal toxicological evaluation will still be necessary.

A key factor for conjugation was to increase the retention time in the peritoneal cavity, the effect of conjugation on permeability was assessed using two *in vitro* assays. In a PAMPA artificial bilayer assay the conjugates were found to have low permeability this was consistent with the low permeability found in Caco-2 epithelial cell permeability assay. However, the half-life of the conjugate in the peritoneal cavity was less than 1 hour. This figure was calculated assuming monophasic drug elimination. Notably, however, 30% of the drug remained after 24 hours, suggesting that the drug elimination may be more complex. One possibility is that the injection fluid is rapidly removed from the peritoneal cavity, and the reduced fluid volume reduces the efficiency of elimination. This may be therapeutically important, because it may allow the drug to accumulate at relatively high concentrations. The relatively short half-life may also be explained by the observation that rodents have an increased amount of α-amylase in the peritoneal cavity compared to humans.[269] The half-life of icodextrin in rodents is known to be significantly less than that in humans due to this increased amount of α-amylase.[269] This may account for the short half-life observed in the murine model. Retention of icodextrin is longer in humans, with a dwell time of more than 12 h.[261] The higher molecular weight fractions, as used in these studies, are anticipated to be eliminated even more slowly. Coupled with the low permeability the conjugate exhibited in *in vitro* models, this suggests that the conjugate could be expected to be retained significantly longer in humans. This is important because it suggests that once daily dosing (or even less frequently) may be possible.

Recovery of the conjugate from the peritoneal cavity was approximately 30% after time 0h of the drug injected. This low recovery was likely to be due to the difficulty in washing out drug from the peritoneal cavity. Therefore, it can be expected that the amount of drug in the peritoneal cavity is higher than the observable concentrations.

5.5 Conclusion

The results from this study suggest that in principle autotaxin inhibitors may be conjugated to icodextrin and retain their pharmacological activity. Conjugation has the potential to improve the pharmacokinetics of the autotaxin inhibitor. The conjugate demonstrated an improved pharmacokinetic profile compared to the free inhibitor. This suggests that conjugation of autotaxin inhibitors to icodextrin has the potential to reduce autotaxin inhibitor clearance from the peritoneal cavity. It will be useful to evaluate the conjugate in an ovarian cancer intraperitoneal xenograft model. Although the focus of the studies described here are to evaluate autotaxin inhibitors for the treatment of ovarian cancer, autotaxin inhibitors have potential in other cancers and other diseases. It will be useful to evaluate the ability of these conjugates to retain pharmacological activity *in vivo.*

Chapter 6

Conclusions and further work

6.1 Introduction

Autotaxin is an extracellular phospholipase D that catalyses the hydrolysis of lysophosphatidyl choline (LPC) to bioactive lipid lysophosphatidic acid (LPA). LPA has been implicated in many pathological processes relevant to cancer, including cell migration and invasion, proliferation, and survival. It has also been shown to be relevant to other pathological diseases such as inflammatory conditions. Autotaxin inhibition is a rapidly expanding field with many potential therapeutic uses. Although autotaxin inhibitors are still in the pre-clinical phase of development, the evidence for therapeutic benefit is mounting.

6.2 Autotaxin as a therapeutic target in cancer

Although there is substantial evidence of *in vitro* autotaxin inhibition with small molecule inhibitors, so far the evaluation of autotaxin inhibitors *in vivo* is limited. The first autotaxin inhibitor to demonstrate *in vivo* activity was BrP-LPA, this was found to reduce tumour burden in an orthotropic breast cancer xenograft model, however BrP-LPA shows activity against LPA receptors, therefore the *in vivo* effects cannot be attributed to autotaxin inhibition alone.[256] Inhibition of autotaxin by a boronic acid based molecule resulted in reduction of LPA *in vivo,*[223] but this reduction was short-lived. The autotaxin inhibitor BoA-3 was shown to reduce levels of LPA in circulation in a murine model.[91] Reduction in circulating LPA levels has also been shown to be reduced with the recently described autotaxin inhibitors PF-8380[226] and ONO-8430506.[228] These inhibitors are the most successful described autotaxin inhibitors to date. The time is ripe to evaluate these molecules in ovarian cancer. It may be worth testing these compounds per oral in an ovarian cancer model. The inhibitor described in this thesis has the advantage of direct delivery to the site of cancer and potential increased retention at this site. However, the use of literature inhibitors, which have been demonstrated to be active with oral administration may overcome the issues associated with intraperitoneal delivery. PF-8380 exhibited a half-life of 1.2 h after intravenous injection and a few hours with oral delivery, this may not provide sufficient autotaxin inhibition. ONO-8430506 was still measurable 24 h after oral administration at levels greater than IC_{90} suggesting this may be long

enough to sufficiently inhibit autotaxin. This requires further investigation in an *in vivo* ovarian cancer model.

6.2.1 Autotaxin and chemoresistance

There is limited evidence showing that inhibition of autotaxin, on its own, promotes cell death. However, autotaxin is over-expressed in ovarian cancer tumours that are resistant to chemotherapy. LPA and autotaxin have been shown to directly confer resistance to chemotherapy in a number of studies. LPA has been associated with the development of resistance to carboplatin in ovarian cancer cells,[176] and colon cancer.[177] Expression of autotaxin delays apoptosis induced by carboplatin in ovarian cancer cells.[178] Additionally apoptosis was accelerated after inhibition of autotaxin by either siRNA silencing or with a small molecule inhibitor.[178] In addition to conferring resistance to platinum-based chemotherapy, LPA and autotaxin also confer resistance to paclitaxel in breast and melanoma cancers.[179,180] In chapter 3, addition of LPC, the substrate of autotaxin, was shown to protect ovarian cancer cells which were engineered to over-express autotaxin, from cell death induced by carboplatin. Treatment with either the autotaxin inhibitor S32826 or conjugate 1 resulted in elimination of this protection. This provides evidence that autotaxin inhibition could be used in combination with chemotherapy in order to overcome chemoresistance. Autotaxin inhibition could be used alongside frontline therapy to improve response or once patients have become resistant to ovarian cancer. The data suggests addition to frontline chemotherapy, this may be the most sensible way it could be tested in clinical trials.

6.2.2 Autotaxin and ovarian cancer

This thesis has focused on the development of novel polymer-autotaxin inhibitor conjugates for the treatment of ovarian cancer. Ovarian cancer is a particular problem as it is often diagnosed at a late stage and although most patients respond to first line chemotherapy they go on to develop resistance. Therefore, the need for new methods for treating ovarian cancer is urgently required.

Patients with ovarian cancer often present with an accumulation of ascites fluid in the intraperitoneal cavity which contains LPA at concentrations up to 80 micromolar.[73] Autotaxin is also found at increased levels in the ascites fluid of patients with ovarian cancer.[270] As autotaxin is the main contributor to the production of LPA, autotaxin inhibitors have the potential to reduce the potentially pathogenic levels of LPA observed in ovarian cancer patient ascites. As discussed, the evidence for a role in cell migration and invasion is extensive. Inhibitors of autotaxin have been shown to reduce lung metastasis and breast metastasis in animal models.[228, 256] Both the polymer-autotaxin inhibitor conjugates described in this thesis were found to inhibit ovarian cancer cell migration in a wound healing assay. Hence autotaxin inhibition has the potential to reduce metastasis in the clinic. However most ovarian cancer patients present with disseminated disease and therefore inhibition of metastasis may be futile. Although it may be beneficial to prevent further metastasis; evaluating the ability of autotaxin inhibitors in the clinic will be challenging. In metastasised disease the major issue is the destruction of the metastasis, however it is possible that reducing further metastasis is therapeutically beneficial. One potential way to examine this would be to administer autotaxin inhibitors after a patient has received chemotherapy.

6.3 Autotaxin as a therapeutic target in other diseases

The potential benefit for autotaxin inhibitors for other indications is also evident. The ATX/LPA signalling pathway has been implicated various other pathophysiological processes. Autotaxin expression is increased in many inflammatory diseases, including in the cerebrospinal fluid of multiple sclerosis patients,[134] the frontal cortex of Alzheimer's like dementia patients,[196] pulmonary fibrosis[194] and in patients with rheumatoid arthritis.[192] Inhibition of autotaxin has already been shown to be therapeutically beneficial in a rat air pouch model of inflammation, the autotaxin inhibitor PF-8380 was able to reduce hyperalgesia with the same efficacy as the non-steroidal anti-inflammatory drug (NSAID), naproxen.[226] Autotaxin inhibition has also been shown to reduce smooth muscle contraction, which is known to be promoted by lysophosphatidic acid. Treating rats with the autotaxin inhibitor ONO-8430506 decreased intraurethral pressure accompanied by urethral

relaxation.[227] The BrP-LPA autotaxin inhibitor was found to attenuate collagen induced arthritis, however as previously discussed BrP-LPA also antagonises LPA receptors and therefore it cannot be concluded that this activity is due to inhibition of autotaxin.[197]

6.4 Icodextrin as a drug carrier

In this thesis the synthesis of a novel icodextrin-autotaxin inhibitor conjugate has been described. Further to its potential to increase autotaxin inhibitor retention in the peritoneal cavity, icodextrin drug carriers also have the potential improve the retention of other drugs in the peritoneal cavity. This may be desirable to ensure a high local drug concentration in the peritoneal cavity that promotes efficacy, but reduced exposure to the drug in plasma may limit systemic toxicity. The residence time of small molecular weight drugs (<20kDa) in the peritoneal cavity may not be adequate because they are quickly absorbed through the peritoneal capillaries into systemic circulation.[236-237] This leads to frequent or continuous dosing and if drugs are delivered by the intraperitoneal route, this creates problems such as increased risk of infection. Conjugation to icodextrin has the potential to overcome these issues. Due to its molecular size, icodextrin is absorbed slowly from the peritoneal cavity mainly via the lymphatic system, icodextrin has a residence time of more than 12 h in the peritoneal cavity.[261] To date there have been several studies investigating icodextrin as an intramolecular drug delivery vehicle. These have included its clinical evaluation for the delivery of the cytotoxic drug 5-fluorouracil and an anti-HIV agent.[271-273] It was also shown to improve retention and peritoneal distribution of adenovirus in a murine model.[274] In these studies the therapeutic agent was made as a solution in icodextrin and the pharmacophore was not covalently linked to icodextrin. Conjugation to icodextrin may be able to further improve peritoneal retention. Drugs which may benefit from conjugation to icodextrin include, but are not limited to, small molecule therapeutics intended for the treatment of cancers localised in the peritoneal cavity. These could be designed based on the requirements of the specific drug. For example, allowing increased retention in the peritoneal cavity or slow release of the drug into the peritoneal cavity. Thus there seem to be many reasons supporting

further exploration of icodextrin for drug delivery in peritoneal cancer due to its chemical properties and its establishment in the clinic.

6.5 Dendrimers as drug carriers

Dendrimers are also widely being investigated as drug delivery systems. The conjugate described in chapter 3 is likely to be rapidly removed from the peritoneal cavity because although conjugation to a dendrimer increases the molecular mass of the drug, it is still only 8 kDa which may not be sufficient to prevent its clearance. Dendrimers above 5th generation may be better retained in the peritoneal cavity as due to their larger molecular weight. It would be worth investigating the retention of dendrimers greater than 5th generation in the peritoneal cavity, as dendrimers are ideal drug carrier candidates due to their uniform size and multiple sites of attachment.

There are other potential therapeutic uses for an autotaxin inhibitor conjugated to a dendrimer. Dendrimers have the potential to improve the pharmacokinetic profiles of lipophilic drugs, such as the autotaxin inhibitor S32826 as was described in chapter 3. The inhibitor was rapidly metabolised in systemic circulation when tested *in vivo*, whereas it had shown high biological activity *in vitro*.[83] Further to increasing the metabolic stability of drugs, the multiple sites of attachment suggest that other molecule could be attached to the dendrimer alongside the drug. These molecules could target the conjugate to the site intended. One such molecule which has been investigated is folate. The folate receptor is associated with tumours, and binds to folate with a high affinity, folate drug conjugates have already been shown to target tumours.[275]

Furthermore, as previously discussed, autotaxin inhibitors also have the potential to be beneficial in inflammatory diseases; a dendrimer-autotaxin inhibitor conjugate could increase the retention time of autotaxin inhibitors in other cavities or at the site of inflammation.

6.6 Further studies

To confirm the icodextrin-autotaxin inhibitor conjugate has therapeutic potential a few key investigations are required. An appropriate xenograft model is required. Initial results suggest that

the 3E3 cell line, which overexpresses autotaxin, could be used. These cells were able to establish ascites forming tumours in the peritoneal cavity. The first step will be to demonstrate the icodextrin-autotaxin inhibitor conjugate can reduce LPA production *in vivo*. This would be achieved by measuring LPA levels at set times after administration of the conjugate. Once LPA reduction has been established demonstration of activity in a xenograft study will be investigated. The conjugate will be investigated in combination with carboplatin for its ability to increase tumour response to carboplatin. The conjugate will also ideally be investigated in a model for ovarian cancer metastasis.

6.7 Concluding remarks

So far there has been limited translation of the autotaxin inhibitors into animal models. Although research into the ATX/LPA signalling pathway has rapidly expanded over the past decade, establishing autotaxin inhibitor activity in animal models will be essential for translating autotaxin inhibitors into the clinic.

This thesis has demonstrated that in principle an autotaxin inhibitor can be attached to a polymer and retain its pharmacological activity. Attaching an autotaxin inhibitor to icodextrin also has the potential to increase the residence time of the inhibitor in the peritoneal cavity. This conjugate has the potential to be therapeutically beneficial for the treatment of ovarian cancer. The icodextrin-autotaxin inhibitor conjugate described in this thesis will be investigated for the ability to reduce LPA in the peritoneal cavity and in a xenograft model of ovarian cancer.

References

1. Statistics, O. f. N. Mortality Statistics: Deaths Registered in England and Wales (Series DR). http://www.ons.gov.uk/ons/index.html (accessed 18/04/2015).

2. Ferlay, J.; Soerjomataram, I.; Ervik, M.; Dikshit, R.; Eser, S.; Mathers, C.; Rebelo, M.; Parkin, D. M.; Forman, D.; Bray, F., Lyon, France: International Agency for Research on Cancer; GLOBOCAN 2012 v1.0, Cancer Incidence and Mortality Worldwide: IARC CancerBase No. 11 [Internet]. In *International Agency for Reseach on Cancer*, 2013.

3. Weiss, N. S.; Homonchuk, T.; Young Jr, J. L., Incidence of the histologic types of ovarian cancer: The U.S. Third National Cancer Survey, 1969–1971. *Gynecol Oncol* 1977, *5* (2), 161-167.

4. Prat, J., Ovarian carcinomas: five distinct diseases with different origins, genetic alterations, and clinicopathological features. *Virchows Arch* 2012, *460* (3), 237-49.

5. Vang, R.; Shih, I. M.; Kurman, R. J., Fallopian tube precursors of ovarian low- and high-grade serous neoplasms. *Histopathology* 2013, *62* (1), 44-58.

6. Dubeau, L., The cell of origin of ovarian epithelial tumors and the ovarian surface epithelium dogma: Does the emperor have no clothes? *Gynecol Oncol* 1999, *72* (3), 437-442.

7. Schubert, E. K.; Lee, M. K.; Mefford, H. C.; Argonza, R. H.; Morrow, J. E.; Hull, J.; Dann, J. L.; King, M. C., BRCA2 in American families with four or more cases of breast or ovarian cancer: Recurrent and novel mutations, variable expression, penetrance, and the possibility of families whose cancer is not attributable to BRCA1 or BRCA2. *Am. J. Hum. Genet.* 1997, *60* (5), 1031-1040.

8. Zweemer, R. P.; van Diest, P. J.; Verheijen, R. H. M.; Ryan, A.; Gille, J. J. P.; Sijmons, R. H.; Jacobs, I. J.; Menko, F. H.; Kenemans, P., Molecular evidence linking primary cancer of the Fallopian tube to BRCA1 germline mutations. *Gynecol Oncol* 2000, *76* (1), 45-50.

9. Piek, J. M. J.; van Diest, P. J.; Zweemer, R. P.; Jansen, J. W.; Poort-Keesom, R. J. J.; Menko, F. H.; Gille, J. J. P.; Jongsma, A. P. M.; Pals, G.; Kenemans, P.; Verheijen, R. H. M., Dysplastic changes in prophylactically removed Fallopian tubes of women predisposed to developing ovarian cancer. *J. Pathol* 2001, *195* (4), 451-456.

10. Gross, A. L.; Kurman, R. J.; Vang, R.; Shih, L. M.; Visvanathan, K., Precursor lesions of high-grade serous ovarian carcinoma: morphological and molecular characteristics. *J. Oncol* 2010, *2010*, 126295-126295.

11. Callahan, M. J.; Crum, C. P.; Medeiros, F.; Kindelberger, D. W.; Elvin, J. A.; Garber, J. E.; Feltmate, C. M.; Berkowitz, R. S.; Muto, M. G., Primary Fallopian tube malignancies in BRCA-positive women undergoing surgery for ovarian cancer risk reduction. *J Clin Oncol* 2007, *25* (25), 3985-3990.

12. Diniz, P. M.; Carvalho, J. P.; Baracat, E. C.; Carvalho, F. M., Fallopian tube origin of supposed ovarian high-grade serous carcinomas. *Clinics* 2011, *66* (1), 73-76.

13. Tone, A. A.; Begley, H.; Sharma, M.; Murphy, J.; Rosen, B.; Brown, T. J.; Shaw, P. A., Gene expression profiles of luteal phase fallopian tube epithelium from BRCA mutation carriers resemble high-grade serous carcinoma. *Clin Cancer Res* 2008, *14* (13), 4067-4078.

14. Williams, T. I.; Toups, K. L.; Saggese, D. A.; Kalli, K. R.; Cliby, W. A.; Muddiman, D. C., Epithelial Ovarian Cancer: Disease Etiology, Treatment, Detection, and Investigational Gene, Metabolite, and Protein Biomarkers. *J Proteome Res* 2007, *6* (8), 2936-2962.

15. Crum, C. P.; Drapkin, R.; Miron, A.; Ince, T. A.; Muto, M.; Kindelberger, D. W.; Lee, Y., The distal fallopian tube: a new model for pelvic serous carcinogenesis. *Curr. Opin. Obstet. Gynecol.* 2007, *19* (1), 3-9.

16. Crum, C. P.; Drapkin, R.; Kindelberger, D.; Medeiros, F.; Miron, A.; Lee, Y., Lessons from BRCA: the tubal fimbria emerges as an origin for pelvic serous cancer. *J Clin Med Res* 2007, *5* (1), 35-44.

17. Medeiros, F.; Muto, M. G.; Lee, Y.; Elvin, J. A.; Callahan, M. J.; Feltmate, C.; Garber, J. E.; Cramer, D. W.; Crum, C. P., The tubal fimbria is a preferred site for early adenocarcinoma in women with familial ovarian cancer syndrome. *Am. J. Surg. Pathol.* 2006, *30* (2), 230-236.

18. Koebel, M.; Kalloger, S. E.; Boyd, N.; McKinney, S.; Mehl, E.; Palmer, C.; Leung, S.; Bowen, N. J.; Ionescu, D. N.; Rajput, A.; Prentice, L. M.; Miller, D.; Santos, J.; Swenerton, K.; Gilks, C. B.; Huntsman, D., Ovarian Carcinoma Subtypes Are Different Diseases: Implications for Biomarker Studies. *PLOS MED* 2008, *5* (12), 1749-1760.

19. Shih, L. M.; Kurman, R. J., Ovarian tumorigenesis - A proposed model based on morphological and molecular genetic analysis. *The American Journal of Pathology* 2004, *164* (5), 1511-1518.

20. Whittemore, A. S.; Harris, R.; Itnyre, J., Characteristics relating to ovarian-cancer risk - collaborative analysis of 12 united-states case -control studies .2. invasive epithelial ovarian cancers in white women. *Am, J. Epidemiol.* 1992, *136* (10), 1184-1203.

21. Schildkraut, J. M.; Thompson, W. D., Familial ovarian cancer a population-based case control study. *Am, J. Epidemiol.* 1988, *128* (3), 456-466.

22. Whittemore, A. S., Characteristics relating to ovarian-cancer risk- implications for prevention and detection. *Gynecol Oncol* 1994, *55* (3), S15-S19.

23. Hankinson, S. E.; Hunter, D. J.; Colditz, G. A.; Willett, W. C.; Stampfer, M. J.; Rosner, B.; Hennekens, C. H.; Speizer, F. E., Tubal-ligation, hysterectomy, and risk of ovarian cancer- a prosective study. *JAMA* 1993, *270* (23), 2813-2818.

24. Rossing, M. A.; Daling, J. R.; Weiss, N. S.; Moore, D. E.; Self, S. G., Ovarian tumours in a cohort of infertile women. *N. Engl. J. Med.* 1994, *331* (12), 771-776.

25. Venn, A.; Watson, L.; Lumley, J.; Giles, G.; King, C.; Healy, D., Breast and ovarian cancer incidence after infertility and in-vitro fertilization. *Lancet* 1995, *346* (8981), 995-1000.

26. Venn, A.; Watson, L.; Bruinsma, F.; Giles, G.; Healy, D., Risk of cancer after use of fertility drugs with in-vitro fertilisation. *Lancet* 1999, *354* (9190), 1586-1590.

27. Ness, R. B.; Cramer, D. W.; Goodman, M. T.; Kjaer, S. K.; Mallin, K.; Mosgaard, B. J.; Purdie, D. M.; Risch, H. A.; Vergona, R.; Wu, A. H., Infertility, fertility drugs, and ovarian cancer: A pooled analysis of case-control studies. *Am, J. Epidemiol.* 2002, *155* (3), 217-224.

28. Wiegand, K. C.; Shah, S. P.; Al-Agha, O. M.; Zhao, Y.; Tse, K.; Zeng, T.; Senz, J.; McConechy, M. K.; Anglesio, M. S.; Kalloger, S. E.; Yang, W.; Heravi-Moussavi, A.; Giuliany, R.; Chow, C.; Fee, J.; Zayed, A.; Prentice, L.; Melnyk, N.; Turashvili, G.; Delaney, A. D.; Madore, J.; Yip, S.; McPherson, A. W.; Ha, G.; Bell, L.; Fereday, S.; Tam, A.; Galletta, L.; Tonin, P. N.; Provencher, D.; Miller, D.; Jones, S. J. M.; Moore, R. A.; Morin, G. B.; Oloumi, A.; Boyd, N.; Aparicio, S. A.; Shih, L. M.; Mes-Masson, A. M.; Bowtell, D. D.; Hirst, M.; Gilks, B.; Marra, M. A.; Huntsman, D. G., ARID1A Mutations in Endometriosis-Associated Ovarian Carcinomas. *N. Engl. J. Med.* 2010, *363* (16), 1532-1543.

29. Pearce, C. L.; Templeman, C.; Rossing, M. A.; Lee, A.; Near, A. M.; Webb, P. M.; Nagle, C. M.; Doherty, J. A.; Cushing-Haugen, K. L.; Wicklund, K. G.; Chang-Claude, J.; Hein, R.; Lurie, G.; Wilkens, L. R.; Carney, M. E.; Goodman, M. T.; Moysich, K.; Kjaer, S. K.; Hogdall, E.; Jensen, A.; Goode, E. L.; Fridley, B. L.; Larson, M. C.; Schildkraut, J. M.; Palmieri, R. T.; Cramer, D. W.; Terry, K. L.; Vitonis, A. F.; Titus, L. J.; Ziogas, A.; Brewster, W.; Anton-Culver, H.; Gentry-Maharaj, A.; Ramus, S. J.; Anderson, A. R.; Brueggmann, D.; Fasching, P. A.; Gayther, S. A.; Huntsman, D. G.; Menon, U.; Ness, R. B.; Pike, M. C.; Risch, H.; Wu, A. H.; Berchuck, A.; Ovarian Canc Assoc, C., Association between endometriosis and risk of histological subtypes of ovarian cancer: a pooled analysis of case-control studies. *Lancet Oncol* 2012, *13* (4), 385-394.

30. Chittenden, B. G.; Fullerton, G.; Maheshwari, A.; Bhattacharya, S., Polycystic ovary syndrome and the risk of gynaecological cancer: a systematic review. *Reprod. Biomed. Online* 2009, *19* (3), 398-405.

31. Merritt, M. A.; Green, A. C.; Nagle, C. M.; Webb, P. M.; Australian Cancer Study Ovarian, C.; Australian Ovarian Cancer Study, G., Talcum powder, chronic pelvic inflammation and NSAIDs in relation to risk of epithelial ovarian cancer. *Int J Cancer* 2008, *122* (1), 170-176.

32. Beral, V.; Gaitskell, K.; Hermon, C.; Moser, K.; Reeves, G.; Peto, R.; Brinton, L.; Marchbanks, P.; Negri, E.; Ness, R.; Peeters, P. H. M.; Vessey, M.; Calle, E. E.; Gapstur, S. M.; Patel, A. V.; Dal Maso, L.; Talamini, R.; Chetrit, A.; Hirsh-Yechezkel, G.; Lubin, F.; Sadetzki, S.; Banks, E.; Beral, V.; Bull, D.; Callaghan, K.; Crossley, B.; Gaitskell, K.; Goodill, A.; Green, J.; Hermon, C.; Key, T.; Moser, K.; Reeves, G.; Sitas, F.; Collins, R.; Doll, R.; Peto, R.; Gonzalez, A.; Lee, N.; Marchbanks, P.; Ory, H. W.; Peterson, H. B.; Wingo, P. A.; Martin, N.; Pardthaisong, T.; Silpisornkosol, S.; Theetranont, C.; Boosiri, B.; Chutivongse, S.; Jimakorn, P.; Virutamasen, P.; Wongsrichanalai, C.; Tjonneland, A.; Titus-Ernstoff, L.; Byers, T.; Rohan, T.; Mosgaard, B. J.; Vessey, M.; Yeates, D.; Freudenheim, J. L.; Chang-Claude, J.; Kaaks, R.; Anderson, K. E.; Folsom, A.; Robien, K.; Hampton, J.; Newcomb, P. A.; Rossing, M. A.; Thomas, D. B.; Weiss, N. S.; Riboli, E.; Clavel-Chapelon, F.; Cramer, D.; Hankinson, S. E.; Tworoger, S. S.; Franceschi, S.; La Vecchia,

C.; Negri, E.; Adami, H. O.; Magnusson, C.; Riman, T.; Weiderpass, E.; Wolk, A.; Schouten, L. J.; van den Brandt, P. A.; Chantarakul, N.; Koetsawang, S.; Rachawat, D.; Palli, D.; Black, A.; Brinton, L. A.; Freedman, D. M.; Hartge, P.; Hsing, A. W.; Lacey, J. V., Jr.; Hoover, R. N.; Schairer, C.; Urban, M.; Graff-Iversen, S.; Selmer, R.; Bain, C. J.; Green, A. C.; Purdie, D. M.; Siskind, V.; Webb, P. M.; Moysich, K.; McCann, S. E.; Hannaford, P.; Kay, C.; Binns, C. W.; Lee, A. H.; Zhang, M.; Ness, R. B.; Nasca, P.; Coogan, P. F.; Palmer, J. R.; Rosenberg, L.; Kelsey, J.; Paffenbarger, R.; Whittemore, A.; Katsouyanni, K.; Trichopoulou, A.; Trichopoulos, D.; Tzonou, A.; Dabancens, A.; Martinez, L.; Molina, R.; Salas, O.; Goodman, M. T.; Lurie, G.; Carney, M. E.; Wilkens, L. R.; Hartman, L.; Manjer, J.; Olsson, H.; Grisso, J. A.; Morgan, M.; Wheeler, J. E.; Bunker, C. H.; Edwards, R. P.; Modugno, F.; Peeters, P. H. M.; Casagrande, J.; Pike, M. C.; Ross, R. K.; Wu, A. H.; Miller, A. B.; Kumle, M.; Gram, I. T.; Lund, E.; McGowan, L.; Shu, X. O.; Zheng, W.; Farley, T. M. M.; Holck, S.; Meirik, O.; Risch, H. A., Ovarian cancer and smoking: individual participant meta-analysis including 28 114 women with ovarian cancer from 51 epidemiological studies. *Lancet Oncol* 2012, *13* (9), 946-956.

33. Parkin, D. M.; Boyd, L.; Walker, L. C., The fraction of cancer attributable to lifestyle and environmental factors in the UK in 2010. *Br J Cancer* 2011, *105 Suppl 2*, S77-81.

34. Rubin, S. C.; Blackwood, M. A.; Bandera, C.; Behbakht, K.; Benjamin, I.; Rebbeck, T. R.; Boyd, J., BRCA1, BRCA2, and hereditary nonpolyposis colorectal cancer gene mutations in an unselected ovarian cancer population: Relationship to family history and implications for genetic testing. *Am. J. Obstet. Gynecol.* 1998, *178* (4), 670-677.

35. King, M. C.; Marks, J. H.; Mandell, J. B.; New York Breast Canc Study, G., Breast and ovarian cancer risks due to inherited mutations in BRCA1 and BRCA2. *Science* 2003, *302* (5645), 643-646.

36. Reedy, M.; Gallion, H.; Fowler, J. M.; Kryscio, R.; Smith, S. A., Contribution of BRCA1 and BRCA2 to familial ovarian cancer: A Gynecologic oncology group study. *Gynecol Oncol* 2002, *85* (2), 255-259.

37. Stratton, J. F.; Pharoah, P.; Smith, S. K.; Easton, D.; Ponder, B. A. J., A systematic review and meta-analysis of family history and risk of ovarian cancer. *Br J Obstet Gynaecol* 1998, *105* (5), 493-499.

38. Scully, R.; Ganesan, S.; Brown, M.; DeCaprio, J. A.; Cannistra, S. A.; Feunteun, J.; Schnitt, S.; Livingston, D. M., Location of BRCA1 in human breast and ovarian cancer cells. *Science* 1996, *272* (5258), 123-125.

39. Struewing, J. P.; Hartge, P.; Wacholder, S.; Baker, S. M.; Berlin, M.; McAdams, M.; Timmerman, M. M.; Brody, L. C.; Tucker, M. A., The risk of cancer associated with specific mutations of BRCA1 and BRCA2 among Ashkenazi Jews. *N. Engl. J. Med.* 1997, *336* (20), 1401-1408.

40. Aletti, G. D.; Gallenberg, M. M.; Cliby, W. A.; Jatoi, A.; Hartmann, L. C., Current management strategies for ovarian cancer. *Mayo Clin. Proc.* 2007, *82* (6), 751-770.

41. Dunlop, M. G.; Farrington, S. M.; Carothers, A. D.; Wyllie, A. H.; Sharp, L.; Burn, J.; Liu, B.; Kinzler, K. W.; Vogelstein, B., Cancer risk associated with germline DNA mismatch repair gene mutations. *Hum Mol Genet* 1997, *6* (1), 105-110.

42. http://www.nice.org.uk/guidance/cg122/chapter/1-recommendations (accessed 10/04/2015).

43. Schmid, B. C.; Oehler, M. K., New perspectives in ovarian cancer treatment. *Maturitas* 2014, *77* (2), 128-136.

44. Sharpe, M.; Easthope, S. E.; Keating, G. M.; Lamb, H. M., Polyethylene glycol-liposomal doxorubicin. *Drugs* 2002, *62* (14), 2089-2126.

45. Herzog, T. J., Clinical experience with topotecan in relapsed ovarian cancer. *Gynecol Oncol* 2003, *90* (3, Supplement), S3-S7.

46. Liu, J. F.; Konstantinopoulos, P. A.; Matulonis, U. A., PARP inhibitors in ovarian cancer: Current status and future promise. *Gynecol Oncol* 2014, *133* (2), 362-369.

47. Ramus, S. J.; Gayther, S. A., The Contribution of BRCA1 and BRCA2 to Ovarian Cancer. *Mol Oncol* 2009, *3* (2), 138-150.

48. Gan, A.; Green, A. R.; Nolan, C. C.; Martin, S.; Deen, S., Poly(adenosine diphosphate-ribose) polymerase expression in BRCA-proficient ovarian high-grade serous carcinoma; association with patient survival. *Hum Pathol* 2013, *44* (8), 1638-1647.

49. Ledermann, J.; Harter, P.; Gourley, C.; Friedlander, M.; Vergote, I.; Rustin, G.; Scott, C. L.; Meier, W.; Shapira-Frommer, R.; Safra, T.; Matei, D.; Fielding, A.; Spencer, S.; Dougherty, B.; Orr, M.; Hodgson, D.; Barrett, J. C.; Matulonis, U., Olaparib maintenance therapy in patients with platinum-sensitive relapsed serous ovarian cancer: a preplanned retrospective analysis of outcomes by BRCA status in a randomised phase 2 trial. *Lancet Oncol* 2014, *15* (8), 852-861.

50. Bryant, H. E.; Schultz, N.; Thomas, H. D.; Parker, K. M.; Flower, D.; Lopez, E.; Kyle, S.; Meuth, M.; Curtin, N. J.; Helleday, T., Specific killing of BRCA2-deficient tumours with inhibitors of poly(ADP-ribose) polymerase (vol 434, pg 913, 2005). *Nature* 2007, *447* (7142), 346-346.

51. Kaye, S. B.; Lubinski, J.; Matulonis, U.; Ang, J. E.; Gourley, C.; Karlan, B. Y.; Amnon, A.; Bell-McGuinn, K. M.; Chen, L.; Friedlander, M.; Safra, T.; Vergote, I.; Wickens, M.; Lowe, E. S.; Carmichael, J.; Kaufman, B., Phase II, Open-Label, Randomized, Multicenter Study Comparing the Efficacy and Safety of Olaparib, a Poly (ADP-Ribose) Polymerase Inhibitor, and Pegylated Liposomal Doxorubicin in Patients With BRCA1 or BRCA2 Mutations and Recurrent Ovarian Cancer. *J Clin Oncol* 2012, *30* (4), 372-379.

52. Perren, T. J.; Swart, A. M.; Pfisterer, J.; Ledermann, J. A.; Pujade-Lauraine, E.; Kristensen, G.; Carey, M. S.; Beale, P.; Cervantes, A.; Kurzeder, C.; du Bois, A.; Sehouli, J.; Kimmig, R.; Staehle, A.; Collinson, F.; Essapen, S.; Gourley, C.; Lortholary, A.; Selle, F.; Mirza, M. R.; Leminen,

A.; Plante, M.; Stark, D.; Qian, W.; Parmar, M. K. B.; Oza, A. M.; Investigators, I., A Phase 3 Trial of Bevacizumab in Ovarian Cancer. *N. Engl. J. Med.* 2011, *365* (26), 2484-2496.

53. Garcia, A. A.; Hirte, H.; Fleming, G.; Yang, D.; Tsao-Wei, D. D.; Roman, L.; Groshen, S.; Swenson, S.; Markland, F.; Gandara, D.; Scudder, S.; Morgan, R.; Chen, H.; Lenz, H. J.; Oza, A. M., Phase II clinical trial of bevacizumab and low-dose metronomic oral cyclophosphamide in recurrent ovarian cancer: A trial of the California, Chicago, and princess Margaret hospital phase II consortia. *J Clin Oncol* 2008, *26* (1), 76-82.

54. Cannistra, S. A.; Matulonis, U. A.; Penson, R. T.; Hambleton, J.; Dupont, J.; Mackey, H.; Douglas, J.; Burger, R. A.; Armstrong, D.; Wenham, R.; McGuire, W., Phase II study of bevacizumab in patients with platinum-resistant ovarian cancer or peritoneal serous cancer. *J Clin Oncol* 2007, *25* (33), 5180-5186.

55. Burger, R. A.; Sill, M. W.; Monk, B. J.; Greer, B. E.; Sorosky, J. I., Phase II trial of bevacizumab in persistent or recurrent epithelial ovarian cancer or primary peritoneal cancer: A Gynecologic oncology group study. *J Clin Oncol* 2007, *25* (33), 5165-5171.

56. Aghajanian, C.; Blank, S. V.; Goff, B. A.; Judson, P. L.; Teneriello, M. G.; Husain, A.; Sovak, M. A.; Yi, J.; Nycum, L. R., OCEANS: A Randomized, Double-Blind, Placebo-Controlled Phase III Trial of Chemotherapy With or Without Bevacizumab in Patients With Platinum-Sensitive Recurrent Epithelial Ovarian, Primary Peritoneal, or Fallopian Tube Cancer. *J Clin Oncol* 2012, *30* (17), 2039-2045.

57. Shaw, D.; Clamp, A.; Jayson, G. C., Angiogenesis as a target for the treatment of ovarian cancer. *Curr Opin Oncol* 2013, *25* (5), 558-565.

58. Bevacizumab in combination with gemcitabine and carboplatin for treating the first recurrence of platinum-sensitive advanced ovarian cancer. https://www.nice.org.uk/guidance/ta285 (accessed 28/06/2015).

59. Bevacizumab in combination with paclitaxel and carboplatin for first-line treatment of advanced ovarian cancer. https://www.nice.org.uk/guidance/ta284 (accessed 28/06/2015).

60. Ling, K. S.; Chen, G.; Tsai, H. J.; Lee, M. S.; Wang, P. H.; Liu, F. S., Mechanisms Involved in Chemoresistance in Ovarian Cancer. *Taiwan J Obstet Gynecol* 2005, *44* (3), 209-217.

61. Fletcher, J. I.; Haber, M.; Henderson, M. J.; Norris, M. D., ABC transporters in cancer: more than just drug efflux pumps. *Nat. Rev. Cancer* 2010, *10* (2), 147-156.

62. Howell, S. B.; Safaei, R.; Larson, C. A.; Sailor, M. J., Copper transporters and the cellular pharmacology of the platinum-containing cancer drugs. *Mol Pharmacol* 2010, *77* (6), 887-94.

63. Joncourt, F.; Buser, K.; Altermatt, H.; Bacchi, M.; Oberli, A.; Cerny, T., Multiple drug resistance parameter expression in ovarian cancer. *Gynecol Oncol* 1998, *70* (2), 176-182.

64. Cherian, M. G.; Jayasurya, A.; Bay, B., Metallothioneins in human tumors and potential roles in carcinogenesis. *Mutat. Res.* 2003, *533* (1–2), 201-209.

65. Kavallaris, M.; Kuo, D. Y. S.; Burkhart, C. A.; Regl, D. L.; Norris, M. D.; Haber, M.; Horwitz, S. B., Taxol-resistant epithelial ovarian tumors are associated with altered expression of specific beta-tubulin isotypes. *J Clin Invest* 1997, *100* (5), 1282-1293.

66. Jordan, M. A.; Toso, R. J.; Thrower, D.; Wilson, L., Mechanism of mitotic block and inhibition of cell-proliferation by taxol at low concentrations. *Proc Natl Acad Sci USA* 1993, *90* (20), 9552-9556.

67. Pommier, Y., DNA topoisomerase-I ans topoisomerase-II in cancer chemotherapy- update and perspectives. *Cancer Chemother. Pharmacol.* 1993, *32* (2), 103-108.

68. Masuda, H.; Tanaka, T.; Matsuda, H.; Kusaba, I., Increased removal of DNA-bound platinum in a human ovarian cancer cell line resistant to Cis-diamminedichloroplatinum(II). *Cancer Res.* 1990, *50* (6), 1863-1866.

69. Zhen, W. P.; Link, C. J.; Oconnor, P. M.; Reed, E.; Parker, R.; Howell, S. B.; Bohr, V. A., Increased gene-specific repair of cisplatin interstrand cross-links in cis-platin resistant human ovarian cancer cell lines. *Molecular and cellular biology* 1992, *12* (9), 3689-3698.

70. Köberle, B.; Tomicic, M. T.; Usanova, S.; Kaina, B., Cisplatin resistance: Preclinical findings and clinical implications. *Biochimica et Biophysica Acta (BBA) - Reviews on Cancer* 2010, *1806* (2), 172-182.

71. Mills, G. B.; May, C.; Hill, M.; Campbell, S.; Shaw, P.; Marks, A., Ascitic Fluid from Human Ovarian Cancer Patients Contains Growth Factors Necessary for Intraperitoneal Growth of Human Ovarian Adenocarcinoma Cells. *J Clin Invest* 1990, *86*, 851-855.

72. Xu, Y.; Gaudette, D. C.; Boynton, J. D.; Frankel, A.; Fang, X. J.; Sharma, A.; Hurteau, J.; Casey, G.; Goodbody, A.; Mellors, A.; Holub, B. J.; Mills, G. B., Characterization of an ovarian cancer activating factor in ascites from ovarian cancer patients. *Clin Cancer Res* 1995, *1* (10), 1223-1232.

73. Westermann, A. M.; Havik, E.; Postma, F. R.; Beijnen, J. H.; Dalesio, O.; Moolenaar, W. H.; Rodenhuis, S., Malignant effusions contain lysophosphatidic acid (LPA)-like activity. *Ann. Oncol.* 1998, *9* (4), 437-42.

74. Umezu-Goto, M.; Kishi, Y.; Taira, A.; Hama, K.; Dohmae, N.; Takio, K.; Yamori, T.; Mills, G. B.; Inoue, K.; Aoki, J.; Arai, H., Autotaxin has lysophospholipase D activity leading to tumor cell growth and motility by lysophosphatidic acid production. *The Journal of cell biology* 2002, *158* (2), 227-33.

75. Stracke, M. L.; Krutzsch, H. C.; Unsworth, E. J.; Arestad, A.; Cioce, V.; Schiffmann, E.; Liotta, L. A., Identification, purification, and partial sequence-analysis of autotaxin, a novel motility-stimulating protein. *J. Biol. Chem.* 1992, *267* (4), 2524-2529.

76. Jansen, S.; Stefan, C.; Creemers, J. W. M.; Waelkens, E.; Van Eynde, A.; Stalmans, W.; Bollen, M., Proteolytic maturation and activation of autotaxin (NPP2), a secreted metastasis-enhancing lysophospholipase D. *J. Cell Sci.* 2005, *118* (14), 3081-3089.

77. Sano, T.; Baker, D.; Virag, T.; Wada, A.; Yatomi, Y.; Kobayashi, T.; Igarashi, Y.; Tigyi, G., Multiple Mechanisms Linked to Platelet Activation Result in Lysophosphatidic Acid and Sphingosine 1-Phosphate Generation in Blood. *J. Biol. Chem.* 2002, *277* (24), 21197-21206.

78. Tokumura, A., A Family of Phospholipid Autacoids- Occurence, Metabolism and Bioactions. *Prog Lipid Res* 1995, *34* (2), 151-184.

79. Aoki, J.; Taira, A.; Takanezawa, Y.; Kishi, Y.; Hama, K.; Kishimoto, T.; Mizuno, K.; Saku, K.; Taguchi, R.; Arai, H., Serum Lysophosphatidic Acid Is Produced through Diverse Phospholipase Pathways. *J. Biol. Chem.* 2002, *277* (50), 48737-48744.

80. Black, E. J.; Clair, T.; Delrow, J.; Neiman, P.; Gillespie, D. A. F., Microarray analysis identifies Autotaxin, a tumour cell motility and angiogenic factor with lysophospholipase D activity, as a specific target of cell transformation by v-Jun. *Oncogene* 2004, *23* (13), 2357-2366.

81. Chen, M.; O'Connor, K. L., Integrin alpha6beta4 promotes expression of autotaxin/ENPP2 autocrine motility factor in breast carcinoma cells. *Oncogene* 2005, *24* (32), 5125-30.

82. McCabe, C. D.; Innis, J. W., A genomic approach to the identification and characterization of HOXA13 functional binding elements. *Nucleic Acids Res* 2005, *33* (21), 6782-6794.

83. Ferry, G.; Moulharat, N.; Pradere, J. P.; Desos, P.; Try, A.; Genton, A.; Giganti, A.; Beucher-Gaudin, M.; Lonchampt, M.; Bertrand, M.; Saulnier-Blache, J. S.; Tucker, G. C.; Cordi, A.; Boutin, J. A., S32826, a nanomolar inhibitor of autotaxin: discovery, synthesis and applications as a pharmacological tool. *J Pharm Exp Ther* 2008, *327* (3), 809-19.

84. Lee, H. Y.; Murata, J.; Clair, T.; Polymeropoulos, M. H.; Torres, R.; Manrow, R. E.; Liotta, L. A.; Stracke, M. L., Cloning, Chromosomal Localization, and Tissue Expression of Autotaxin from Human Teratocarcinoma Cells. *Biochem. Biophys. Res. Commun.* 1996, *218* (3), 714-719.

85. Murata, J.; Lee, H. Y.; Clair, T.; Krutzsch, H. C.; Arestad, A.; Sobel, M. E.; Liotta, L. A.; Stracke, M. L., cDNA cloning of the human tumor motility-stimulating protein, autotaxin, reveals a homology with phosphodiesterases. *J. Biol. Chem.* 1994, *269* (48), 30479-30484.

86. Narita, M.; Goji, J.; Nakamura, H.; Sano, K., Molecular cloning, expression, and localization of a brain-specific phosphodiesterase I/nucleotide pyrophosphatase (PD-I alpha) from rat brain. *J. Biol. Chem.* 1994, *269* (45), 28235-42.

87. Boutin, J. A.; Ferry, G., Autotaxin. *Cell Mol Life Sci* 2009, *66* (18), 3009-21.

88. Tania, M.; Khan, M. A.; Zhang, H.; Li, J.; Song, Y., Autotaxin: a protein with two faces. *Biochem. Biophys. Res. Commun.* 2010, *401* (4), 493-7.

89. Nishimasu, H.; Okudaira, S.; Hama, K.; Mihara, E.; Dohmae, N.; Inoue, A.; Ishitani, R.; Takagi, J.; Aoki, J.; Nureki, O., Crystal structure of autotaxin and insight into GPCR activation by lipid mediators. *Nat Struct Mol Biol* 2011, *18* (2), 205-U271.

90. Hausmann, J.; Kamtekar, S.; Christodoulou, E.; Day, J. E.; Wu, T.; Fulkerson, Z.; Albers, H. M.; van Meeteren, L. A.; Houben, A. J. S.; van Zeijl, L.; Jansen, S.; Andries, M.; Hall, T.; Pegg, L. E.; Benson, T. E.; Kasiem, M.; Harlos, K.; Kooi, C. W. V.; Smyth, S. S.; Ovaa, H.; Bollen, M.;

Morris, A. J.; Moolenaar, W. H.; Perrakis, A., Structural basis of substrate discrimination and integrin binding by autotaxin. *Nat Struct Mol Biol* 2011, *18* (2), 198-U262.

91. Kawaguchi, M.; Okabe, T.; Okudaira, S.; Nishimasu, H.; Ishitani, R.; Kojima, H.; Nureki, O.; Aoki, J.; Nagano, T., Screening and X-ray Crystal Structure-based Optimization of Autotaxin (ENPP2) Inhibitors, Using a Newly Developed Fluorescence Probe. *ACS Chem. Biol.* 2013, *8* (8), 1713-1721.

92. Tabchy, A.; Tigyi, G.; Mills, G. B., Location, location, location: a crystal-clear view of autotaxin saturating LPA receptors. *Nat Struct Mol Biol* 2011, *18* (2), 117-8.

93. Koyama, M.; Nishimasu, H.; Ishitani, R.; Nureki, O., Molecular Dynamics Simulation of Autotaxin: Roles of the Nuclease-like Domain and the Glycan Modification. *J. Phys. Chem. B* 2012, *116* (39), 11798-11808.

94. Zalatan, J. G.; Fenn, T. D.; Brunger, A. T.; Herschlag, D., Structural and functional comparisons of nucleotide pyrophosphatase/phosphodiesterase and alkaline phosphatase: Implications for mechanism and evolution. *Biochemistry* 2006, *45* (32), 9788-9803.

95. Tanyi, J. L.; Hasegawa, Y.; Lapushin, R., Role of Decreased Levels of Lipid Phosphate Phosphatase-1 in Accumulation of Lysophosphatidic Acid in Ovarian Cancer. *Clin Cancer Res* 2003, *9*, 3534-3545.

96. Imai, A.; Furui, T.; Tamaya, T.; Mills, G. B., A Gonadotropin-Releasing Hormone-Responsive Phosphatase Hydrolyses Lysophosphatidic Acid within the Plasma Membrane of Ovarian Cancer Cells. *The Journal of Clinical Endocrinology & Metabolism* 2000, *85* (9), 3370-3375.

97. Fang, X. J.; Schummer, M.; Mao, M. L.; Yu, S. X.; Tabassam, F. H.; Swaby, R.; Hasegawa, Y.; Tanyi, J. L.; LaPushin, R.; Eder, A.; Jaffe, R.; Erickson, J.; Mills, G. B., Lysophosphatidic acid is a bioactive mediator in ovarian cancer. *Biochim. Biophys. Acta Mol. Cell Biol. Lipids* 2002, *1582* (1-3), 257-264.

98. Tanyi, J. L.; Morris, A. J.; Wolf, J. K., The Human Lipid Phosphate Phosphatase-3 Decreases the Growth, Survival, and Tumorigenesis of Ovarian Cancer Cells : Validation of the Lysophosphatidic Acid Signaling Cascade as a Target for Therapy in Ovarian Cancer

Cancer Res. 2003, *63*, 1073-1082.

99. Samadi, N.; Bekele, R.; Capatos, D.; Venkatraman, G.; Sariahmetoglu, M.; Brindley, D. N., Regulation of lysophosphatidate signaling by autotaxin and lipid phosphate phosphatases with respect to tumor progression, angiogenesis, metastasis and chemo-resistance. *Biochimie* 2011, *93* (1), 61-70.

100. Hecht, J. H.; Weiner, J. A.; Post, S. R.; Chun, J., Ventricular zone gene-1 (vzg-1) encodes a lysophosphatidic acid receptor expressed in neurogenic regions of the developing cerebral cortex. *The Journal of cell biology* 1996, *135* (4), 1071-1083.

101. Bandoh, K.; Aoki, J.; Hosono, H.; Kobayashi, S.; Kobayashi, T.; Murakami-Murofushi, K.; Tsujimoto, M.; Arai, H.; Inoue, K., Molecular cloning and characterization of a novel human G-protein-coupled receptor, EDG7, for lysophosphatidic acid. *J. Biol. Chem.* 1999, *274* (39), 27776-27785.

102. Chun, J.; Goetzl, E. J.; Hla, T.; Igarashi, Y.; Lynch, K. R.; Moolenaar, W.; Pyne, S.; Tigyi, G., International Union of Pharmacology. XXXIV. Lysophospholipid receptor nomenclature. *Pharmacol Rev.* 2002, *54* (2), 265-269.

103. Noguchi, K.; Ishii, S.; Shimizu, T., Identification of p2y(9)/GPR23 as a novel G protein-coupled receptor for lysophosphatidic acid, structurally distant from the Edg family. *J. Biol. Chem.* 2003, *278* (28), 25600-25606.

104. Lee, C. W.; Rivera, R.; Gardell, S.; Dubin, A. E.; Chun, J., GPR92 as a new G(12/13)- and G(q)-coupled lysophosphatidic acid receptor that increases cAMP, LPA(5). *J. Biol. Chem.* 2006, *281* (33), 23589-23597.

105. Kotarsky, K.; Boketoft, A.; Bristulf, J.; Nilsson, N. E.; Norberg, A.; Hansson, S.; Owman, C.; Sillard, R.; Leeb-Lundberg, L. M. F.; Olde, B., Lysophosphatidic acid binds to and activates GPR92, a G protein-coupled receptor highly expressed in gastrointestinal lymphocytes. *J Pharm Exp Ther* 2006, *318* (2), 619-628.

106. Pasternack, S. M.; von Kuegelgen, I.; Al Aboud, K.; Lee, Y. A.; Rueschendorf, F.; Voss, K.; Hillmer, A. M.; Molderings, G. J.; Franz, T.; Ramirez, A.; Nuernberg, P.; Noethen, M. M.; Betz, R. C., G protein-coupled receptor P2Y5 and its ligand LPA are involved in maintenance of human hair growth. *Nature Genet* 2008, *40* (3), 329-334.

107. Yanagida, K.; Masago, K.; Nakanishi, H.; Kihara, Y.; Hamano, F.; Tajima, Y.; Taguchi, R.; Shimizu, T.; Ishii, S., Identification and Characterization of a Novel Lysophosphatidic Acid Receptor, p2y5/LPA(6). *J. Biol. Chem.* 2009, *284* (26), 17731-17741.

108. Lee, M.; Choi, S.; Hallden, G.; Yo, S. J.; Schichnes, D.; Aponte, G. W., P2Y5 is a G alpha(i), G alpha(12/13) G protein-coupled receptor activated by lysophosphatidic acid that reduces intestinal cell adhesion. *Am. J. Physiol. Gastrointest. Liver Physiol.* 2009, *297* (4), G641-G654.

109. Oka, S.; Ota, R.; Shima, M.; Yamashita, A.; Sugiura, T., GPR35 is a novel lysophosphatidic acid receptor. *Biochem. Biophys. Res. Commun.* 2010, *395* (2), 232-237.

110. Tabata, K. I.; Baba, K.; Shiraishi, A.; Ito, M.; Fujita, N., The orphan GPCR GPR87 was deorphanized and shown to be a lysophosphatidic acid receptor. *Biochem. Biophys. Res. Commun.* 2007, *363* (3), 861-866.

111. Murakami, M.; Shiraishi, A.; Tabata, K.; Fujita, N., Identification of the orphan GPCR, P2Y(10) receptor as the sphingosine-1-phosphate and lysophosphatidic acid receptor. *Biochem. Biophys. Res. Commun.* 2008, *371* (4), 707-712.

112. Houben, A. J. S.; Moolenaar, W. H., Autotaxin and LPA receptor signaling in cancer. *Cancer Metastasis Rev.* 2011, *30* (3-4), 557-565.

113. Parri, M.; Chiarugi, P., Rac and Rho GTPases in cancer cell motility control. *Cell Commun Signal* 2010, *8*, 23.

114. Boucharaba, A.; Serre, C. M.; Guglielmi, J.; Bordet, J. C.; Clezardin, P.; Peyruchaud, O., The type 1 lysophosphatidic acid receptor is a target for therapy in bone metastases. *Proc Natl Acad Sci USA* 2006, *103* (25), 9643-8.

115. Furui, T.; LaPushin, R.; Mao, M., Overexpression of Edg-2/vzg-1 Induces Apoptosis and Acid-independent Manner Anoikisin Ovarian Cancer Cells in a Lysophosphatidic. *Clin Cancer Res* 1999, *5*, 4308-4318.

116. Wang, P.; Wu, X.; Chen, W.; Liu, J.; Wang, X., The lysophosphatidic acid (LPA) receptors their expression and significance in epithelial ovarian neoplasms. *Gynecol Oncol* 2007, *104* (3), 714-20.

117. Murph, M. M.; Nguyen, G. H.; Radhakrishna, H.; Mills, G. B., Sharpening the edges of understanding the structure/function of the LPA1 receptor: expression in cancer and mechanisms of regulation. *Biochim Biophys Acta* 2008, *1781* (9), 547-57.

118. Wang, G. L.; Wen, Z. Q.; Xu, W. P.; Wang, Z. Y.; Du, X.; Wang, F., Inhibition of Lysophosphatidic Acid Receptor-2 Expression by RNA Interference Decreases Lysophosphatidic Acid-induced Urokinase Plasminogen Activator Activation, Cell Invasion, and Migration in Ovarian Cancer SKOV-3 Cells. *Croat Med J* 2008, *49* (2), 175-181.

119. Liu, S.; Umezu-Goto, M.; Murph, M.; Lu, Y.; Liu, W.; Zhang, F.; Yu, S.; Stephens, L. C.; Cui, X.; Murrow, G.; Coombes, K.; Muller, W.; Hung, M. C.; Perou, C. M.; Lee, A. V.; Fang, X.; Mills, G. B., Expression of Autotaxin and Lysophosphatidic Acid Receptors Increases Mammary Tumorigenesis, Invasion, and Metastases. *Cancer Cell* 2009, *15* (6), 539-550.

120. Hayashi, M.; Okabe, K.; Kato, K.; Okumura, M.; Fukui, R.; Fukushima, N.; Tsujiuchi, T., Differential function of lysophosphatidic acid receptors in cell proliferation and migration of neuroblastoma cells. *Cancer Lett* 2012, *316* (1), 91-96.

121. Zhang, G. Y.; Ahmed, N.; Riley, C.; Oliva, K.; Barker, G.; Quinn, M. A.; Rice, G. E., Enhanced expression of peroxisome proliferator-activated receptor gamma in epithelial ovarian carcinoma. *Br J Cancer* 2005, *92* (1), 113-119.

122. Davidson, B.; Hadar, R.; Stavnes, H. T.; Trope, C. G.; Reich, R., Expression of the peroxisome proliferator-activated receptors-alpha, -beta, and -gamma in ovarian carcinoma effusions is associated with poor chemoresponse and shorter survival. *Hum Pathol* 2009, *40* (5), 705-713.

123. Yang, Y. C.; Tsao, Y. P.; Ho, T. C.; Choung, I. P., Peroxisome proliferator-activated receptor-gamma agonists cause growth arrest and apoptosis in human ovarian carcinoma cell lines. *Int J Gynecol Cancer* 2007, *17* (2), 418-425.

124. Girnun, G. D.; Naseri, E.; Vafai, S. B.; Qu, L.; Szwaya, J. D.; Bronson, R.; Alberta, J. A.; Spiegelman, B. M., Synergy between PPAR gamma ligands and platinum-based drugs in cancer. *Cancer Cell* 2007, *11* (5), 395-406.

125. van Meeteren, L. A.; Ruurs, P.; Stortelers, C.; Bouwman, P.; van Rooijen, M. A.; Pradere, J. P.; Pettit, T. R.; Wakelam, M. J.; Saulnier-Blache, J. S.; Mummery, C. L.; Moolenaar, W. H.; Jonkers, J., Autotaxin, a secreted lysophospholipase D, is essential for blood vessel formation during development. *Molecular and cellular biology* 2006, *26* (13), 5015-22.

126. Fotopoulou, S.; Oikonomou, N.; Grigorieva, E.; Nikitopoulou, I.; Paparountas, T.; Thanassopoulou, A.; Zhao, Z.; Xu, Y.; Kontoyiannis, D. L.; Remboutsika, E.; Aidinis, V., ATX expression and LPA signalling are vital for the development of the nervous system. *Dev. Biol.* 2010, *339* (2), 451-464.

127. Tanaka, M.; Okudaira, S.; Kishi, Y.; Ohkawa, R.; Iseki, S.; Ota, M.; Noji, S.; Yatomi, Y.; Aoki, J.; Arai, H., Autotaxin stabilizes blood vessels and is required for embryonic vasculature by producing lysophosphatidic acid. *J. Biol. Chem.* 2006, *281* (35), 25822-25830.

128. Yukiura, H.; Kano, K.; Kise, R.; Inoue, A.; Aoki, J., Autotaxin Overexpression Causes Embryonic Lethality and Vascular Defects. *PLOS ONE* 2015, *10* (5).

129. Nakamura, K.; Nangaku, M.; Ohkawa, R.; Okubo, S.; Yokota, H.; Ikeda, H.; Aoki, J.; Yatomi, Y., Analysis of serum and urinary lysophospholipase D/autotaxin in nephrotic syndrome. *Clin. Chem. Lab. Med.* 2008, *46* (1), 150-151.

130. Zhao, C.; Fernandes, M. J.; Prestwich, G. D.; Turgeon, M.; Di Battista, J.; Clair, T.; Poubelle, P. E.; Bourgoin, S. G., Regulation of lysophosphatidic acid receptor expression and function in human synoviocytes: Implications for rheumatoid arthritis? *Mol Pharmacol* 2008, *73* (2), 587-600.

131. Nochi, H.; Tomura, H.; Tobo, M.; Tanaka, N.; Sato, K.; Shinozaki, T.; Kobayashi, T.; Takagishi, K.; Ohta, H.; Okajima, F.; Tamoto, K., Stimulatory role of lysophosphatidic acid in cyclooxygenase-2 induction by synovial fluid of patients with rheumatoid arthritis in fibroblast-like synovial cells. *J. Immunol* 2008, *181* (7), 5111-5119.

132. Mabey, T.; Taleongpong, P.; Udomsinprasert, W.; Jirathanathornnukul, N.; Honsawek, S., Plasma and synovial fluid autotaxin correlate with severity in knee osteoarthritis. *Clin. Chim. Acta* 2015, *444*, 72-77.

133. Sato, K.; Malchinkhuu, E.; Muraki, T.; Ishikawa, K.; Hayashi, K.; Tosaka, M.; Mochiduki, A.; Inoue, K.; Tomura, H.; Mogi, C.; Nochi, H.; Tamoto, K.; Okajima, F., Identification of autotaxin as a neurite retraction-inducing factor of PC12 cells in cerebrospinal fluid and its possible sources. *J Neurochem* 2005, *92* (4), 904-914.

134. Hammack, B. N.; Fung, K. Y. C.; Hunsucker, S. W.; Duncan, M. W.; Burgoon, M. P.; Owens, G. P.; Gilden, D. H., Proteomic analysis of multiple sclerosis cerebrospinal fluid. *Mult. Scler.* 2004, *10* (3), 245-260.

135. Ferry, G.; Tellier, E.; Try, A.; Grés, S.; Naime, I.; Simon, M. F.; Rodriguez, M.; Boucher, J.; Tack, I.; Gesta, S.; Chomarat, P.; Dieu, M.; Raes, M.; Galizzi, J. P.; Valet, P.; Boutin, J. A.; Saulnier-Blache, J. S., Autotaxin Is Released from Adipocytes, Catalyzes Lysophosphatidic Acid

Synthesis, and Activates Preadipocyte Proliferation: Up-Regulated Expression with Adipocyte Differentiation and Obesity. *J. Biol. Chem.* 2003, *278* (20), 18162-18169.

136. Kanda, H.; Newton, R.; Klein, R.; Morita, Y.; Gunn, M. D.; Rosen, S. D., Autotaxin, an ectoenzyme that produces lysophosphatidic acid, promotes the entry of lymphocytes into secondary lymphoid organs. *Nature Immunol* 2008, *9* (4), 415-423.

137. Clair, T.; Aoki, J.; Koh, E.; Bandle, R. W.; Nam, S. W.; Ptaszynska, M. M.; Mills, G. B.; Schiffmann, E.; Liotta, L. A.; Stracke, M. L., Autotaxin hydrolyzes sphingosylphosphorylcholine to produce the regulator of migration, sphingosine-1-phosphate. *Cancer Res.* 2003, *63* (17), 5446-5453.

138. van Meeteren, L. A.; Moolenaar, W. H., Regulation and biological activities of the autotaxin-LPA axis. *Prog Lipid Res* 2007, *46* (2), 145-160.

139. Katsifa, A.; Kaffe, E.; Nikolaidou-Katsaridou, N.; Economides, A. N.; Newbigging, S.; McKerlie, C.; Aidinis, V., The Bulk of Autotaxin Activity Is Dispensable for Adult Mouse Life. *PLOS ONE* 2015, *10* (11), e0143083.

140. Kishi, Y.; Okudaira, S.; Tanaka, M.; Hama, K.; Shida, D.; Kitayama, J.; Yamori, T.; Aoki, J.; Fujimaki, T.; Arai, H., Autotaxin is overexpressed in glioblastoma multiforme and contributes to cell motility of glioblastoma by converting lysophosphatidylcholine to lysophosphatidic acid. *J. Biol. Chem.* 2006, *281* (25), 17492-500.

141. Gaetano, C. G.; Samadi, N.; Tomsig, J. L.; Macdonald, T. L.; Lynch, K. R.; Brindley, D. N., Inhibition of autotaxin production or activity blocks lysophosphatidylcholine-induced migration of human breast cancer and melanoma cells. *Mol Carcinog* 2009, *48* (9), 801-9.

142. Harper, K.; Arsenault, D.; Boulay-Jean, S.; Lauzier, A.; Lucien, F.; Dubois, C. M., Autotaxin promotes cancer invasion via the lysophosphatidic acid receptor 4: participation of the cyclic AMP/EPAC/Rac1 signaling pathway in invadopodia formation. *Cancer Res.* 2010, *70* (11), 4634-43.

143. Suk, W. N.; Clair, T.; Campo, C. K.; Hoi Young, L.; Liotta, L. A.; Stracke, M. L., Autotaxin (ATX), a potent tumor motogen, augments invasive and metastatic potential of ras-transformed cells. *Oncogene* 2000, *19*, 241-247.

144. Zhang, R.; Wang, J.; Ma, S.; Huang, Z.; Zhang, G., Requirement of Osteopontin in the migration and protection against Taxol-induced apoptosis via the ATX-LPA axis in SGC7901 cells. *BMC Cell Biol* 2011, *12*, 11.

145. Haga, A.; Nagai, H.; Deyashiki, Y., Autotaxin promotes the expression of matrix metalloproteinase-3 via activation of the MAPK cascade in human fibrosarcoma HT-1080 cells. *Cancer Invest* 2009, *27* (4), 384-90.

146. Jung, I. D.; Lee, J.; Yun, S. Y.; Park, C. G.; Choi, W. S.; Lee, H. W.; Choi, O. H.; Han, J. W.; Lee, H. Y., Cdc42 and Rac1 are necessary for autotaxin-induced tumor cell motility in A2058 melanoma cells. *FEBS Lett* 2002, *532* (3), 351-6.

147. Hoelzinger, D. B.; Nakada, M.; Demuth, T.; Rosensteel, T.; Reavie, L. B.; Berens, M. E., Autotaxin: a secreted autocrine/paracrine factor that promotes glioma invasion. *J Neurooncol* 2008, *86* (3), 297-309.

148. David, M.; Wannecq, E.; Descotes, F.; Jansen, S.; Deux, B.; Ribeiro, J.; Serre, C. M.; Gres, S.; Bendriss-Vermare, N.; Bollen, M.; Saez, S.; Aoki, J.; Saulnier-Blache, J. S.; Clezardin, P.; Peyruchaud, O., Cancer cell expression of autotaxin controls bone metastasis formation in mouse through lysophosphatidic acid-dependent activation of osteoclasts. *PLOS ONE* 2010, *5* (3), e9741.

149. Huang, R. Y.; Wang, S. M.; Hsieh, C. Y.; Wu, J. C., Lysophosphatidic acid induces ovarian cancer cell dispersal by activating Fyn kinase associated with p120-catenin. *Int J Cancer* 2008, *123* (4), 801-9.

150. Do, T. V.; Symowicz, J. C.; Berman, D. M.; Liotta, L. A.; Petricoin, E. F., 3rd; Stack, M. S.; Fishman, D. A., Lysophosphatidic acid down-regulates stress fibers and up-regulates pro-matrix metalloproteinase-2 activation in ovarian cancer cells. *Mol. Cancer Res.* 2007, *5* (2), 121-31.

151. Kim, E. K.; Park, J. M.; Lim, S.; Choi, J. W.; Kim, H. S.; Seok, H.; Seo, J. K.; Oh, K.; Lee, D. S.; Kim, K. T.; Ryu, S. H.; Suh, P. G., Activation of AMP-activated protein kinase is essential for lysophosphatidic acid-induced cell migration in ovarian cancer cells. *J. Biol. Chem.* 2011, *286* (27), 24036-45.

152. Bian, D.; Mahanivong, C.; Yu, J.; Frisch, S. M.; Pan, Z. K.; Ye, R. D.; Huang, S., The G12/13-RhoA signaling pathway contributes to efficient lysophosphatidic acid-stimulated cell migration. *Oncogene* 2006, *25* (15), 2234-44.

153. Sawada, K.; Morishige, K.; Tahara, M.; Ikebuchi, Y.; Kawagishi, R.; Tasaka, K.; Murata, Y., Lysophosphatidic Acid Induces Focal Adhesion Assembly through Rho/Rho-Associated Kinase Pathway in Human Ovarian Cancer Cells. *Gynecol Oncol* 2002, *87* (3), 252-259.

154. Bian, D.; Su, S.; Mahanivong, C.; Cheng, R. K.; Han, Q.; Pan, Z. K.; Sun, P.; Huang, S., Lysophosphatidic Acid Stimulates Ovarian Cancer Cell Migration via a Ras-MEK Kinase 1 Pathway. *Cancer Res.* 2004, *64* (12), 4209-17.

155. Fishman, D. A.; Liu, Y.; Ellerbroek, S. M.; Stack, M. S., Lysophosphatidic Acid Promotes Matrix Metalloproteinase (MMP) Activation and MMP-dependent Invasion in Ovarian Cancer Cells. *Cancer Res.* 2001, *61*, 3194–3199.

156. Wang, F. Q.; Fisher, J.; Fishman, D. A., MMP-1-PAR1 axis mediates LPA-induced epithelial ovarian cancer (EOC) invasion. *Gynecol Oncol* 2011, *120* (2), 247-255.

157. Park, S. Y.; Jeong, K. J.; Panupinthu, N.; Yu, S.; Lee, J.; Han, J. W.; Kim, J. M.; Lee, J. S.; Kang, J.; Park, C. G.; Mills, G. B.; Lee, H. Y., Lysophosphatidic acid augments human hepatocellular carcinoma cell invasion through LPA1 receptor and MMP-9 expression. *Oncogene* 2011, *30* (11), 1351-1359.

158. Sengupta, S.; Kim, K. S.; Berk, M. P.; Oates, R.; Escobar, P.; Belinson, J.; Li, W.; Lindner, D. J.; Williams, B.; Xu, Y., Lysophosphatidic acid downregulates tissue inhibitor of

metalloproteinases, which are negatively involved in lysophosphatidic acid-induced cell invasion. *Oncogene* 2007, *26* (20), 2894-2901.

159. Gil, O. D.; Lee, C.; Ariztia, E. V.; Wang, F. Q.; Smith, P. J.; Hope, J. M.; Fishman, D. A., Lysophosphatidic acid (LPA) promotes E-cadherin ectodomain shedding and OVCA429 cell invasion in an uPA-dependent manner. *Gynecol Oncol* 2008, *108* (2), 361-9.

160. Kang, Y. C.; Kim, K. M.; Lee, K. S.; Namkoong, S.; Lee, S. J.; Han, J. A.; Jeoung, D.; Ha, K. S.; Kwon, Y. G.; Kim, Y. M., Serum bioactive lysophospholipids prevent TRAIL-induced apoptosis via PI3K/Akt-dependent cFLIP expression and Bad phosphorylation. *Cell Death Differ* 2004, *11* (12), 1287-98.

161. Meng, Y.; Graves, L.; Do, T. V.; So, J.; Fishman, D. A., Upregulation of FasL by LPA on ovarian cancer cell surface leads to apoptosis of activated lymphocytes. *Gynecol Oncol* 2004, *95* (3), 488-95.

162. Meng, Y.; Kang, S.; Fishman, D. A., Lysophosphatidic acid stimulates fas ligand microvesicle release from ovarian cancer cells. *Cancer Immunol. Immunother.* 2005, *54* (8), 807-14.

163. Kamrava, M.; Simpkins, F.; Alejandro, E.; Michener, C.; Meltzer, E.; Kohn, E. C., Lysophosphatidic acid and endothelin-induced proliferation of ovarian cancer cell lines is mitigated by neutralization of granulin-epithelin precursor (GEP), a prosurvival factor for ovarian cancer. *Oncogene* 2005, *24* (47), 7084-93.

164. Song, J.; Clair, T.; Noh, J. H.; Eun, J. W.; Ryu, S. Y.; Lee, S. N.; Ahn, Y. M.; Kim, S. Y.; Lee, S. H.; Park, W. S.; Yoo, N. J.; Lee, J. Y.; Nam, S. W., Autotaxin (lysoPLD/NPP2) protects fibroblasts from apoptosis through its enzymatic product, lysophosphatidic acid, utilizing albumin-bound substrate. *Biochem. Biophys. Res. Commun.* 2005, *337* (3), 967-75.

165. Yu-Long, H.; Albanese, C.; Pestell, R. G.; Jaffe, R., Dual Mechanisms for Lysophosphatidic Acid Stimulation of Human Ovarian Carcinoma Cells. *J Natl Cancer Inst* 2003, *95* (10), 733.

166. Xu, Y.; Fang, X. J.; Casey, T. G.; Mills, G. B., Lysophospholipids activate ovarian and breast cancer cells. *J. Biol. Chem.* 1995, *309*, 933-940.

167. Hurst, J. H.; Hooks, S. B., Lysophosphatidic acid stimulates cell growth by different mechanisms in SKOV-3 and Caov-3 ovarian cancer cells: distinct roles for Gi- and Rho-dependent pathways. *Pharmacology* 2009, *83* (6), 333-47.

168. Lee, Z.; Swaby, R. F.; Liang, Y.; Yu, S.; Liu, S.; Lu, K. H.; Bast, R. C.; Mills, G. B.; Fang, X., Lysophosphatidic Acid Is a Major Regulator of Growth-Regulated Oncogene α in Ovarian Cancer. *Cancer Res.* 2006, *66* (5), 2740-2748.

169. Lee, J.; Park, S. Y.; Lee, E. K.; Park, C. G.; Chung, H. C.; Rha, S. Y.; Kim, Y. K.; Bae, G. U.; Kim, B. K.; Han, J. W.; Lee, H. Y., Activation of hypoxia-inducible factor-1alpha is necessary for lysophosphatidic acid-induced vascular endothelial growth factor expression. *Clin Cancer Res* 2006, *12* (21), 6351-8.

170. Ptaszynska, M. M.; Pendrak, M. L.; Stracke, M. L.; Roberts, D. D., Autotaxin signaling via lysophosphatidic acid receptors contributes to vascular endothelial growth factor-induced endothelial cell migration. *Mol. Cancer Res.* 2010, *8* (3), 309-21.

171. Yu, S.; Murph, M. M.; Lu, Y.; Liu, S.; Hall, H. S.; Liu, J.; Stephens, C.; Fang, X.; Mills, G. B., Lysophosphatidic acid receptors determine tumorigenicity and aggressiveness of ovarian cancer cells. *J. Natl. Cancer Inst.* 2008, *100* (22), 1630-42.

172. Murph, M. M.; Hurst-Kennedy, J.; Newton, V.; Brindley, D. N.; Radhakrishna, H., Lysophosphatidic acid decreases the nuclear localization and cellular abundance of the p53 tumor, suppressor in A549 lung carcinoma cells. *Mol. Cancer Res.* 2007, *5* (11), 1201-1211.

173. Kortlever, R. M.; Brummelkamp, T. R.; van Meeteren, L. A.; Moolenaar, W. H.; Bernards, R., Suppression of the p53-dependent replicative senescence response by lysophosphatidic acid signaling. *Mol. Cancer Res.* 2008, *6* (9), 1452-60.

174. Bermudez, Y.; Yang, H.; Saunders, B. O.; Cheng, J. Q.; Nicosia, S. V.; Kruk, P. A., VEGF- and LPA-induced telomerase in human ovarian cancer cells is Sp1-dependent. *Gynecol Oncol* 2007, *106* (3), 526-37.

175. Yang, K.; Zheng, D. H.; Deng, X. L.; Bai, L.; Xu, Y.; Cong, Y. S., Lysophosphatidic Acid Activates Telomerase in Ovarian Cancer Cells Through Hypoxia-Inducible Factor-1 alpha and the PI3K Pathway. *J. Cell. Biochem* 2008, *105* (5), 1194-1201.

176. Frankel, A.; Mills, G. B., Peptide and Lipid growth factors decrease cis-diamminedichloroplatinum-induced cell death in Human Ovarian Cancer Cells. *Clin Cancer Res* 1996, *2*, 1307-1313.

177. Sun, H., Effects of lysophosphatidic acid on human colon cancer cells and its mechanisms of action. *World J Gastroenterol* 2009, *15* (36), 4547.

178. Vidot, S.; Witham, J.; Agarwal, R.; Greenhough, S.; Bamrah, H. S.; Tigyi, G. J.; Kaye, S. B.; Richardson, A., Autotaxin delays apoptosis induced by carboplatin in ovarian cancer cells. *Cell. Signal.* 2010, *22* (6), 926-935.

179. Samadi, N.; Gaetano, C.; Goping, I. S.; Brindley, D. N., Autotaxin protects MCF-7 breast cancer and MDA-MB-435 melanoma cells against Taxol-induced apoptosis. *Oncogene* 2009, *28* (7), 1028-1039.

180. Samadi, N.; Bekele, R. T.; Goping, I. S.; Schang, L. M.; Brindley, D. N., Lysophosphatidate induces chemo-resistance by releasing breast cancer cells from taxol-induced mitotic arrest. *PLOS ONE* 2011, *6* (5), e20608.

181. Deng, W.; E, S.; Tsukahara, R.; Valentine, W. J.; Durgam, G.; Gududuru, V.; Balazs, L.; Manickam, V.; Arsura, M.; Vanmiddlesworth, L.; Johnson, L. R.; Parrill, A. L.; Miller, D. D.; Tigyi, G., The Lysophosphatidic Acid Type 2 Receptor Is Required for Protection Against Radiation-Induced Intestinal Injury. *Gastroenterology* 2007, *132* (5), 1834-1851.

182. Deng, W.; Balazs, L.; Wang, D. A.; Van Middlesworth, L.; Tigyi, G.; Johnson, L. R., Lysophosphatidic acid protects and rescues intestinal epithelial cells from radiation- and chemotherapy-induced apoptosis. *Gastroenterology* 2002, *123* (1), 206-216.

183. Shuyu, E.; Lai, Y. J.; Tsukahara, R.; Chen, C. S.; Fujiwara, Y.; Yue, J.; Yu, J. H.; Guo, H.; Kihara, A.; Tigyi, G.; Lin, F. T., Lysophosphatidic acid 2 receptor-mediated supramolecular complex formation regulates its antiapoptotic effect. *J. Biol. Chem.* 2009, *284* (21), 14558-71.

184. Barkinge, J. L.; Gudi, R.; Sarah, H.; Chu, F.; Borthakur, A.; Prabhakar, B. S.; Prasad, K. V., The p53-induced Siva-1 plays a significant role in cisplatin-mediated apoptosis. *Journal of carcinogenesis* 2009, *8*, 2.

185. Lin, F. T.; Lai, Y. J.; Makarova, N.; Tigyi, G.; Lin, W. C., The Lysophosphatidic Acid 2 Receptor Mediates Down-regulation of Siva-1 to Promote Cell Survival. *J. Biol. Chem.* 2007, *282* (52), 37759-37769.

186. Witham, J.; Valenti, M. R.; De-Haven-Brandon, A. K.; Vidot, S.; Eccles, S. A.; Kaye, S. B.; Richardson, A., The Bcl-2/Bcl-XL family inhibitor ABT-737 sensitizes ovarian cancer cells to carboplatin. *Clin Cancer Res* 2007, *13* (23), 7191-8.

187. Xue, L.; Chu, F.; Cheng, Y.; Sun, X.; Borthakur, A.; Ramarao, M.; Pandey, P.; Wu, M.; Schlossman, S. F.; Prasad, K. V., Siva-1 binds to and inhibits BCL-X(L)-mediated protection against UV radiation-induced apoptosis. *Proc Natl Acad Sci USA* 2002, *99* (10), 6925-30.

188. Hurst, J. H.; Mendpara, N.; Hooks, S. B., Regulator of G-protein signalling expression and function in ovarian cancer cell lines. *Cell Mol Biol Lett* 2009, *14* (1), 153-74.

189. Hooks, S. B.; Callihan, P.; Altman, M. K.; Hurst, J. H.; Ali, M. W.; Murph, M. M., Regulators of G-Protein signaling RGS10 and RGS17 regulate chemoresistance in ovarian cancer cells. *Mol Cancer* 2010, *9*, 289.

190. Pamuklar, Z.; Federico, L.; Liu, S. Y.; Umezu-Goto, M.; Dong, A. P.; Panchatcharam, M.; Fulerson, Z.; Berdyshev, E.; Natarajan, V.; Fang, X. J.; Van Meeteren, L. A.; Moolenaar, W. H.; Mills, G. B.; Morris, A. J.; Smyth, S. S., Autotaxin/Lysopholipase D and Lysophosphatidic Acid Regulate Murine Hemostasis and Thrombosis. *J. Biol. Chem.* 2009, *284* (11), 7385-7394.

191. Dusaulcy, R.; Rancoule, C.; Grès, S.; Wanecq, E.; Colom, A.; Guigné, C.; van Meeteren, L. A.; Moolenaar, W. H.; Valet, P.; Saulnier-Blache, J. S., Adipose-specific disruption of autotaxin enhances nutritional fattening and reduces plasma lysophosphatidic acid. *J Lipid Res* 2011, *52* (6), 1247-1255.

192. Nikitopoulou, I.; Oikonomou, N.; Karouzakis, E.; Sevastou, I.; Nikolaidou-Katsaridou, N.; Zhao, Z. W.; Mersinias, V.; Armaka, M.; Xu, Y.; Masu, M.; Mills, G. B.; Gay, S.; Kollias, G.; Aidinis, V., Autotaxin expression from synovial fibroblasts is essential for the pathogenesis of modeled arthritis. *J. Exp. Med.* 2012, *209* (5), 923-931.

193. Zahednasab, H.; Balood, M.; Harirchian, M. H.; Mesbah-Namin, S. A.; Rahimian, N.; Siroos, B., Increased autotaxin activity in multiple sclerosis. *J Neuroimmunol* 2014, *273* (1-2), 120-123.

194. Oikonomou, N.; Mouratis, M. A.; Tzouvelekis, A.; Kaffe, E.; Valavanis, C.; Vilaras, G.; Karameris, A.; Prestwich, G. D.; Bouros, D.; Aidinis, V., Pulmonary Autotaxin Expression Contributes to the Pathogenesis of Pulmonary Fibrosis. *Am. J. Respir. Cell Mol. Biol.* 2012, *47* (5), 566-574.

195. Watanabe, N.; Ikeda, H.; Nakamura, K.; Ohkawa, R.; Kume, Y.; Aoki, J.; Hama, K.; Okudaira, S.; Tanaka, M.; Tomiya, T.; Yanase, M.; Tejima, K.; Nishikawa, T.; Arai, M.; Arai, H.; Omata, M.; Fujiwara, K.; Yatomi, Y., Both plasma lysophosphatidic acid and serum autotaxin levels are increased in chronic hepatitis C. *J Clin Gastroenterol* 2007, *41* (6), 616-623.

196. Umemura, K.; Yamashita, N.; Yu, X. N.; Arima, K.; Asada, T.; Makifuchi, T.; Murayama, S.; Saito, Y.; Kanamaru, K.; Goto, Y.; Kohsaka, S.; Kanazawa, I.; Kimura, H., Autotaxin expression is enhanced in frontal cortex of Alzheimer-type dementia patients. *Neurosci. Lett* 2006, *400* (1-2), 97-100.

197. Nikitopoulou, I.; Kaffe, E.; Sevastou, I.; Sirioti, I.; Samiotaki, M.; Madan, D.; Prestwich, G. D.; Aidinis, V., A Metabolically-Stabilized Phosphonate Analog of Lysophosphatidic Acid Attenuates Collagen-Induced Arthritis. *PLOS ONE* 2013, *8* (7).

198. Park, G. Y.; Lee, Y. G.; Berdyshev, E.; Nyenhuis, S.; Du, J.; Fu, P.; Gorshkova, I. A.; Li, Y.; Chung, S.; Karpurapu, M.; Deng, J.; Ranjan, R.; Xiao, L.; Jaffe, H. A.; Corbridge, S. J.; Kelly, E. A. B.; Jarjour, N. N.; Chun, J.; Prestwich, G. D.; Kaffe, E.; Ninou, I.; Aidinis, V.; Morris, A. J.; Smyth, S. S.; Ackerman, S. J.; Natarajan, V.; Christman, J. W., Autotaxin Production of Lysophosphatidic Acid Mediates Allergic Asthmatic Inflammation. *Am. J. Respir. Crit. Care Med.* 2013, *188* (8), 928-940.

199. Tager, A. M.; LaCamera, P.; Shea, B. S.; Campanella, G. S.; Selman, M.; Zhao, Z.; Polosukhin, V.; Wain, J.; Karimi-Shah, B. A.; Kim, N. D.; Hart, W. K.; Pardo, A.; Blackwell, T. S.; Xu, Y.; Chun, J.; Luster, A. D., The lysophosphatidic acid receptor LPA1 links pulmonary fibrosis to lung injury by mediating fibroblast recruitment and vascular leak. *Nat. Med.* 2008, *14* (1), 45-54.

200. Watanabe, N.; Ikeda, H.; Nakamura, K.; Ohkawa, R.; Kume, Y.; Tomiya, T.; Tejima, K.; Nishikawa, T.; Arai, M.; Yanase, M.; Aoki, J.; Arai, H.; Omata, M.; Fujiwara, K.; Yatomi, Y., Plasma lysophosphatidic acid level and serum autotaxin activity are increased in liver injury in rats in relation to its severity. *Life Sci.* 2007, *81* (12), 1009-1015.

201. Clair, T.; Koh, E.; Ptaszynska, M.; Bandle, R. W.; Liotta, L. A.; Schiffmann, E.; Stracke, M. L., L-histidine inhibits production of lysophosphatidic acid by the tumor-associated cytokine, autotaxin. *Lipids in health and disease* 2005, *4*, 5.

202. Tokumura, A.; Miyake, M.; Yoshimoto, O.; Shimizu, M.; Fukuzawa, K., Metal-ion stimulation and inhibition of lysophospholipase D which generates bioactive lysophosphatidic acid in rat plasma. *Lipids* 1998, *33* (10), 1009-1015.

203. van Meeteren, L. A.; Ruurs, P.; Christodoulou, E.; Goding, J. W.; Takakusa, H.; Kikuchi, K.; Perrakis, A.; Nagano, T.; Moolenaar, W. H., Inhibition of autotaxin by lysophosphatidic acid and sphingosine 1-phosphate. *J. Biol. Chem.* 2005, *280* (22), 21155-21161.

204. Durgam, G. G.; Virag, T.; Walker, M. D.; Tsukahara, R.; Yasuda, S.; Liliom, K.; van Meeteren, L. A.; Moolenaar, W. H.; Wilke, N.; Siess, W.; Tigyi, G.; Miller, D. D., Synthesis, structure-activity relationships, and biological evaluation of fatty alcohol phosphates as lysophosphatidic acid receptor ligands, activators of PPAR gamma, and inhibitors of autotaxin. *J Med Chem* 2005, *48* (15), 4919-4930.

205. Gududuru, V.; Zeng, K.; Tsukahara, R.; Makarova, N.; Fujiwara, Y.; Pigg, K. R.; Baker, D. L.; Tigyi, G.; Miller, D. D., Identification of Darmstoff analogs as selective agonists and antagonists of lysophosphatidic acid receptors. *Bioorg Med Chem Lett* 2006, *16* (2), 451-456.

206. Mukai, M.; Imamura, F.; Ayaki, M.; Shinkai, K.; Iwasaki, T.; Murakami-Murofushi, K.; MUROFUSHI, H.; Kobayashi, S.; Yamamoto, T.; Nakamura, H.; Akedo, H., Inhibtion of tumour invasion and metastasis by a novel Lysophosphatidic acid (cyclic LPA). *Int J Cancer* 1999, *81*, 918-922.

207. Ishihara, R.; Tatsuta, M.; Iishi, H.; Baba, M.; Uedo, N.; Higashino, K.; Mukai, M.; Ishiguro, S.; Kobayashi, S.; Murakami-Murofushi, K., Attenuation by cyclic phosphatidic acid of peritoneal metastasis of azoxymethane-induced intestinal cancers in Wistar rats. *Int J Cancer* 2004, *110* (2), 188-93.

208. Baker, D. L.; Fujiwara, Y.; Pigg, K. R.; Tsukahara, R.; Kobayashi, S.; Murofushi, H.; Uchiyama, A.; Murakami-Murofushi, K.; Koh, E.; Bandle, R. W.; Byun, H. S.; Bittman, R.; Fan, D.; Murph, M.; Mills, G. B.; Tigyi, G., Carba analogs of cyclic phosphatidic acid are selective inhibitors of autotaxin and cancer cell invasion and metastasis. *J. Biol. Chem.* 2006, *281* (32), 22786-93.

209. Gupte, R.; Siddam, A.; Lu, Y.; Li, W.; Fujiwara, Y.; Panupinthu, N.; Pham, T. C.; Baker, D. L.; Parrill, A. L.; Gotoh, M.; Murakami-Murofushi, K.; Kobayashi, S.; Mills, G. B.; Tigyi, G.; Miller, D. D., Synthesis and pharmacological evaluation of the stereoisomers of 3-carba cyclic-phosphatidic acid. *Bioorg Med Chem Lett* 2010, *20* (24), 7525-8.

210. Nozaki, E.; Gotoh, M.; Hotta, H.; Hanazawa, S.; Kobayashi, S.; Murakami-Murofushi, K., Synthesis of enantiopure 2-carba-cyclic phosphatidic acid and effects of its chirality on biological functions. *Biochim Biophys Acta* 2011, *1811* (4), 271-7.

211. Cui, P.; Tomsig, J. L.; McCalmont, W. F.; Lee, S.; Becker, C. J.; Lynch, K. R.; Macdonald, T. L., Synthesis and biological evaluation of phosphonate derivatives as autotaxin (ATX) inhibitors. *Bioorg Med Chem Lett* 2007, *17* (6), 1634-40.

212. Jiang, G. W.; Xu, Y.; Fujiwara, Y.; Tsukahara, T.; Tsukahara, R.; Gajewiak, J.; Tigyi, G.; Prestwich, G. D., alpha-substituted phosphonate analogues of lysophosphatidic acid (LPA) selectively inhibit production and action of LPA. *ChemMedChem* 2007, *2* (5), 679-690.

213. Cui, P.; McCalmont, W. F.; Tomsig, J. L.; Lynch, K. R.; Macdonald, T. L., alpha- and beta-Substituted phosphonate analogs of LPA as autotaxin inhibitors. *Bioorg Med Chem* 2008, *16* (5), 2212-2225.

214. East, J. E.; Kennedy, A. J.; Tomsig, J. L.; De Leon, A. R.; Lynch, K. R.; Macdonald, T. L., Synthesis and structure-activity relationships of tyrosine-based inhibitors of autotaxin (ATX). *Bioorg Med Chem Lett* 2010, *20* (23), 7132-6.

215. Brinkmann, V.; Davis, M. D.; Heise, C. E.; Albert, R.; Cottens, S.; Hof, R.; Bruns, C.; Prieschl, E.; Baumruker, T.; Hiestand, P.; Foster, C. A.; Zollinger, M.; Lynch, K. R., The immune modulator FTY720 targets sphingosine 1-phosphate receptors. *J. Biol. Chem.* 2002, *277* (24), 21453-7.

216. Kim, S.; Lee, H.; Lee, M.; Lee, T., Efficient Synthesis of the Immunosuppressive Agent FTY720. *Synthesis* 2006, *2006* (05), 753-755.

217. van Meeteren, L. A.; Brinkmann, V.; Saulnier-Blache, J. S.; Lynch, K. R.; Moolenaar, W. H., Anticancer activity of FTY720: phosphorylated FTY720 inhibits autotaxin, a metastasis-enhancing and angiogenic lysophospholipase D. *Cancer Lett* 2008, *266* (2), 203-8.

218. Valentine, W. J.; Kiss, G. N.; Liu, J.; E, S.; Gotoh, M.; Murakami-Murofushi, K.; Pham, T. C.; Baker, D. L.; Parrill, A. L.; Lu, X.; Sun, C.; Bittman, R.; Pyne, N. J.; Tigyi, G., (S)-FTY720-vinylphosphonate, an analogue of the immunosuppressive agent FTY720, is a pan-antagonist of sphingosine 1-phosphate GPCR signaling and inhibits autotaxin activity. *Cell. Signal.* 2010, *22* (10), 1543-53.

219. Gupte, R.; Patil, R.; Liu, J.; Wang, Y.; Lee, S. C.; Fujiwara, Y.; Fells, J.; Bolen, A. L.; Emmons-Thompson, K.; Yates, C. R.; Siddam, A.; Panupinthu, N.; Pham, T. C.; Baker, D. L.; Parrill, A. L.; Mills, G. B.; Tigyi, G.; Miller, D. D., Benzyl and naphthalene methylphosphonic acid inhibitors of autotaxin with anti-invasive and anti-metastatic activity. *ChemMedChem* 2011, *6* (5), 922-35.

220. Jiang, G.; Madan, D.; Prestwich, G. D., Aromatic phosphonates inhibit the lysophospholipase D activity of autotaxin. *Bioorg Med Chem Lett* 2011, *21* (17), 5098-5101.

221. Parrill, A. L.; Echols, U.; Nguyen, T.; Pham, T. C.; Hoeglund, A.; Baker, D. L., Virtual screening approaches for the identification of non-lipid autotaxin inhibitors. *Bioorg Med Chem* 2008, *16* (4), 1784-95.

222. Hoeglund, A. B.; Howard, A. L.; Wanjala, I. W.; Pham, T. C. T.; Parrill, A. L.; Baker, D. L., Characterization of non-lipid autotaxin inhibitors. *Bioorg Med Chem* 2010, *18* (2), 769-776.

223. Albers, H. M.; Dong, A.; van Meeteren, L. A.; Egan, D. A.; Sunkara, M.; van Tilburg, E. W.; Schuurman, K.; van Tellingen, O.; Morris, A. J.; Smyth, S. S.; Moolenaar, W. H.; Ovaa, H.,

Boronic acid-based inhibitor of autotaxin reveals rapid turnover of LPA in the circulation. *Proc Natl Acad Sci USA* 2010, *107* (16), 7257-62.

224. Albers, H. M.; van Meeteren, L. A.; Egan, D. A.; van Tilburg, E. W.; Moolenaar, W. H.; Ovaa, H., Discovery and optimization of boronic acid based inhibitors of autotaxin. *J Med Chem* 2010, *53* (13), 4958-67.

225. Albers, H. M.; Hendrickx, L. J.; van Tol, R. J.; Hausmann, J.; Perrakis, A.; Ovaa, H., Structure-based design of novel boronic acid-based inhibitors of autotaxin. *J Med Chem* 2011, *54* (13), 4619-26.

226. Gierse, J.; Thorarensen, A.; Beltey, K.; Bradshaw-Pierce, E.; Cortes-Burgos, L.; Hall, T.; Johnston, A.; Murphy, M.; Nemirovskiy, O.; Ogawa, S.; Pegg, L.; Pelc, M.; Prinsen, M.; Schnute, M.; Wendling, J.; Wene, S.; Weinberg, R.; Wittwer, A.; Zweifel, B.; Masferrer, J., A novel autotaxin inhibitor reduces lysophosphatidic acid levels in plasma and the site of inflammation. *J Pharm Exp Ther* 2010, *334* (1), 310-7.

227. Saga, H.; Ohhata, A.; Hayashi, A.; Katoh, M.; Maeda, T.; Mizuno, H.; Takada, Y.; Komichi, Y.; Ota, H.; Matsumura, N.; Shibaya, M.; Sugiyama, T.; Nakade, S.; Kishikawa, K., A novel highly potent autotaxin/ENPP2 inhibitor produces prolonged decreases in plasma lysophosphatidic acid formation in vivo and regulates urethral tension. *PLOS ONE* 2014, *9* (4), e93230.

228. Benesch, M. G.; Tang, X.; Maeda, T.; Ohhata, A.; Zhao, Y. Y.; Kok, B. P.; Dewald, J.; Hitt, M.; Curtis, J. M.; McMullen, T. P.; Brindley, D. N., Inhibition of autotaxin delays breast tumor growth and lung metastasis in mice. *FASEB J* 2014, *28* (6), 2655-66.

229. Staehle, W.; Schultz, M.; Schiemann, K. Benzonaphthyridinamines as autotaxin inhibitors. US 09029387, May 12 2015, 2015.

230. Staehle, W.; Schiemann, K.; Schultz, M. Heterocyclic compounds as autotaxin inhibitors. US 08841324, Sep 23 2014, 2014.

231. Schiemann, K.; Schultz, M.; Staehle, W. Piperidine and piperazine derivatives as autotaxin inhibitors. US 08822476, Sep 2 2014, 2014.

232. Long, S. A.; Thorarensen, A.; Schnute, M. E. New pyrimidine and pyridine derivatives are autotaxin inhibitors useful for treating e.g. ovarian cancer, breast cancer, prostate cancer, atherosclerosis, thrombosis, psoriasis, multiple sclerosis, Keloid, Cirrhosis and rheumatoid arthritis. WO2013054185-A1.

233. Roppe, J. R.; Parr, T. A.; Stock, N. S.; Volkots, D.; Hutchinson, J. H. Autotaxin inhibitors and uses thereof. US 09000025, Apr 7 2015, 2015.

234. Bleisch, T. J.; Doti, R. A.; Pfeifer, L. A.; Norman, B. H. New substituted 2-(indan-2-ylamino)-7,8-dihydro-5H-pyrido(4,3-d)pyrimidine-6-carbaldehyd e compounds are autotaxin inhibitors useful for treating pain associated with osteoarthritis. WO2014168824-A1; TW201500356-A.

235. Guckian, K.; Kumaravel, G.; Ma, B.; Mi, S.; Peng, H.; Shao, Z.; Sun, L.; Taveras, A.; Wang, D.; Xin, Z.; Zhang, L. New substituted naphthalene derivatives are autotaxin inhibitors, used to treat an inflammatory disorder, an autoimmune disorder, a fibrosis and a malignancy of lung, chronic pain and chronic inflammatory demyelinating polyneuropathy. WO2014018881-A1; TW201416340-A; WO2014018881-A8; CA2879360-A1; AU2013295584-A1; KR2015038273-A; AR91930-A1.

236. Lukas, G.; Brindle, S. D.; Greengar.P, Route of absorbption of intraperitoneally administered compounds. *J Pharm Exp Ther* 1971, *178* (3), 562-&.

237. Hirano, K.; Hunt, C. A., Lymphatic transport of liposome encapsulated agents- effects of liposome size following intraperitoneal administration. *J. Pharm. Sci* 1985, *74* (9), 915-921.

238. Ulbrich, K.; Šubr, V., Structural and chemical aspects of HPMA copolymers as drug carriers. *Adv. Drug Deliv. Rev.* 2010, *62* (2), 150-166.

239. Veronese, F. M.; Pasut, G., PEGylation, successful approach to drug delivery. *Drug Discov. Today* 2005, *10* (21), 1451-1458.

240. Esfand, R.; Tomalia, D. A., Poly(amidoamine) (PAMAM) dendrimers: from biomimicry to drug delivery and biomedical applications. *Drug Discov. Today* 2001, *6* (8), 427-436.

241. Haley, B.; Frenkel, E., Nanoparticles for drug delivery in cancer treatment. *Urol. Oncol.* 2008, *26* (1), 57-64.

242. Ringsdorf, H., Structure and properties of pharmacologically active polymers. *J. Polym Sci, Polym Symp* 1975, *51* (1), 135-153.

243. Maeda, H.; Wu, J.; Sawa, T.; Matsumura, Y.; Hori, K., Tumor vascular permeability and the EPR effect in macromolecular therapeutics: a review. *J. Controlled Release* 2000, *65* (1-2), 271-284.

244. Markman, M., Intraperitoneal chemotherapy in the management of malignant disease. *Expert Rev Anticancer Ther* 2001, *1* (1), 142-8.

245. Butini, S.; Brindisi, M.; Gemma, S.; Minetti, P.; Cabri, W.; Gallo, G.; Vincenti, S.; Talamonti, E.; Borsini, F.; Caprioli, A.; Stasi, M. A.; Di Serio, S.; Ros, S.; Borrelli, G.; Maramai, S.; Fezza, F.; Campiani, G.; Maccarrone, M., Discovery of potent inhibitors of human and mouse fatty acid amide hydrolases. *J Med Chem* 2012, *55* (15), 6898-915.

246. Ferguson, C. G.; Bigman, C. S.; Richardson, R. D.; van Meeteren, L. A.; Moolenaar, W. H.; Prestwich, G. D., Fluorogenic phospholipid substrate to detect lysophospholipase D/autotaxin activity. *Org Lett* 2006, *8* (10), 2023-2026.

247. Witham, J.; Vidot, S.; Agarwal, R.; Kaye, S. B.; Richardson, A., Transient ectopic expression as a method to detect genes conferring drug resistance. *Int J Cancer* 2008, *122* (11), 2641-2645.

248. Malik, N.; Wiwattanapatapee, R.; Klopsch, R.; Lorenz, K.; Frey, H.; Weenerc, J. W.; Meijerc, E. W.; Paulusd, W.; Duncan, R., Dendrimers: Relationship between structure and biocompatibility in vitro, and preliminary studies on the biodistribution of ^{125}I-labelled polyamidoamine dendrimers in vivo. *J. Controlled Release* 2000, *63*, 133-1448.

249. Ihre, H. R.; De Jesus, O. L. P.; Szoka, F. C.; Frechet, J. M. J., Polyester dendritic systems for drug delivery applications: Design, synthesis, and characterization. *Bioconjug. Chem.* 2002, *13* (3), 443-452.

250. Cheng, Y.; Xu, Z.; Ma, M.; Xu, T., Dendrimers as drug carriers: applications in different routes of drug administration. *J. Pharm. Sci* 2008, *97* (1), 123-43.

251. Seymour, L. W.; Miyamoto, Y.; Maeda, H.; Brereton, M.; Strohalm, J.; Ulbrich, K.; Duncan, R., Influence of molecular-weight on passive tumor accumulation of a soluble macromolecular drug carrier. *Eur. J. Cancer* 1995, *31A* (5), 766-770.

252. Maeda, H.; Seymour, L. W.; Miyamoto, Y., Conjugates of anticancer agents and polymers: advantages of macromolecular therapeutics in vivo. *Bioconjug. Chem.* 1992, *3* (5), 351-362.

253. Campbell, I. G.; Jones, T. A.; Foulkes, W. D.; Trowsdale, J., Folate-binding Protein Is a Marker for Ovarian Cancer. *Cancer Res.* 1991, *51* (19), 5329-5338.

254. Najlah, M.; Freeman, S.; Attwood, D.; D'Emanuele, A., Synthesis, characterization and stability of dendrimer prodrugs. *Int J Pharm* 2006, *308* (1–2), 175-182.

255. Malik, N.; Evagorou, E. G.; Duncan, R., Dendrimer-platinate: a novel approach to cancer chemotherapy. *Anticancer Drugs* 1999, *10* (8), 767-776.

256. Zhang, H.; Xu, X.; Gajewiak, J.; Tsukahara, R.; Fujiwara, Y.; Liu, J.; Fells, J. I.; Perygin, D.; Parrill, A. L.; Tigyi, G.; Prestwich, G. D., Dual Activity Lysophosphatidic Acid Receptor Pan-Antagonist/Autotaxin Inhibitor Reduces Breast Cancer Cell Migration In vitro and Causes Tumor Regression In vivo. *Cancer Res.* 2009, *69* (13), 5441-5449.

257. Saunders, L. P.; Ouellette, A.; Bandle, R.; Chang, W. C.; Zhou, H. W.; Misra, R. N.; De La Cruz, E. M.; Braddock, D. T., Identification of small-molecule inhibitors of autotaxin that inhibit melanoma cell migration and invasion. *Mol Cancer Ther* 2008, *7* (10), 3352-3362.

258. Murph, M. M.; Liu, W.; Yu, S.; Lu, Y.; Hall, H.; Hennessy, B. T.; Lahad, J.; Schaner, M.; Helland, A.; Kristensen, G.; Borresen-Dale, A. L.; Mills, G. B., Lysophosphatidic acid-induced transcriptional profile represents serous epithelial ovarian carcinoma and worsened prognosis. *PLOS ONE* 2009, *4* (5), e5583.

259. Jazaeri, A. A.; Avvtrey, C. S.; Chandramouli, G. V. R.; Chuang, Y. E.; Khan, J.; Sotiriou, C.; Aprelikova, O.; Yee, C. J.; Zorn, K. K.; Birrer, M. J.; Barrett, J. C.; Boyd, J., Gene expression profiles associated with response to chemotherapy in epithelial ovarian cancers. *Clin Cancer Res* 2005, *11* (17), 6300-6310.

260. Wilbur, D. S.; Pathare, P. M.; Hamlin, D. K.; Buhler, K. R.; Vessella, R. L., Biotin Reagents for Antibody Pretargeting. 3. Synthesis, Radioiodination, and Evaluation of Biotinylated Starburst Dendrimers. *Bioconjug. Chem.* 1998, *9* (6), 813-825.

261. Moberly, J. B.; Mujais, S.; Gehr, T.; Hamburger, R.; Sprague, S.; Kucharski, A.; Reynolds, R.; Ogrinc, F.; Martis, L.; Wolfson, M., Pharmacokinetics of icodextrin in peritoneal dialysis patients. *Kidney Int Suppl* 2002, (81), S23-S33.

262. McOmie, J. F. W.; Watts, M. L.; West, D. E., Demethylation of aryl methyl ethers by boron tribromide. *Tetrahedron* 1968, *24* (5), 2289-2292.

263. Plourde, G. L.; Spaetzel, R. R., Regioselective Protection of the 4-Hydroxyl of 3,4-dihydroxy-benzaldehyde. *Molecules* 2002, (7), 697-705.

264. Zhou, Q.; Zhang, L. N.; Okamura, H.; Minoda, M.; Miyamoto, T., Synthesis and properties of O-2- 2-(2-methoxyethoxy) ethoxy acetyl cellulose. *Journal of Polymer Science Part A-Polymer Chemistry* 2001, *39* (3), 376-382.

265. Liu, C.; Baumann, H., Exclusive and complete introduction of amino groups and their N-sulfo and N-carboxymethyl groups into the 6-position of cellulose without the use of protecting groups. *Carbohydr. Res.* 2002, *337* (14), 1297-1307.

266. Smith, A. B.; Risatti, C. A.; Atasoylu, O.; Bennett, C. S.; Liu, J.; Cheng, H.; TenDyke, K.; Xu, Q., Design, Synthesis, and Biological Evaluation of Diminutive Forms of (+)-Spongistatin 1: Lessons Learned. *Journal of the American Chemical Society* 2011, *133* (35), 14042-14053.

267. Zhang, C.; Liu, R.; Xiang, J.; Kang, H.; Liu, Z.; Huang, Y., Dissolution Mechanism of Cellulose in N,N-Dimethylacetamide/Lithium Chloride: Revisiting through Molecular Interactions. *J. Phys. Chem. B* 2014, *118* (31), 9507-9514.

268. Dedrick, R. L.; Flessner, M. F., Pharmacokinetic Problems in Peritoneal Drug Administration: Tissue Penetration and Surface Exposure. *J Natl Cancer Inst* 1997, *89* (7), 480-487.

269. de Waart, D. R.; Zweers, M. M.; Struijk, D. G.; Krediet, R. T., Icodextrin degradation products in spent dialysate of CAPD patients and the rat, and its relation with dialysate osmolality. *Perit Dial Int.* 2001, *21* (3), 269-274.

270. Tokumura, A.; Kume, T.; Fukuzawa, K.; Tahara, M.; Tasaka, K.; Aoki, J.; Arai, H.; Yasuda, K.; Kanzaki, H., Peritoneal fluids from patients with certain gynecologic tumor contain elevated levels of bioactive lysophospholipase D activity. *Life Sci.* 2007, *80* (18), 1641-1649.

271. Shaunak, S.; Thornton, M.; John, S.; Teo, I.; Peers, E.; Mason, P.; Krausz, T.; Davies, D. S., Reduction of the viral load of HIV-1 after the intraperitoneal administration of dextrin 2-sulphate in patients with AIDS. *AIDS* 1998, *12* (4), 399-409.

272. Kerr, D. J.; Young, A. M.; Neoptolemos, J. P.; Sherman, M.; Van-Geene, P.; Stanley, A.; Ferry, D.; Dobbie, J. W.; Vincke, B.; Gilbert, J.; el Eini, D.; Dombros, N.; Fountzilas, G., Prolonged intraperitoneal infusion of 5-fluorouracil using a novel carrier solution. *Br J Cancer* 1996, *74* (12), 2032-5.

273. McArdle, C. S.; Kerr, D. J.; O'Gorman, P.; Wotherspoon, H. A.; Warren, H.; Watson, D.; Vinke, B. J.; Dobbie, J. W.; el Eini, D. I., Pharmacokinetic study of 5-fluorouracil in a novel dialysate solution: a long-term intraperitoneal treatment approach for advanced colorectal carcinoma. *Br J Cancer* 1994, *70* (4), 762-6.

274. Engler, H.; Machemer, T. R.; Schluep, T.; Wen, S. F.; Quijano, E.; Wills, K. N.; Harper, A. E.; Maneval, D. C.; Conroy, S. E., Development of a formulation that enhances gene expression and efficacy following intraperitoneal administration in rabbits and mice. *Mol Ther* 2003, *7* (4), 558-64.
275. Leamon, C. P., Folate-targeted drug strategies for the treatment of cancer. *Curr Opin Investig Drugs* 2008, *9* (12), 1277-86.